NASA/CR-1999-209324

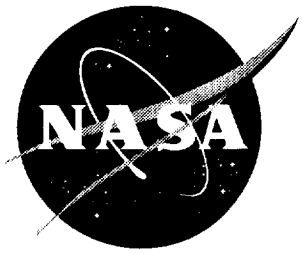

High Reynolds Number Hybrid Laminar Flow Control (HLFC) Flight Experiment II. Aerodynamic Design

Boeing Commercial Airplane Group, Seattle, Washington

National Aeronautics and
Space Administration

Langley Research Center
Hampton, Virginia 23681-2199

Prepared for Langley Research Center
under Contract NAS1-18574

April 1999

The data in this volume, D6-55648-2, was collected by members of The Boeing Company in a cooperative effort with the National Aeronautics and Space Administration and the United States Air Force under contract NAS1-18574.

Available from:

NASA Center for AeroSpace Information (CASI)
7121 Standard Drive
Hanover, MD 21076-1320
(301) 621-0390

National Technical Information Service (NTIS)
5285 Port Royal Road
Springfield, VA 22161-2171
(703) 605-6000

CONTENTS

FIGURES

FIGURES

FIGURES

FIGURES

PREFACE

The program was jointly sponsored by NASA; the United States Air Force, Wright Laboratory, Flight Dynamics Directorate; and The Boeing Company. The contract was managed by Mr. R. D. Wagner, Head of Laminar Flow Control Project Office, and Mr. D. V. Maddalon, Technical Monitor. Mr. R. L. Clark was the Wright Laboratory (WL/FIMM, Wright-Patterson Air Force Base, OH) Program Manager. The period of performance was from December 1987 through August 1991.

The program was conducted by the Advanced Development Aerodynamics organization of Boeing Commercial Airplane Group (BCAG), supported by the BCAG Nacelle, Strut, and Propulsion System Engineering, BCAG Structures Engineering, BCAG Mechanical/Electrical Systems Engineering, and BCAG Flight Test organizations.

The principal contributors to the work described herein are Mr. D. George-Falvy, principal analyst; Mr. A. W. Chen, wing contour design; Ms. R. Behbehani, stability calculations; and Mr. D. W. Lund, low-speed wind tunnel testing. Mr. F. J. Davenport provided technical and document integration services. Mr. A. L. Nagel of BCAG Aerodynamics Technology, HLFC program manager, gave guidance and suggestions throughout the course of the design effort.

Special thanks are owed to Mr. R. D. Wagner and Mr. D. V. Maddalon of NASA Langley Research Center, who generously contributed time and effort to make their unique backgrounds of laminar flow expertise and flight test experience available to Boeing personnel.

Finally, the authors wish to acknowledge the vital contribution of Dr. Werner Pfenninger. In addition to being a mentor to all participants in modern laminar flow control work, he made several specific contributions to the present flight test program.

SYMBOLS AND ABBREVIATIONS

A	Disturbance amplitude
A_O	Disturbance amplitude at neutral stability point
c	Wing chord (local), ft
c_l	Section lift coefficient
C_L	Airplane lift coefficient
C_D	Airplane drag coefficient
C_{RM}	Airplane rolling moment coefficient
C_P	Local pressure coefficient
c_q'	Local suction flow coefficient, (mass flow per unit area)/$\rho_\infty V_\infty$
c_q	Chord suction flow coefficient, (mass flow per unit area)/$\rho_\infty V_\infty$
C_Q	Total suction flow coefficient (referred to suction panel reference area)
D	Drag, lb
d	Width in protuberance
g	Acceleration of gravity
GW	Airplane gross weight, lb
h	Altitude, ft, or surface wave height, in
k	Protuberance height, in
L	Lift, l
M	Mach number
N	Natural logarithm of disturbance amplification factor
P	Pressure, lb/ft^2
R	Airfoil nose radius, in
R_c	Reynolds number based on wing chord
R_l	Unit Reynolds number, V/ν, ft^{-1}
$R_{\theta al}$	Attachment-line Reynolds number, $W_{\theta al})/\nu$
q	Dynamic pressure, $\rho V^2/2$, lb/ft^2
Q	Suction volume flow rate, ft^3/s

SYMBOLS AND ABBREVIATIONS

s	Streamwise distance from attachment line along wing surface, ft
S	Wing reference area, ft^2
S_{sp}	Suction panel reference area, ft^2
U	Velocity component normal to the leading edge, ft/s
v_w	Equivalent suction inflow velocity (uniformly distributed), ft/s
V	Velocity component parallel to free stream, ft/s
$\dot{w}$	Suction weight flow, lb/s
W	Velocity component parallel to the leading edge, ft/s
x	Chordwise distance, in
y_{sp}	Spanwise length of suction panel, ft
Z	Vertical coordinate, in
α	Disturbance wave number, ft^{-1}
$ß$	Angle of side slip, deg
δ	Boundary layer velocity thickness, ft, or Krueger flap deflection, deg
δ^*	Boundary layer displacement thickness, ft
ΔZ	Krueger trailing edge height above chord plane, in, or vertical coordinate, in
θ	Boundary layer momentum thickness, ft
η	Fractional semispan location
λ	Wave length, ft
Λ	Wing sweepback angle
μ	Viscosity, $lb\text{-}s/ft^2$
ν	Kinematic viscosity (μ/ρ), ft-lb-s/slug
ρ	Density, $slugs/ft^3$
ω	Disturbance frequency, Hz
ψ	Wave angle

SUPERSCRIPTS

•	Time rate of change

SUBSCRIPTS

∞	Freestream condition
al	Attachment line
e	Edge of the boundary layer
K	Krueger flap
LE	Leading edge
Max	Maximum
o	Initial condition
sp	Suction panel
w	Condition at the wall

ABBREVIATIONS

BSTA	Body station
CF	Crossflow
CFD	Computational fluid dynamics
HLFC	Hybrid laminar flow control
MAC	Mean aerodynamic chord
NLF	Natural laminar flow
OSS	Outboard slat station
Rn	Reynolds number
TS	Tollmien-Schlichting
USS	Unified Stability System
UWAL	University of Washington Aeronautical Laboratory
WBL	Wing buttock line

1.0 SUMMARY

The aerodynamic design of an experimental hybrid laminar flow control (HLFC) wing panel on a Boeing 757 airplane has been developed. The modified wing is intended both to provide a facility for flight research on high Reynolds number HLFC and to demonstrate practical HLFC operation on a full-scale commercial transport airplane. The 17-ft-long test panel provides a flow-controlled span of nearly 14 ft, beginning just outboard of the left engine nacelle.

The aerodynamic design comprises—

a. A revised wing contour designed to produce a pressure distribution favorable to laminar flow.

b. Definition of suction flow requirements to laminarize the boundary layer and predict the extent of laminar flow achievable in the test area.

c. Design of provisions at the leading edge of the inboard end of the test panel to prevent attachment-line boundary layer transition.

d. Geometric design and experimental verification of the effectiveness of a Krueger leading edge flap that serves both as a high-lift device equivalent to the original 757 leading edge slat and as a shield to prevent insect impingement on the laminar flow surface.

The development of the revised wing contour was carried out using an enhanced version of Jameson's transonic inviscid flow code (ref. 1) in conjunction with a Boeing-developed three-dimensional boundary layer analysis code (ref. 2). No high-speed wind tunnel testing was done in support of this effort. The selected design point was $M = 0.80$ and $C_L = 0.50$ at 39,000-ft altitude, which is the same as the recommended long-range cruise condition of the Boeing 757 airplane. The HLFC wing profile modification was limited to the portion ahead of the front spar. A slightly blunter leading edge was used, providing more rapid initial acceleration than the original 757 wing. Aft of the front spar, the desired gently favorable pressure gradient and aft pressure recovery were already present. The lower surface of the leading edge formed the upper contour of the Krueger flap when it was deployed. To increase the Krueger's effectiveness as a leading edge device, the very flat 757 contour was replaced by a slightly bulged form.

The suction flow rates were determined using the Unified Stability System (USS) computer code developed by Boeing under NASA sponsorship (ref. 3). The USS code calculates disturbance amplification ratios for crossflow (CF) and Tollmien-Schlichting (TS) instabilities, including the effects of suction, in three-dimensional compressible flow according to Mack's stability code (ref. 4). The transition criterion used in the present study was a curve on a plot of TS versus CF amplification ratios based on data from flight experiments on the F-111 and Boeing 757 natural laminar flow "gloves" (refs. 5 and 6). It showed high sensitivity to crossflow instability, resulting in a requirement for high suction rates near the leading edge.

The stability and suction requirement calculations were carried out over a range of lift coefficient and Mach number surrounding the design point. The calculations indicated that laminar flow could usually be sustained back to the pressure recovery point (or shock location), normally around 45% to 50% of chord. However, the predicted laminar run was less than 45% chord over the inboard

portion of the HLFC test panel, because of early pressure recovery. At lower C_Ls, (around 0.40), more suction was required and less laminar flow predicted than at high lift coefficients (around 0.60) because of changes in the pressure distributions. The calculations also indicated that, because of decreasing Reynolds number, a greater extent of laminar flow could be expected as altitude increased, and less suction flow would be required to attain it.

The predicted total suction flow coefficient (C_Q) at the design condition (M = 0.80 and C_L = 0.50 at 39,000 ft altitude) was 4.72×10^{-5} and the corresponding total volume and mass flow rates were 6.97 ft^3/s and 0.1368 lb/s (8.2 lb/min), respectively.

After the suction requirements had been defined and the suction system had been designed to meet them, additional data became available from flight experiments on the variable-sweep F-14 VSTFE airplane (ref. 3), indicating that somewhat higher crossflow amplification would be acceptable, so lower suction rates near the leading edge would be adequate. However, it was not considered prudent to redesign the system for a lower suction capability at that point, and it was decided to regard the USS code's prediction as a conservative upper boundary. The suction system controls would permit inflight verification of the lower suction requirements.

The attachment-line boundary layer momentum thickness Reynolds number was expected to be at or near the critical value of 100 along most of the span affected by HLFC, so it was considered advisable to take steps to reduce it. A suction "patch" was therefore provided at the leading edge just inboard of the HLFC test area, vented to a low-pressure point further downstream on the lower surface. The passive suction provided was estimated to have reduced the attachment-line Reynolds number to about 30.

A low-speed wind tunnel test of a Boeing 757 model with modified leading edge devices showed that the maximum lift capability was only slightly compromised by replacing two of the five slats with dual-purpose Krueger flaps, and the test also showed that the HLFC leading edge modification would not significantly alter the low-speed performance and handling qualities of the test airplane.

2.0 INTRODUCTION

2.1 BACKGROUND

The potential for reducing wing friction drag by increasing the extent of laminar flow was recognized more than half a century ago. However, boundary layer instabilities associated with high Reynolds number and with sweepback prevented achievement of significant laminar runs on the wings of large high-performance airplanes. In the 1960s, the USAF X-21 program (ref. 7) showed that those problems could be overcome by using slot suction to stabilize the boundary layer, provided that care was taken to control wing surface roughness and waviness. The program failed as a demonstration of practical laminar flow control because of a flawed joint design that required continual repair or replacement of aerodynamic smoothing material. There was also debate as to whether the complexity of a suction system that covered the entire wing with slots and subsurface ducts was justified by the performance gain.

The concept of Hybrid Laminar Flow Control (HLFC), invented by L. B. Gratzer of The Boeing Company (U.S. Patent No. 4,575,030), greatly simplifies laminar flow control by confining suction surfaces and pneumatic system components to the leading edge. HLFC maintains laminar flow downstream of the wing front spar solely by tailoring the pressure distribution.

Other concerns relating to anti-icing and to clogging or roughening of suction surfaces as a result of insect accretion were addressed by the NASA Leading Edge Flight Test Program (refs. 8, 9, and 10). A modified Lockheed Jetstar airplane equipped with a partial-span leading edge suction system was flown in a variety of hostile environments and demonstrated reliable operation of the system.

The present program was sponsored by NASA, with partial USAF sponsorship and Boeing participation, in order to—

a. Perform high Reynolds number flight research on HLFC.

b. Obtain data on the effectiveness of HLFC on a large, high-subsonic-speed transport airplane.

c. Develop and demonstrate practical design concepts for HLFC systems.

2.2 TECHNICAL APPROACH

A Boeing-owned 757 airplane was modified to include all the critical systems for a full-scale HLFC application, plus flight-operable suction controls and extensive instrumentation to meet HLFC research requirements. The 757 was ideally suited for the program because its advanced aerodynamic technology wing permitted attainment of the needed HLFC pressure distribution with only a small contour change ahead of the front spar, and the smoothness of the existing between-spar structure allowed the test to be conducted with minimal fairing or coating beyond normal paint. This ensured that the data obtained would have practical application to standard production wings, and not be restricted to ideally smooth surfaces.

2.3 PROGRAM TASKS

The program effort consisted of—

Aerodynamic Design. Definition of the surface pressures and suction quantities required to achieve extended laminar flow, followed by geometric design of the wing contours needed to obtain the surface pressures. This task is treated in detail in this volume.

Leading Edge Structural Design and Fabrication. The design, construction, and installation of a 22-ft section of wing leading edge, having provisions for suction through a porous outer skin and for a Krueger-type leading edge flap serving both as an integral part of the airplane high-lift system and as a shield against insect accretion at low altitude. The leading edge was required to meet stringent aerodynamic smoothness and waviness requirements under load, as well as to provide structural integrity. This task is treated in detail in volume III.

Suction System Design and Manufacture. The design of the system of air passages, ducts, valves, and pump, and the specification of leading edge outer skin porosities. The system was required not only to provide the suction flows required for laminarization, but also to demonstrate anti-icing capability. To achieve this, hot pressurized air was required to flow out through certain portions of the porous skin. The system was also required to provide for a wide range of suction flow adjustment, so as to permit optimization of HLFC suction quantities and to permit generation of boundary layer behavior data under a variety of suction conditions, in support of research on boundary layer analysis methods. This task is reported in detail in volume IV.

Flight Test and Data Analysis. The definition and installation of suitable instrumentation to evaluate boundary layer conditions and suction system performance, followed by the conduct of the tests, data acquisition, and evaluation of test results. This task is reported in volume I, along with an overview of the program.

2.4 BOEING 757 WING DESCRIPTION

The HLFC test panel replaced part of the left wing of a Boeing 757. The general arrangement and principal dimensions of the airplane are shown in figure 2.4-1, and the wing structural arrangement is shown in figure 2.4-2. The wing primary structure consisted of outboard spar boxes cantilevered from a center section box contained within the fuselage. All three boxes were sealed to form integral fuel tanks. Each box was built up of front and rear spars, lower panels, and upper panels. The outboard wing boxes incorporated ribs normal to the outboard rear spar. The inboard wing had a trailing edge extension to accommodate the landing gear support beam. The movable elements of the wing included an aileron at the wingtip, six spoilers aft of the rear spar, two double-segment trailing edge flaps, and five leading edge slats.

Various components of the wing were defined in different coordinate systems for design and manufacturing convenience. For aerodynamic analysis, spanwise location was given by the wing buttock line (WBL), and the fore-and-aft coordinate was given as a fraction of local wing chord (sometimes supplemented by body station (BSTA) where an absolute reference was needed). For HLFC structural and suction system design and analysis, outboard slat station (OSS) was used for spanwise locations. Definitions of BS, OSS, and WBL are shown in figure 2.4-3.

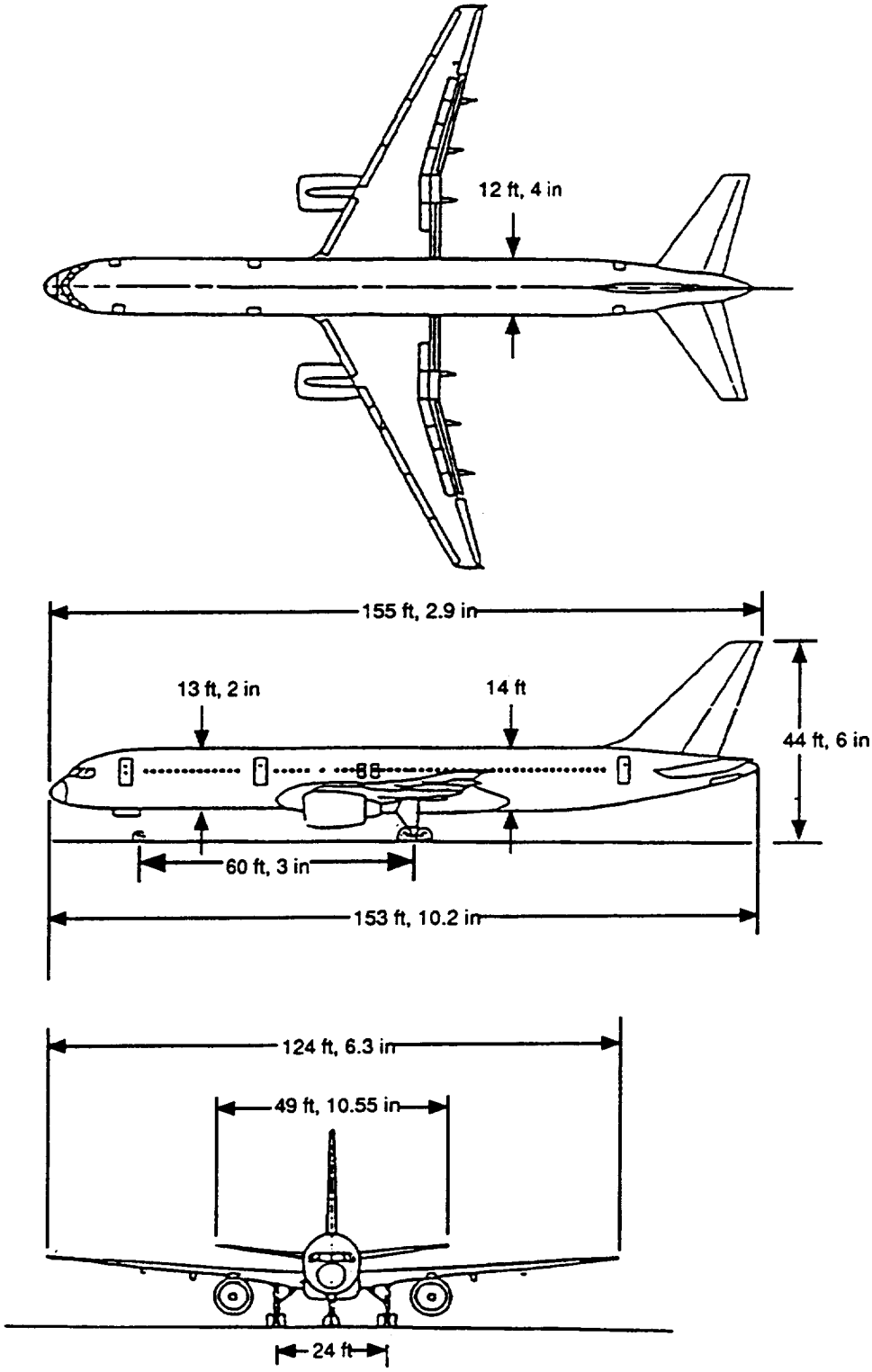

Figure 2.4-1. General Arrangement and Main Dimensions of the Boeing 757-200

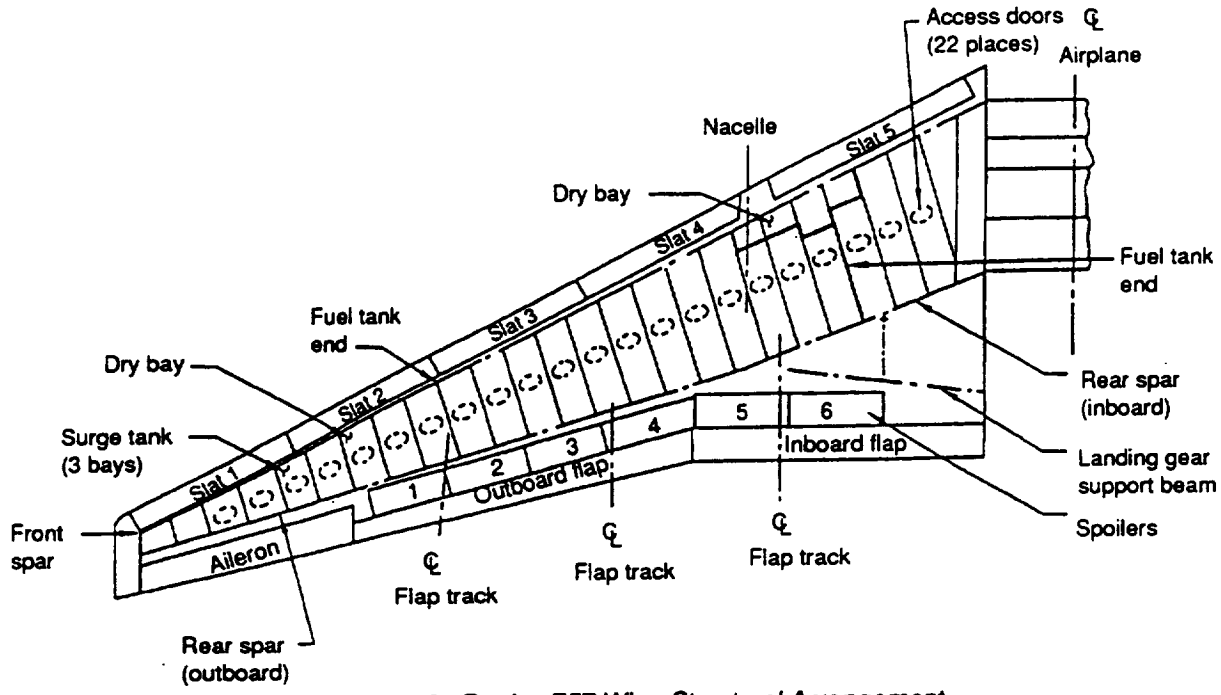

Figure 2.4-2. Boeing 757 Wing Structural Arrangement

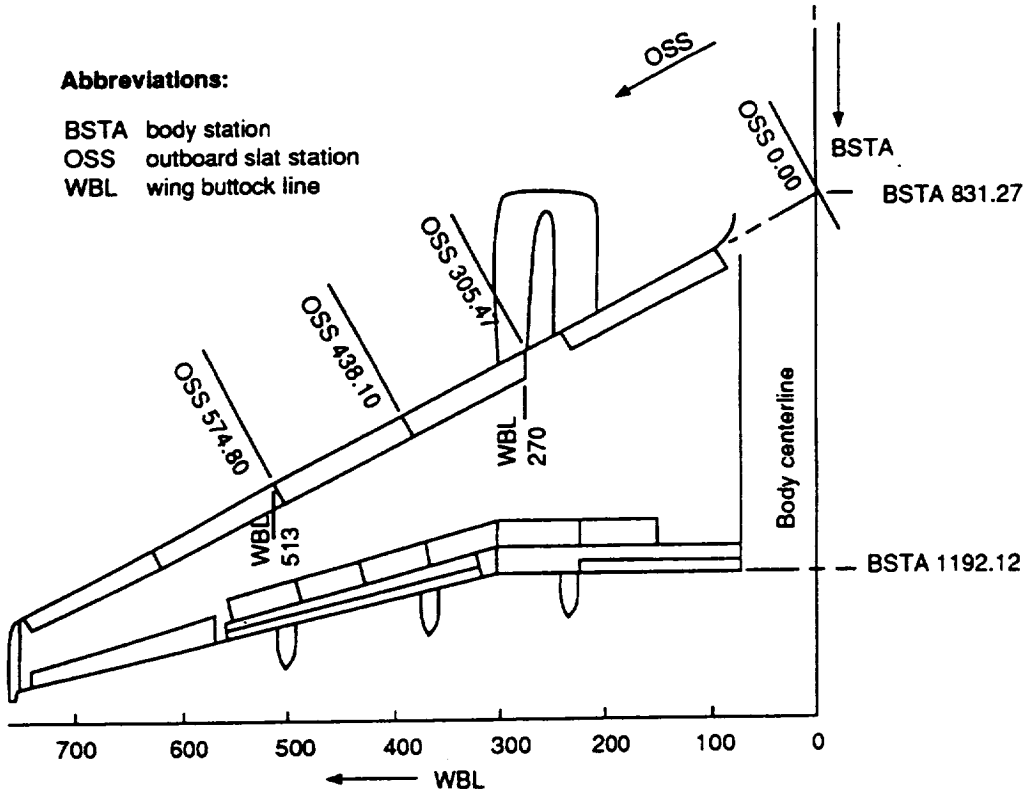

Figure 2.4-3. Wing Planform and Coordinate Definitions

Leading edge features are shown in figure 2.4-4. The fixed part of the leading edge structure consisted of machined aluminum alloy ribs with bonded fiberglass honeycomb stabilized surfaces. The lower surface was made up of Kevlar laminate panels that were removable for access. Four individual tapered-chord slats were outboard of the engine nacelle, and a single constant-chord slat was inboard of the nacelle. Each slat was supported by two circular arc steel tracks and moved by two rotary actuators driven by an electric motor via a torque tube. The slats had two deployment positions: ungapped for takeoff and gapped for landing, as depicted in figure 2.4-5. (Note that actuation of the Krueger flap on the HLFC test panel was required to be integrated with the actuation of the slats on either side of it.)

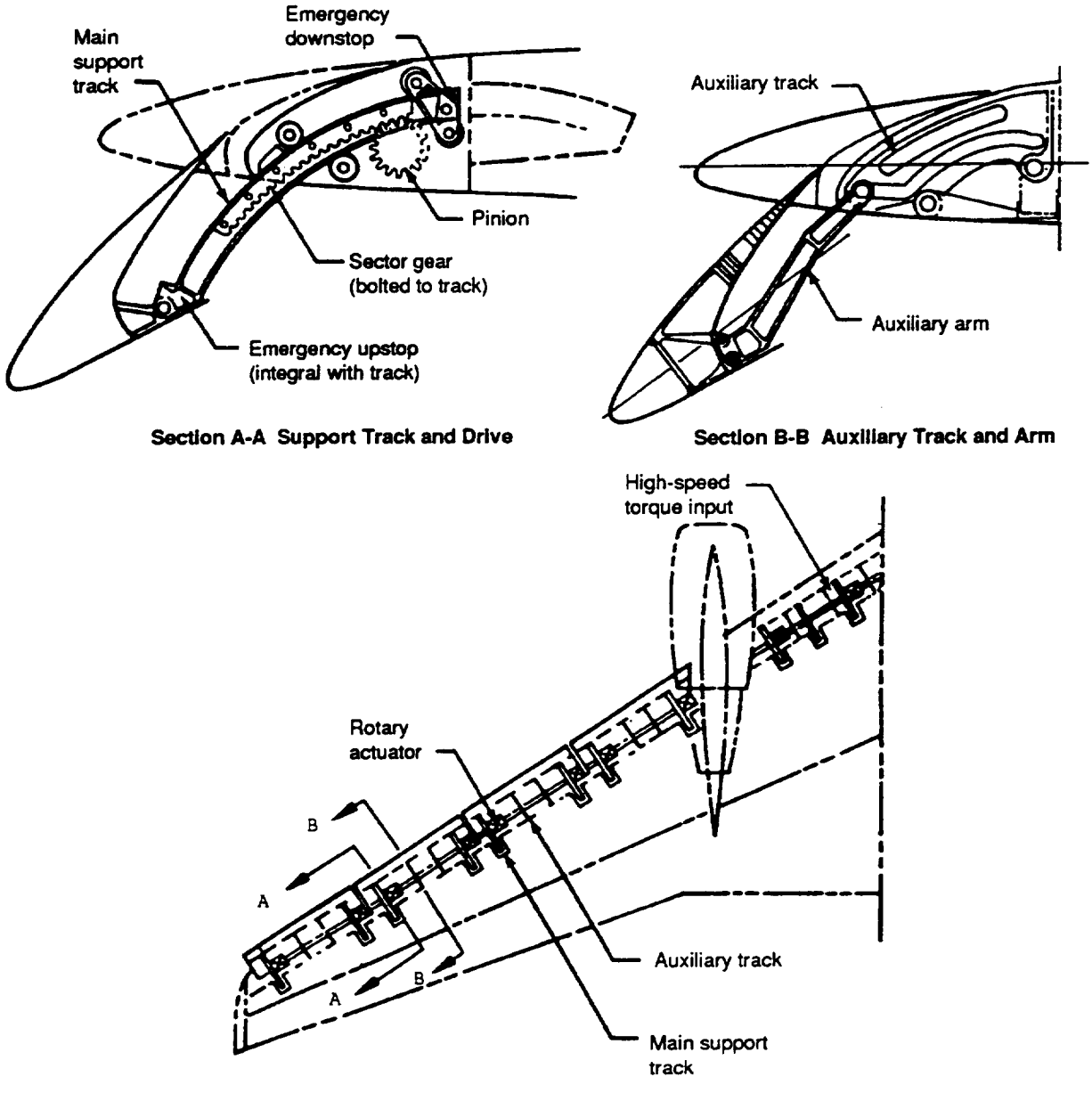

Figure 2.4-4. Boeing 757 Leading Edge Slat Design

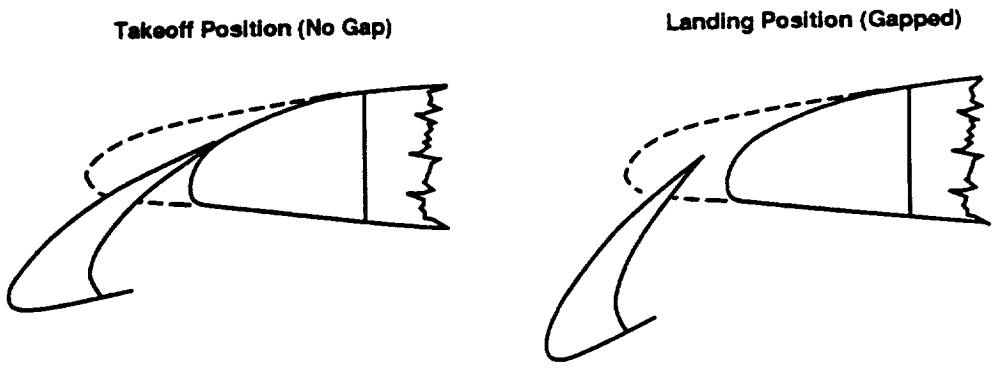

Figure 2.4-5. Leading Edge Slat Positions

2.5 DESIGN OBJECTIVES AND CONSTRAINTS

The 757 long-range cruise condition, $M = 0.80$ at $C_L = 0.50$, was the design point chosen for the HLFC flight experiment. This was slightly faster than the point for highest M(L/D), as shown in figure 2.5-1. The variation of altitude with gross weight at the design point condition is also shown. The applicable weight range of the test airplane was from 160,000 to 220,000 lb.

Because the portion of the test panel forward of the front spar was to be completely rebuilt, it was possible to refine the external contours to provide a pressure distribution more favorable to HLFC than the pressure distribution of the original 757s. Previous studies (refs. 11 and 12) had indicated a number of desirable features for HLFC airfoil sections on a sweptback wing. As shown in figure 2.5-2, these features included—

a. Rapid initial acceleration to limit the extent of the region where suppressing crossflow instability required intensive suction.

b. A slight negative pressure peak at the end of the initial acceleration to attenuate the crossflow boundary layer.

c. Gentle acceleration aft of the suction region just sufficient to keep the Tollmien-Schlichting (TS) instability in check.

d. Late recovery (i.e., shock location), possibly aft of 65% chord, with local Mach number not exceeding 1.15.

While a stronger pressure gradient aft of the suction region would be favorable for the TS amplification, the associated crossflow boundary layer would be vulnerable to CF instability. Furthermore, because of the limitation on Mach number at the shock, the favorable pressure gradient would reduce the achievable lift coefficient.

The modifications to the wing contours in the HLFC test section were aimed at fulfilling the above objectives as far as the constraints imposed on the design permitted.

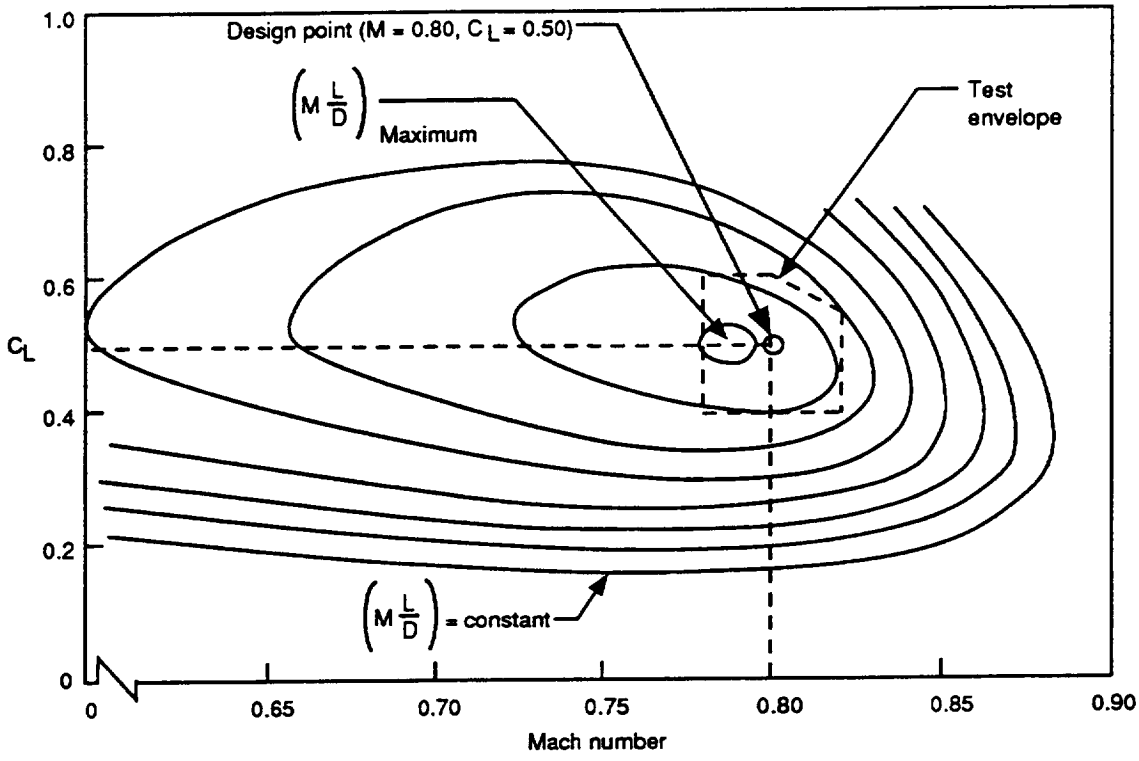

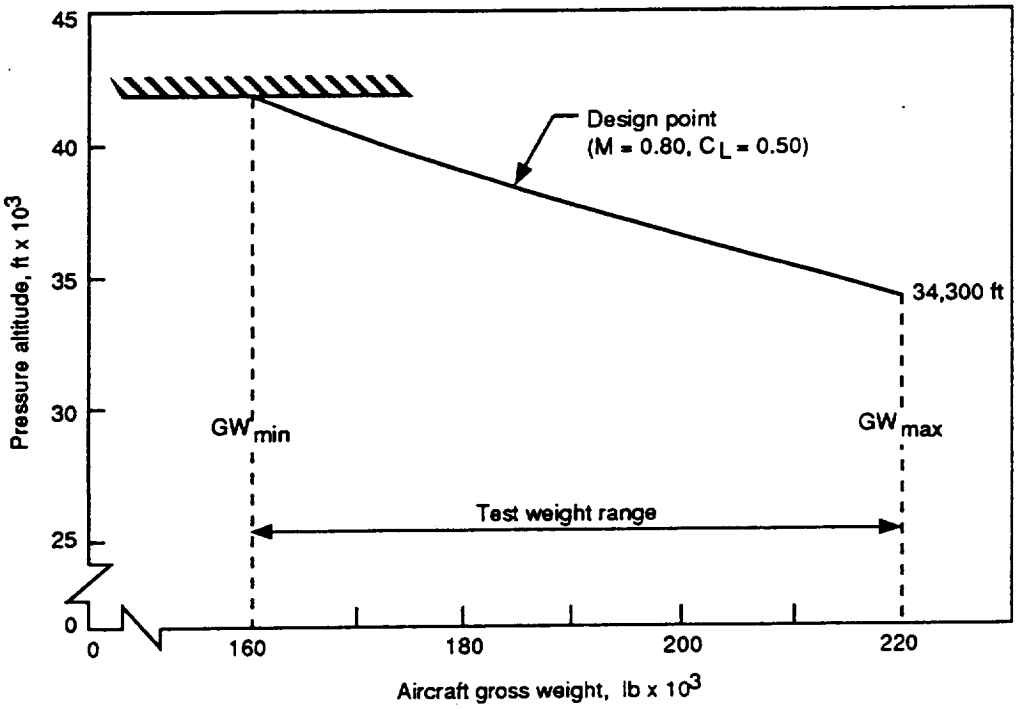

Figure 2.5-1. Design Point Selection

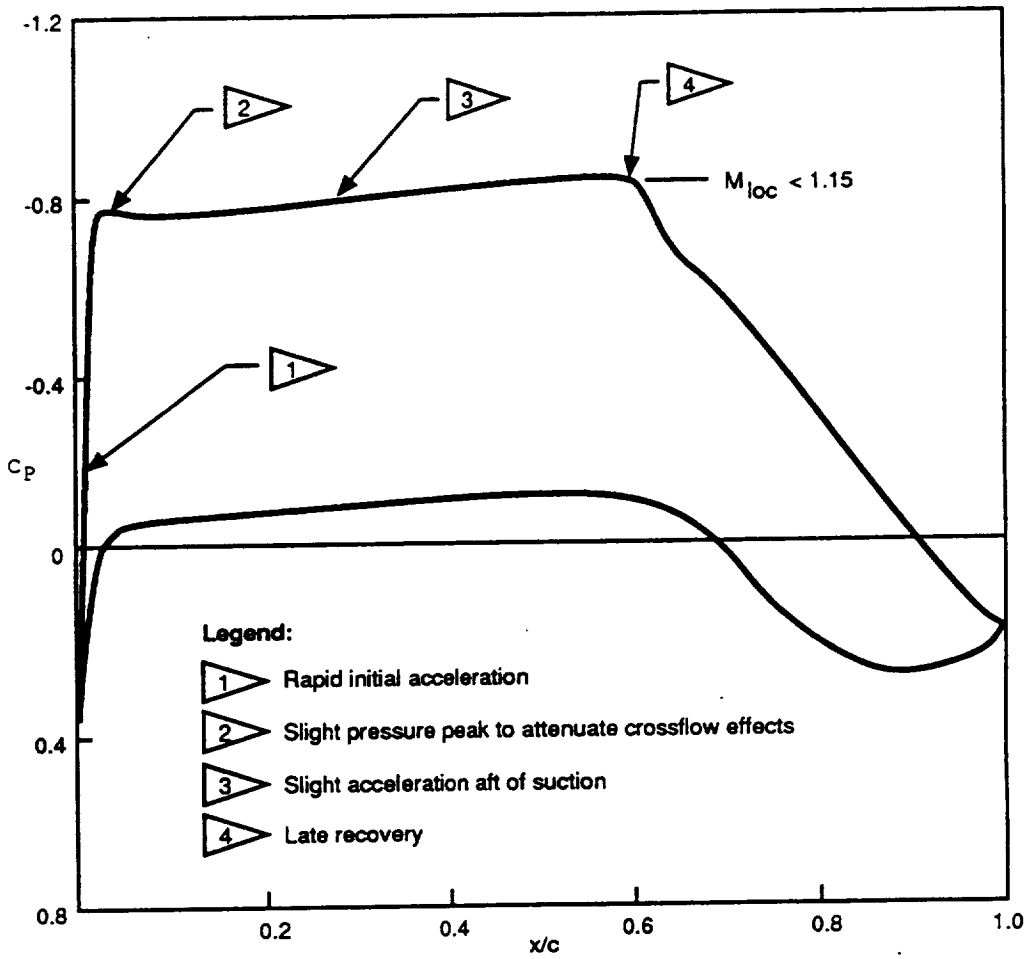

Figure 2.5-2. Desired Features of HLFC Wing Pressure Distribution

One such constraint was that no contour changes were allowed aft of the front spar, preventing postponement of the pressure recovery point. Another was that no change in slope was permitted at the mating point of the leading edge and the spar box. This, in conjunction with other design guidelines regarding the curvature distribution of practical transonic airfoils, limited the allowable steepening of the initial pressure gradient.

Because of the requirement to protect the leading edge from insect accretion during landing and takeoff and the need to eliminate gaps on the upper surface, leading edge slats Nos. 3 and 4 were replaced by Krueger flaps. These flaps were required to provide low-speed flight characteristics comparable to those of the original 757.

The initial design called for suction to be applied along the entire 22-ft length of the new leading edge, but the suction region was later reduced by 5 ft to adapt the design to the capacity of the available suction pump.

2.6 SURFACE QUALITY REQUIREMENTS

Guidelines for two-dimensional (2D) surface quality requirements on laminar flow airplanes were first established during the Northrop/USAF X-21 LFC research program (ref. 7), using the extensive database of previous boundary layer research and the results of specific LFC-related experiments. More recent flight and wind tunnel tests by NASA, Boeing, and others (refs. 13, 14, and 15) have added to this database, resulting in further refinements but not substantially changing the Northrop criteria.

There are two categories of surface imperfections to be dealt with: 2D imperfections, such as waviness, steps, gaps, joints, rivets, and dents (depending on the value of d/k), and three-dimensional (3D) types, such as insect residue, paint graininess, and accumulated dirt, all of which behave in the same manner whether they are individual protuberances or sparsely distributed when the values of d/k are in the general vicinity of 0.5 to 10. At Mach numbers up to moderate supersonic speeds, 2D imperfections introduce TS-type disturbances into the boundary layer, and their effects on transition are affected by boundary layer stability, whereas 3D surface imperfections bypass stability effects and cause premature transition very near the individual imperfection when it is a critical size.

Surface tolerances are generally more stringent in the forward region, where the boundary layer is relatively thin, but other factors may mitigate this rule. For example, suction or a strong favorable pressure gradient may allow wider tolerances for waviness but they may also promote transition due to a 3D discontinuity. Increasing unit Reynolds numbers (decreasing altitude) leads to tighter tolerances for both 2D and 3D protuberances, but in a different manner. For 2D, increasing unit Reynolds number increases the growth of the 2D type of boundary layer disturbances, leading to a forward movement in transition. For 3D, increasing unit Reynolds number decreases the height of 3D roughness that triggers immediate transition near the roughness. Also, crossflow in the leading edge may reduce the size of the tolerable 3D protuberances. The limits specified for the 757 HLFC test section at the design condition are summarized in figures 2.6-1 and 2.6-2 for the most common types of surface imperfections. Surface quality requirements are also discussed in volume III of this report.

Finally, figure 2.6-3 illustrates so called "aerodynamic" roughness, which arises from the fact that the streamtubes sucked in to perforations create an uneven "virtual surface" that is analogous to a physical surface with distributed roughness. While there are no data available to prove that this effect actually exists, it was regarded as prudent to allow for the possibility. An unpublished analysis attributed to Pfenninger (who also provided the figure) indicates that the originally contemplated hole spacing of 0.025 in would produce an equivalent roughness height K = 0.003 in, but a maximum value of k of only 0.001 in was allowable close to the airfoil nose. The analysis also showed that reducing the spacing to 0.010 in would reduce k to the required value. The 0.010-in spacing was accordingly adopted for the most forward perforation area.

Allowable Waviness

- Multiple waves; for single waves, triple the indicated allowable wave height.
- Wavecrests are parallel to span; for wavecrests parallel to chord, double the allowable wave height.

Allowable Roughness Height

- Rivets, dents $\left(\frac{d}{k} \sim 150\right)$

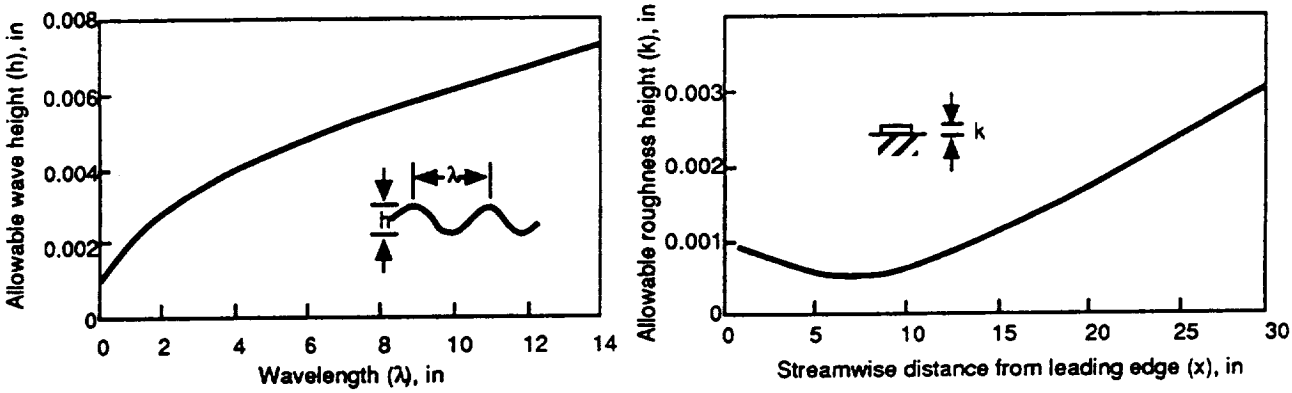

Spar-Joint Step or Gap—Maximum Allowable Discontinuity

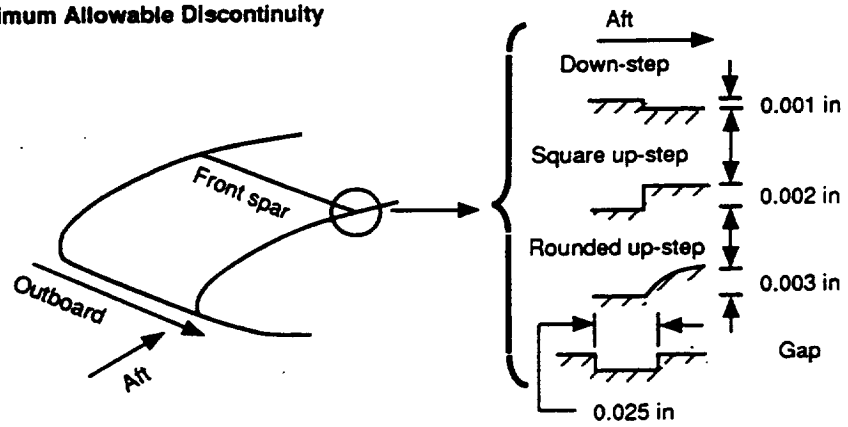

Suction Surface Splice Step or Gap—Maximum Allowable Discontinuity

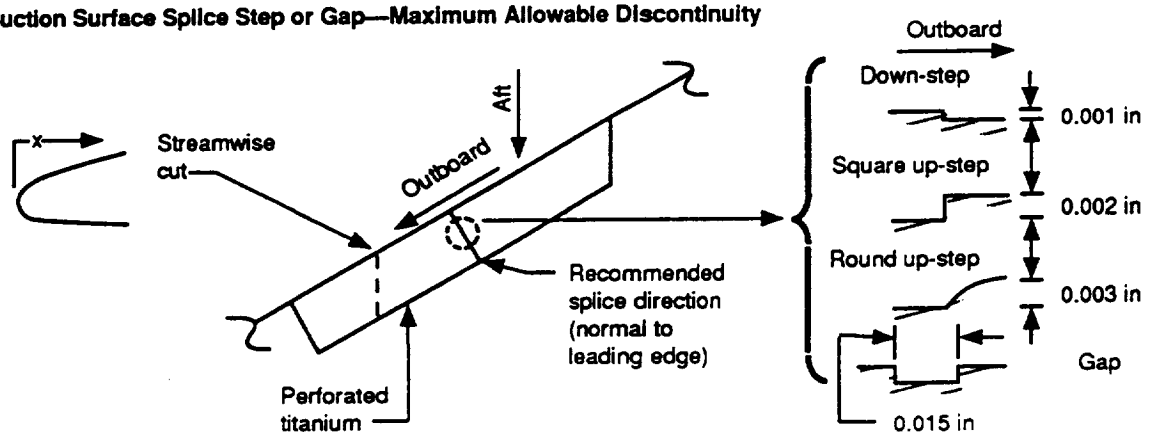

Figure 2.6-1. Surface Quality Specifications for the Suction Region

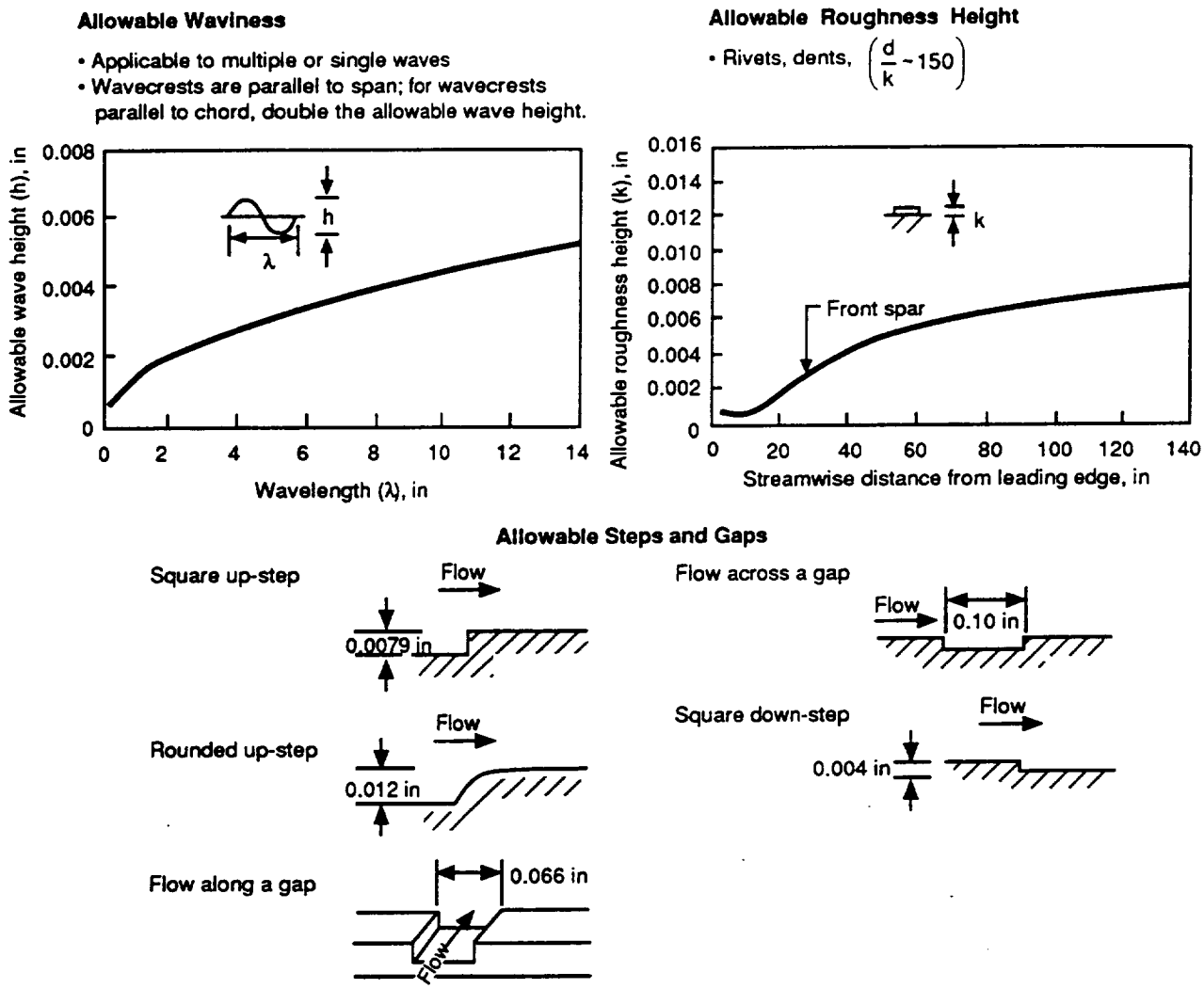

Figure 2.6-2. Surface Quality Specifications for the Nonsuction Region

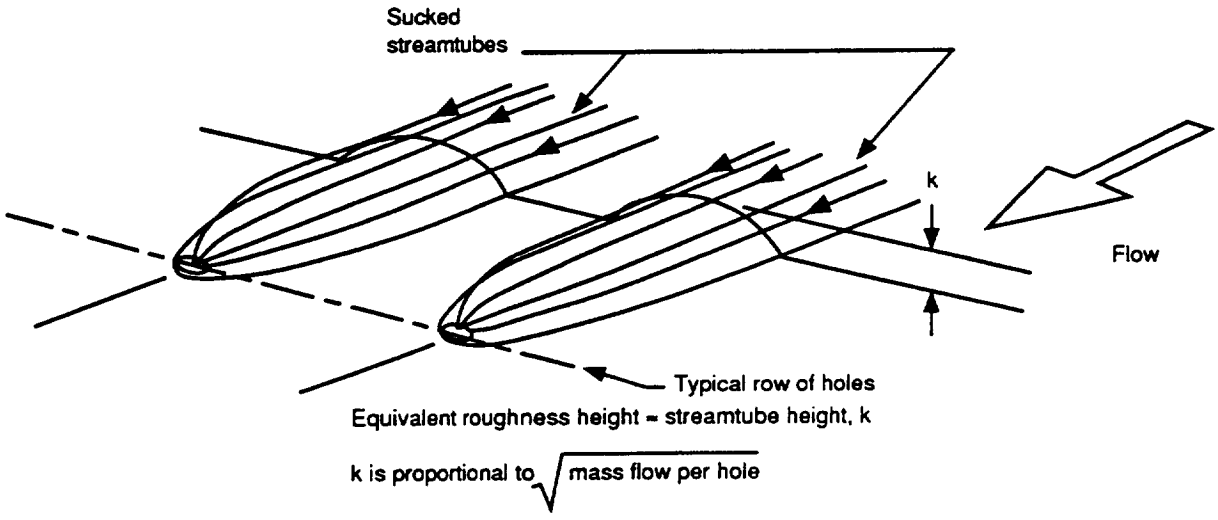

Figure 2.6-3. Equivalent Roughness of Suction Streamtubes

This page intentionally left blank.

3.0 HLFC WING SECTION EXTERNAL CONTOUR ANALYSIS AND DESIGN

Before the present contract, preliminary studies had been carried out regarding the feasibility of the HLFC experiments on the Boeing 757 airplane. This work included computation of pressure distributions, boundary layer stability characteristics, and preliminary estimates of suction requirements, as well as the extent of laminar flow achievable on the basic 757 wing. The conclusion of these studies was that the 757 was well suited for the proposed flight experiment.

Preliminary work on the design of the HLFC wing modification had also been started. It focused mainly on delineating trades between airfoil contour changes, suction requirements, and the achievable extent of laminar flow. By the time the contract was awarded, the applicable trades and limitations were fairly well understood, and a sound basis for the final design was established. These studies confirmed Pfenninger's recommendations (ref. 16) that it would be advantageous to start the suction as close to the attachment line as possible and to make the forward suction peak high and narrow, rather than low and wide. The required suction could be reduced by shortening the zone of acceleration (i.e., by steepening the initial pressure gradient) and allowing a slight pressure peak to form following the initial acceleration. This could be achieved by using a blunter leading edge.

3.1 ANALYTICAL METHODS

The principal analytical design tool for the wing contour modifications was a three-dimensional (3D) transonic viscous flow computer code system capable of computing flows around wing/body/nacelle configurations. Major components of this system are an enhanced version of Jameson's FLO28 transonic inviscid flow code (ref. 1) and a 3D boundary layer analysis by McLean (ref. 2). Other components include a grid-generation program that treats the wing, fuselage, nacelles, and struts simultaneously, so that all mutual interference effects are included. Figure 3.1-1 shows the grid on the airplane surface.

The flowfield is discretized by the the grid-generation program, and a finite-volume method is used to solve the full potential equation for the external flow. Artificial viscosities are applied to all three directions in the supersonic region to capture shocks. The surface velocities, together with Reynolds number and temperature, are used to calculate the boundary layer on the wing. Boundary layer transition on the wing is assumed at the first appearance either of an adverse pressure gradient or of laminar separation, and is assumed fixed at 2% chord on the lower surface.

The wing geometry is then updated by the displacement thickness of the boundary layer, and the inviscid flow is computed again. The new surface velocities are then used to compute the wing boundary layer, and the process is repeated until the the solutions stabilize, usually within six to eight cycles.

The gridding of the 757 wing for the 3D boundary layer analysis is shown in figure 3.1-2. Near the expected shock location and the leading and trailing edges, the chordwise paneling was made more dense. In the vicinity of the engine nacelle and the side of the body, denser spanwise spacing was also provided.

Figure 3.1-3 shows a comparison of pressure distributions computed by this system of codes with wind tunnel test data for the original 757 wing. The agreement is generally fairly good, although some tendency for underpredicting the peak pressures can be observed. (The pressures encountered in flight can be expected to differ even more, because the analysis paneling is more faithful to the wind

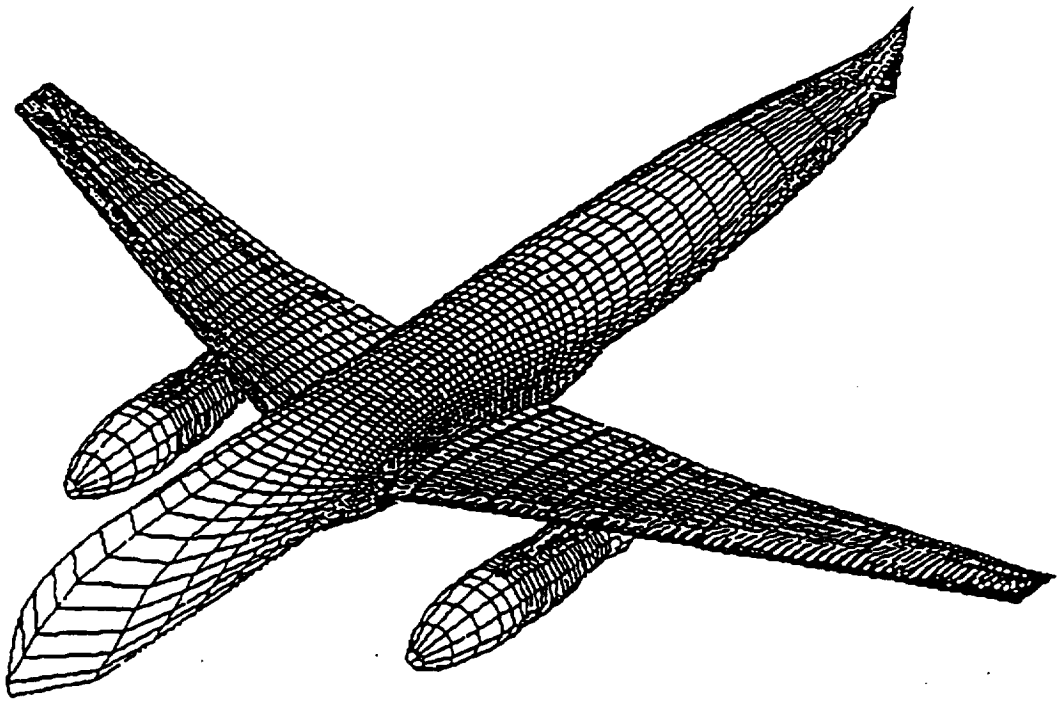

Figure 3.1-1. Numerical Model for Three-Dimensional Transonic Flow Analysis

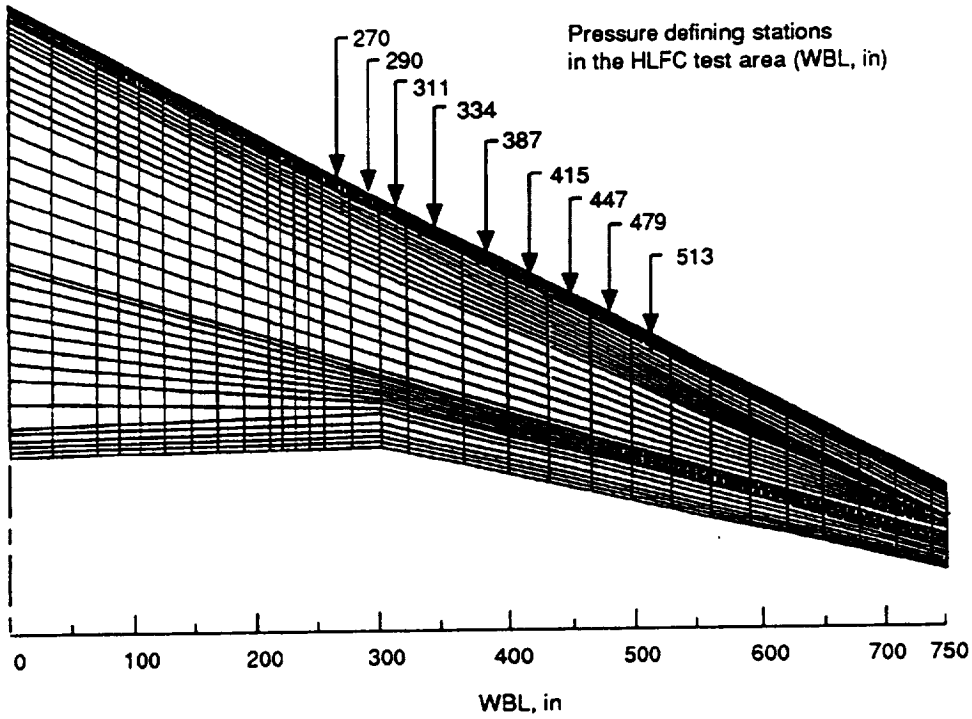

Figure 3.1-2. Gridding of the 757 Wing for Flow Analysis

tunnel model than it can be to the real airplane wing, which not only is more complex in detail, but is subject to varying aeroelastic deformation at different weight conditions. Furthermore, computational fluid dynamics code calibration has mostly been done using plentiful wind tunnel pressure data at relatively low Reynolds number, rather than with flight test surveys at full scale.)

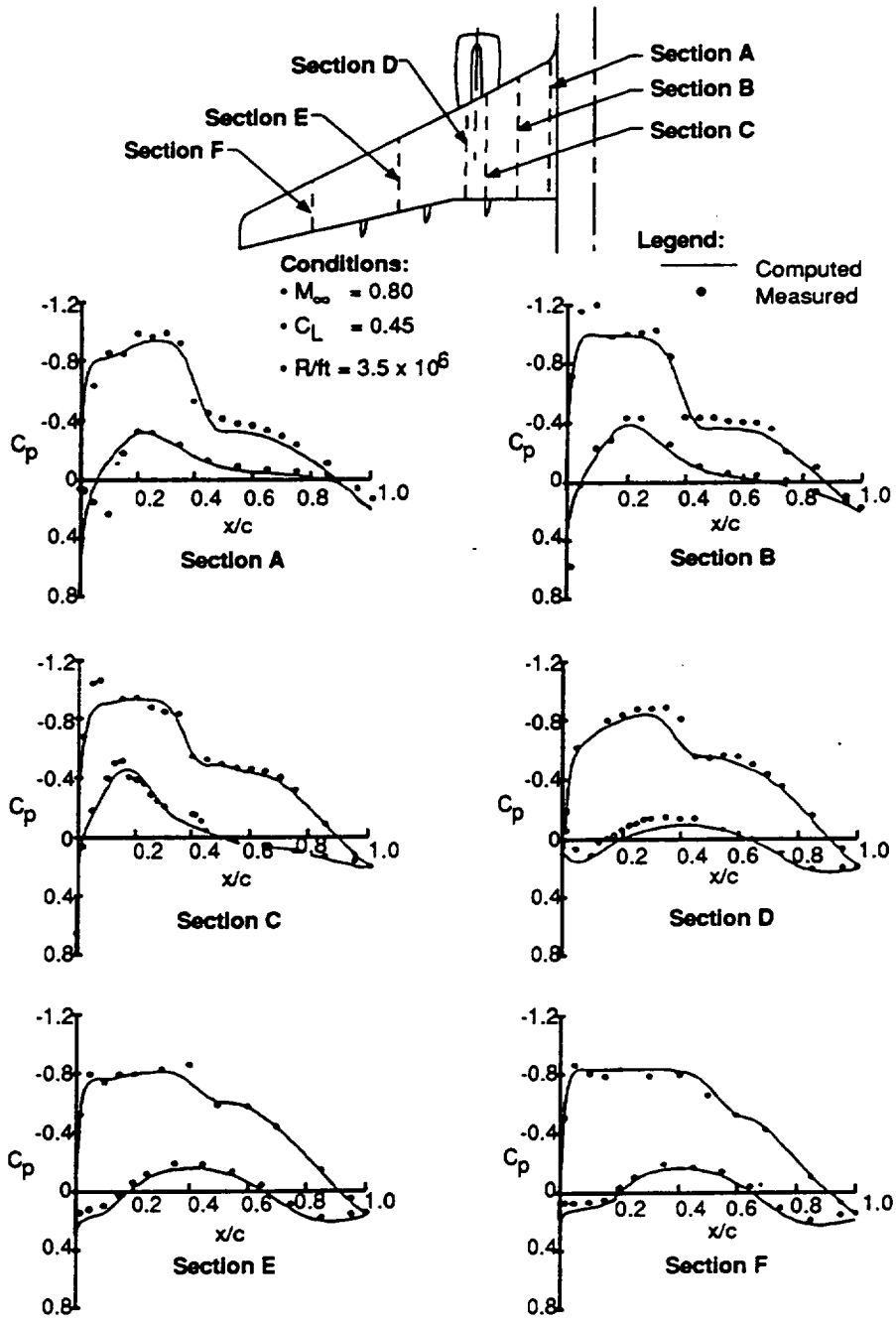

Figure 3.1-3. Correlation of Computed 757 Wing Pressure Distributions With Wind Tunnel Test Data

3.2 ORIGINAL 757 WING SURFACE PRESSURES

Computed pressure distributions for the original 757 wing geometry at three spanwise stations within the prospective HLFC test region are shown in figure 3.2-1. The CP distributions at the center and outboard sections closely resemble the one desired for HLFC (fig. 2.5-2) in that they show a rapid acceleration at the leading edge, followed by a gentle favorable pressure gradient until the recovery point is reached at about 40% to 50% chord. However, in the vicinity of the nacelle, the pressure distribution is less favorable, having an early recovery point preceded by a moderately strong acceleration due to local unsweeping of the isobars. This behavior is attributed to interference due to the engine nacelle, and it caused some difficulty in the design of the HLFC leading edge.

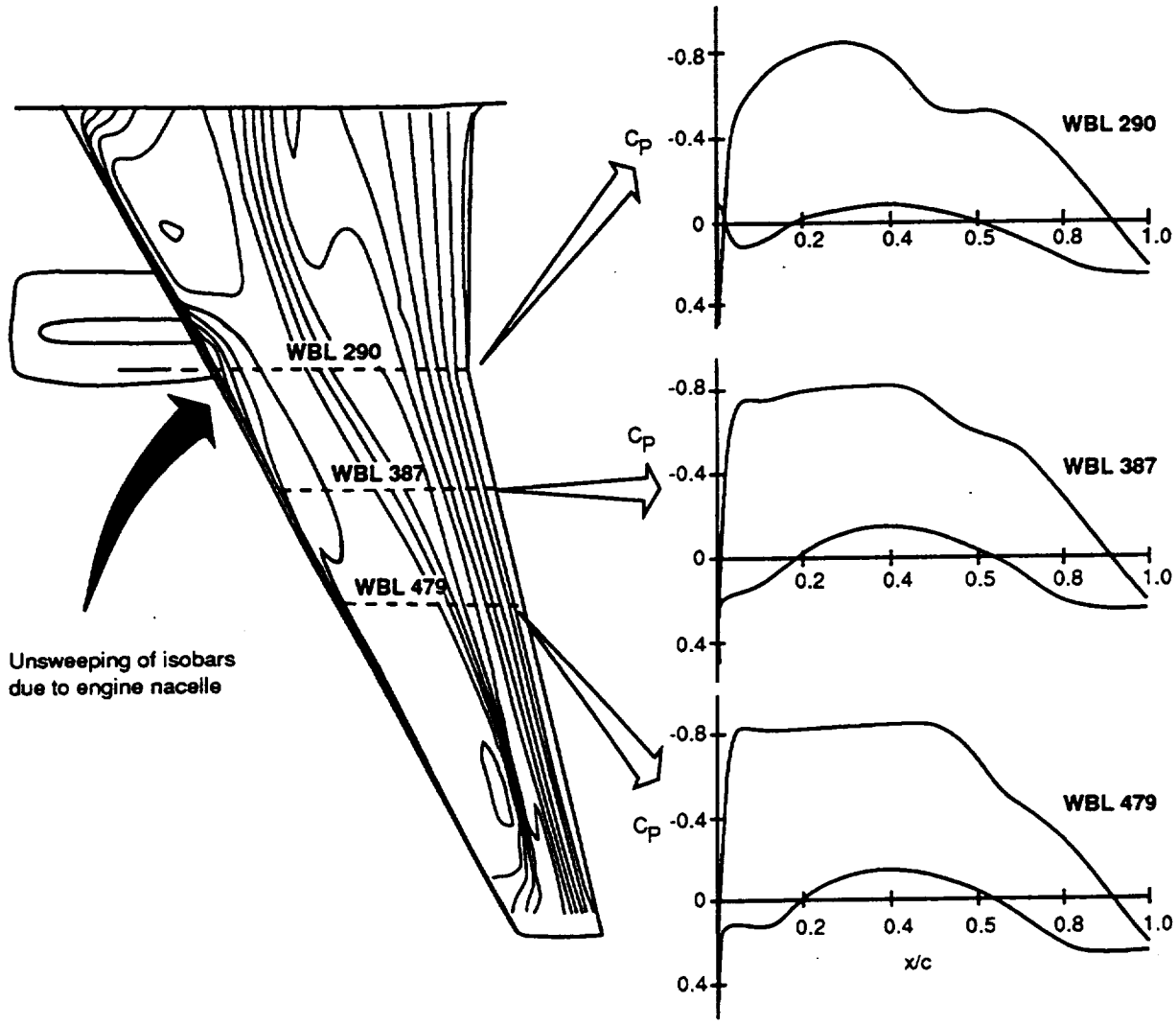

Figure 3.2-1. Theoretical Pressure Distribution on the Basic 757 Wing at Design Condition $M = 0.80$, $C_L = 0.50$

3.3 DESIGN OF THE MODIFIED WING CONTOUR

Figure 3.3-1 illustrates the approach to contour modifications: A more rapid initial acceleration for crossflow attenuation could be obtained by a slight blunting of the leading edge. At the same time, the lower surface of the leading edge could also be revised to improve the characteristics of the Krueger flap, which replaced the slat used on the basic 757 airplane. The lower surface contour ahead of the front spar forms the upper side of the extended Krueger flap. It is very flat where a curved contour would be more desirable. This could readily be achieved by adding a shallow bulge to the lower surface and by adding a folding blunt leading edge (called a "bullnose"). The extent of actual leading edge contour modifications relative to the basic 757 wing contours is shown in figure 3.3-2 for four sections of the HLFC test panel. (Appendix A provides additional cross sections on gridded plots. Data relating to leading edge radii, which affect attachment-line flow characteristics (discussed in sec. 5), are given in appendices B and C.)

At the beginning of the program, it was planned that the suction area would start just outboard of the nacelle, at WBL 270 (36% semispan), and extend through the area occupied by slats Nos. 3 and 4, ending at WBL 495 (66% semispan). Later, the inboard boundary of the suction zone was moved outboard to WBL 330 (42% semispan) to eliminate the need for a second turbocompressor. Because this was done after completion of the aerodynamic analysis, airfoil contours and computation results are shown for inboard sections that were subsequently excluded from the HLFC test span.

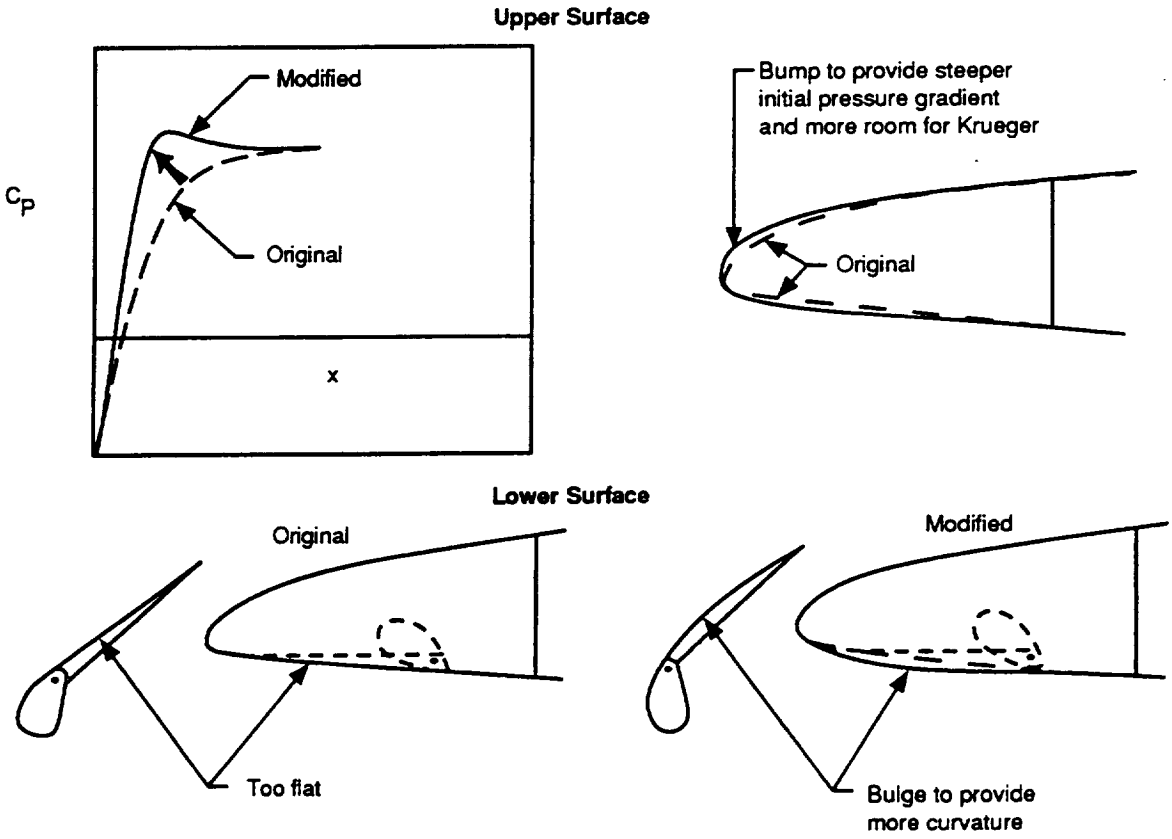

Figure 3.3-1. Philosophy of Wing Contour Modifications

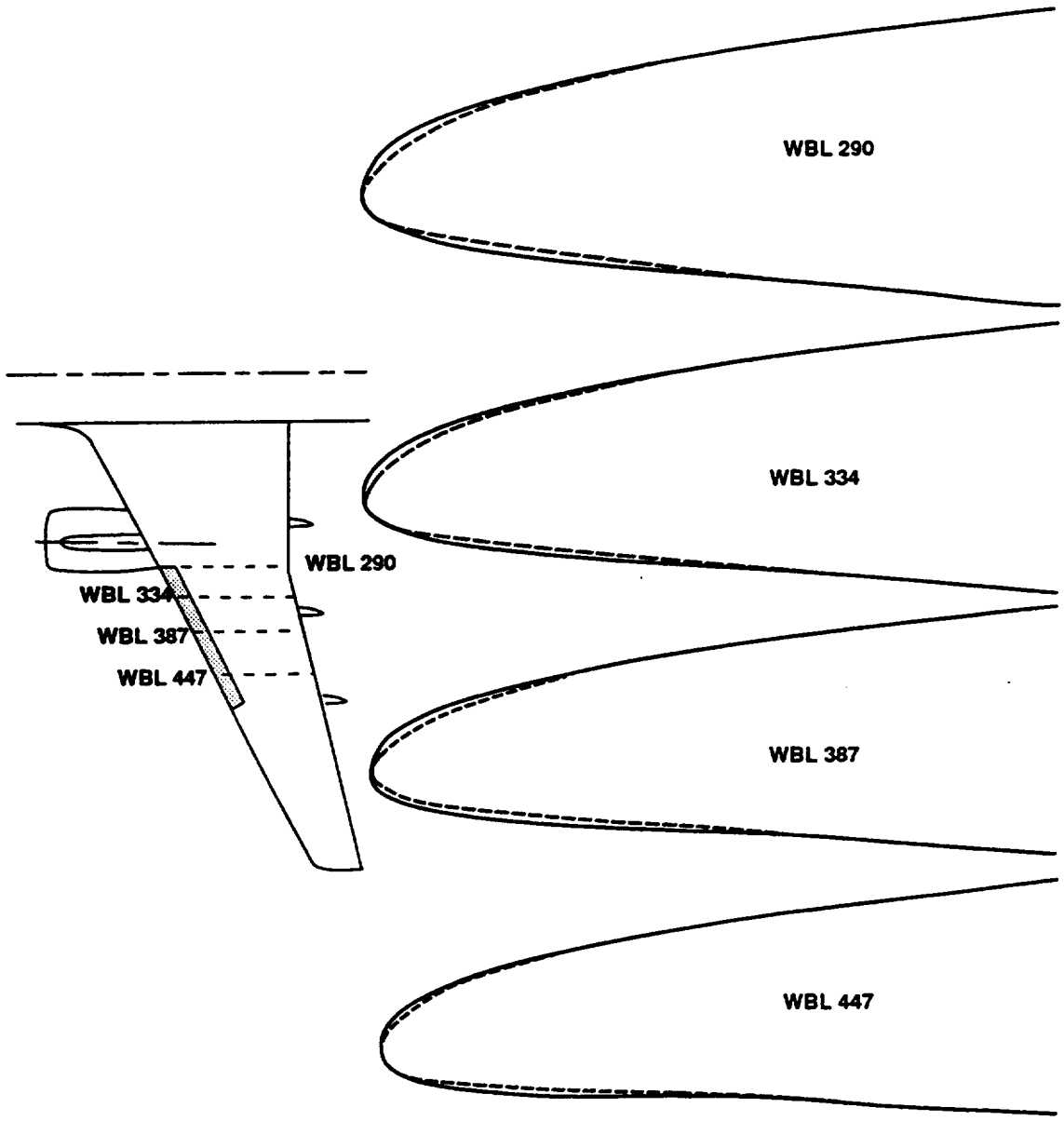

Figure 3.3-2. Extent of Leading Edge Contour Modifications on the HLFC Test Panel

The unsweeping of the isobars in the vicinity of the nacelle had significant impact on the design of the HLFC suction surface. It was not desirable to have large pressure variations along the "flutes" (spanwise channels under the perforated skin that collect the suction flow), so the flutes were laid out along isobars. Curved isobars require curved flutes, adding to fabrication complexity. It was therefore desirable to design an HLFC wing leading edge with parallel isobars. However, the distortion of the pressure pattern resulting from to the high-bypass-ratio turbofan engine's large nacelle limited compliance with this objective.

After the modified contours were tentatively defined, an attempt was made to eliminate the unsweeping of the isobars near the nacelle by further increasing the bluntness of the leading edge to increase the initial acceleration. This exercise, however, did not significantly improve the isobar

pattern, even with a very large bump on the leading edge near the nacelle. Figure 3.3-3 shows the airfoil shapes and pressure distributions for the basic 757 wing, the baseline HLFC modification, and the blunt leading edge alternative. The nacelle effects evidently overpowered the airfoil shape effects, because the pressure distributions did not change much, even though the airfoil was considerably more blunt. Furthermore, past experience has shown that under off-design conditions, that is, at lower Mach numbers, the blunt airfoils tend to develop a strong pressure peak near the leading edge that could have some adverse effects, such as premature shock and increased drag. Therefore, the blunter leading edge design was not accepted for the final HLFC configuration.

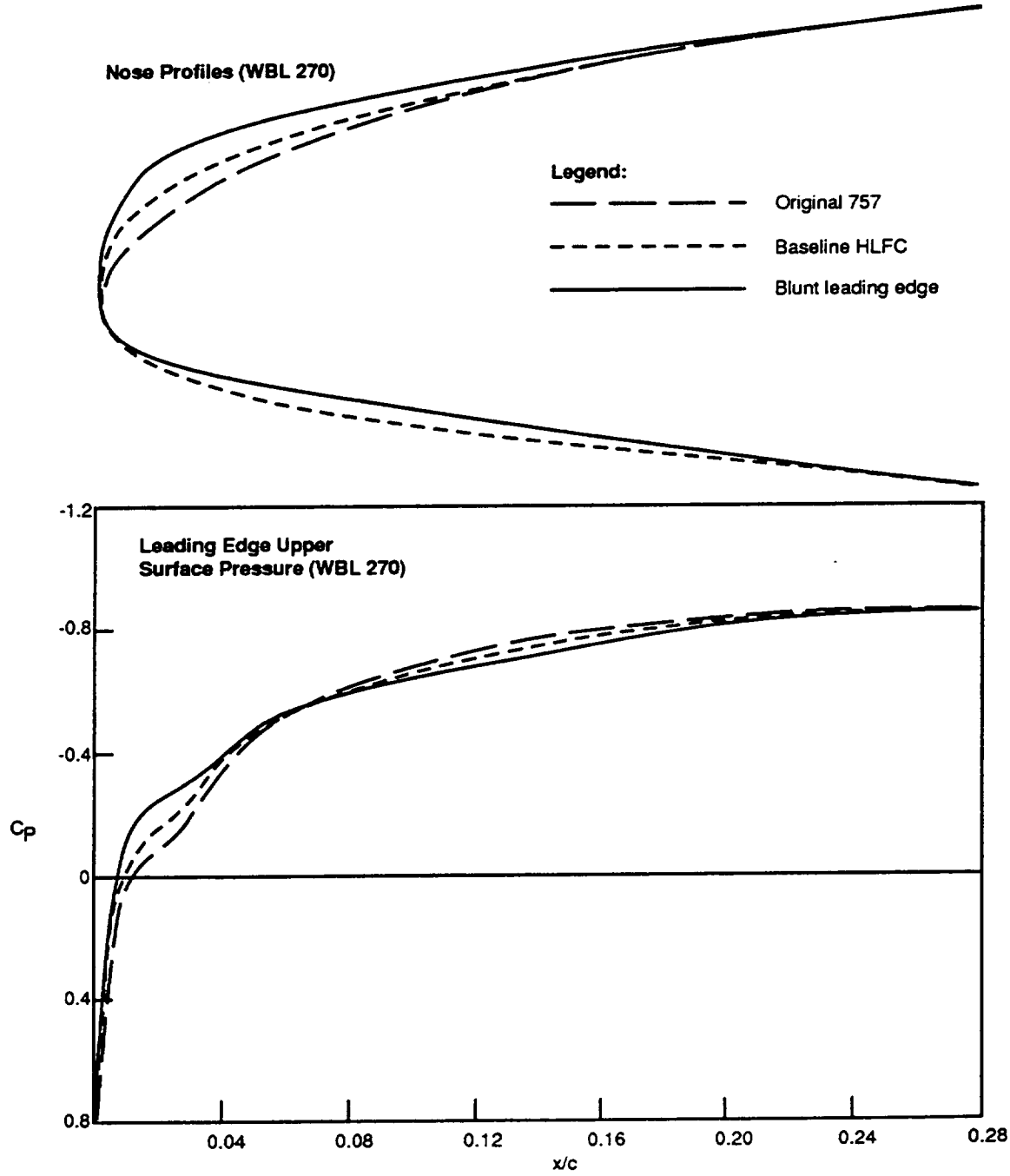

Figure 3.3-3. Effect of Leading Edge Blunting Near the Nacelle

The design process was completed by smoothing the wing contour lines in both spanwise and chordwise directions. This was necessary because airfoil sections were defined at given stations, while coordinates of intermediate sections were derived by interpolation. This resulted in a slightly bumpy initial shape that did not have continuous curvature in the chordwise direction (which is desirable aerodynamically), and that was not wave-free in the spanwise direction (which is desirable for fabrication as well as for aerodynamic reasons). Figures 3.3-4 and 3.3-5 show the results of the smoothing process.

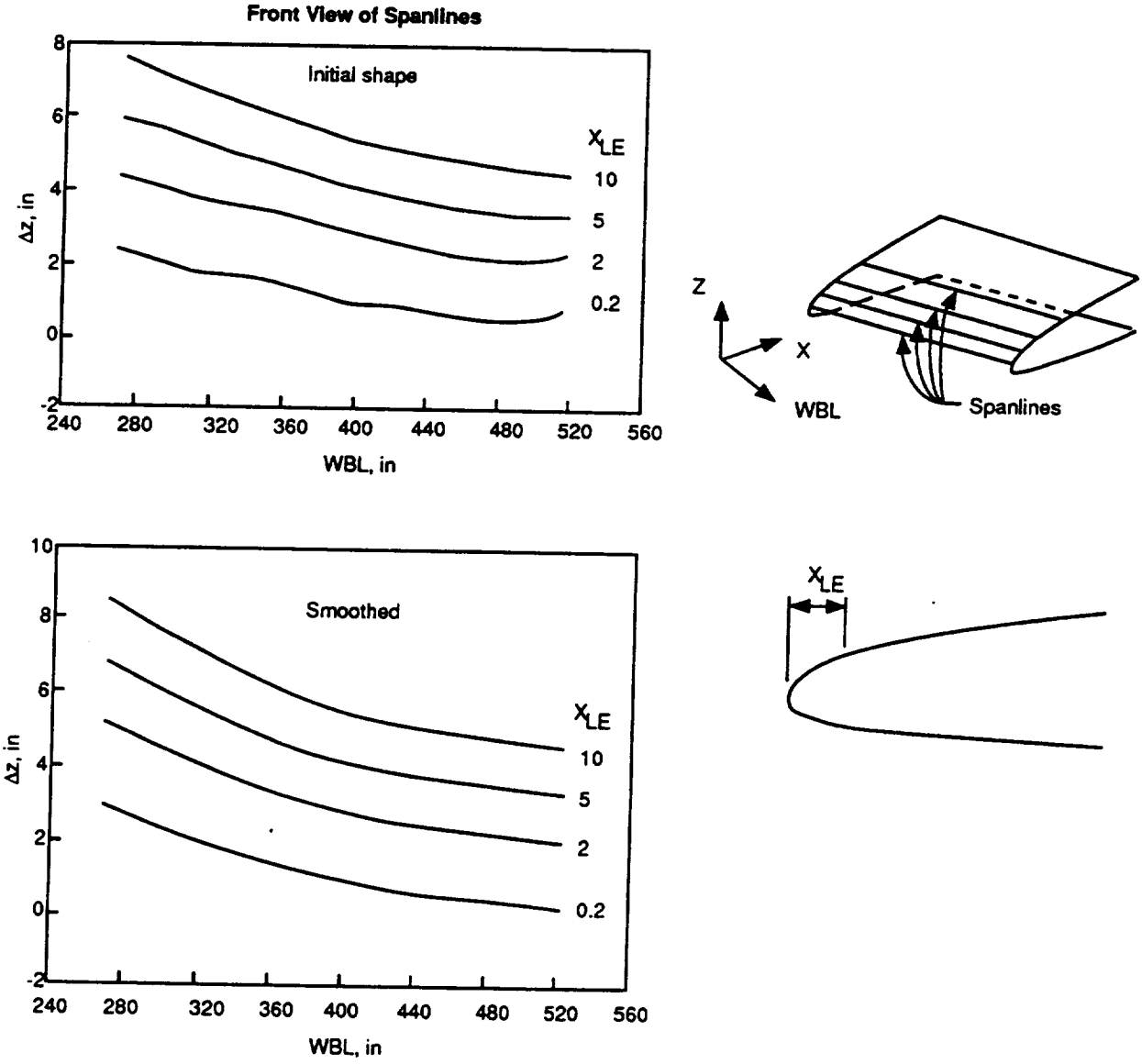

Figure 3.3-4. Wing Geometry Smoothing—Spanwise

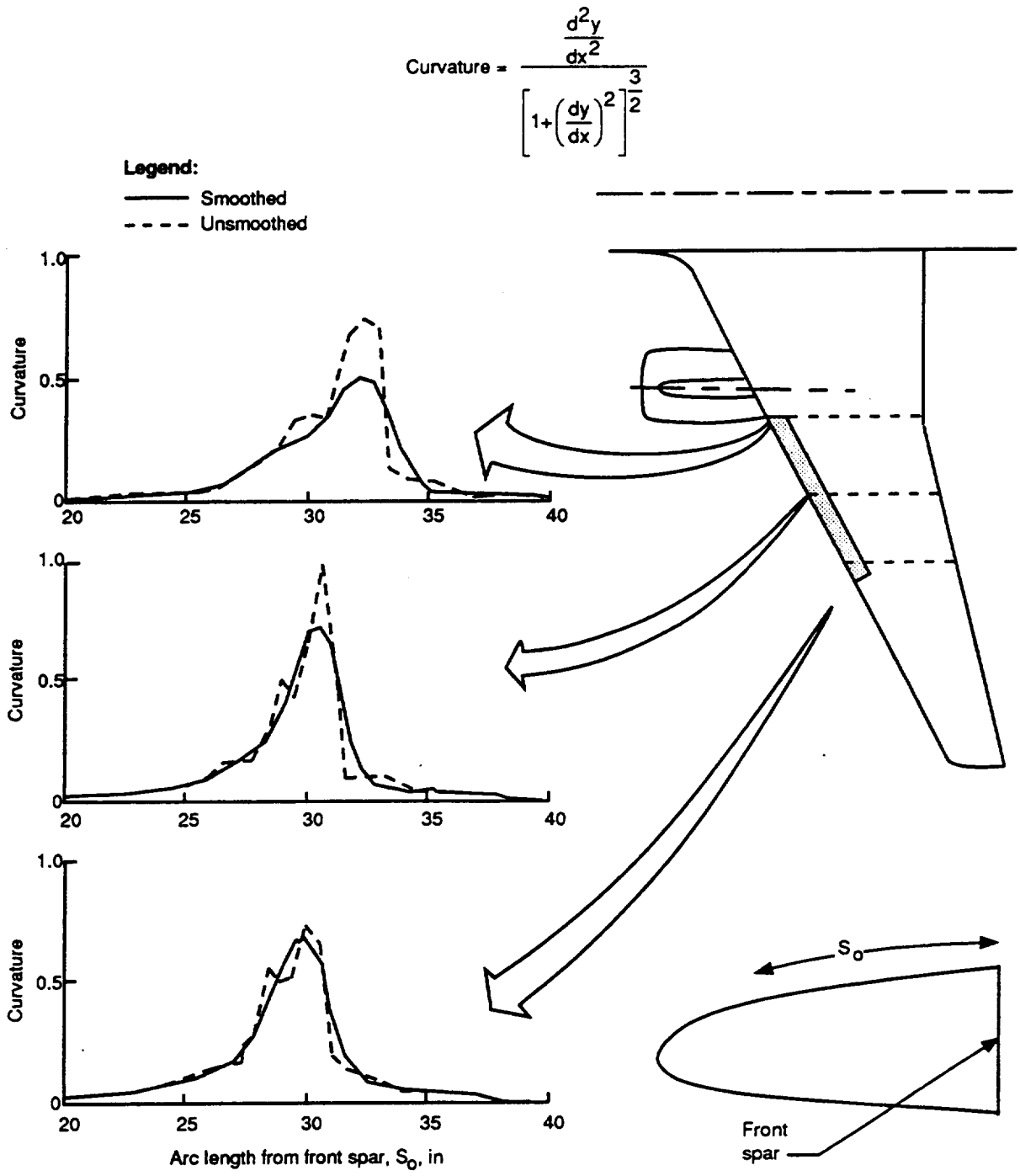

Figure 3.3-5. Wing Geometry Smoothing—Chordwise

3.4 CALCULATED PRESSURE DISTRIBUTIONS ON THE MODIFIED WING

3.4.1 Design Conditions

Theoretical pressure distributions for the modified HLFC test panel at M = 0.80 and C_L = 0.50 are shown in figure 3.4-1. (Gridded plots, for all stations analyzed, are presented in app. D.) Comparison with figure 3.2-1 shows that the contour changes succeeded in steepening the initial pressure gradient at midpanel and outboard, but the pressure recovery point was not affected much because the modification was entirely ahead of the front spar. The unsweeping of isobars near the nacelle causes large spanwise pressure variations along constant chord lines near the leading edge, as illustrated in figure 3.4-2. If the internal flutes had been located along these lines, the external pressure variation could have resulted in excessive suction inboard and inadequate suction, or even outflow, outboard. (Outflow could have been expected to cause immediate boundary layer transition, and so was not permissible.) It was therefore necessary to choose between placing separator dams in the flutes or laying out the flutes along isobars. While dams in the flutes appeared to be a simple solution, they could have caused abrupt spanwise steps in suction level, which would have had unpredictable effects on transition. Therefore, it was decided to take the conservative approach of building curved flutes that ran along isobars. The theoretical isobar pattern within the front 0.5 in of the suction surface is shown at left in figure 3.4-3. The flute layout in this region followed the same pattern. (Larger scale isobar plots are provided in app. E.)

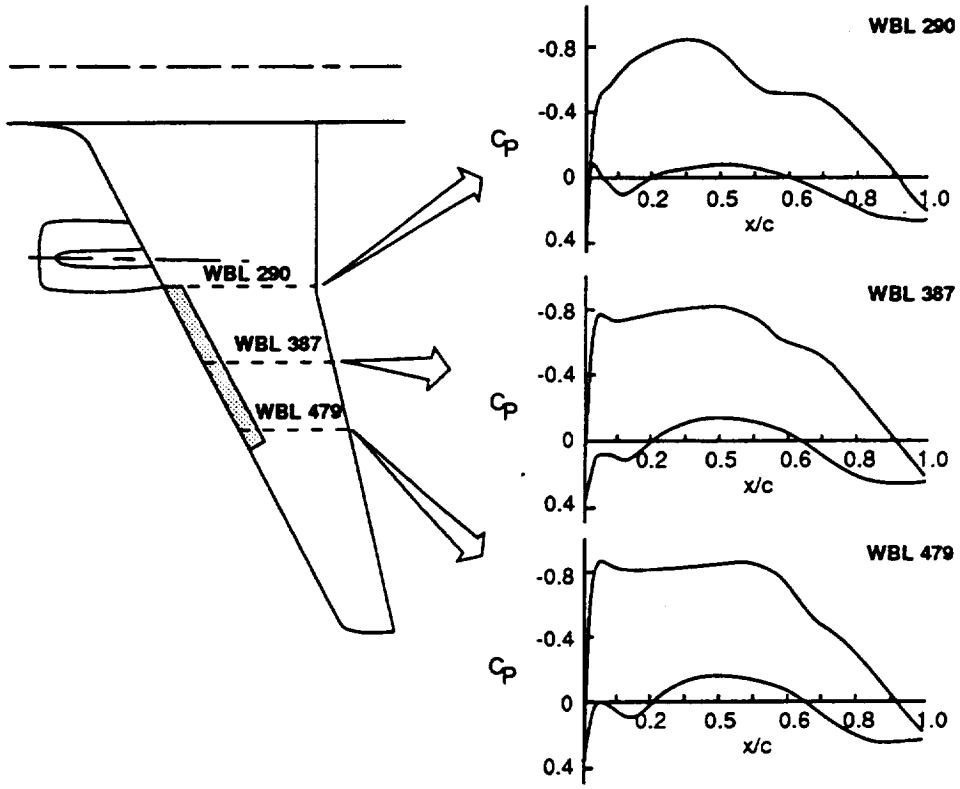

Figure 3.4-1. Theoretical Pressure Distributions for the Modified 757 HLFC Wing; M = 0.80, C_L = 0.50, and R/ft = 1.61 million (h = 39,000 ft)

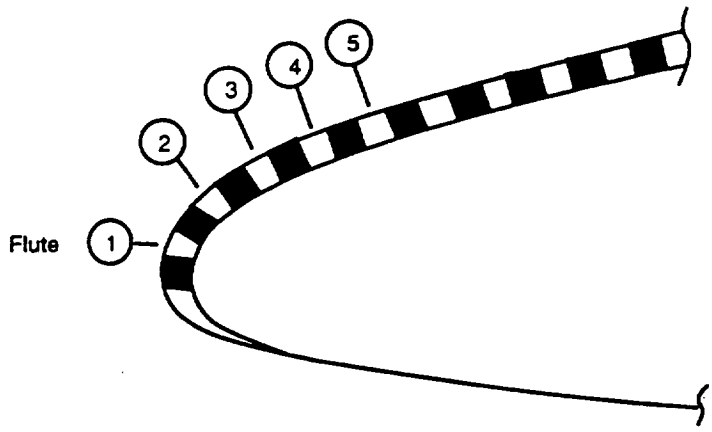

Dams would be required in the flutes to prevent large differences in suction rates or outflow at the low-pressure end.

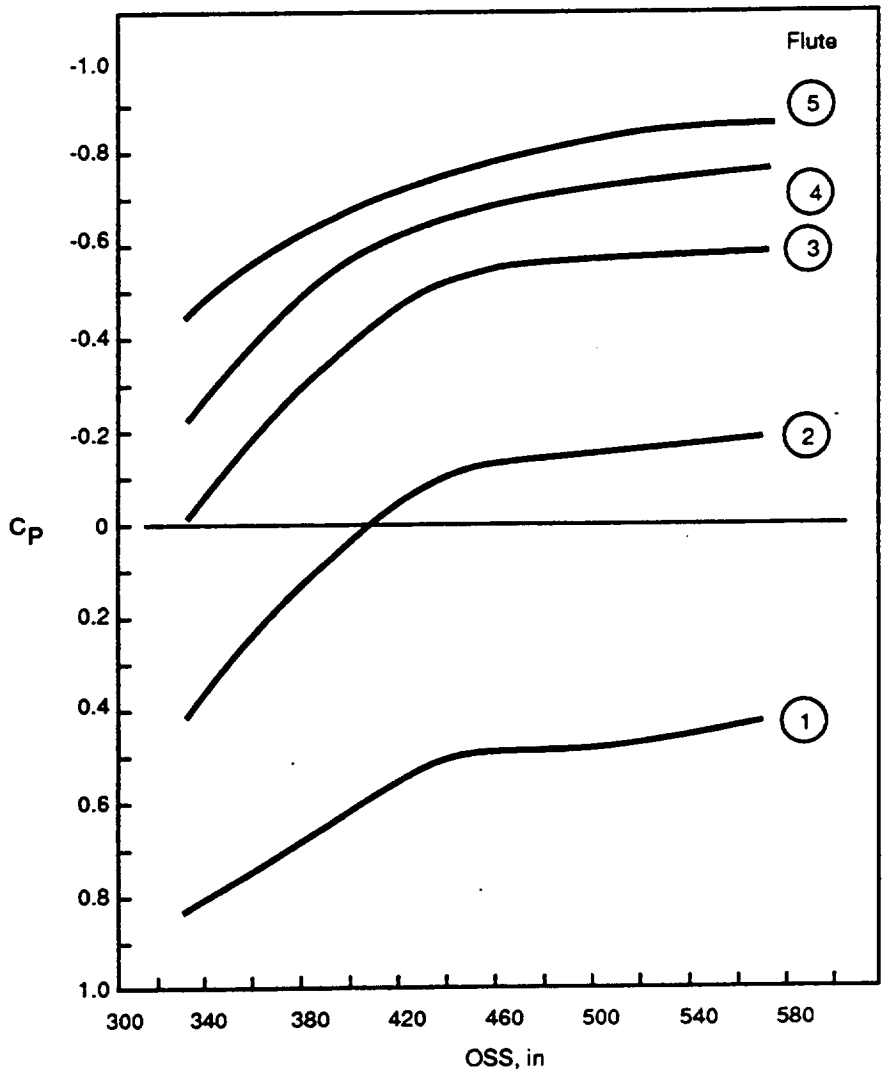

Figure 3.4-2. External Pressure Variations Along Constant Chord Lines

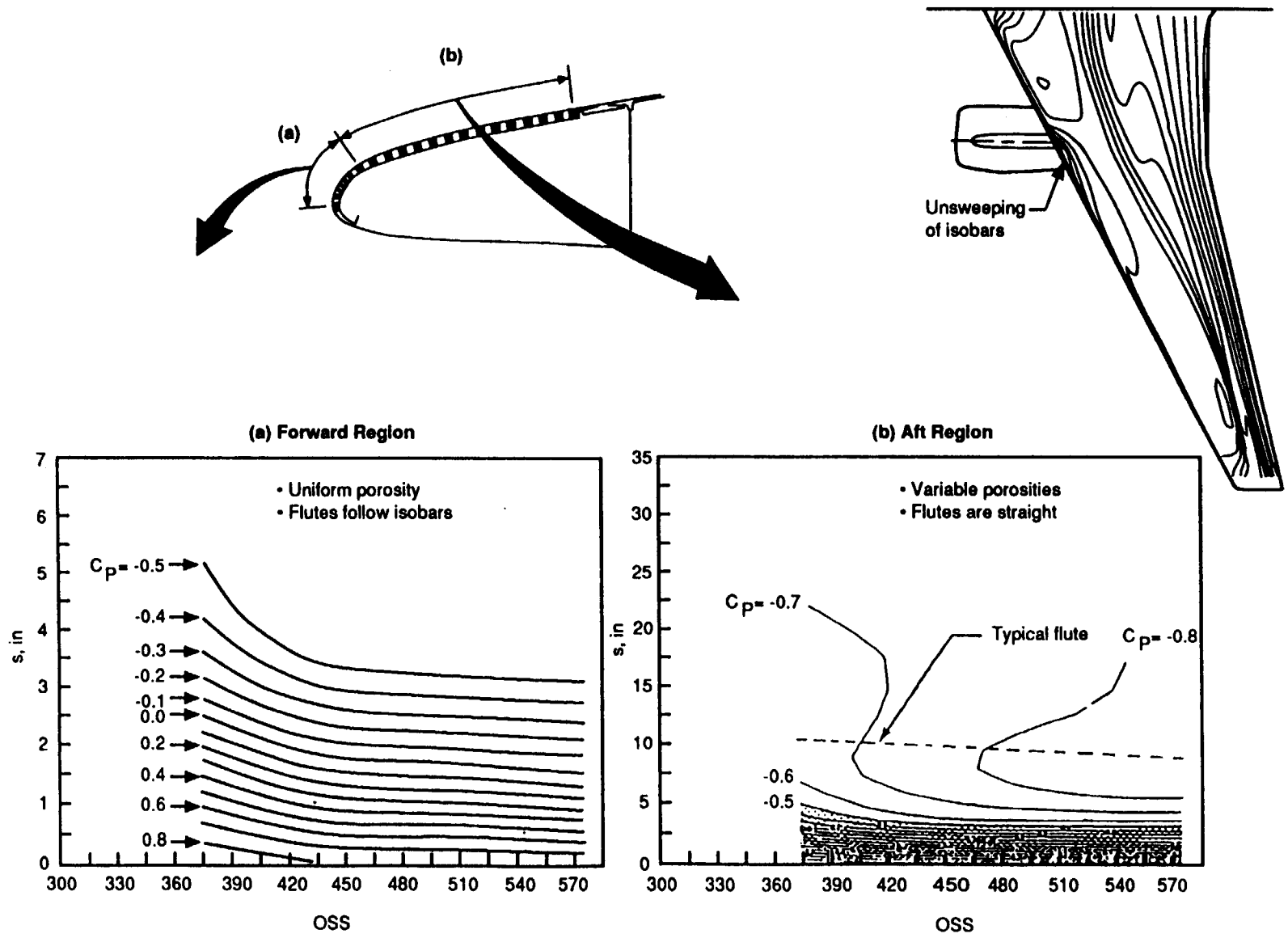

Figure 3.4-3. Isobar Patterns Along the Suction Surface

Farther aft, the isobars curved back sharply, as illustrated at the upper right of figure 3.4-3. There, it was not feasible to lay out the flutes along the isobars. At the design condition, the desired distribution of suction quantity could have been obtained by varying the skin porosity over flutes laid out along approximately straight lines. There is a penalty, however, for departing from the isobars. Because outflow can be expected to cause immediate transition, the entire flute must always be sucked hard enough to prevent outflow over its entire length. At off-design conditions, a mismatch in external and internal pressures will inevitably be present, requiring local oversuction and a consequent increase in compressor load.

3.4.2 Off-Design Conditions

After the airfoil contours were finalized, the flow analysis was extended to a number of off-design flight conditions where operation of the HLFC system was planned. These conditions included variations in Mach number and lift coefficient at cruise, as well as climb, descent, and holding at various speeds and altitudes. Figure 3.4-4 illustrates the range of off-design conditions analyzed.

An overview of the effects of Mach number and lift coefficient on the chordwise pressure distributions at the test panel midspan (WBL 387) is presented in figure 3.4-5. It is evident that at low Mach numbers ($M < 0.78$) an acute pressure peak develops near the leading edge and the subsequent adverse pressure gradient will not allow much laminar flow. On the other hand, at Mach numbers and lift coefficients higher than the design values ($M > 0.80$ and $C_L > 0.50$), the pressure recovery point shifts rearward and the extended region of mildly favorable pressure gradient may allow more laminar flow. In fact, the most extensive laminar flow could be expected not at the design point of $M = 0.80$ and $C_L = 0.50$, but at somewhat higher Mach numbers and lift coefficients.

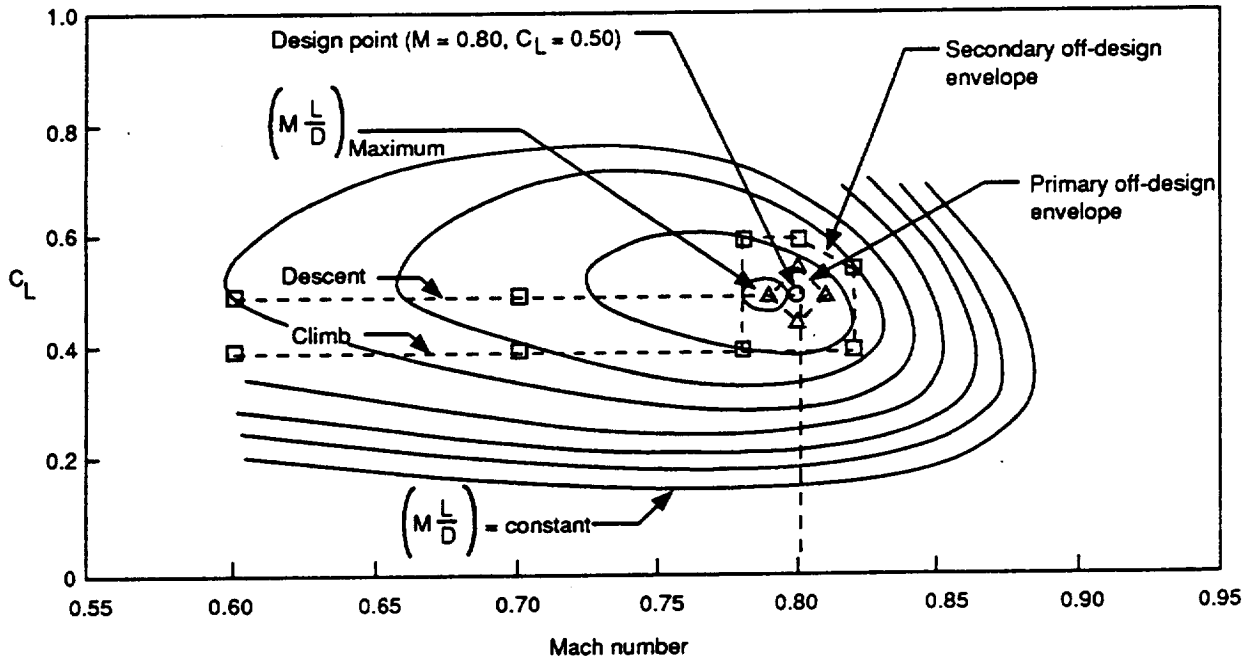

Figure 3.4-4. Off-Design Analysis Plan

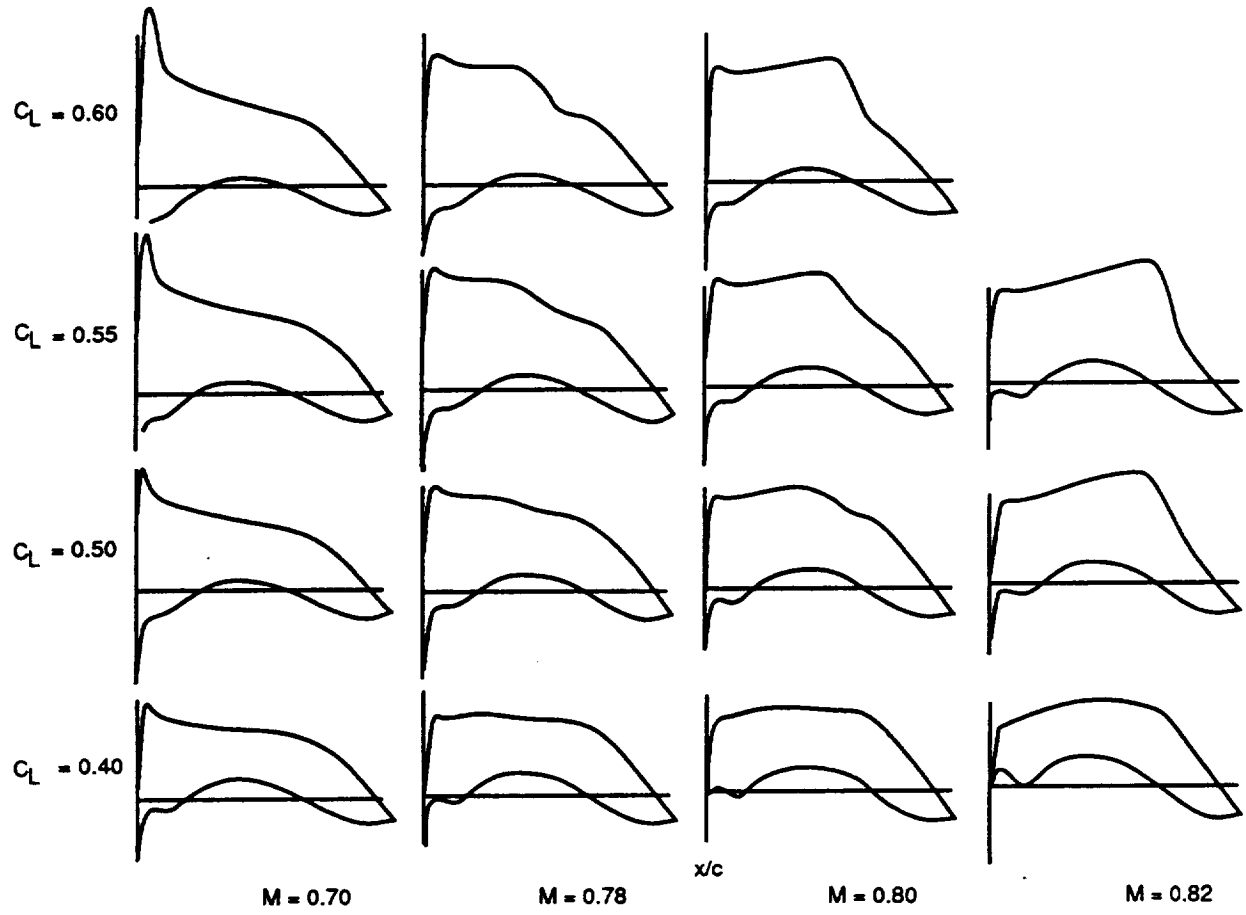

Figure 3.4-5. Theoretical Wing Pressure Distributions

More detailed comparisons for the effects of Mach number and lift coefficient within the primary and secondary test envelopes are presented in figures 3.4-6 and 3.4-7. These comparisons give further support to the observation that the most favorable conditions for extended laminar flow would be found at somewhat higher Mach numbers and lift coefficients than the design condition.

Figure 3.4-8 shows pressure distributions for climb and descent conditions at M = 0.60 and M = 0.70, respectively. Normal climb above 10,000 ft takes place at a calibrated airspeed of 290 kn, corresponding to a lift coefficient of approximately C_L = 0.40, with gradually increasing Mach number as the airplane gains altitude. Optimum calibrated airspeed for descent is 250 kn (approximately C_L = 0.50) with gradually decreasing Mach number from M = 0.80 to M = 0.38 as the airplane loses altitude. In both climb and descent, a pronounced pressure peak is present near the leading edge, which is expected to preclude the achievement of extensive laminar flow.

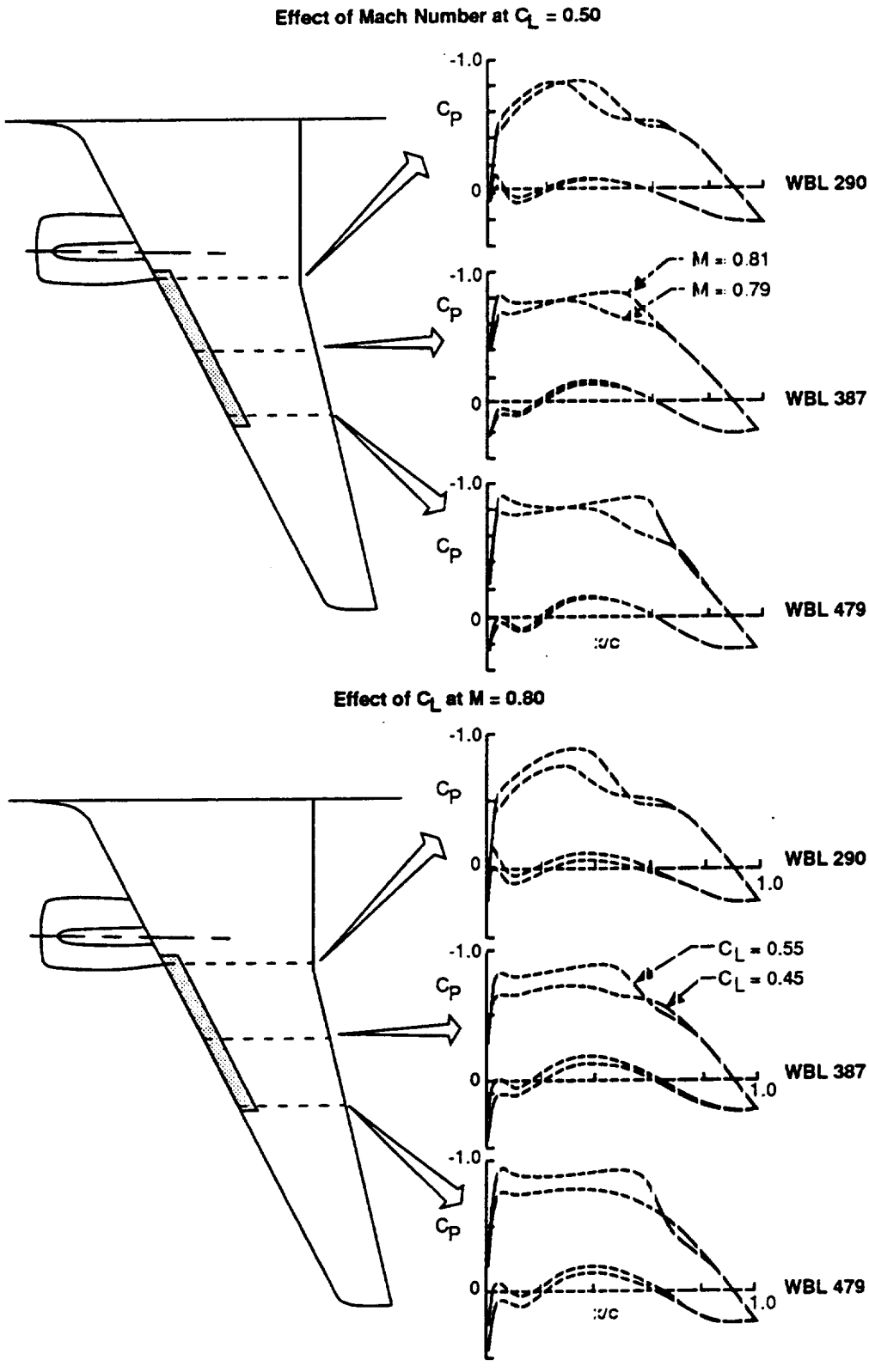

Figure 3.4-6. Theoretical Pressure Distributions for Off-Design Conditions

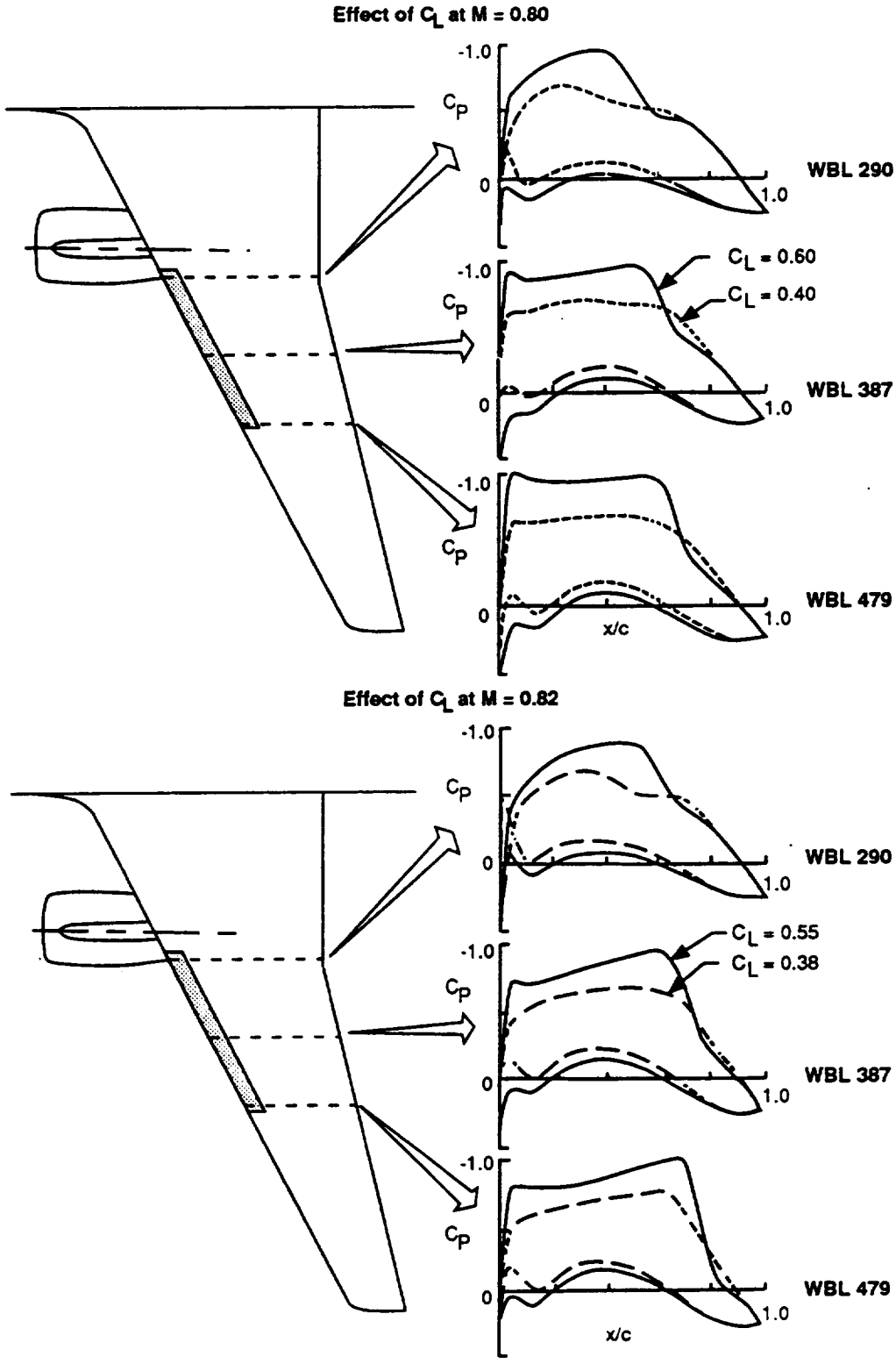

Figure 3.4-7. Theoretical Pressure Distributions for Off-Design Conditions (Continued)

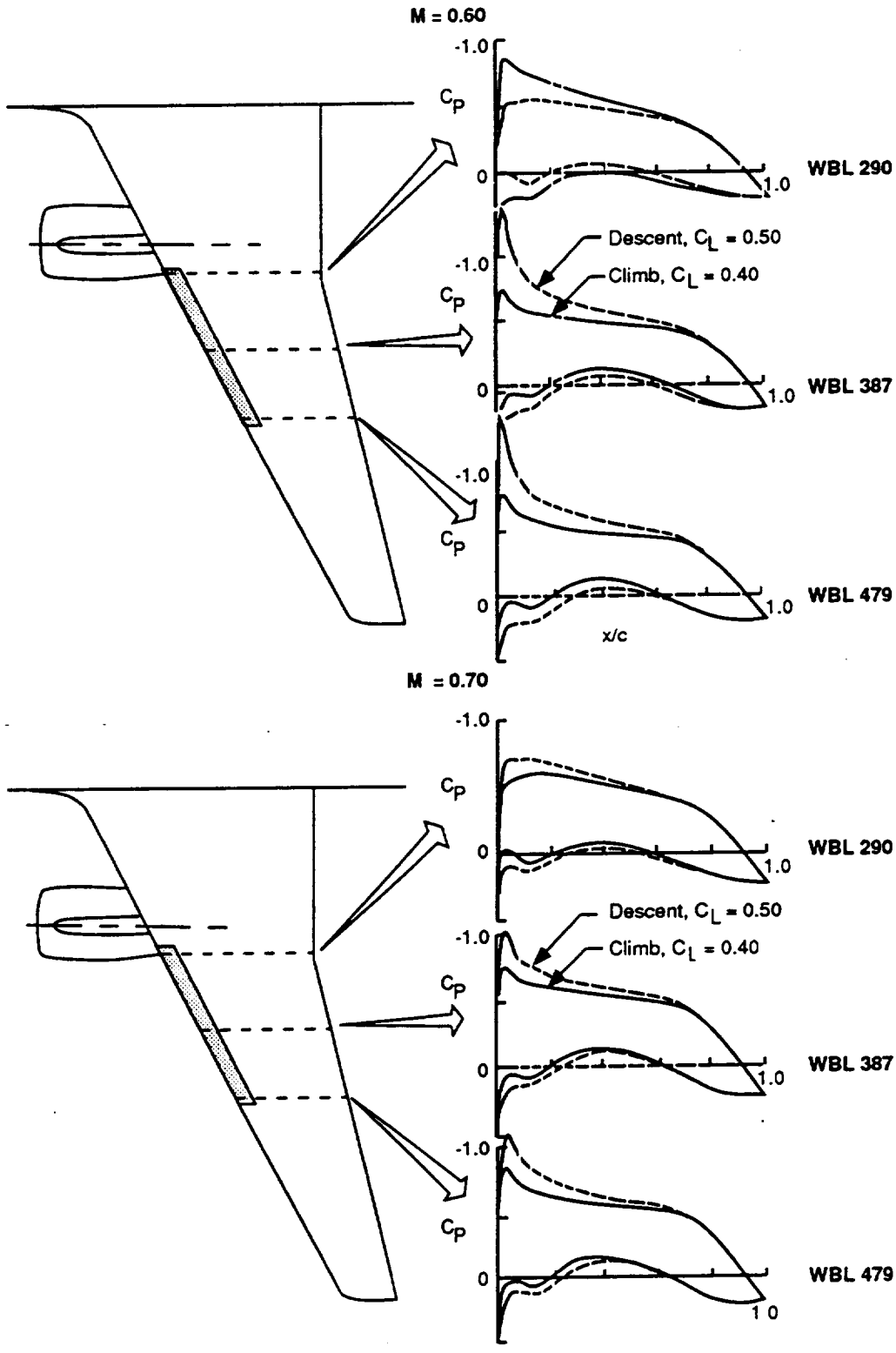

Figure 3.4-8. Theoretical Pressure Distributions for Climb and Descent

This page intentionally left blank.

4.0 BOUNDARY LAYER STABILITY ANALYSIS AND DETERMINATION OF SUCTION REQUIREMENTS

Once a geometry for the test panel had been determined on the basis of the HLFC guidelines and the corresponding pressure distributions were known, the next aerodynamic design task was to define an economical suction distribution that would provide the maximum practical extent of laminar flow.

4.1 STABILITY PREDICTION METHODOLOGY

The principal analytical tool for this work was the Unified Stability System (USS) computer code, developed by Boeing under NASA contract (ref. 3). This code uses Mack's method (ref. 4) to generate the disturbance amplification characteristics of the two major boundary layer instability modes in three-dimensional compressible flow, for given distributions of external pressure and suction flow.

The code is a combination of several subprograms: First, boundary layer velocity profiles (both tangential and crossflow (CF), including the effects of suction) are calculated using the method of reference 2. This is followed by analyses of both Tollmien-Schlichting (TS) and CF instabilities to determine amplification rates. The mathematical basis and solution procedure in both are very similar, but the TS procedure treats waves that propagate more or less in the direction of the local external flow, while the CF procedure analyzes waves that propagate across it.* The amplification rates are integrated separately to obtain amplification ratios. The natural logarithms of the amplification ratios (referred to as "N-factors") are more convenient to plot and discuss than the ratios themselves. Figure 4.1-1 shows the computation sequence and indicates the appearance of the data.

The method of transition prediction is illustrated in figure 4.1-2. The TS amplification exponent, N_{TS}, is plotted against the CF amplification exponent, N_{CF}, with the distance along the surface, s/c, as a parameter. Transition is predicted when this curve crosses the transition criterion line, an empirically derived boundary. When CF effects are dominant, the trajectory of N-factors leans to the right, but when the amplification is mainly due to TS instability, it runs more or less parallel to the N_{TS} axis. Where N_{CF} remains very small, the analysis may carry into the pressure recovery region, and computation of N_{TS} may be subject to considerable uncertainty. In those cases, judgment must be applied to estimate a transition point. (The stability calculations for WBL 447, discussed below in sec. 4.2, are an example.)

Figure 4.1-3 shows the transition criterion used in the present design study. It was based on correlation of N-factor computations by the USS code with experimental transition data for the NASA F-111 NLF glove (ref. 5) and the Boeing 757 NLF glove (ref. 6).† A point from Boeing experiments on a T-33 with an NLF glove (ref. 15) is also shown. Boundaries of the data scatter band are shown by the dotted lines.

---

* The wave angle, defined as the angle between a normal to the wave front and the flow direction, will be near 0 deg for TS waves in incompressible flow, or 0 to 70 deg in compressible flow. Wave angles for CF disturbances are from 70 to 90 deg.

† Correlation of N-factor computations by the USS code with experimental transition data shows considerable scatter. Use of such a criterion is an empirical expedient in the absence of a more rigorous method. One of the objectives of the present program is to provide additional experimental data to support development of improved transition prediction methods.

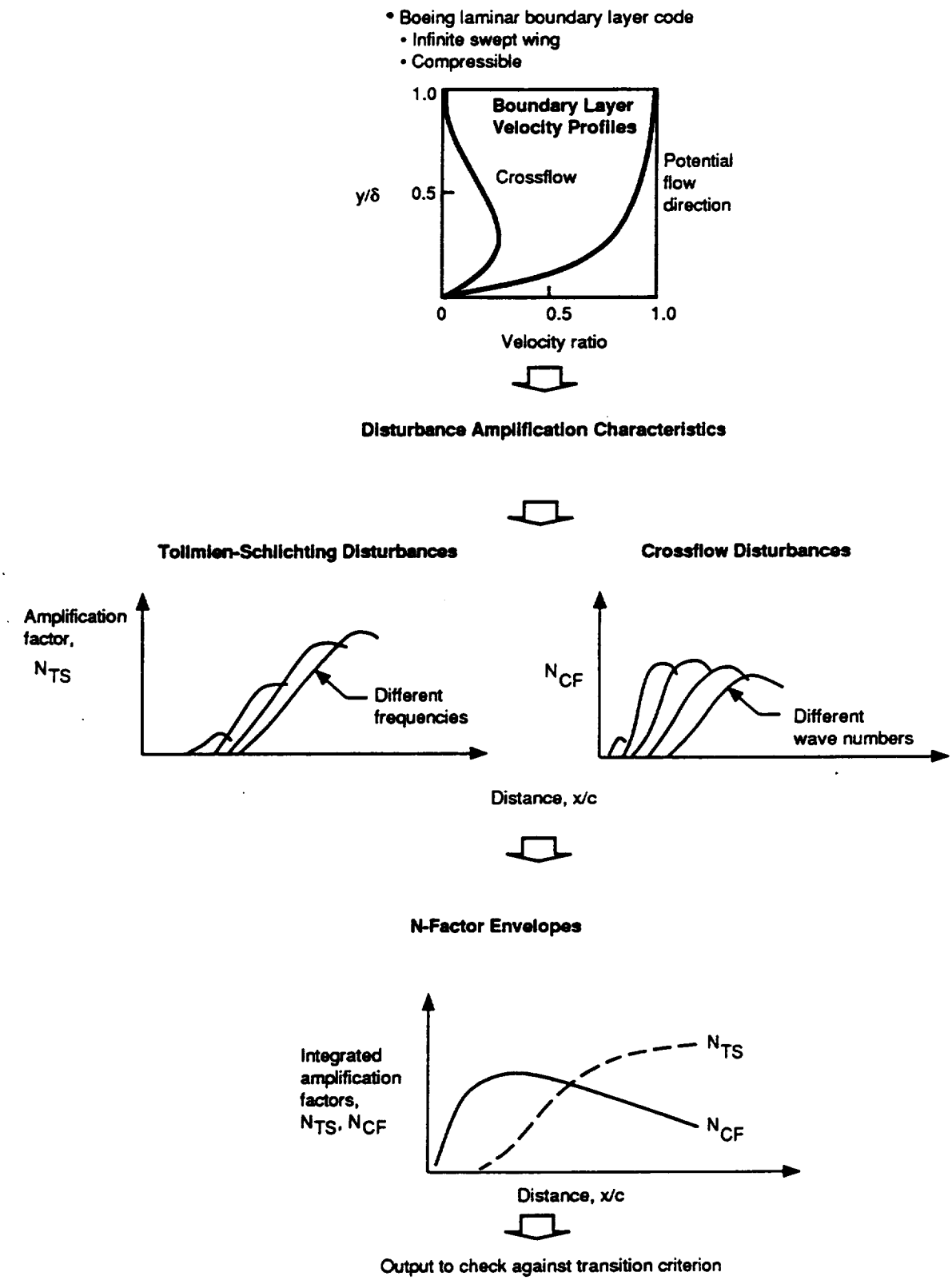

Figure 4.1-1. Main Steps of the Computation Sequence in the USS Code

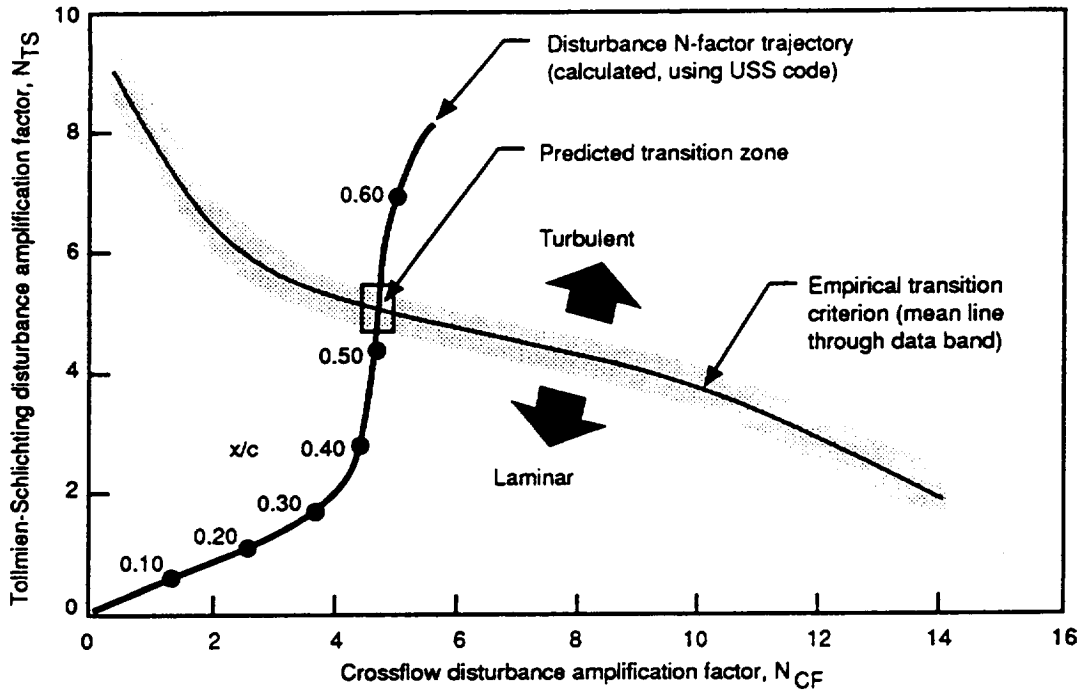

Figure 4.1-2. Scheme of Transition Prediction Method

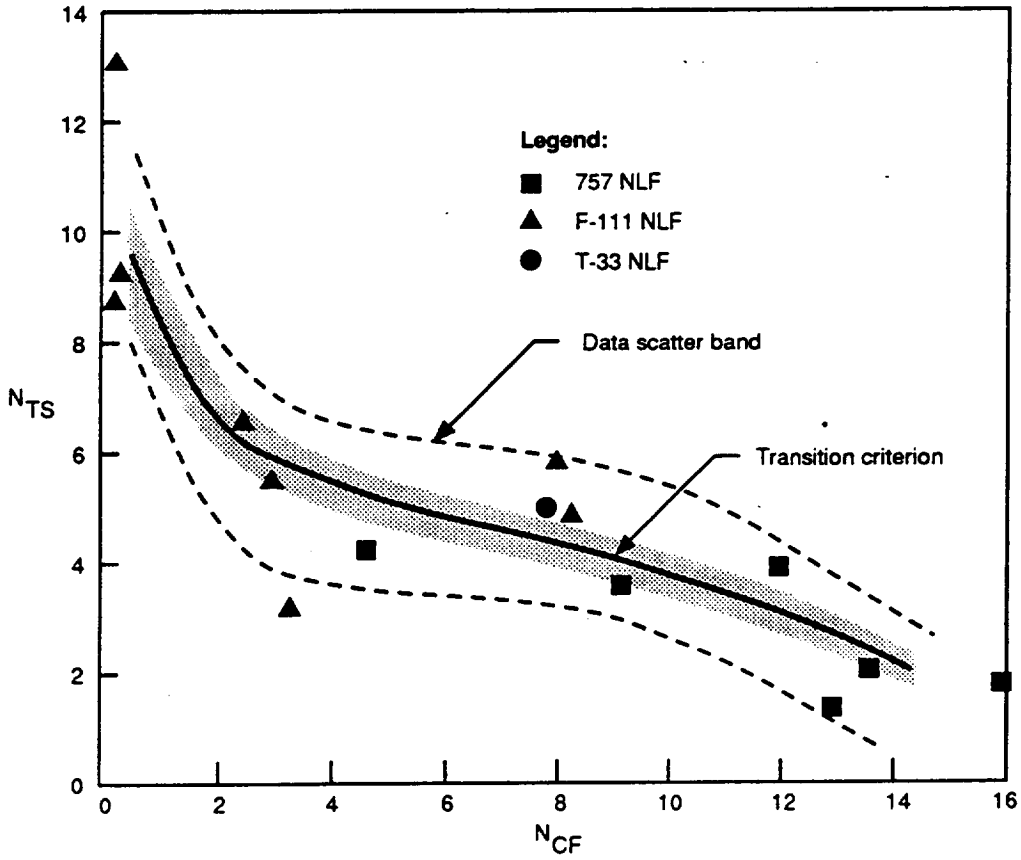

Figure 4.1-3. Empirical Trend of Crossflow and Tollmien-Schlichting Amplification Factors at Transition

4.2 SUCTION REQUIREMENTS AT INDIVIDUAL SPAN STATIONS

Moderately swept transport airplane wings usually have sufficient CF to cause early transition. Controlling CF instability is therefore of paramount importance. CF instability can, to some extent, be mitigated by geometric means (that is, airfoil tailoring) but boundary-layer suction is the most direct means of preventing crossflow-induced transition. The influence of suction on the N-factor trajectory is illustrated in figure 4.2-1. Without suction, the uncontrolled CF instability pushes the amplification trajectory to the right, where it intersects the transition criterion line at a low value of s/c. For the case shown, transition would be expected to take place at about 14% chord. With adequate suction, the trajectory moves closer to the NTS axis (i.e., showing low CF amplification), and N_{TS} is somewhat reduced as well. The intersection with the transition boundary now takes place at about 50% chord. Generally, the practice was to apply sufficient suction to bring the trajectory close to the N_{TS} axis, and if possible, to keep it clear of the transition data scatter band.

In the discussions below, three different nondimensional suction quantity parameters are used. They are—

C_Q = total suction coefficient = (total suction mass flow)/$\rho_\infty V_\infty S_{sp}$,

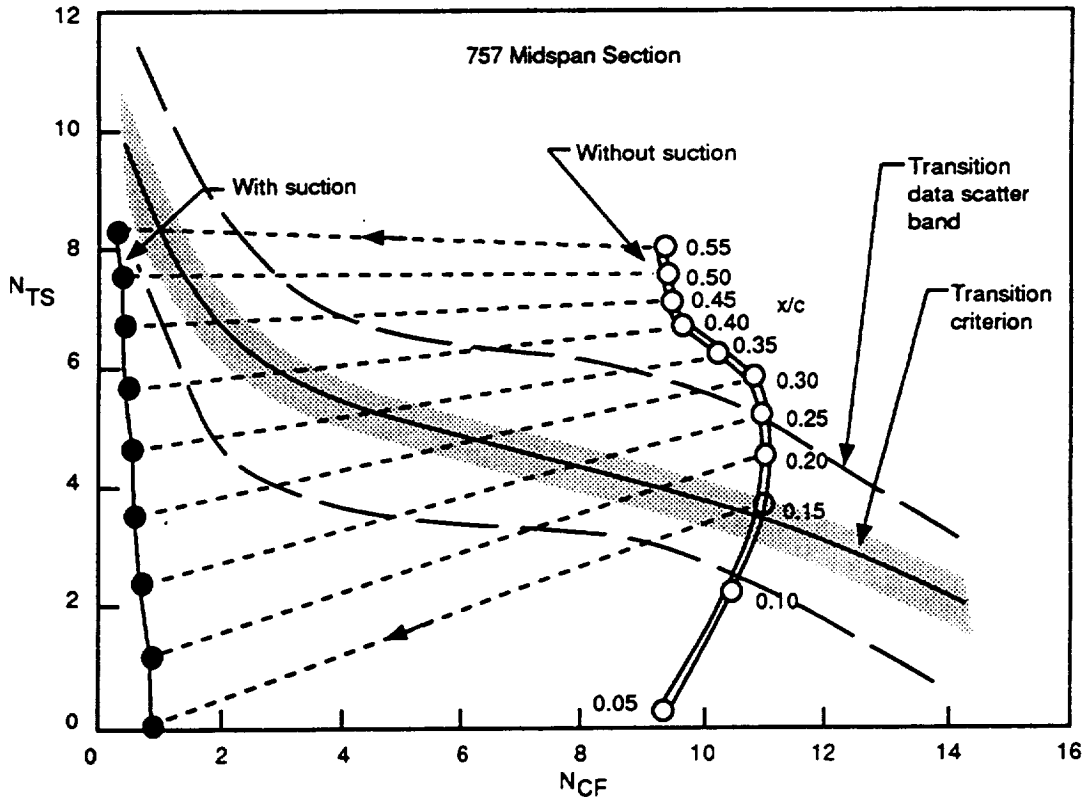

Figure 4.2-1. Effect of Suction on Amplification Characteristics

where S_{sp} is the area of the HLFC suction panel. (The "HLFC suction panel" includes all the wing chord, to the trailing edge, over the span where suction is applied. In the present case, S_{sp} = 190.78 ft^2

c_q = chord suction coefficient = (suction mass flow per unit span)/$\rho_\infty V_\infty c$,

where c is the local streamwise wing chord, and

c_q' = local suction coefficient = (suction mass flow per unit area)/$\rho_\infty V_\infty$

The actual process of determining suction requirements for the HLFC test panel began with stability analyses at several spanwise stations, using an assumed initial c_q' distribution. The calculations then were repeated with revised c_q' values until c_q was minimized, while maintaining the maximum extent of laminar flow. The typical tailoring sequence is illustrated in figure 4.2-2.

First, the suction peak (A) in the high-crossflow region was made narrower (B), resulting in lower c_q, but at the expense of slightly N_{CF}. Then the peak itself was lowered (C) until the predicted transition moved forward. Finally, adding a little more suction in the region between the high-crossflow and low-crossflow sectors (D) reduced N_{CF} to the level lost in the first suction peak reduction, while still giving a net reduction in c_q, relative to the starting point.

Stability calculations were also carried out for a number of off-design conditions. Their extent is illustrated in figure 4.2-3. Altogether, nearly 100 cases were analyzed, including 10 flight conditions each at three spanwise stations (WBL 290, 387, and 479) with suction variations, plus six additional spanwise stations (WBL 270, 311, 360, 416, 477, and 513) at the design condition. Altitude variations were also included in the calculations, to investigate Reynolds number effects. A summary of boundary layer growth at the stations is given in appendix F. Detailed results of boundary layer analysis are included as appendix G.

Because of the differences in pressure distribution between inboard and outboard stations, two distinct behaviors were found in the effects of c_q' tailoring on transition. WBL 311 and WBL 447 will be discussed. At WBL 311 the initial flow acceleration is more gradual than at WBL 447 because of the nacelle interference effect described in section 3.3, resulting in a longer CF region, whereas at WBL 447 the acceleration takes place within the first 5% of chord. Figure 4.2-4 compares the pressure and suction distributions at these two stations. The computed amplification factors are shown in figure 4.2-5. The graphs show the CF amplification factors for a range of wave numbers at zero frequency and the TS amplification factors for a range of frequencies at a wave angle of 50 deg, which are the most critical conditions. The dominance of CF amplification at WBL 311 is very evident, whereas TS amplification is approximately the same at both stations. The range of CF wave numbers and TS frequencies is illustrated in the contour plots of figure 4.2-6. Finally, the impact of pressure distribution on the boundary layer instability and predicted transition is illustrated in figure 4.2-7, where the pressure distributions, the N_{TS} and N_{CF} envelopes, and the transition criterion (N_{TS}-N_{CF}) diagrams for the two cases are shown together. (Note that in constructing the N_{TS}-N_{CF} diagram, the *envelopes* of the individual amplification factor curves were used. For the remainder of this discussion, only the envelope curves will be shown.) At WBL 311, transition is predicted at about 36% chord, while at WBL 447 it is near 50%, but in both cases the limits are imposed by the onset of pressure recovery. At WBL 311 more suction could further reduce the CF instability, but not much laminar flow could be gained because of the early recovery point. At WBL 447 the CF instability is almost entirely eliminated, but again the pressure recovery at 50% chord limits the extent of laminar flow.

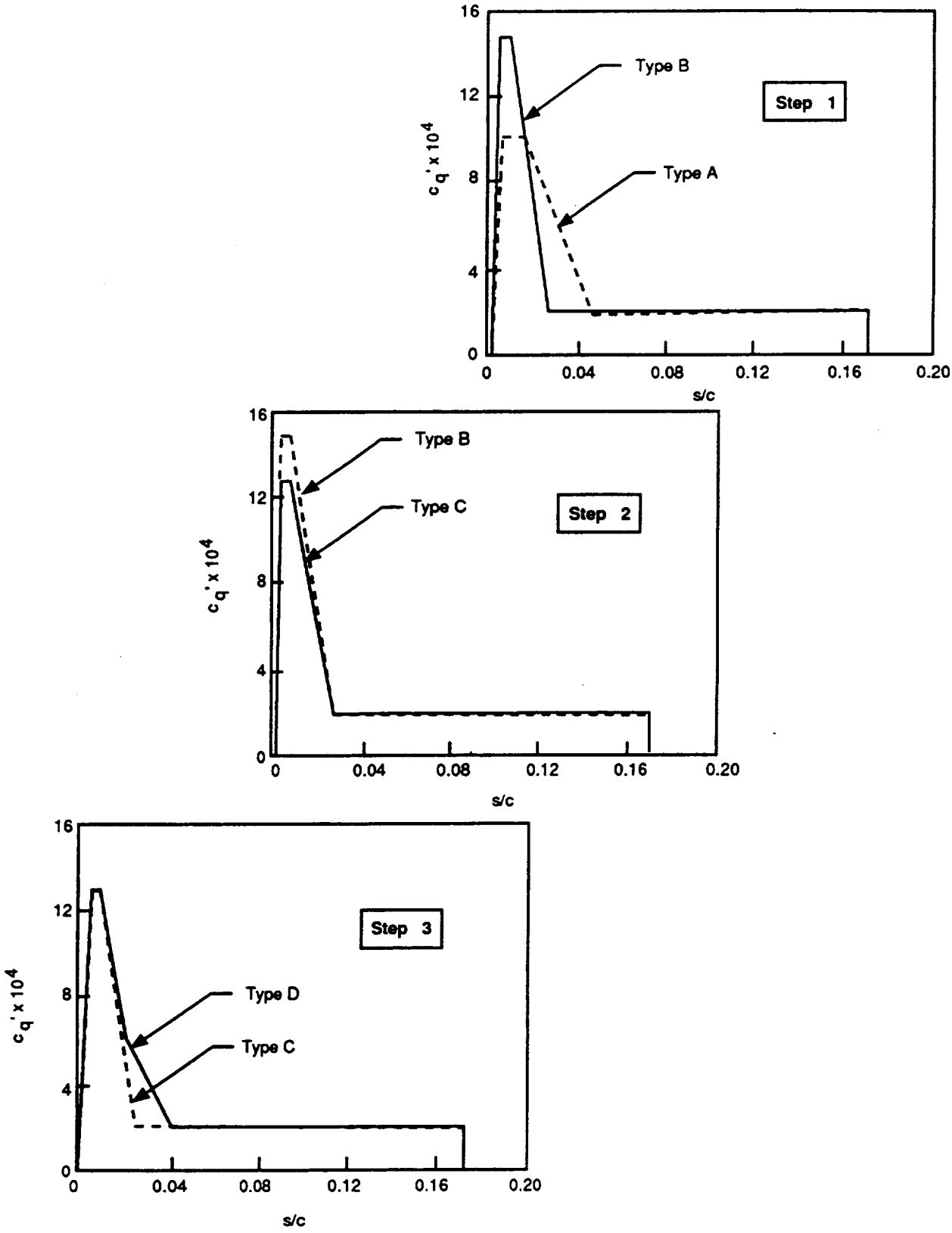

Figure 4.2-2. Suction Distribution Tailoring Sequence

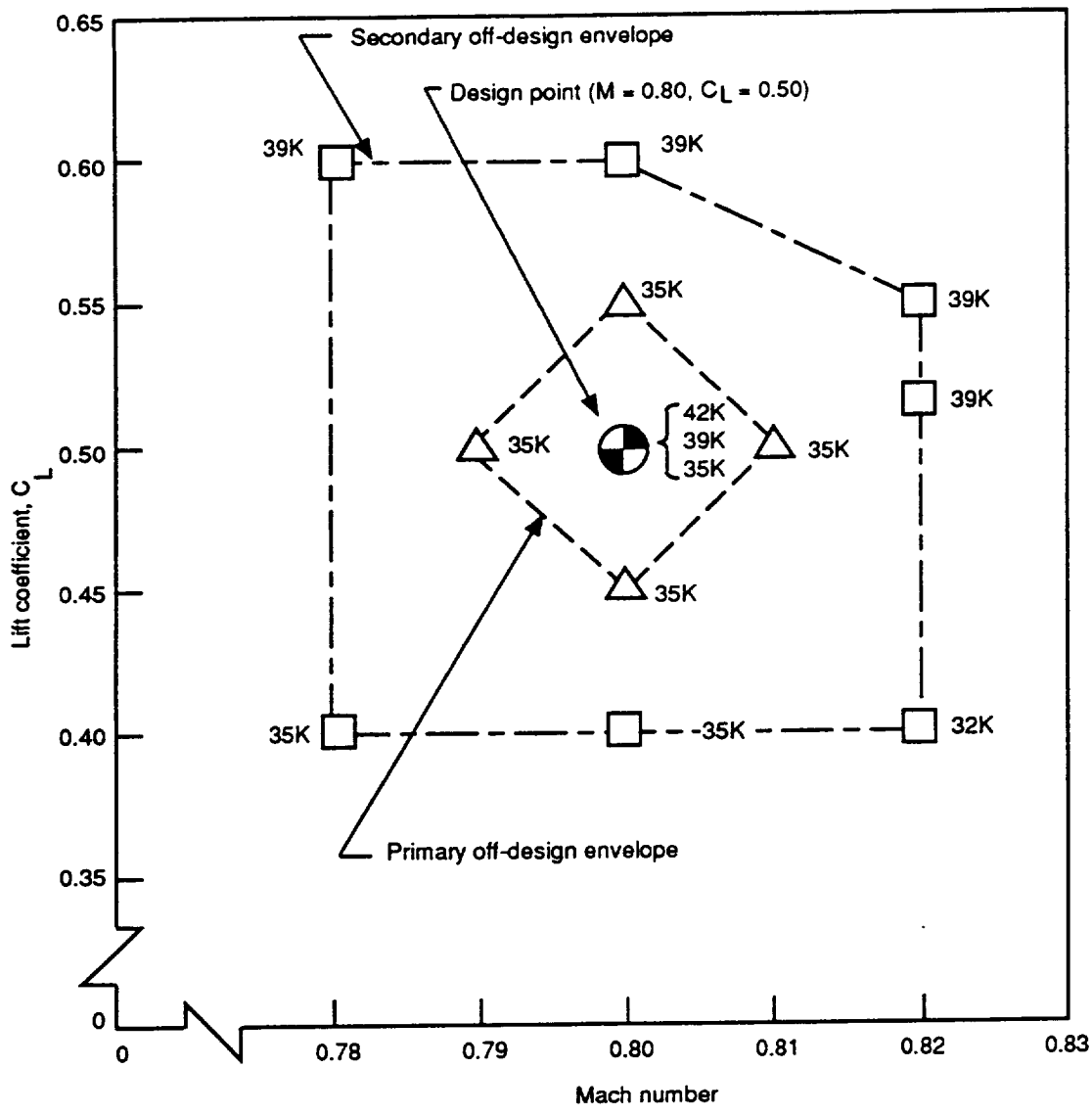

Note: At each condition at or above M = 0.79, three spanwise stations (WBL 290, 387, and 479) were analyzed, except for the design condition at 39K-ft altitude, in which case five additional stations were also analyzed (WBL 311, 360, 416, 447, and 513).

Figure 4.2-3. Scope of Boundary Layer Stability Calculations

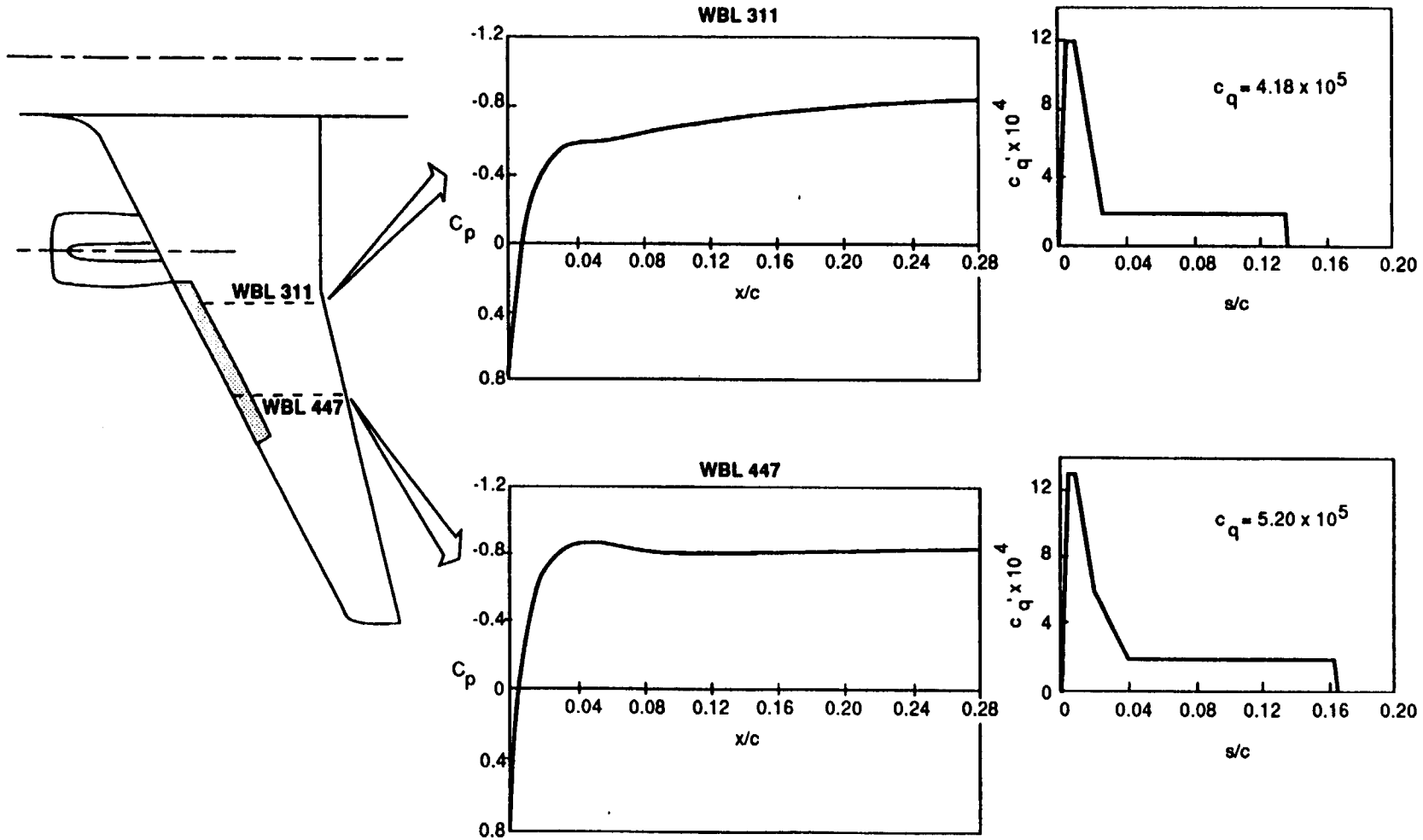

Figure 4.2-4. Comparison of Pressure and Suction Distributions at WBL 311 and 477; M = 0.80, CL = 0.50, and R/ft = 1.61 million (h = 39,000 ft)

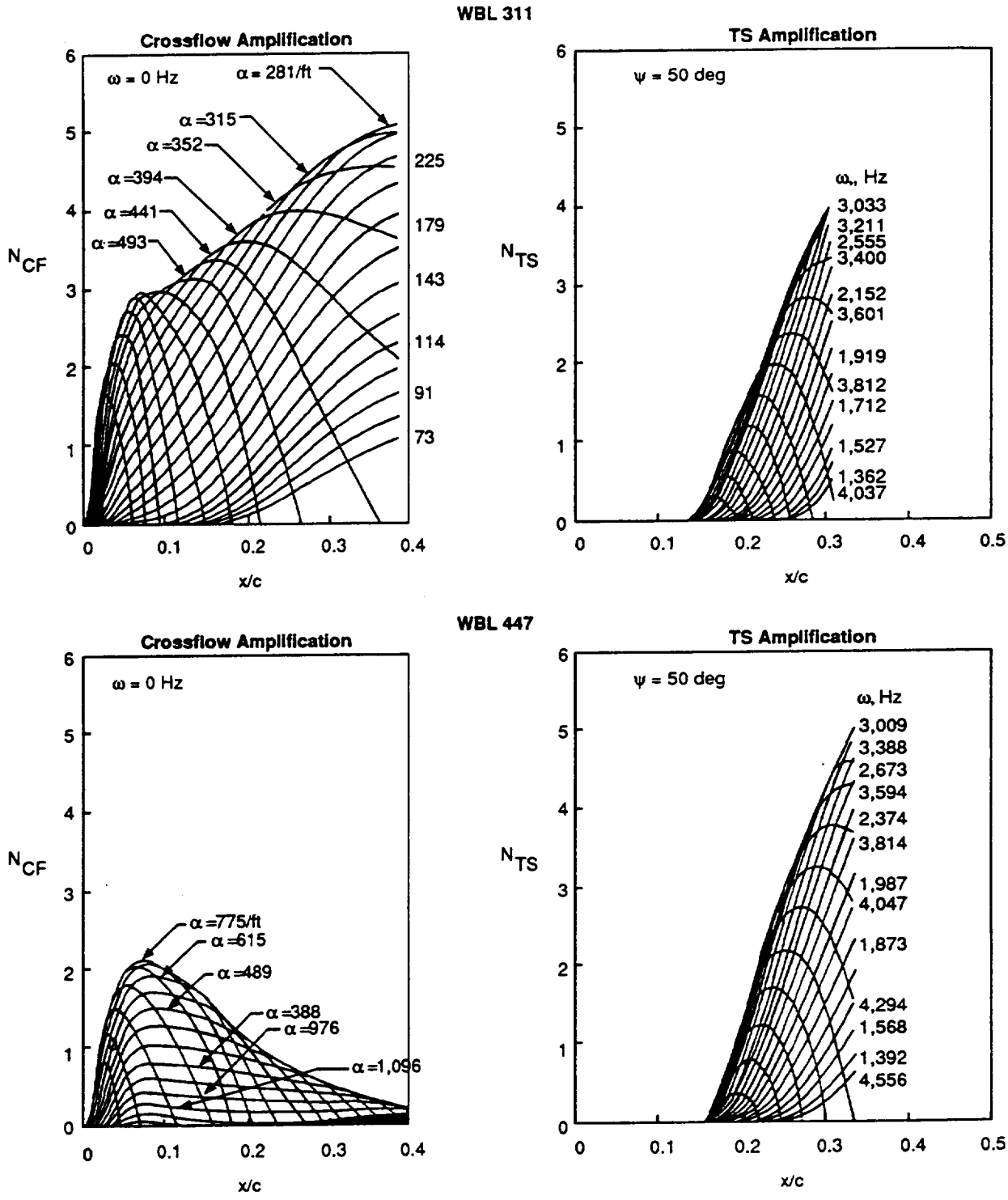

Figure 4.2-5. CF and TS Amplification Factors at WBL 311 and 447; M = 0.80, C_L = 0.50, and R/ft = 1.61 million (h = 39,000 ft)

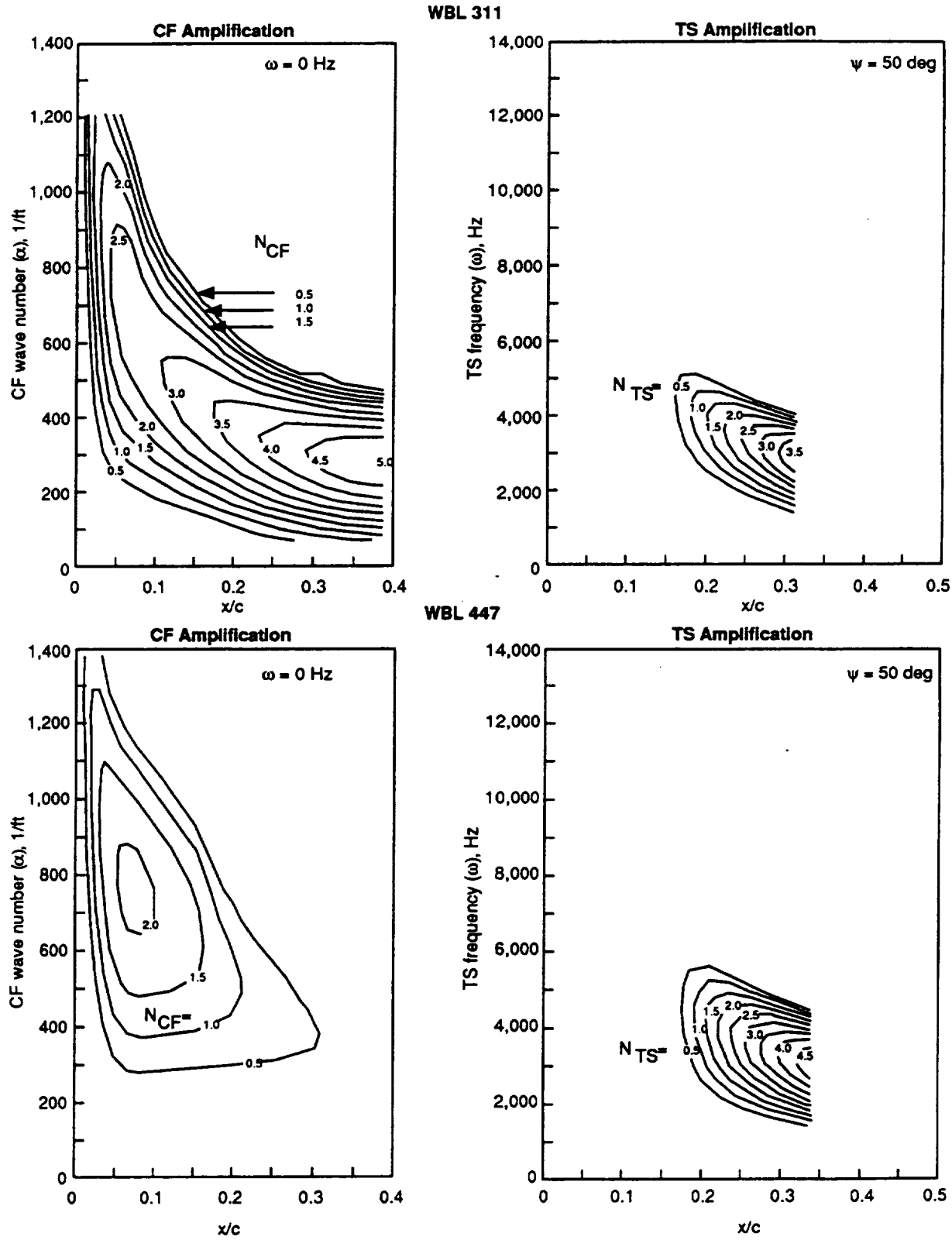

Figure 4.2-6. Comparison of Contour Plots of Amplification Factors at WBL 311 and 447; M = 0.80, CL = 0.50 and R/ft = 1.61 million (h = 39,000 ft)

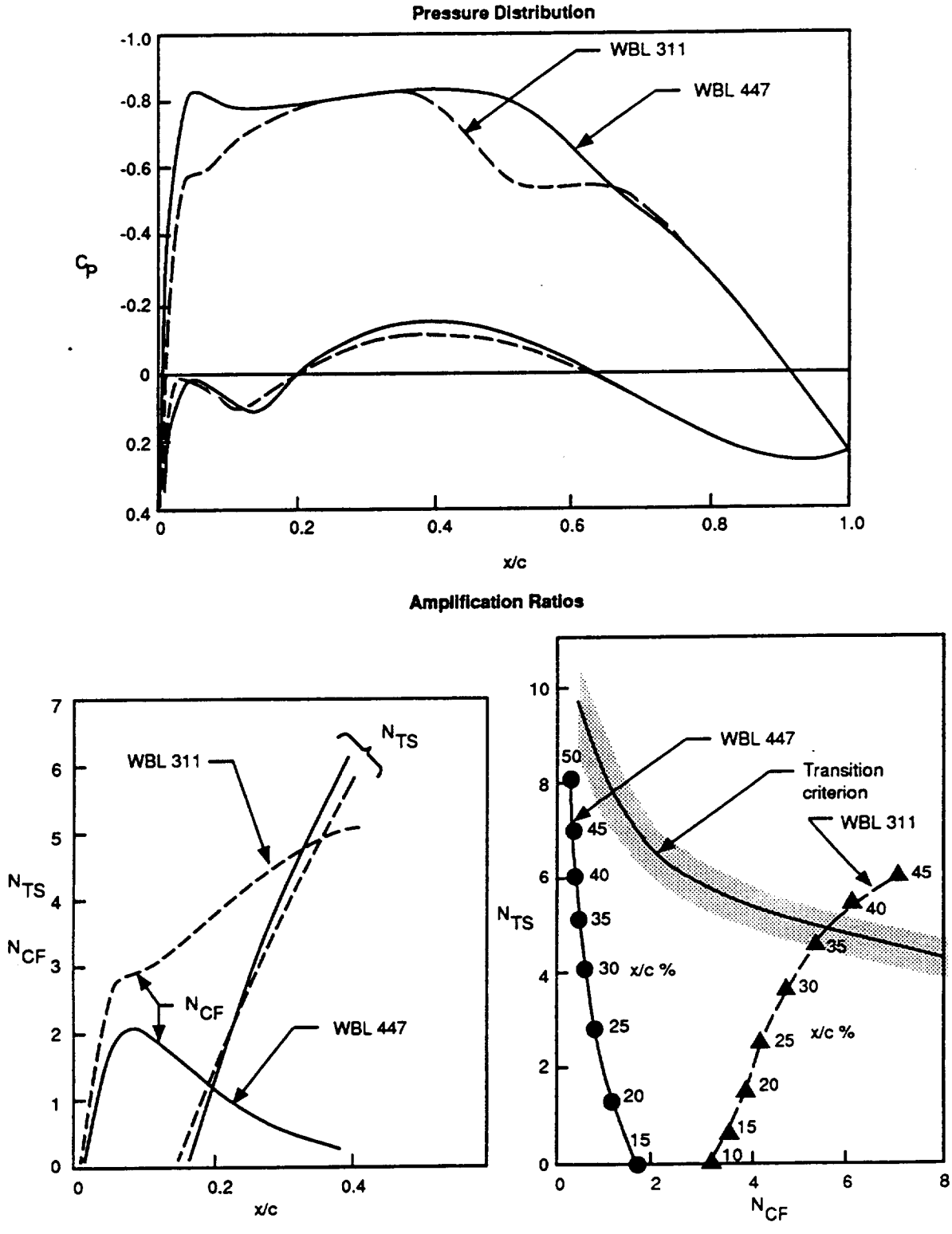

Figure 4.2-7. Summary of Stability Analysis Results at WBL 311 and 447; M = 0.80, C_L = 0.50, and R/ft = 1.61 million (h = 39,000 ft)

The effects of suction distribution tailoring are illustrated in figures 4.2-8 through 4.2-10. Narrowing the high suction region (i.e., going from type A suction to type B as indicated in fig. 4.2-2) allows some reduction in c_q at the expense of slightly increased CF amplification (fig. 4.2-8). A small increase in c_q' at the "corner" (a type D distribution) can restore the condition of near-zero N_{CF} at transition (fig. 4.2-9). While this remedy was effective over the outer portion of the HLFC panel, it did not work at the inboard end, where the slow acceleration caused the CF instability to be very strong. Figure 4.2-10 shows the stability analysis results for WBL 270 (just outboard of the nacelle) with a type C suction distribution at $c_q = 2.74 \times 10^{-5}$ and also with an unorthodox distribution (E) that puts a large amount of extra suction in the corner at $c_q = 5.79 \times 10^{-5}$. With the conventional suction distribution, crossflow-induced instability is the dominant factor, and transition is predicted at about 26% chord. The extra suction does bring the amplification trajectory closer to the N_{TS} axis but not enough to affect transition very much. Thus a 211% increase in suction produced only a 5% chord increase in the extent of laminar flow. The effect of a further increase of suction (F) could not be evaluated because the stability code would not converge on a solution. In any case, because pressure recovery at this station begins not far past 30% chord, the potential for additional improvement is small. (When the test panel span was later reduced to adapt to the capacity of a single turbocompressor, WBL 270 was outside the laminarized region anyway.)

The typical effects of altitude (more precisely, of unit Reynolds number) are shown in figure 4.2-11. The data pertain to WBL 479 at $C_L = 0.50$, $M = 0.80$, and $h = 39{,}000$ and 42,000 ft ($R_1 = 1.61$ million/ft and 1.40 million/ft, respectively). At the higher altitude, both the CF and the TS amplification factors are reduced, but the effect is more pronounced on the TS amplification. In both cases, transition is caused by TS instability, but it is postponed by 5% chord at the higher altitude.

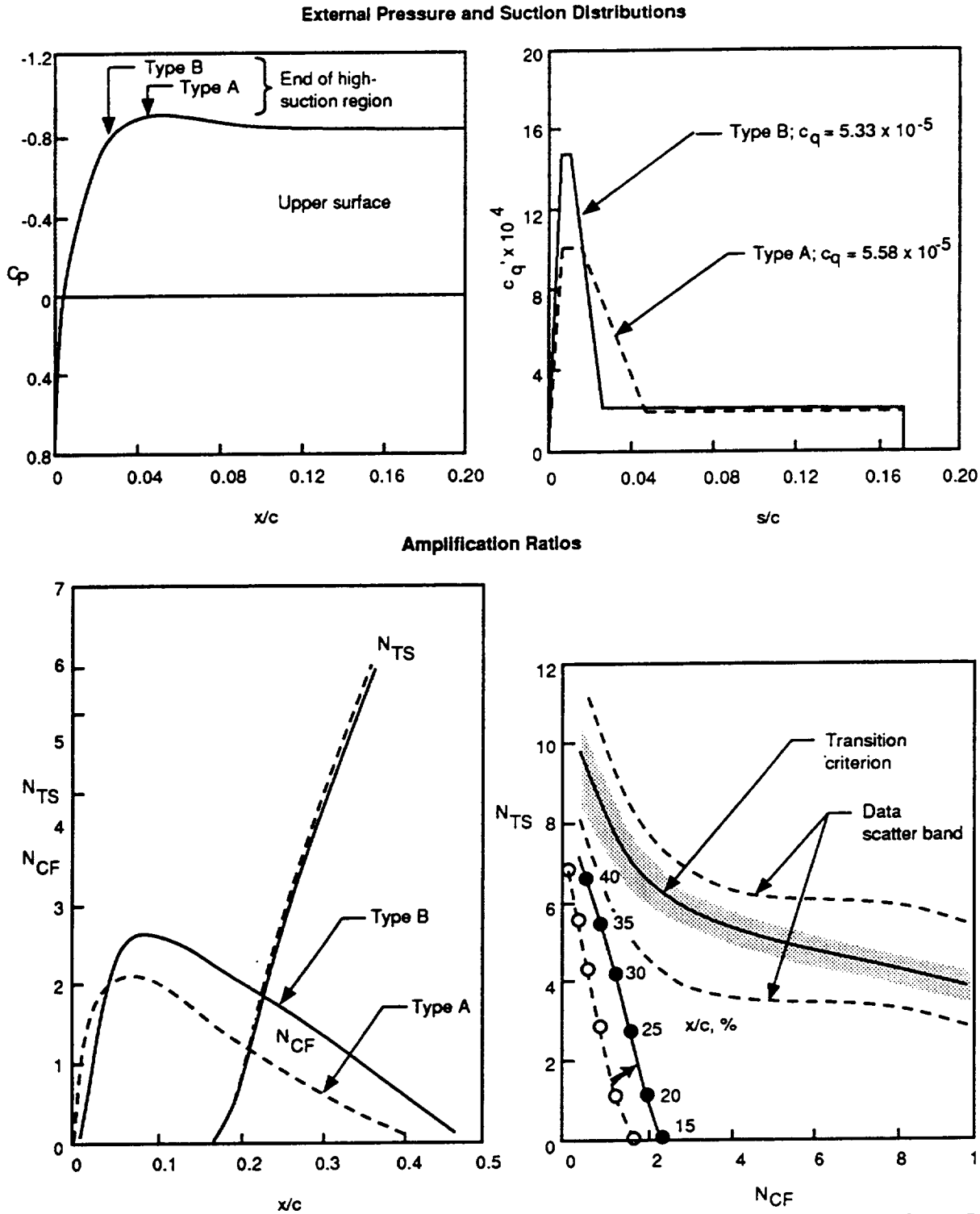

Figure 4.2-8. Typical Effects of Suction Tailoring—Type A to Type B Distribution; M = 0.80, C_L = 0.50, h = 35,500 ft, $R_C = 23.1 \times 10^6$, WBL 479

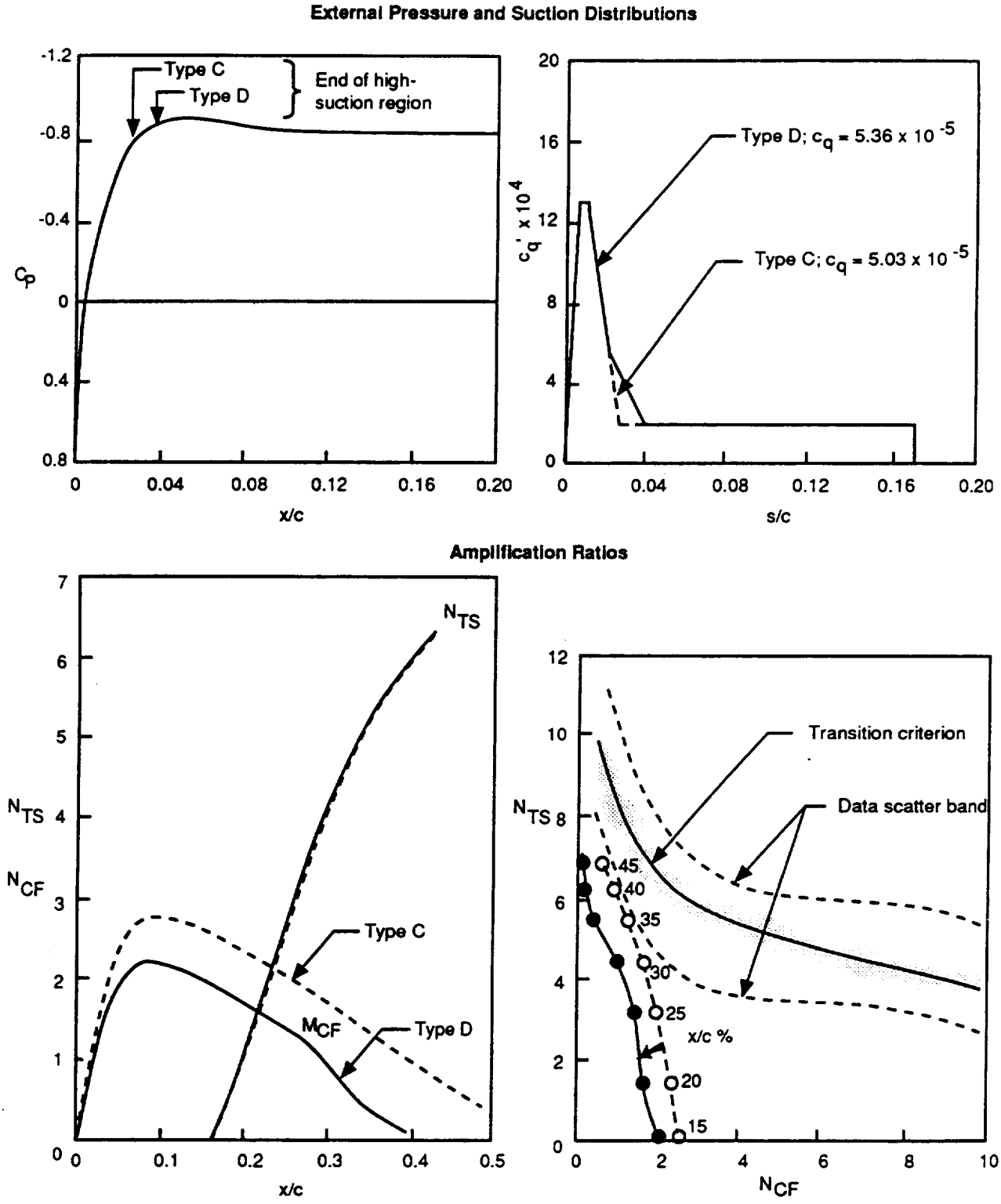

Figure 4.2-9. Typical Effects of Suction Tailoring—Type C to Type D Distribution; M = 0.80, C_L = 0.52, h = 39,000 ft, $R_C = 19.77 \times 10^6$, WBL 479

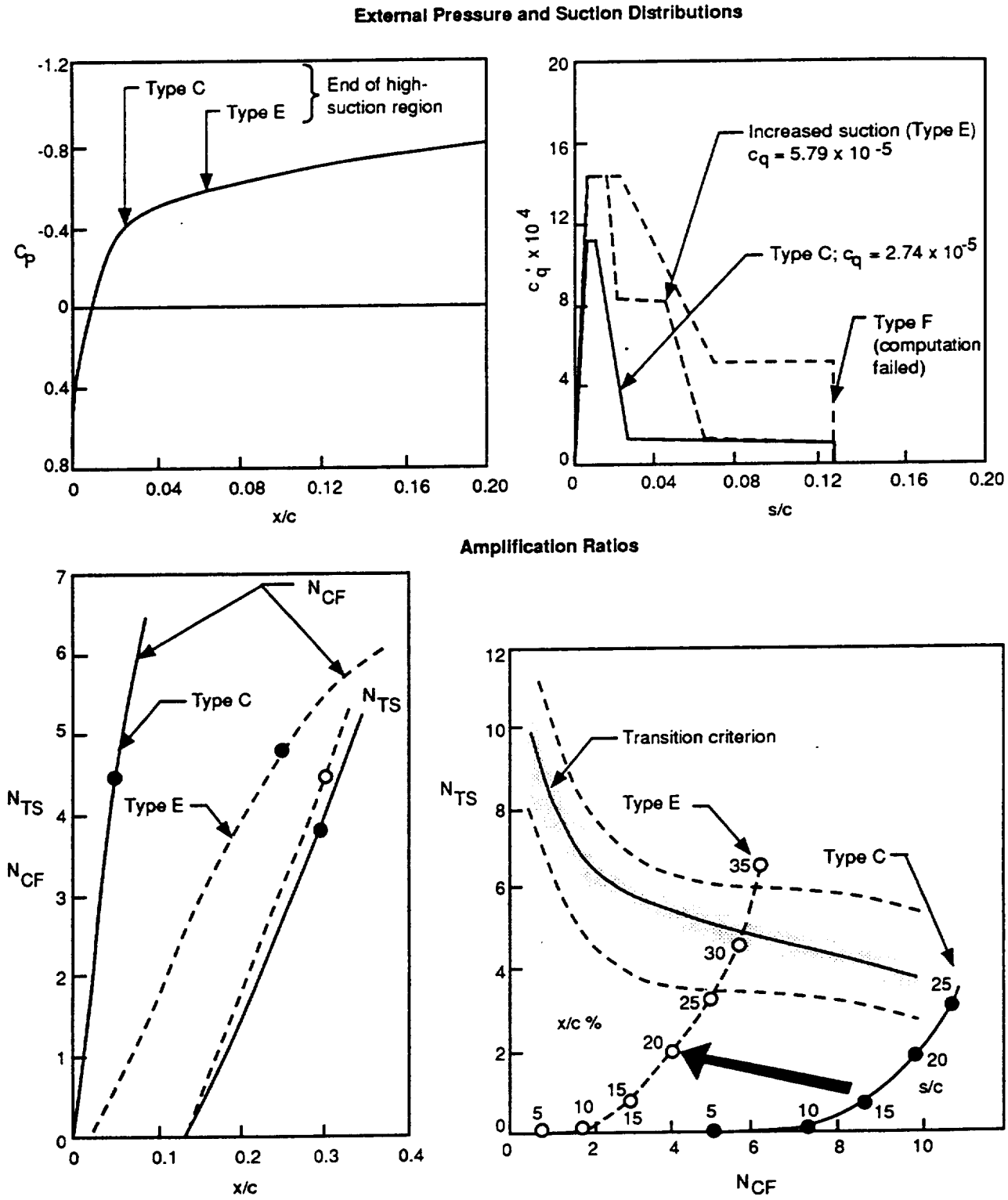

Figure 4.2-10. Effect of Increased Suction in the Vicinity of the Engine Nacelle; M = 0.80, C_L = 0.50, h = 39,000 ft, $R_C = 28.8 \times 10^6$, WBL 270

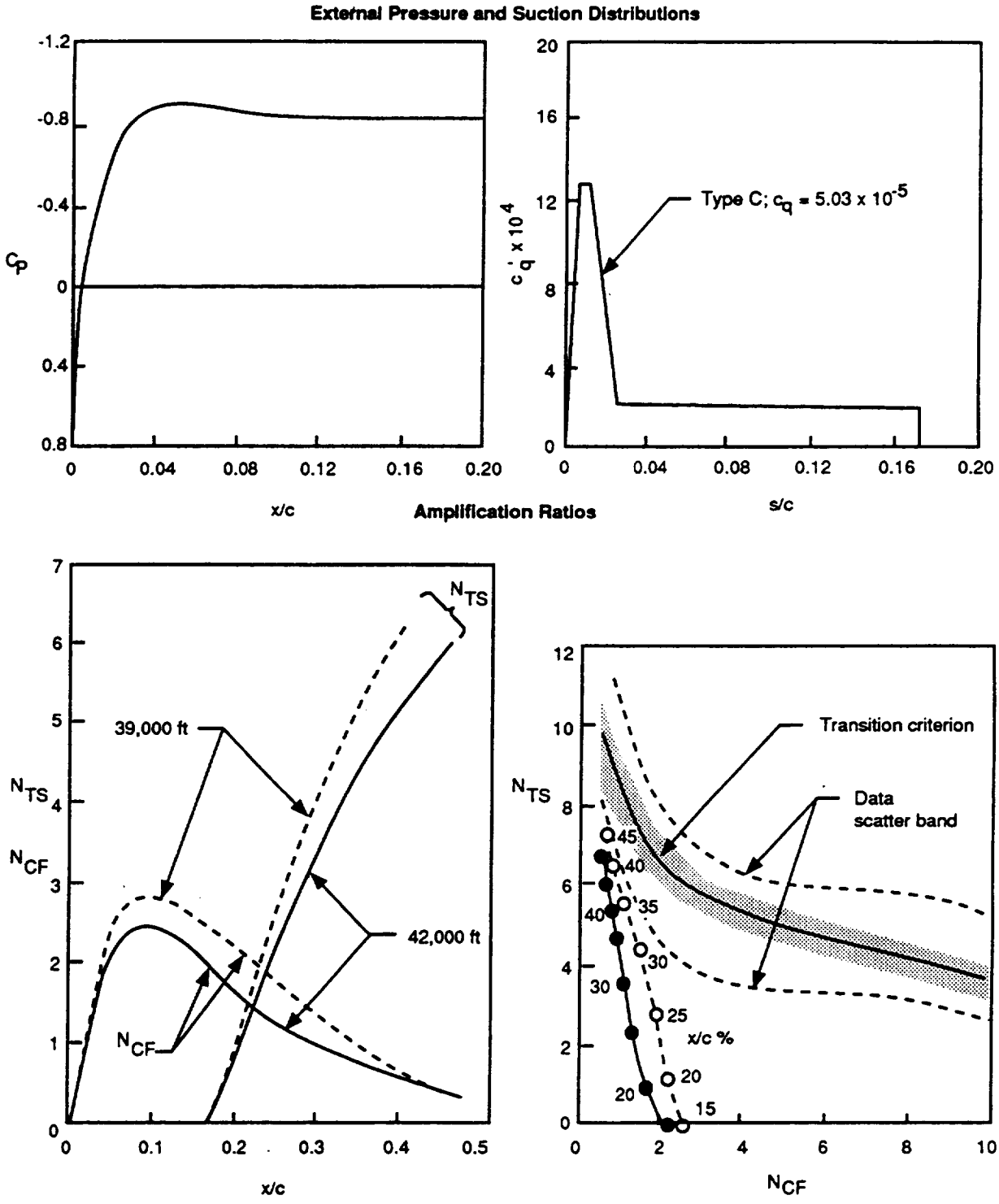

Figure 4.2-11 Effect of Altitude on Amplification Characteristics; M = 0.80, C_L = 0.50, WBL 479

4.3 OVERALL SUCTION REQUIREMENTS

Figure 4.3-1 shows the calculated suction requirement over the whole span of the HLFC panel for the design condition (M = 0.80, C_L = 0.50, and h = 39,000 ft). The symbols show theWBL span stations where calculations were made. The section c_q increases going outboard, but the suction flow per unit span (proportional to c times c_q) diminishes, except at the inboard end. There, the early pressure recovery limits the extent of laminar flow, so additional suction would have no effect. The mean values of c_q and cc_q over the HLFC panel are 4.9×10^{-5} and 6.8×10^{-4} ft, respectively. The slight dip in c_q at WBL 387 amd 416 is not considered significant because of the "cut and try" nature of the optimization procedure.

The stability calculations indicate laminar flow at least up to the pressure recovery line (the approximate location of the shock), as shown in figure 4.3-2 by the dashed line. It runs approximately along the 45% chord line outboard, then moves forward to about 24% chord at the inboard end. However, prediction of the recovery line by the computer code is somewhat uncertain because the computation tends to smooth out abrupt changes in pressure, such as at the shock. Therefore the actual pressure recovery point may lie somewhat downstream of the computed one, and an additional 5% to 10% chord laminar flow may be possible. This region is marked by shading in the figure. The potential laminar zone may therefore reach 50% to 55% chord over the outboard half of the test area, decreasing gradually to about 30% to 40% chord at the inboard edge of the suction region (WBL 330).

For off-design conditions, the stability calculations were carried out for only three spanwise stations, resulting in a sparse definition of the cq distribution. Nevertheless, the trends with Mach number, C_L, and altitude are clearly identifiable. Figure 4.3-3 shows the effect of varying C_L in the range from 0.40 to 0.55 on the required cq and predicted transition at M = 0.80 and h = 35,000 ft. More suction is required at lower C_Ls but in spite of this, less laminar flow would be obtainable. This is true because the pressure distributions are more conducive to laminar flow at higher lift coefficients, particularly in the central and inboard regions of the test panel.

The effects of altitude at M = 0.80 and C_L = 0.50 are illustrated in figure 4.3-4, for h = 35,000 and 42,000 ft. At the higher altitude, less suction is required and the extent of laminar flow is increased. Because both cases have the same pressure distributions, the difference is due to the decreased disturbance growth at the lower unit Reynolds number.

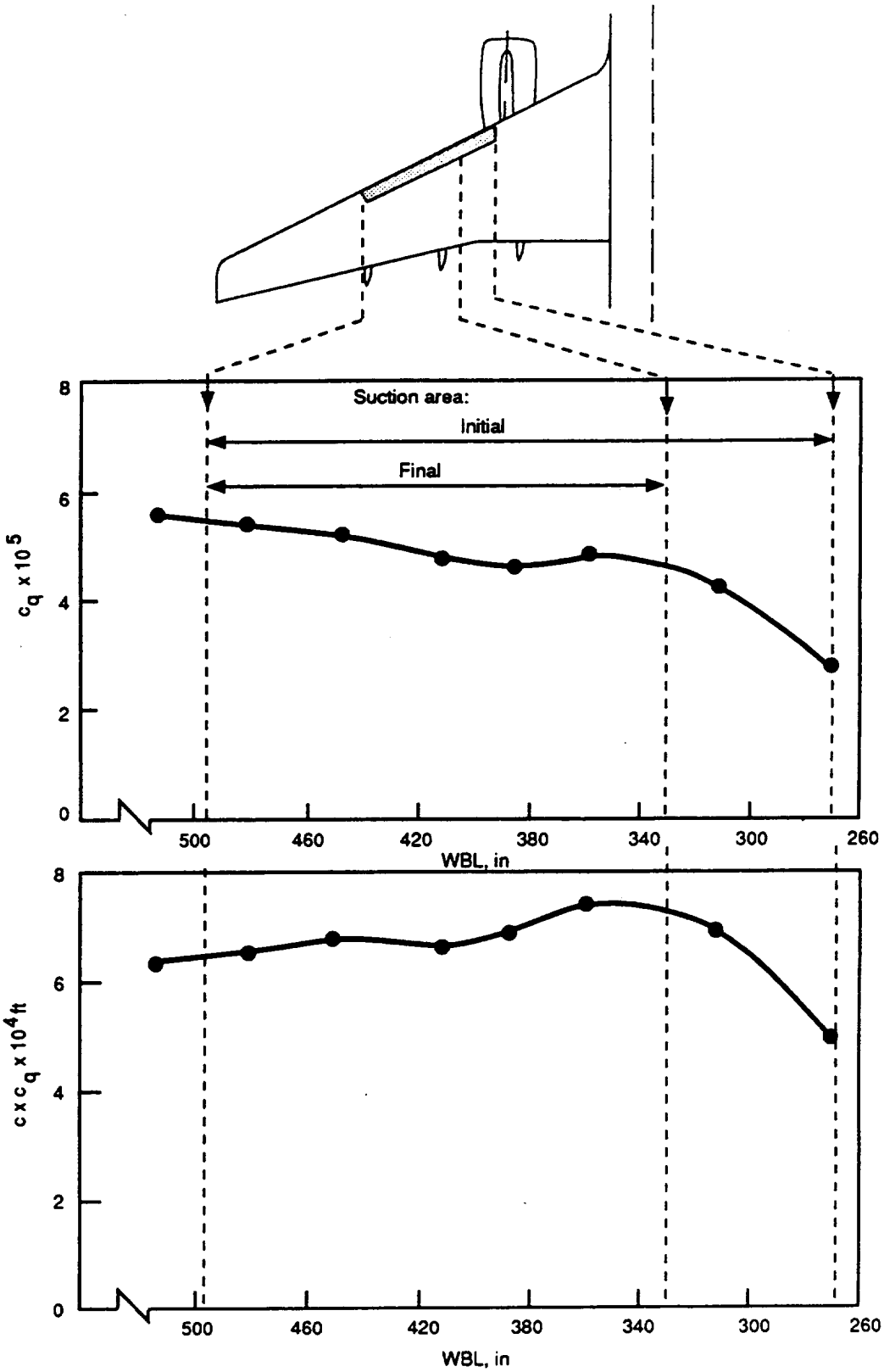

Figure 4.3-1. Spanwise Variation of Tailored Suction Flow Rates

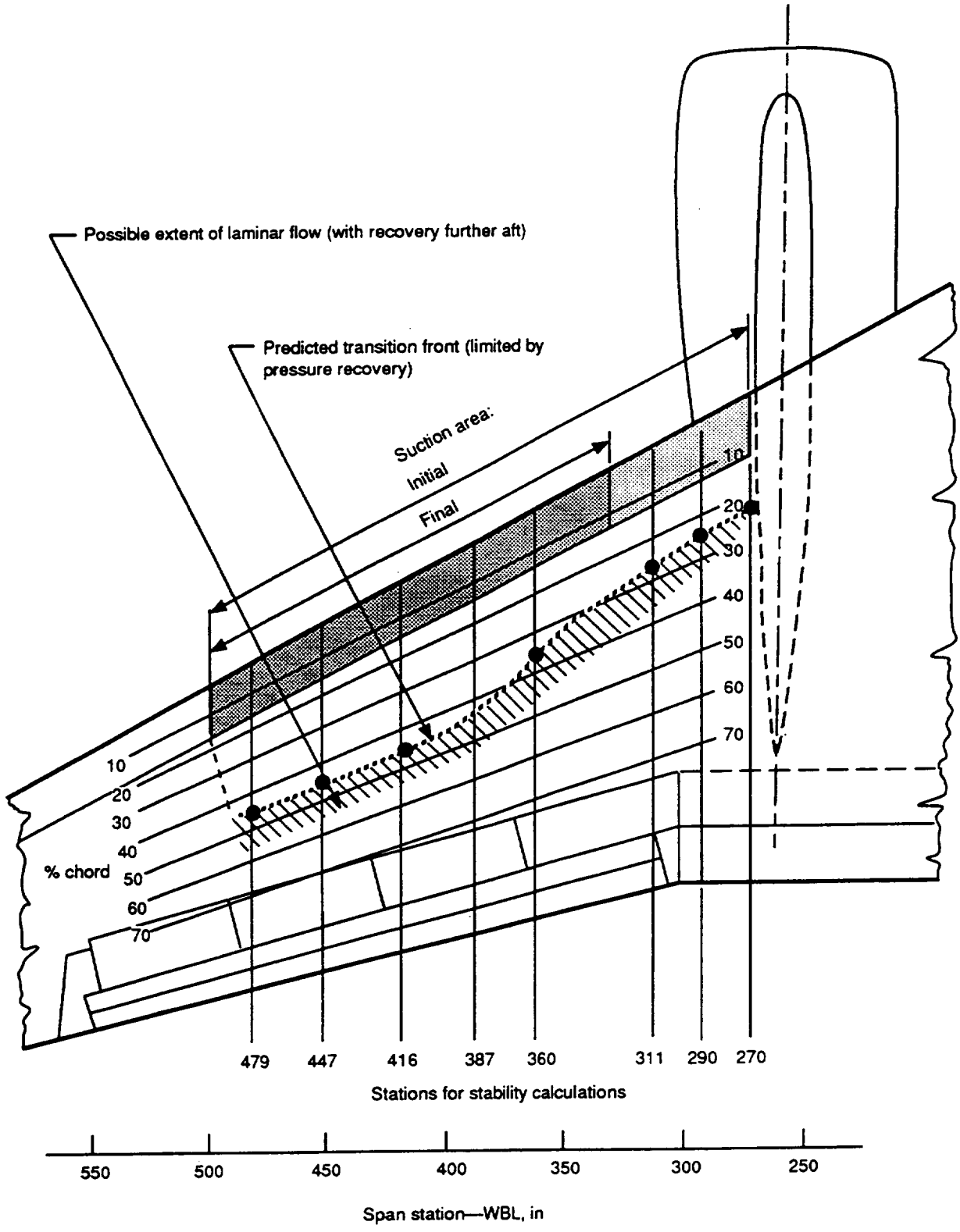

Figure 4.3-2. Predicted Extent of Laminar Flow, Design Condition

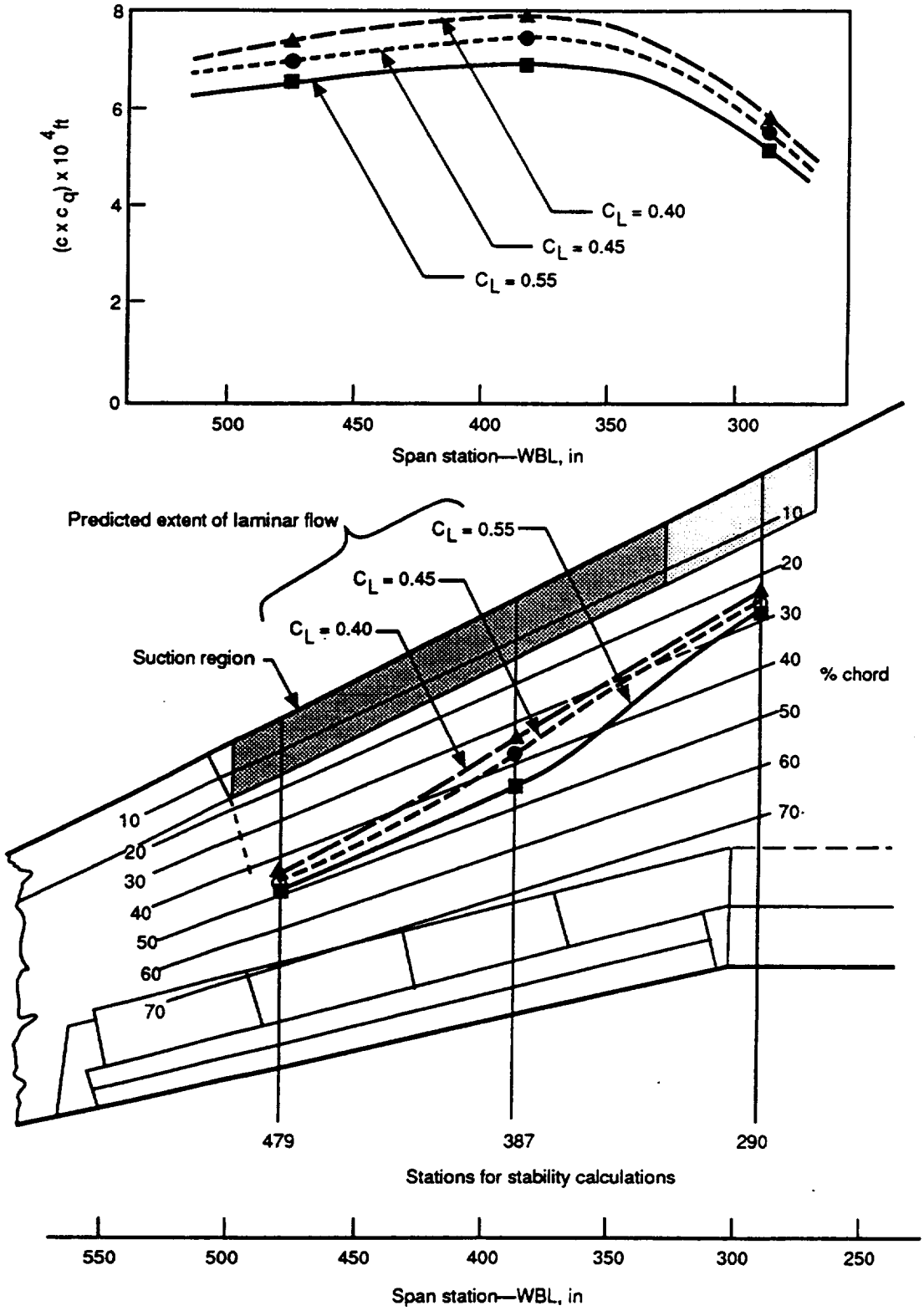

Figure 4.3-3. Effect of Lift Coefficient on Suction Rates and Transition; M = 0.80, h = 35,000 ft

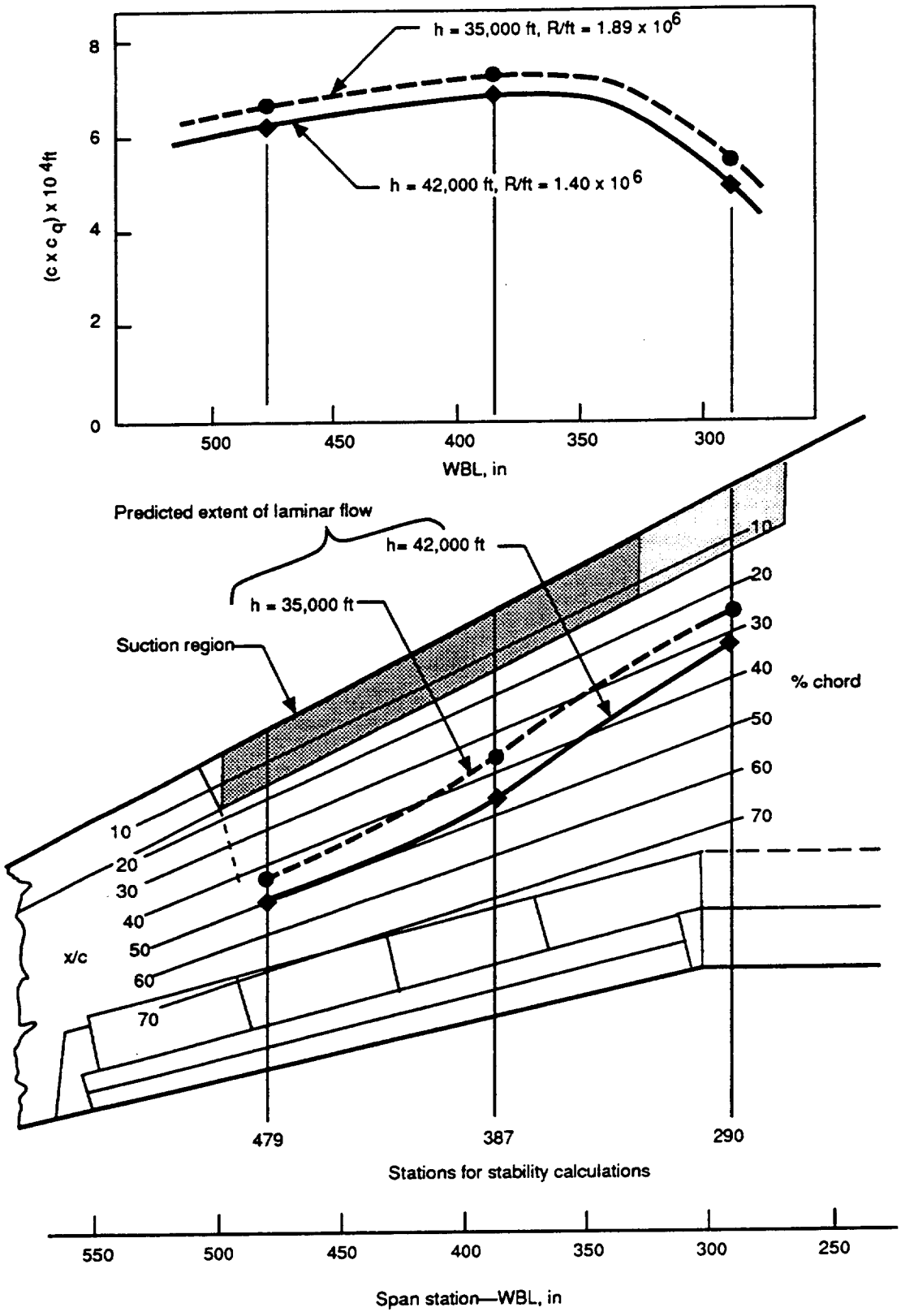

Figure 4.3-4. Effect of Altitude on Suction Rates and Transition; M = 0.80, C_L = 50

4.4 ADJUSTMENTS TO THEORETICAL SUCTION DISTRIBUTIONS

The analyses described above were done before the final configuration of the suction surface and flute arrangement were established. The calculations were carried out independently for individual sections. Consequently, the cq distributions showed some spanwise variation, as noted above in the discussion of figure 4.3-1. Therefore, the theoretical c_q' distributions were adjusted to make them mutually consistent and compatible with the hardware design. The adjustments affected both the forward region, where the flutes are curved to follow the external isobars, and the suction termination point. The aftmost flute was eliminated to provide space for the joint between the suction surface and the front spar. The adjusted c_q' distributions are shown in figure 4.4-1. The peak values of c_q' are 14×10^{-4} for $C_L = 0.40$, 13×10^{-4} for $C_L = 0.50$, and 12×10^{-4} for $C_L = 0.60$, respectively (see fig. 4.4-1 for connecting points A-B). The intermediate zone between the high- and low-suction regions is defined by point C, where $c_q' = 4.00 \times 10^{-4}$, and point D, where s/c = 0.04. The low-suction region, with $c_q' = 2 \times 10^{-4}$, terminates at a fixed distance from the leading edge, and therefore at increasing s/c with distance outboard (point E).

The adjusted spanwise distributions of c_q and cc_q for the design condition are shown in figure 4.4-2. The irregularities have been eliminated and the c_q levels somewhat reduced. The average cc_q is 6.54×10^{-4} ft. The resulting total flow coefficient for the entire test area is

$$C_Q = \int (cc_q) dy_{sp} / S_{panel} = 4.72 \times 10^{-5} \qquad \frac{1}{S_{sp}} = \int (cc_q) dy_{sp} = 4.72 \times 10^{-5}$$

The corresponding total volume flow rate is

$$Q = V_\infty S_{panel} C_Q = 6.97 \text{ ft}^3/\text{s}$$

where

$V_\infty = 774.4$ ft/s at M = 0.80 and h = 39,000 ft,

and the mass flow rate is

$$w = \rho_\infty g Q = 0.1368 \text{ lb/s} = 8.2 \text{ lb/min}$$

These adjusted suction distributions were the basis for the internal flow system design. That activity is described in volume IV of this report.

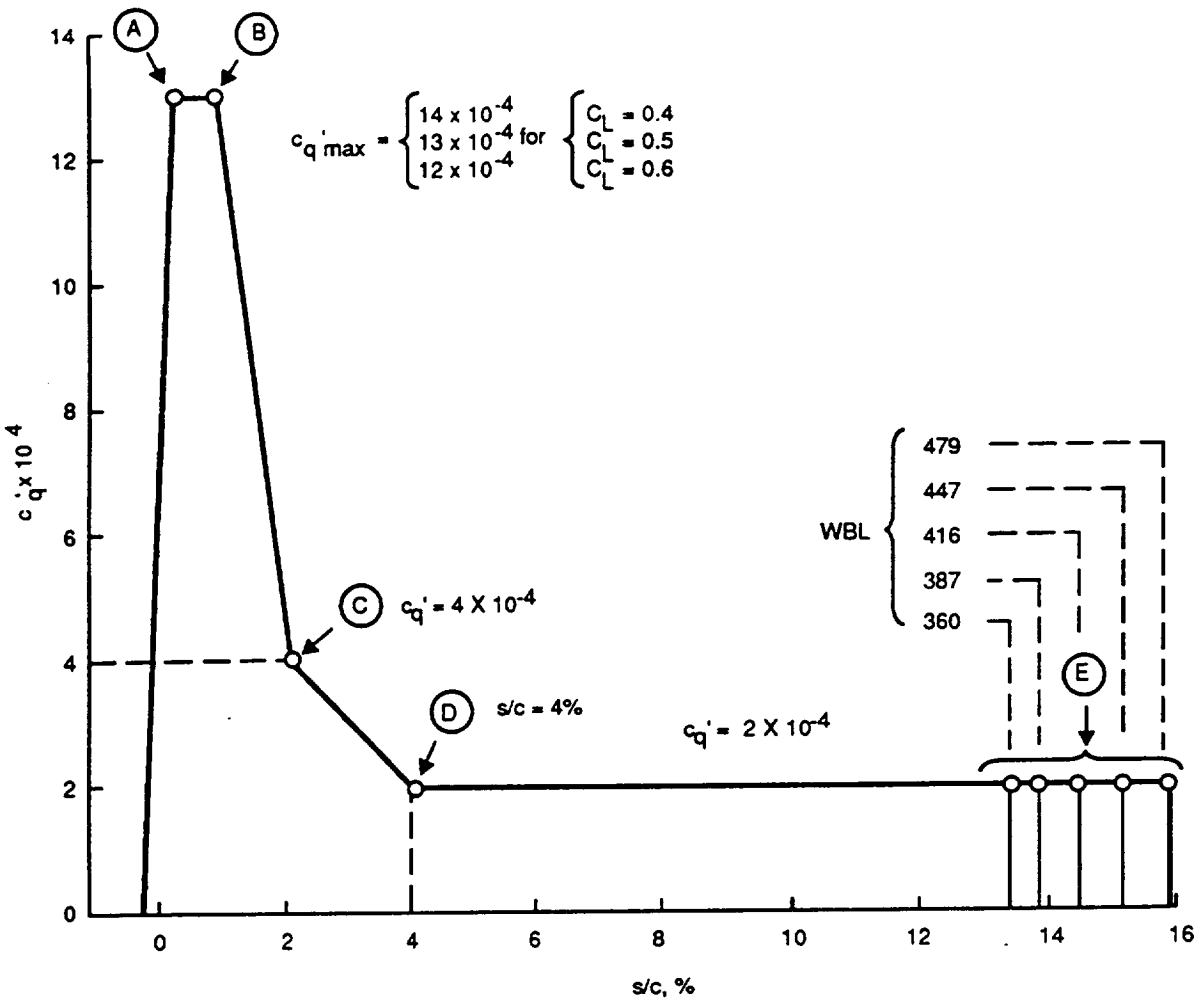

WBL, in	c, ft	s/c at Ⓔ, %	c_q x 10^5	(c x c_q) x 10^4
360	15.16	13.40	4.495	6.817
387	14.50	13.80	4.575	6.633
416	13.75	14.35	4.685	6.441
447	13.00	15.10	4.835	6.285
479	12.20	15.85	4.985	6.085

Figure 4.4-1. Adjusted Final Suction Requirements

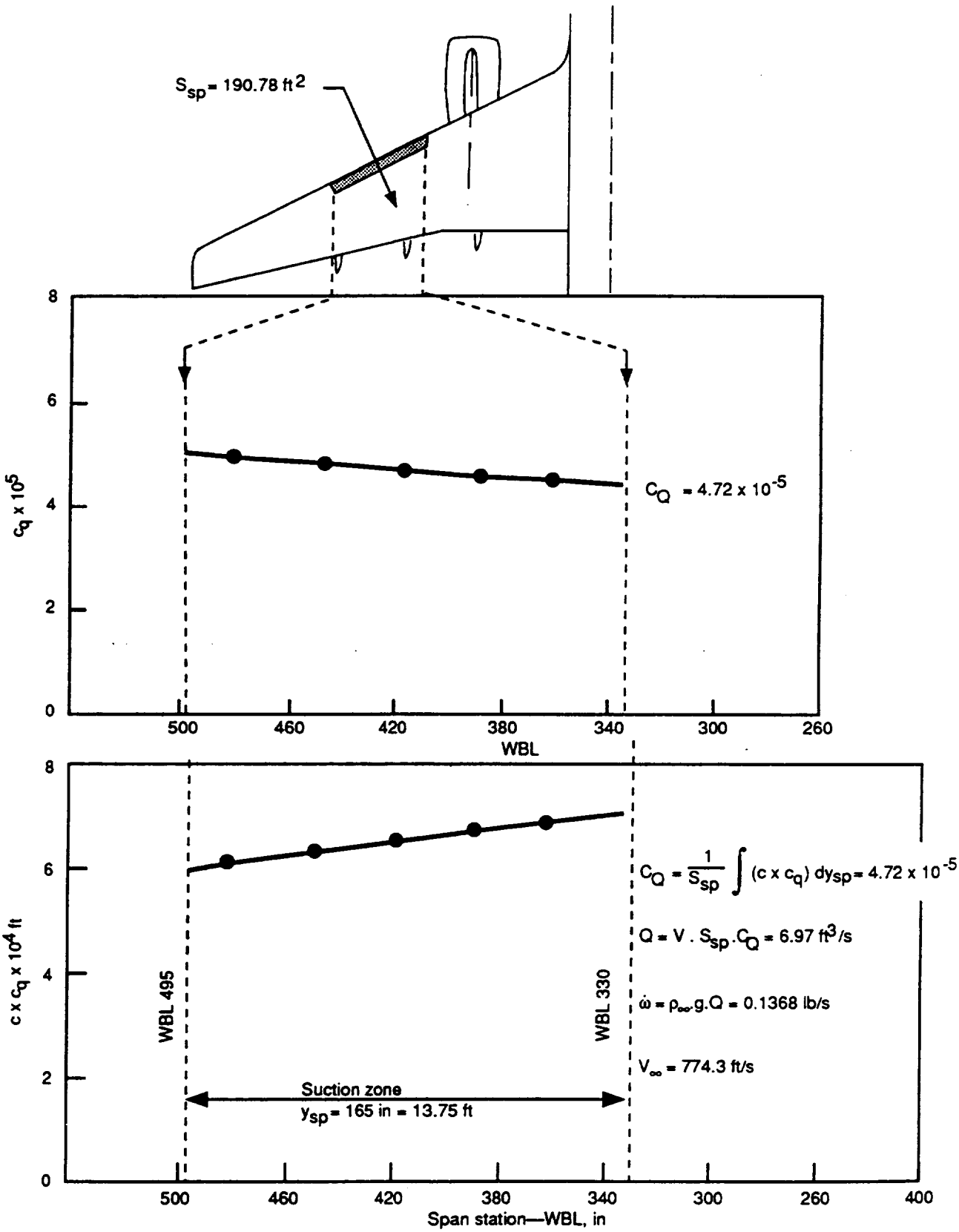

Figure 4.4-2. Spanwise Variation of Adjusted Suction Flow Rates; M = 0.80, CL = 0.50, R/ft = 1.61 million (h = 39,000 ft)

5.0 ATTACHMENT-LINE FLOW TREATMENT

5.1 BACKGROUND AND DESIGN CRITERIA

The third form of boundary layer instability that may cause early transition on swept wings is called "attachment-line turbulence contamination." It was first observed during early laminar flow flight experiments in England (refs. 17 and 18) and was encountered also on the Northrop/USAF X-21 research airplane (ref. 19). Premature transition may be caused by turbulence convected by the boundary layer of the spanwise flow along the leading edge attachment line, that is, the surface streamline separating the flows above and below the wing. Disturbances may originate from turbulent eddies in the fuselage boundary layer, from vortices forming at the wing/fuselage intersection, or they may arise within the attachment-line boundary layer itself. The behavior of the attachment-line boundary layer depends on its momentum thickness Reynolds number

$$R_{\theta_{al}} = \frac{\rho_{al} W_{al} \theta_{al}}{\mu_{al}}$$

where the subscript "al" denotes "attachment line." The attachment-line boundary layer momentum thickness, θ_{al}, depends on the sweepback angle, the unit Reynolds number, and the velocity gradient normal to the attachment line. That gradient is strongly influenced by leading edge geometry. Appendices B and C include wing cross sections normal to the leading edge and leading edge radius data.

According to references 19, 20, and 21, $R_{\theta_{al}}$ should be kept less than 94 to 100 to ensure that the flow stays laminar.

5.2 ATTACHMENT-LINE FLOW CONDITIONS ON THE MODIFIED WING

Figure 5.2-1 shows $R_{\theta_{al}}$ (as calculated by a subroutine included in the transonic flow computer code discussed in sec. 3.1, above) for several flight conditions in the cruise envelope. It can be seen that in the test region, $R_{\theta_{al}}$ often approaches and sometimes exceeds the critical value of 100, particularly at cruise altitudes below 35,000 ft. Consequently, some kind of treatment against attachment line transition was deemed necessary.

5.3 ATTACHMENT-LINE FLOW STABILIZATION BY PASSIVE SUCTION

Initially, the application of a "Gaster-bump" (a bump on the leading edge that creates a local stagnation point and thus diverts the leading edge boundary layer (ref. 22)) was considered. It had been proven effective by previous experiments, such as the laminar flow test fixture on the Avro Lancaster (ref. 23) and the NASA Jetstar/LEFT suction glove (ref. 8). Other schemes that had been used before with success, such as a notch in the leading edge, used on the NASA/Boeing 757 NLF glove (ref. 6), or a laminarized fence on the leading edge, used on the X-21 (ref. 7), were also considered but judged not practical for the present case.

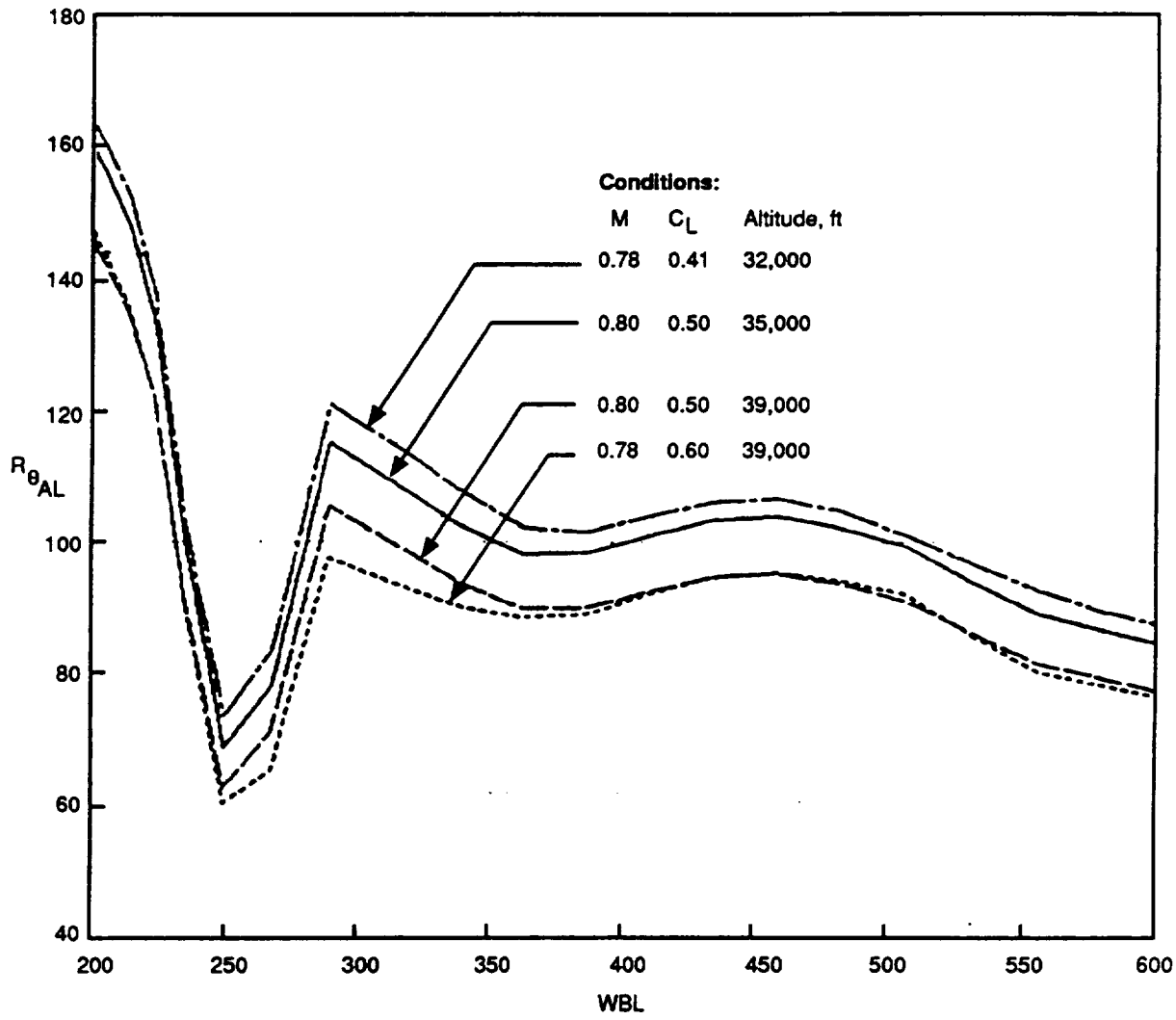

Figure 5.2-1. Attachment-Line Reynolds Number

It was finally decided to apply suction at the leading edge inboard of the HLFC test panel, because a Gaster bump could always be added later if it were needed, whereas retrofitting suction would be much more difficult. Two arrangements were considered (fig. 5.3-1), one using chordwise slots across the leading edge and the other using perforated skin. The former scheme had been tried previously on the X-21, but perforations were chosen here because large areas of skin were to be perforated anyway, and forming problems were foreseen for the slotted skin. It was convenient to make the attachment-line suction independent of the main suction system, using the relatively high external pressure at the attachment line and venting to a low pressure region on the wing lower surface, as shown in figure 5.3-2.

In selecting the size and location of the attachment-line suction area, the movement of the attachment line with changing flight conditions and the associated variations of external pressures were considered. The position of the attachment line could be inferred from the calculated pressures (sec. 3.3). Figure 5.3-3 shows the theoretical location of the attachment line along the HLFC test span for the design condition and the two extreme off-design conditions. At the design

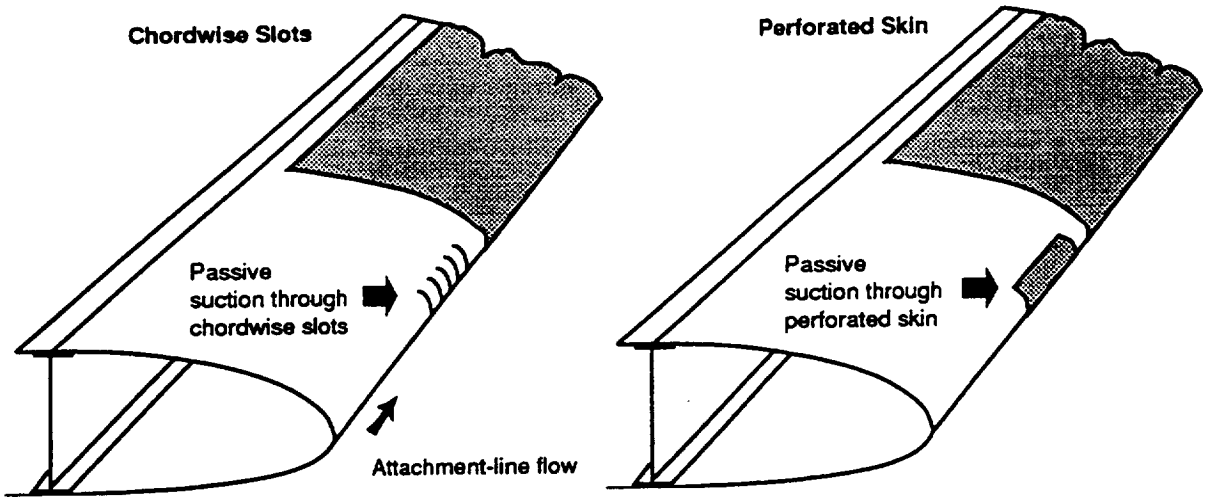

Figure 5.3-1. Attachment-Line Suction Concepts

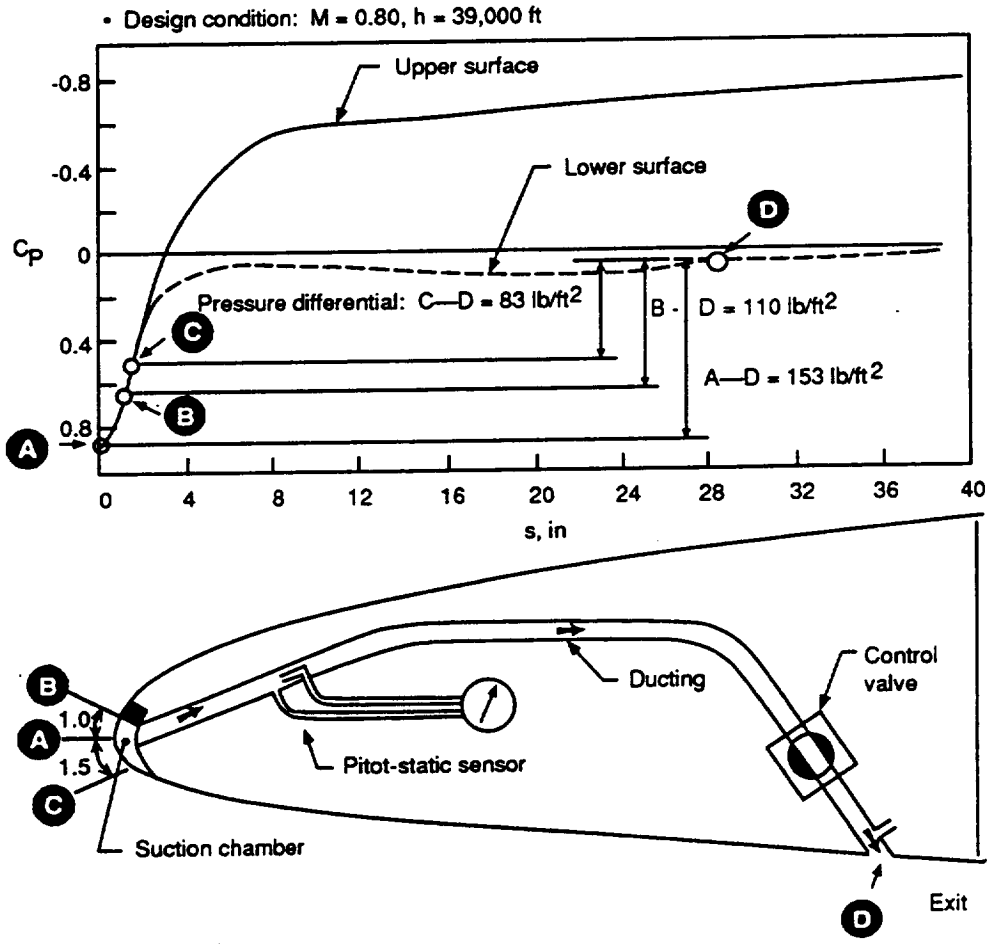

Figure 5.3-2. Automatic Suction Arrangement for Attachment-Line Flow Control

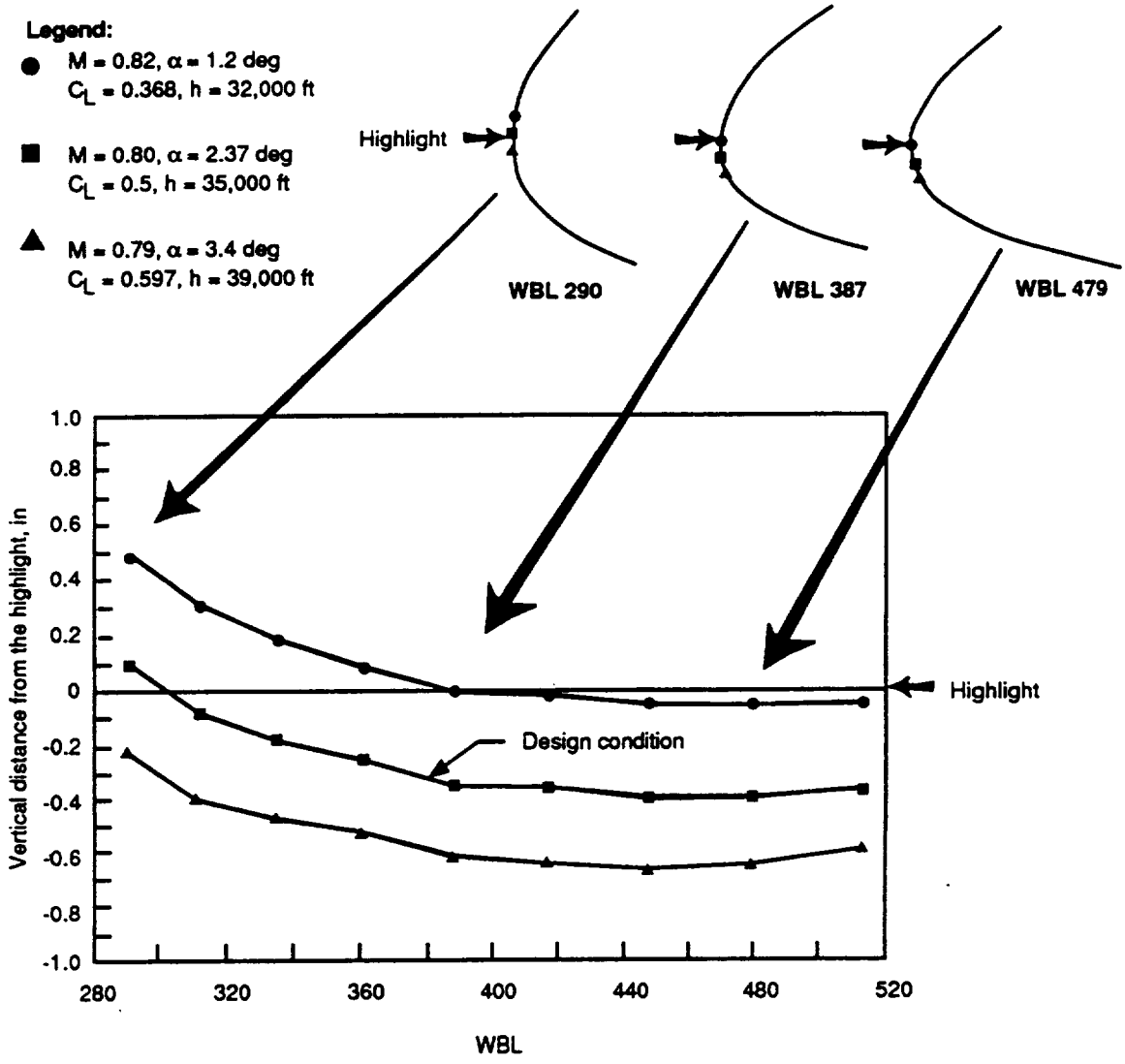

Figure 5.3-3. Range of Movement of the Attachment Line at Cruise Conditions

condition, the attachment line lies 0.2 to 0.4 in below the leading edge (highlight). At lower C_Ls it moves upward (closer to the highlight) and at higher C_Ls it moves downward. The total excursion is about 0.6 in. The upper and lower boundaries of the suction area were placed 1 in above and 1.5 in below the highlight. The span of the attachment-line suction area was 6 in. At the estimated suction rates, $R\theta_{al}$ in the most critical region could be reduced from the original level of 100 to about 30.

6.0 LEADING EDGE DEVICE AERODYNAMIC DESIGN

As part of the HLFC flight experiment, a dual-purpose leading edge Krueger flap was incorporated to serve both as a high-lift device and as an insect and debris shield. Before the contract effort was begun, a Boeing-sponsored, two-dimensional wind tunnel test had been performed to investigate the high-lift geometry trades and insect protection effectiveness of a Krueger flap (ref. 24). The design of the leading edge device used in the HLFC flight experiment was guided by the knowledge gained from these preliminary experiments. Later, as part of the contract effort, a three-dimensional low-speed test was conducted to evaluate the effects of the modified high-lift system on the low-speed performance and handling characteristics of the test airplane.

6.1 DESIGN REQUIREMENTS AND APPROACH

The design requirements for the leading-edge device were—

a. The Krueger flap that replaces the Nos. 3 and 4 slats on the left wing must provide comparable high-lift capabilities to the slats, and the resulting asymmetrical leading-edge configuration must not cause unacceptable handling characteristics in low-speed flight.

b. The Krueger flap and its actuating mechanism must be compact, in order to leave room for the suction system ducting.

c. The Krueger flap in the deployed position must shield the suction surface leading edge from contamination resulting from insect accretion and other forms of flying debris during takeoff and landing.

d. The power to actuate the Krueger flap must be provided by the same torque tube that drives the rest of the slats to ensure simultaneous operation.

Because of the difficult kinematics of matching deployment of the Krueger and the three-position (retracted, gapped, or sealed) slat it was decided to modify the leading edge device control system to eliminate the sealed-leading-edge (takeoff) slat position. Therefore, only a two-position Krueger was required (retracted or deployed-with-gap).

6.2 PRELIMINARY STUDIES

Figure 6.2-1 shows the test setup and model configuration of the two-dimensional tests referred to previously. The chord of the Krueger flap was 12% of the wing chord. The main geometry variables were the flap deflection angle, the height of the flap trailing edge above the wing chord plane, and the gap between the flap trailing edge and the wing. The best high-lift characteristics were obtained at 45 deg deflection, with both gap and height at 2.2% chord.

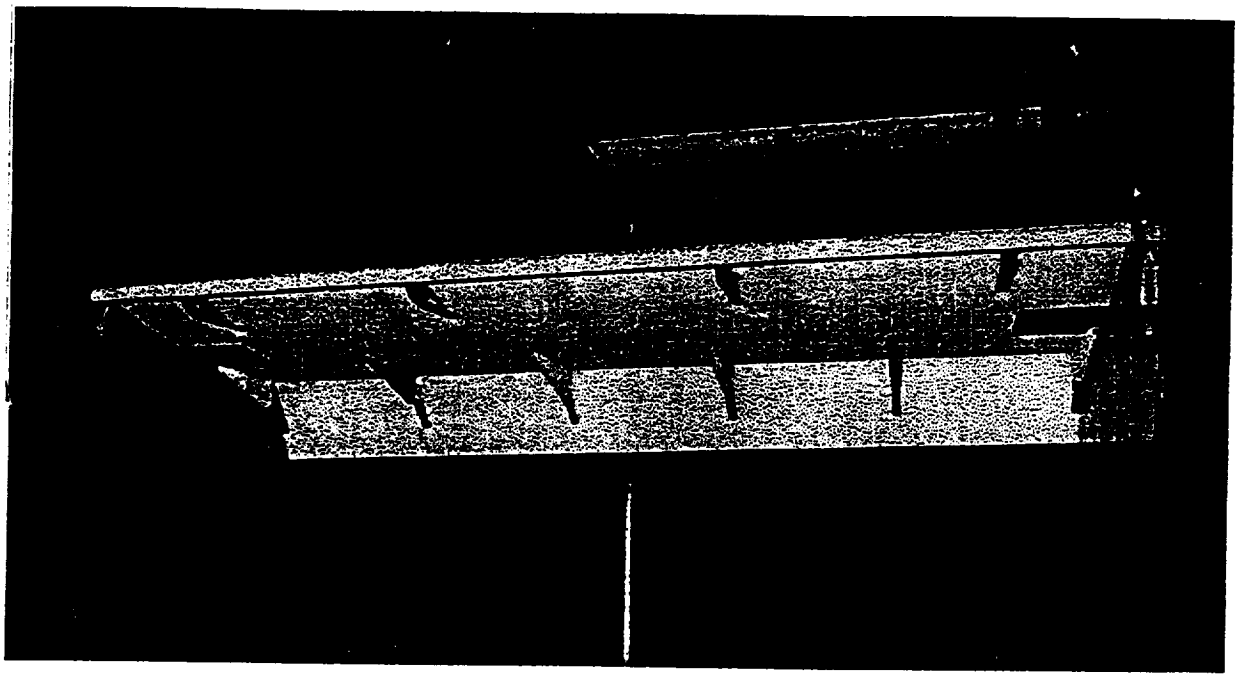

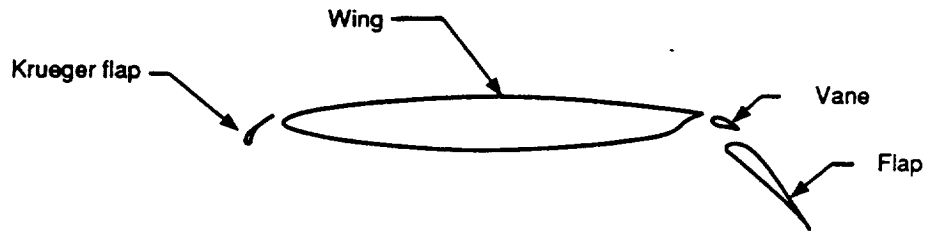

High-Lift Airfoil With Leading Edge Krueger Flap

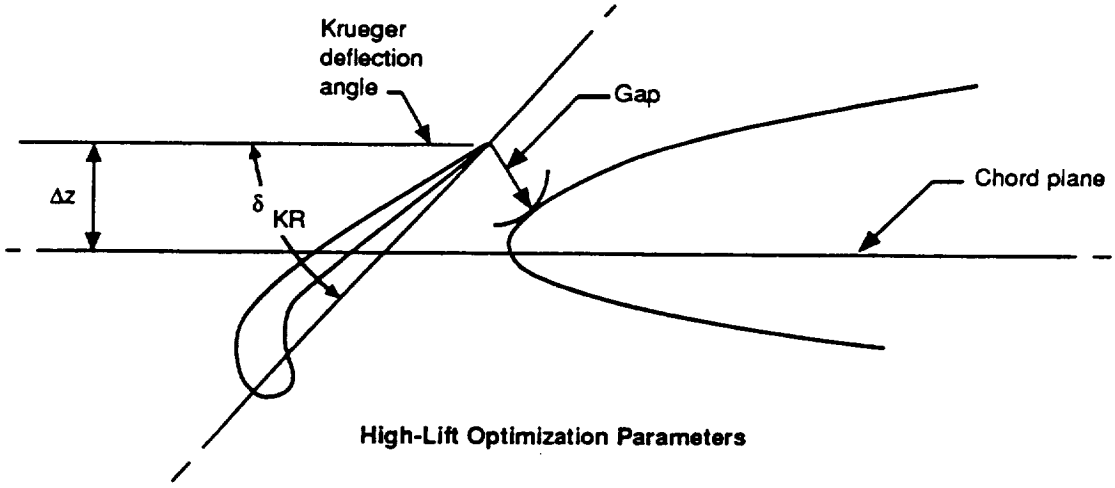

High-Lift Optimization Parameters

Figure 6.2-1. Two-Dimensional Wind Tunnel Test of a Dual-Purpose Krueger Flap

An apparatus was developed to inject insects into the wind tunnel flow. Three types of insects (spring tails, aphids, and fruit flies) were used for size variations, which at full scale would represent larger insects. Two critical conditions were investigated with the Krueger flap at the optimum high-lift position: (1) heavy insects at low angle of attack, as would be encountered during takeoff roll, and (2) light insects at high angle of attack, as encountered during climbout and approach. Results of this experiment are shown in figure 6.2-2 for all three species at the critical angles. These results are

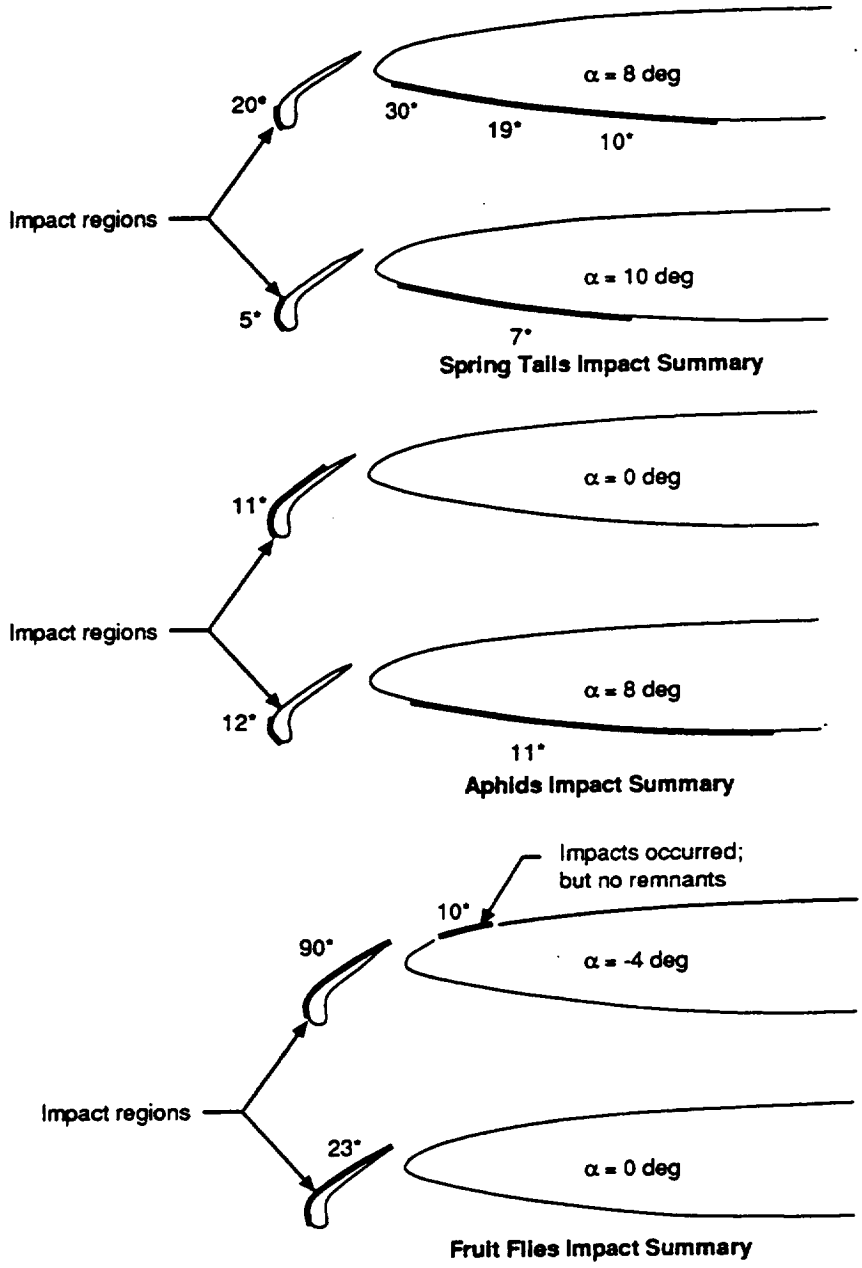

*Number of impacts.

Figure 6.2-2. Test Results on the Effectiveness of the Krueger Flap as Insect Shield

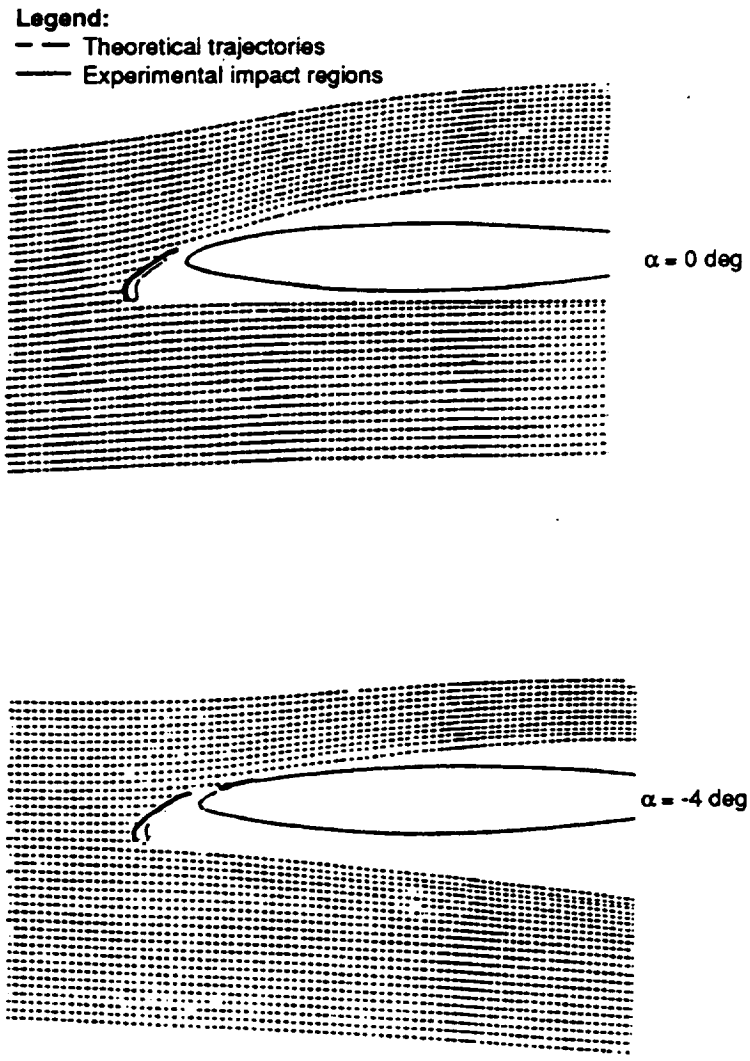

Figure 6.2-3. Comparison of Theoretical Trajectory Predictions of Fruit Flies Versus Test Results at 0 and -4 deg Angle of Attack

consistent with predictions based on particle trajectories computed using a two-dimensional multielement airfoil code (ref. 25) with an empirical model for lift and drag of insects derived by Bragg and Maresh (ref. 26) as shown in figure 6.2-3.

6.3 DESIGN INTEGRATION

A variable-camber Krueger flap similar to the one used on the Boeing 747 would have been needed to match the optimum geometry determined in the two-dimensional test discussed above, but it also would have added cost and complexity without contributing to the principal objectives of the program. It was found that the design goals could be met by changing the shape of the wing lower surface and incorporating a folding "bull-nose" leading edge as described in section 3.3. Figure 6.3-1

compares the desired aerodynamic contours and the final design. Some compromises were allowed in the hardware design to meet volume and kinematic constraints. For example, four small notches were cut in the bull-nose to provide clearance from the supporting ribs with the Krueger flap stowed. These are described in more detail in volume III of this report.

6.4 LOW-SPEED WIND TUNNEL TEST

A three-dimensional low-speed wind tunnel test was performed on a 0.055 scale model of the 757 in the 8- by 12-ft wind tunnel of the University of Washington Aeronautical Laboratory (UWAL), with the HLFC Krueger and modified leading edge installed. The purpose was to identify

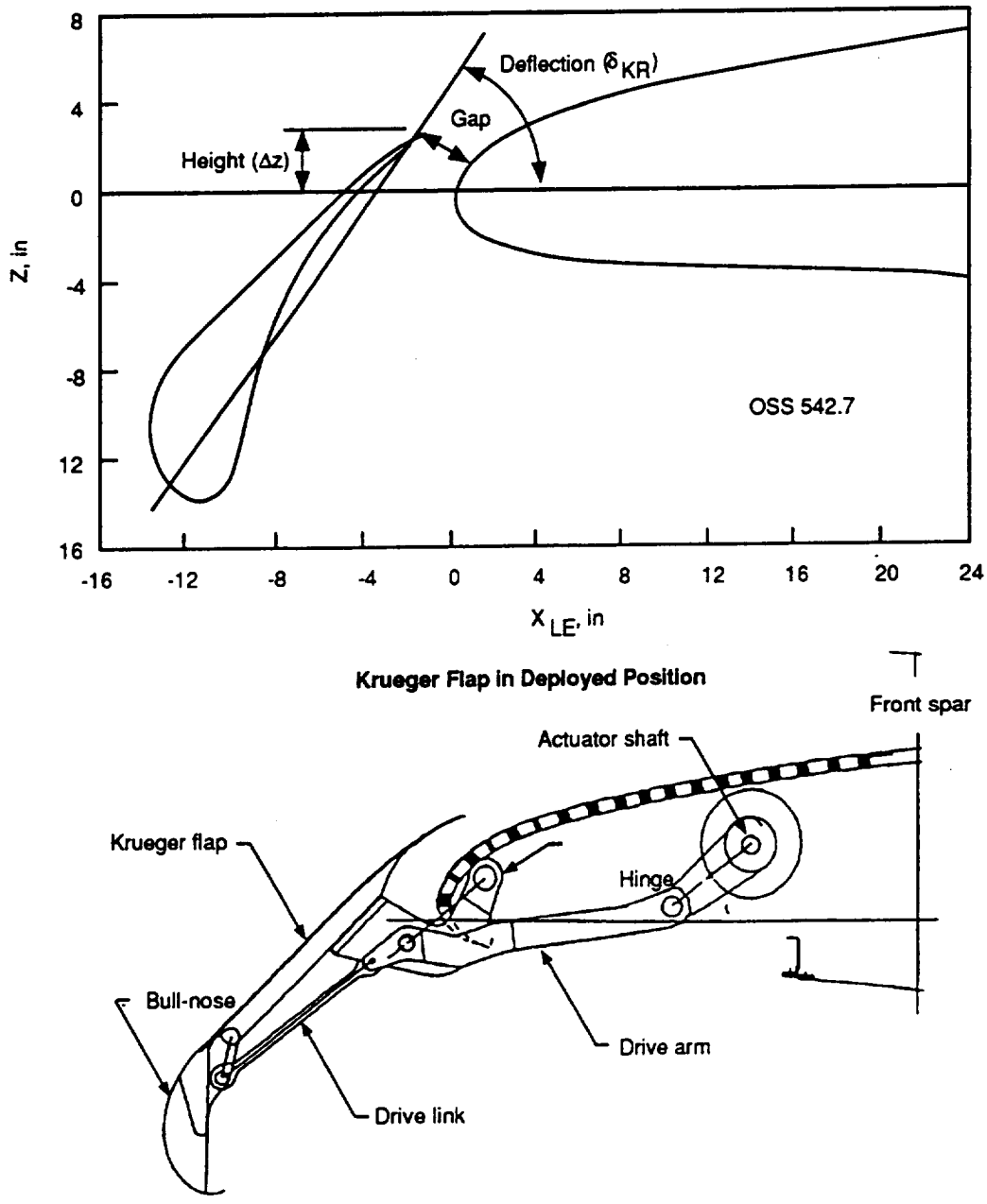

Figure 6.3-1. Comparison of the Requested and Produced Krueger Geometries

incremental low-speed performance and stability and control changes attributable to the HLFC modifications. The model was tested both in free air and in ground effect, as shown in figure 6.4-1. Testing was conducted at a dynamic pressure of 60 lb/ft^2, which corresponds to a Reynolds number of 1.3 million, based on mean aerodynamic chord.

The test included several trailing edge flap positions used during takeoff and landing. In addition to the basic Krueger configuration, notches in the leading-edge bull-nose (fig. 6.4-2) were also evaluated. A feature that caused some concern was the discontinuity between the Krueger and the slat at the outboard end of the HLFC test span, as shown in figure 6.4-3. This discontinuity was unavoidable because of the geometric differences between the two systems. Flow visualization photographs revealed that there was a large area of separated flow downstream of the leading edge discontinuity at high angles of attack. A large rolling moment resulted from the unsymmetrical stall, as shown in figure 6.4-4. A Krueger end-seal was installed between the Krueger and the slat (see fig. 6.4-2) was found to reduce the maximum unsymmetrical moment by more than 50% up to 24 deg angle of attack. Figure 6.4-5 shows the observed flow patterns for the baseline wing and for the modified wing with and without the Krueger end-seal at 18 deg angle of attack (just beyond stall).

The test showed that the lift capability of the modified wing was only slightly impaired, resulting in a $C_{L_{max}}$ decrement of 0.05, corresponding to about a 1.3-kn increase in stall speed. The Krueger end-seal at the end of the Krueger made the stall less abrupt, but did not increase $C_{L_{max}}$. Figure 6.4-6 shows the lift curves with the Krueger flaps installed, with and without the Krueger end-seal, in comparison to the baseline configuration with the slats in both the takeoff and the landing positions.

The drag of the modified configuration did not change much relative to the baseline when the slats were in the landing position. In the takeoff position, the slats showed somewhat lower drag. Thus, the Krueger, in landing configuration required to prevent insect accretion, would have a drag penalty during initial climb. The measured drag characteristics are shown in figure 6.4-7 for the case of 20 deg trailing edge flap deflection.

The pitching moment data did not indicate changes in the longitudinal characteristics great enough to require different handling or trimming of the airplane. Furthermore, the notches in the Krueger leading edge had no significant effects on airplane performance and stability characteristics. However, the rolling moment due to unsymmetrical stall was still a matter of great concern. While the problem could have been significantly alleviated by the Krueger end-seal, it was decided not to use it because of the complexity and cost. Instead, safety was ensured by prohibiting intentional stalls and by adjusting the stall warning stick shaker.

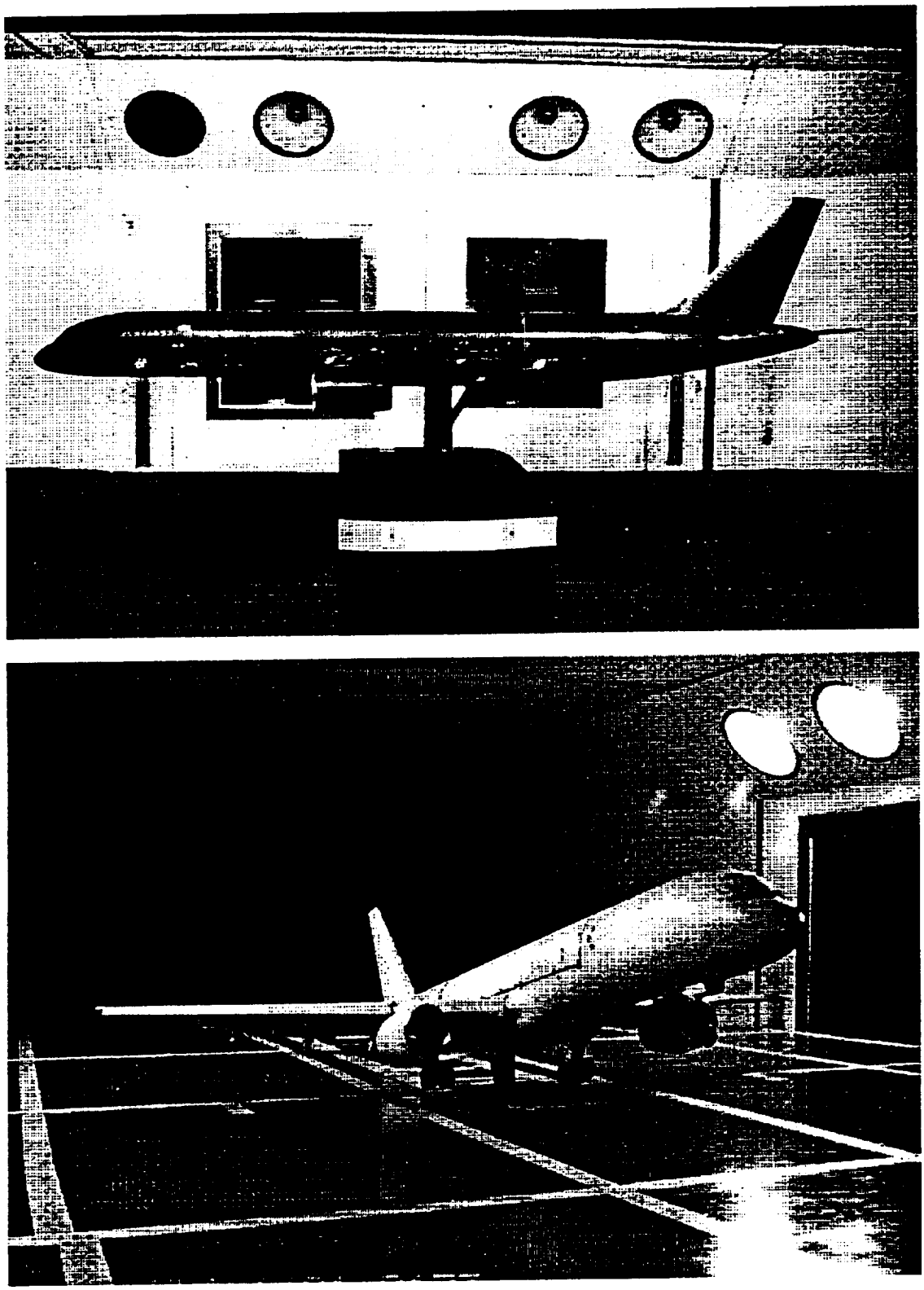

Figure 6.4-1. Low-Speed Wind Tunnel Model of the Boeing 757 With HLFC Modifications Installed in the UWAL Wind Tunnel

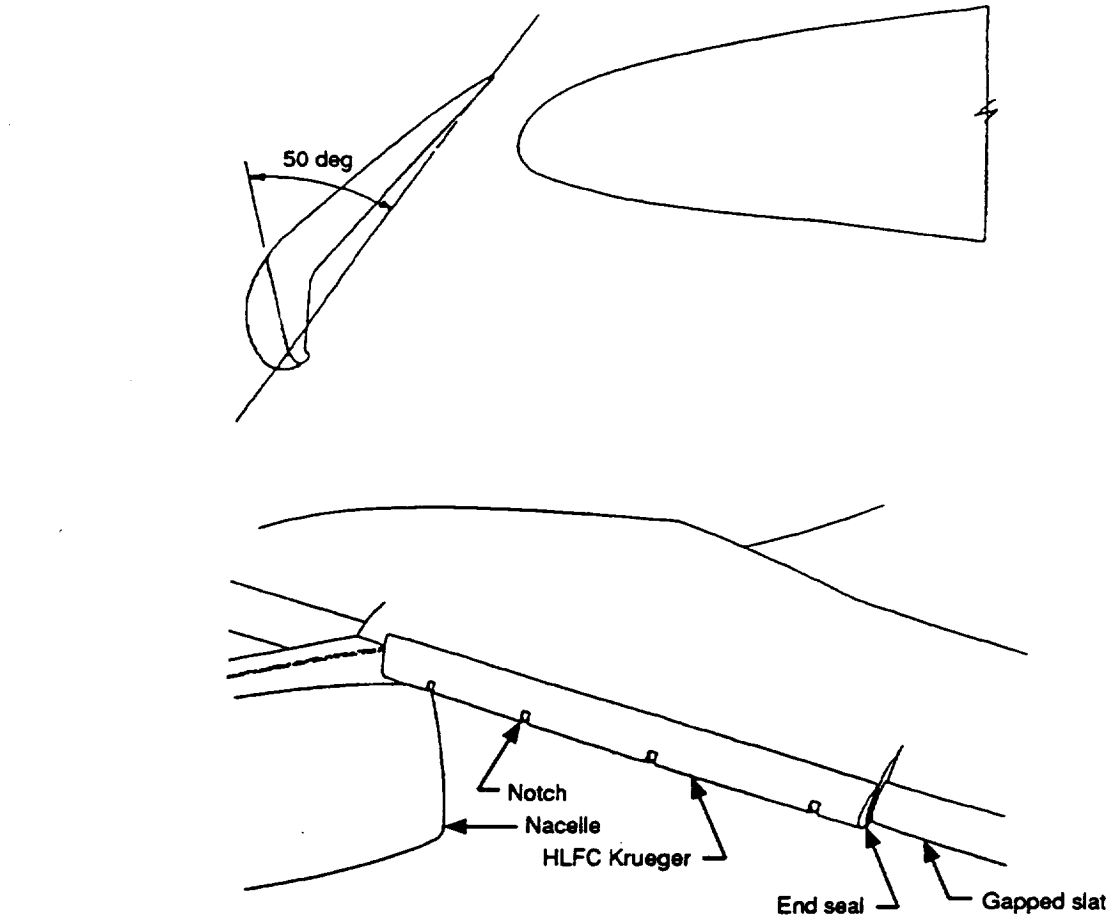

Figure 6.4-2. Notches in the Krueger Leading Edge

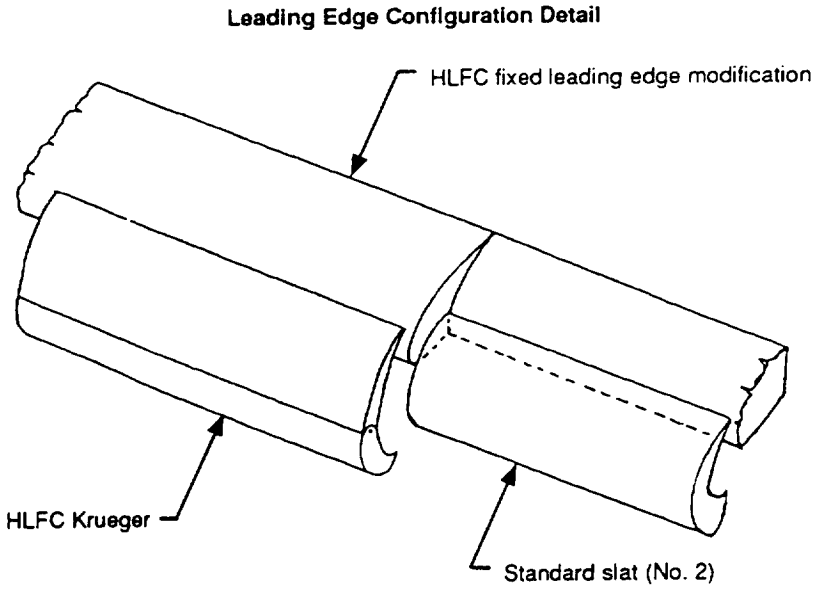

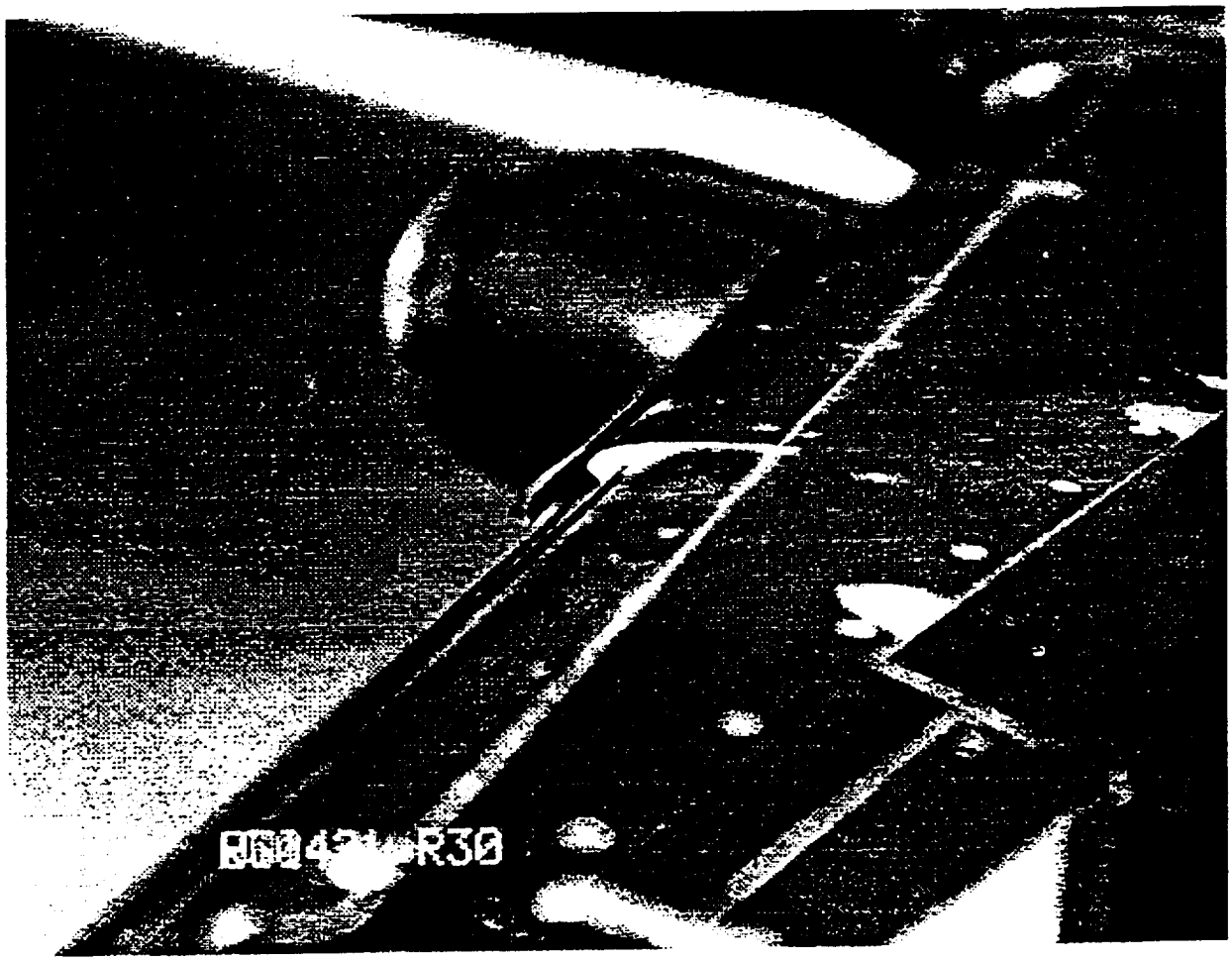

Figure 6.4-3. Mismatch of Krueger and Slat Contours at the Outboard Edge of the HLFC Test Area

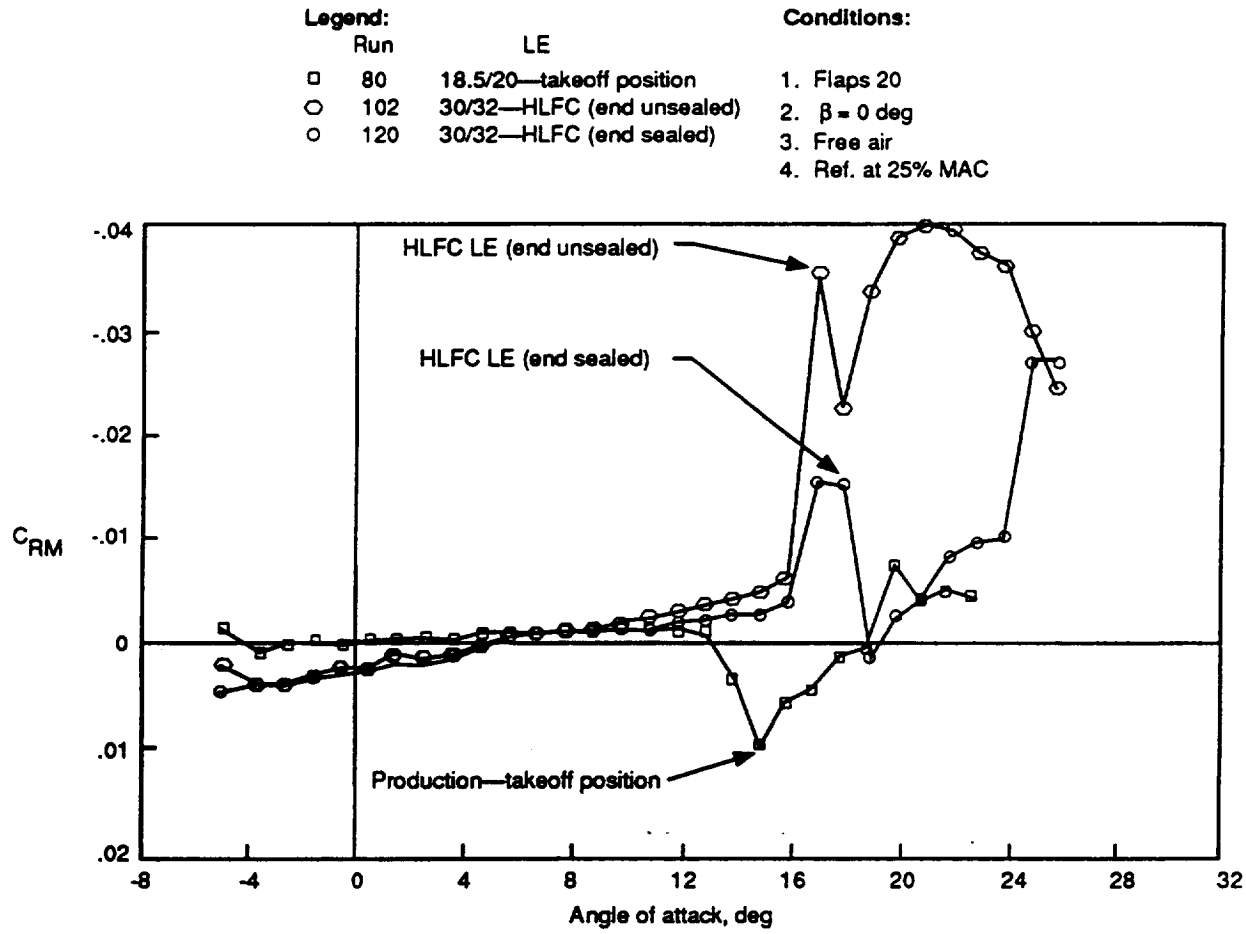

Figure 6.4-4. Low-Speed Test Results—Rolling Moment

Baseline Production Gapped

$\alpha = 18$ deg

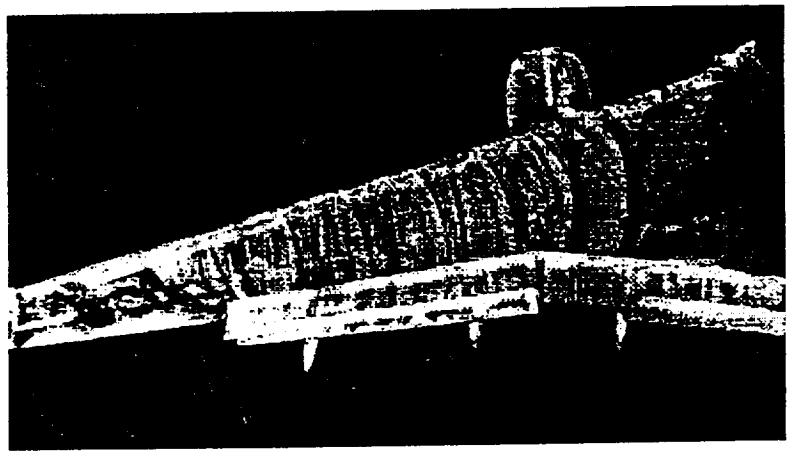

Krueger Without End Seal

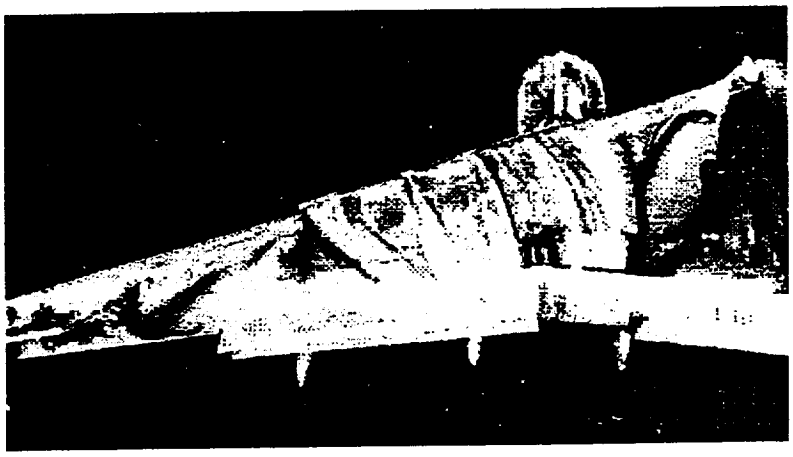

Krueger With End Seal

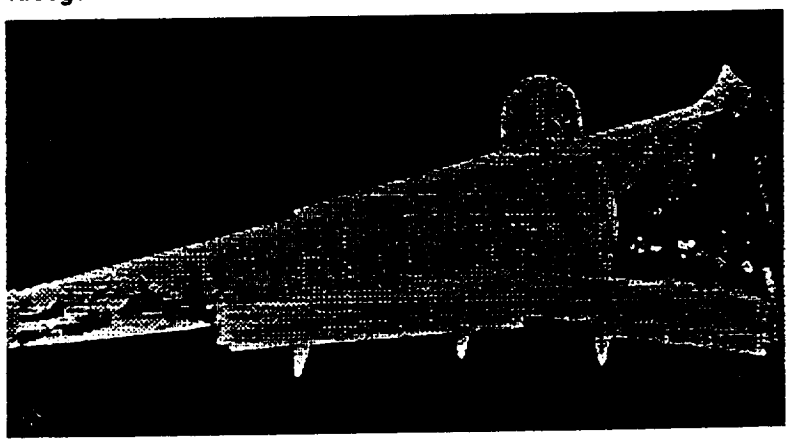

Figure 6.4-5. Effect of Krueger End Seal on Wing Flow Pattern—China Clay Flow Visualization

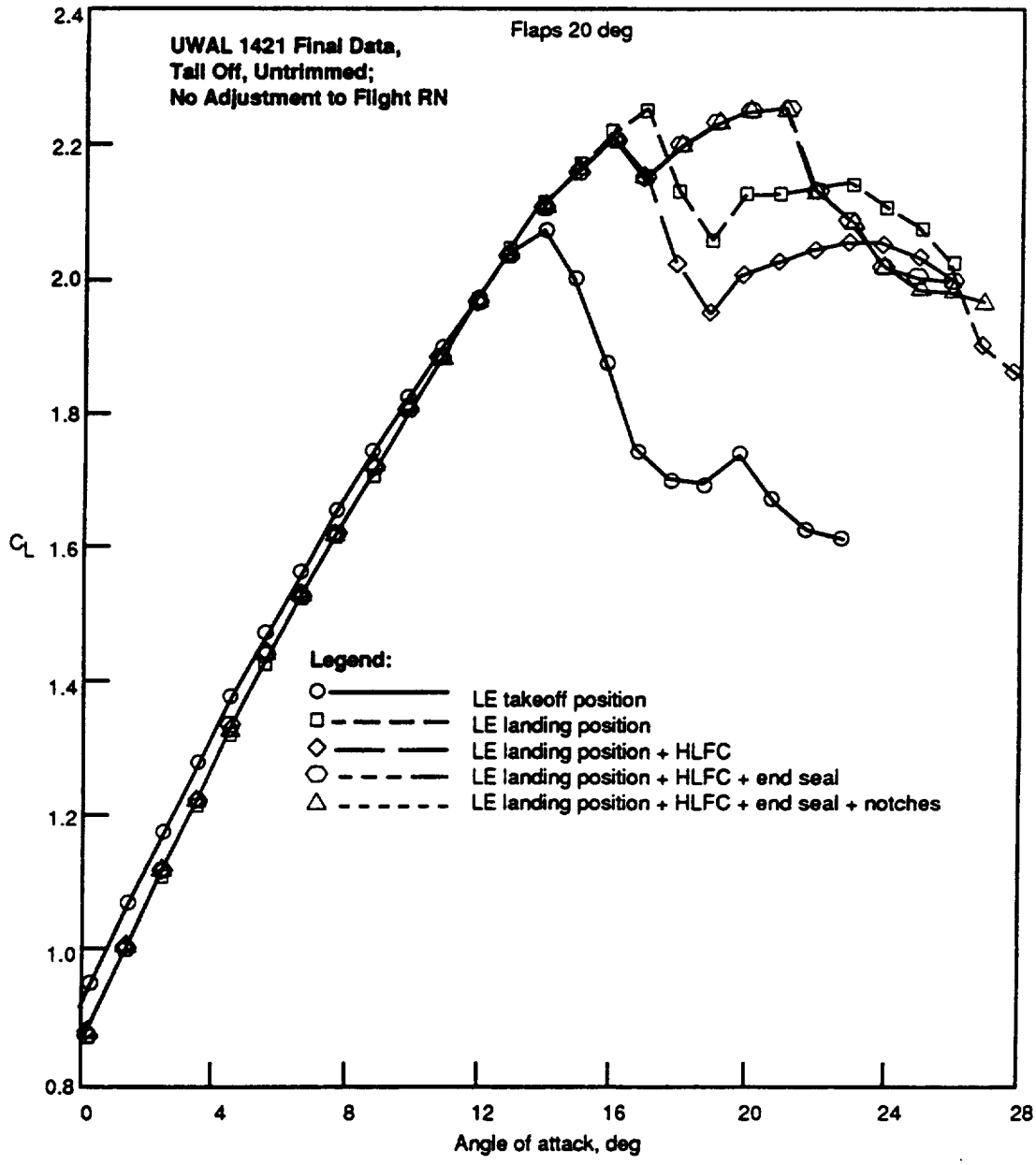

Figure 6.4-6. Low-Speed Test Results—Lift Curves

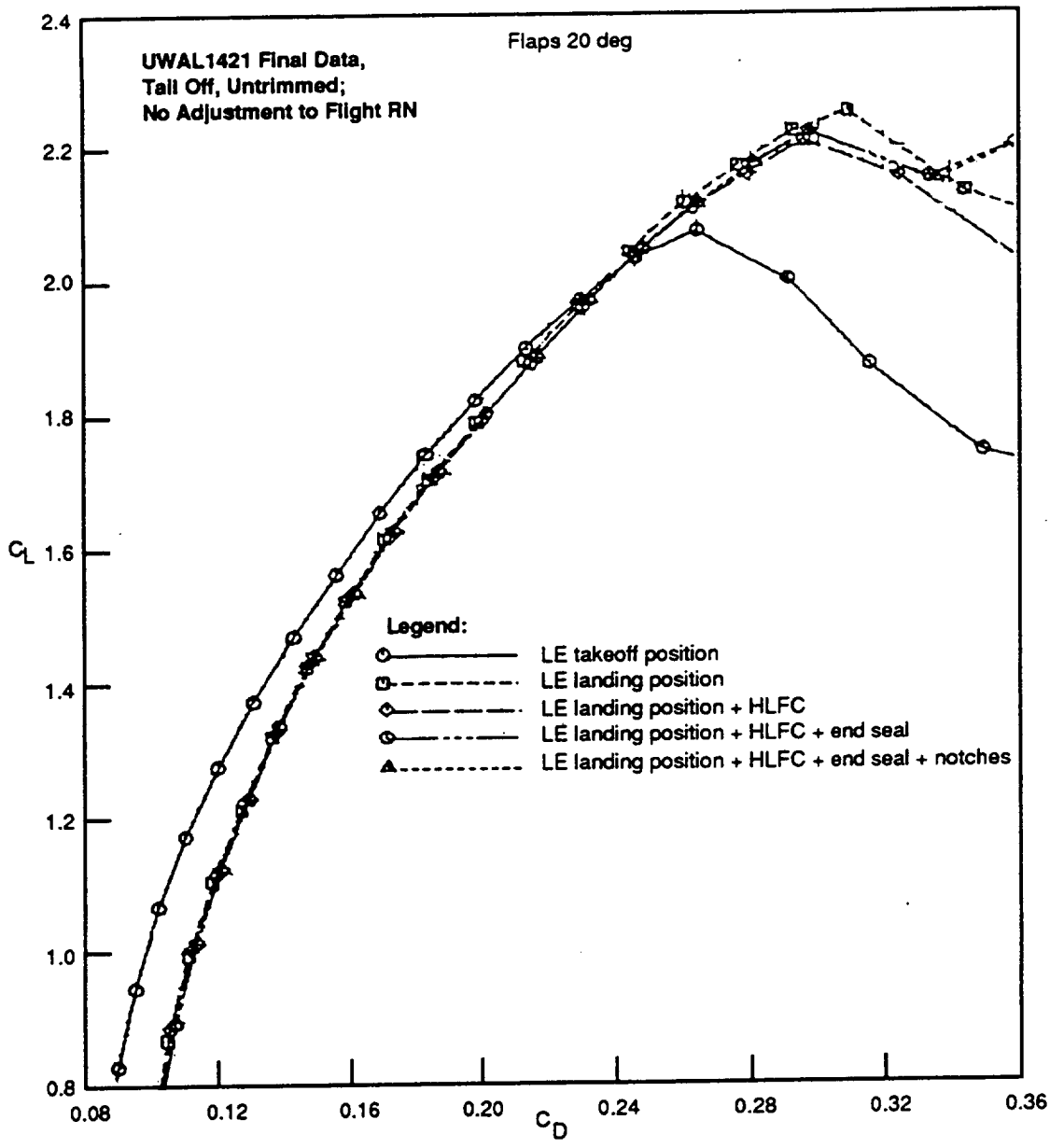

Figure 6.4-7. Low-Speed Test Results—Drag Polars

This page intentionally left blank

7.0 CONCLUDING REMARKS

7.1 LESSONS LEARNED

The remarks below summarize salient points and lessons learned from the design study reported here, which provided the geometry and suction requirements for a 20-ft long hybrid laminar flow control test panel for a Boeing 757 wing.

a. The design was based entirely on analysis, except for a wind tunnel test to validate the flaps-down characteristics of the modified airplane. Design of the HLFC leading edge contours was accomplished using a three-dimensional, transonic viscous-flow computer code system. The estimates of suction requirements and achievable extent of laminar flow were made on the basis of boundary layer stability analysis using the USS computer code and an empirically determined transition criterion.

b. The requirements of HLFC added a dimension to the wing aerodynamic design problem, because restricting suction to the area forward of the front spar puts new constraints on tailoring the profile for compressibility drag and lift coefficient.

c. The original contours of the outboard wing provided pressure distributions that would be acceptable for HLFC. However, a slight modification of the leading edge geometry ahead of the front spar further enhanced the flow characteristics, resulting in reduced crossflow instability and therefore a reduced suction requirement. Repeated smoothing of the computer-generated contours was necessary in both chordwise and spanwise directions to arrive at a surface definition that met the stringent waviness criteria for laminar flow.

d. Desirable pressure distributions for HLFC in the vicinity of the engine nacelle could not be provided within the design constraints. Nacelle interference effects caused an extended pressure gradient there, which increased crossflow instability.

e. Investigation of off-design flight conditions showed the most favorable pressure distributions for extensive laminar flow in cruise occur at somewhat higher values of both Mach number and lift coefficient than the design point (Mach 0.80 at $C_L = 0.50$). In both climb and descent a pronounced pressure peak near the leading edge would likely preclude achievement of extensive laminar flow.

f. Accurate pressure predictions are very important to the design of a laminar-flow wing because boundary layer stability, and hence suction requirements, critically depend on them. Flight test results obtained later in the program (to be reported in volume I) revealed certain characteristic differences from the CFD predictions, such as shock locations farther aft and more pronounced pressure peaks.

g. The transition prediction method used in this study was based on an empirical criterion derived from data showing significant scatter. Computed transition locations and suction requirements are therefore uncertain. After the analytical work described in this report had been completed, a revised transition criterion was proposed with the inclusion of the latest data obtained with the F-14 VSTFE airplane. The revised criterion indicated less sensitivity to crossflow amplification than the one used in the present study, and it would have reduced the predicted suction requirement.

h. The best suction distributions obtained in the study had a high-suction region extending from the leading edge to the end of the steep initial pressure gradient, followed by a longer low-suction zone. A gradual transition between the high- and low-suction regions was found to be advantageous. The required suction flow coefficient (C_Q) at the design condition is

4.72×10^{-5}, requiring a mass flow rate for the HLFC test panel of 8.2 lb/min.

i. The stability analyses indicated that laminar flow could be sustained at least back to the pressure recovery line (or shock location), at about 45% chord over the outboard half of the HLFC test panel. Inboard, because of nacelle interference effects, the pressure recovery and transition front would be farther forward, at about 35% chord.

j. The HLFC test panel leading edge was calculated to be marginal with respect to attachment-line turbulence contamination. A leading edge suction patch was therefore provided just inboard of the panel, vented to a low-pressure point on the lower surface to provide suction independently of the main suction system.

k. A low-speed wind tunnel test of a 757 model with the modified leading edge devices showed that the maximum lift capability would be slightly compromised by replacing two slats by the dual-purpose Krueger flap, but that the modification would not significantly alter the low-speed performance of the test airplane.

7.2 RECOMMENDATIONS

Further studies are recommended in the following areas:

a. **Pressure Prediction Methods.** CFD codes should be correlated with flight test pressure survey results, as well as with wind tunnel data, and means should be sought to improve the accuracy of shock location and pressure peak prediction.

b. **Wing/Nacelle Integration.** Nacelle, strut, and wing contours that minimize spanwise pressure gradients and provide straight isobars are needed in order to maximize the extent of laminar flow and simplify HLFC suction system design.

c. **Transition Prediction Methods.** Further analysis and correlation efforts are needed to reduce the uncertainty of the predicted transition point.

d. **Leading Edge High-Lift/Insect Protection Devices.** The drag penalty resulting from the gap between the Krueger flap and the fixed leading edge at the takeoff flap setting should be reduced or eliminated.

8.0 REFERENCES

1. Jameson, A., and Caughey, D. A., "Recent Progress in Finite Volume Calculations for Wing-Fuselage Combinations," AIAA Paper No. 79-1513, July 1979.

2. McLean, J. D., and Randall, J. L., "Computer Program To Calculate Three-Dimensional Boundary Layer Flows Over Wings With Mass Transfer," Program User's Document, NASA CR-158967, December 1978.

3. Rozendaal, R. A., and Behbehani, R., "Variable Sweep Transition Flight Experiment (VSTFE) - Unified Stability System (USS), Description and User's Manual," NASA CR-181918, July 1989.

4. Mack, L. M., "Boundary Layer Stability Theory," AGARD Report No. 709, 1984.

5. Runyan, L. J., Navran, B. H., and Rozendaal, R. H., "F-111 Natural Laminar Flow Glove Flight Test Data Analysis and Boundary Layer Stability Analysis," NASA CR-166051, January 1984.

6. Boeing Commercial Airplane Company, "Flight Survey of the 757 Wing Noise Field and Its Effects on Laminar Boundary Layer Transition," NASA CR-178216, March 1987.

7. Northrop Corporation, "Final Report on LFC Aircraft Design Data, Laminar Flow Control Demonstration Program," Northrop Report NOR 67-136, June 1967.

8. Fisher, D. F., and Fischer, M. C., "The Development Flight Tests of the JetStar LFC Leading Edge Flight Test Experiment," NASA CP 2487, 1987.

9. Wagner, R. D., Maddalon, D. V., Bartlett, D. W., Collier, F. S., and Braslow, A. L., "Laminar Flow Flight Experiments," NASA CP 3020, Transonic Aerodynamics Symposium, NASA Langley Research Center, 1988.

10. Maddalon, D. V., and Braslow, A. L., "Simulated-Airline-Service Flight Tests of Laminar Flow Control With a Perforated Surface Suction System," NASA TP 2966, March 1990.

11. Boeing Commercial Airplane Company, "Hybrid Laminar Flow Control Study—Final Technical Report," NASA CR-165930, October 1982.

12. Boeing Commercial Airplane Company, "Evaluation of Laminar Flow Control System Concepts for Subsonic Commercial Transport Aircraft—Final Technical Report," NASA CR-158976, December 1978.

13. Carmichael, B. H., "Summary of Past Experience in Natural Laminar Flow," NASA CR-152276, May 1979.

14. Holmes, B. J., et al., "Manufacturing Tolerances for Natural Laminar Flow Airframe Surfaces," SAE Paper No. 85-0863, April 1985.

15. George-Falvy, D., "In Quest of the Laminar Flow Airliner: Flight Experiments on a T-33 Jet Trainer," paper presented at the IXth Hungarian Aeronautical Sciences Conference, Budapest, Hungary, November 1988.

16. Pfenninger, W., and Vemuru, C. S., "High Subsonic LFC Transport Airplanes: Boundary Layer Crossflow Stabilization, Wing Analysis and Design," AIAA Paper No. 88-0275, AIAA 26th Aerospace Sciences Meeting, Reno, Nevada, January 1988.

17. Gray, W. E., "The Effect of Wing Sweep on Laminar Flow," RAE TM Aero 255, 1952.

18. Landeryou, R. R., and Trayford, R. S., "Flight Tests of a Laminar Flow Swept Wing With Boundary Layer Control by Suction," Report Aero No. 174, The College of Aeronautics, Cranfield, June 1964.

19. Pfenninger, W., "Flow Problems of Swept Low-Drag Suction Wings of Practical Construction at High Reynolds Numbers," Annals of the New York Academy of Sciences, Vol. 154, Art. 2, November 1968.

20. Maddalon, D. V., Collier Jr., F. S. Montoya, L. L., and Land, C. K., "Transition Flight Experiments on a Swept Wing With Suction," AIAA Paper No. 89-1893, June 1989.

21. Gaster, M., "On the Flow Along Swept Leading Edges," Aeronautical Quarterly, May 1967.

22. Gaster, M., "A Simple Device for Preventing Turbulent Contamination on Swept Leading Edges," Journal of the Royal Aeronautical Society, November 1965.

23. Landeryou, R. R., and Porter, P. G., "Further Tests of a Laminar Flow Swept Wing with Boundary Layer Control by Suction," Report Aero No. 192, The College of Aeronautics, Cranfield, May 1966.

24. Brune, G. W., Tamigniaux, T. L. B., and Stark, S. E., "An Experimental Investigation of the Insect Shielding Effectiveness of a Krueger Flap/Wing Airfoil Configuration," AIAA Paper No. 87-2615, August 1987.

25. Tamigniaux, T. L. B., Stark, S. E., and Brune, G. W., "An Experimental Investigation of the Insect Shielding Effectiveness of a Krueger Flap/Wing Airfoil Configuration," AIAA Paper No. 87-2615-CP, August 1987.

26. Bragg, M. B., and Maresh, J. L., "A Numerical Method to Predict the Effect of Insect Contamination on Airfoil Drag," Ohio State University A&A Engineering Report, AARL 86-01, March 1986.

Appendix A

Geometry Comparisons Between the HLFC and the 757 Wings

This appendix presents comparisons of airfoil contours between the basic Boeing 757 wing and the modified HLFC test section at 10 spanwise stations from WBL 270 to WBL 513.

The x coordinates are body station values, and the z coordinates are measured vertically from the wing definition plane. The units are inches for both.

The dashed lines are the original 757 profiles, while the solid lines show the HLFC contours.

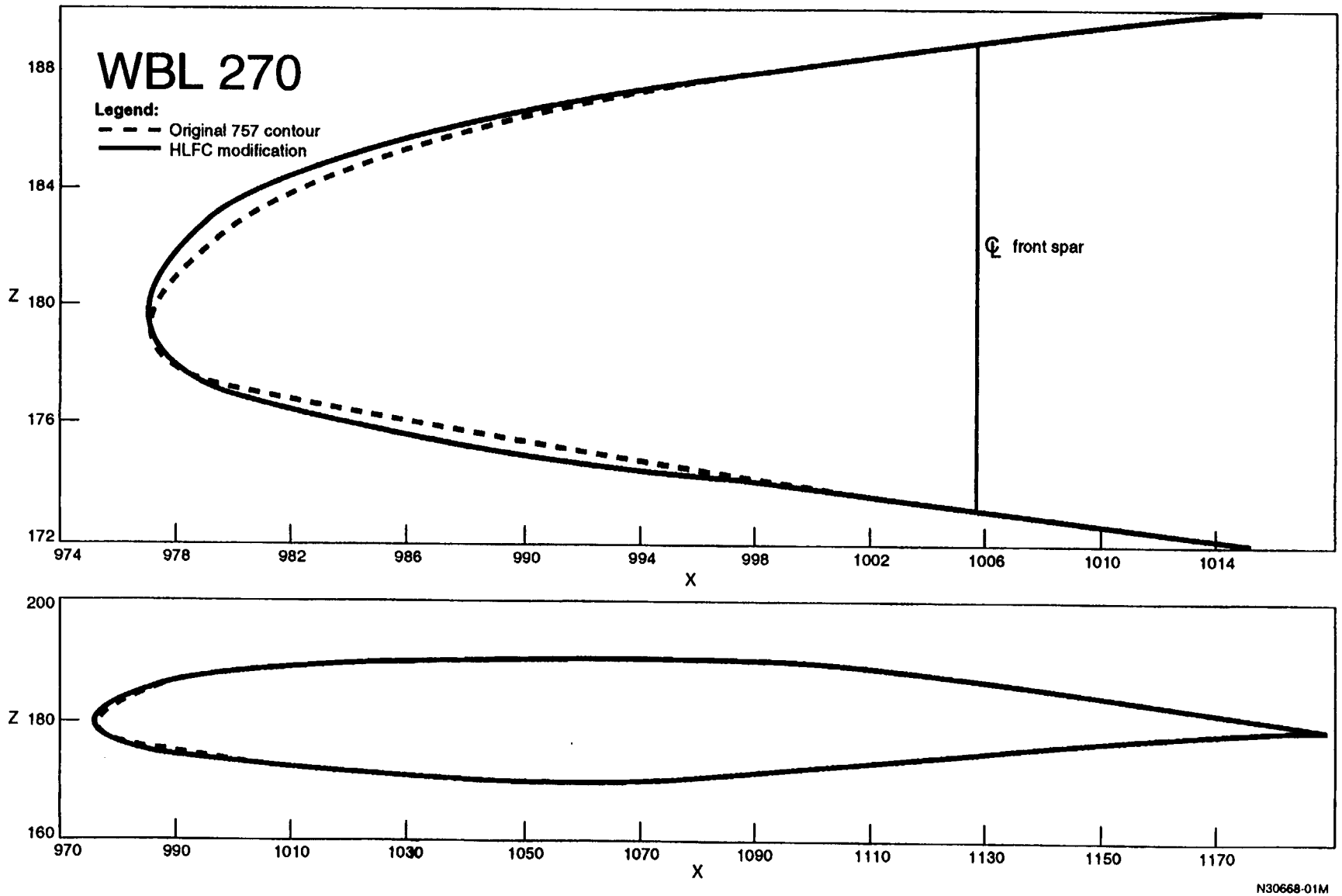

Figure A-1. HLFC and Original 757 Airfoil Contours, WBL 270

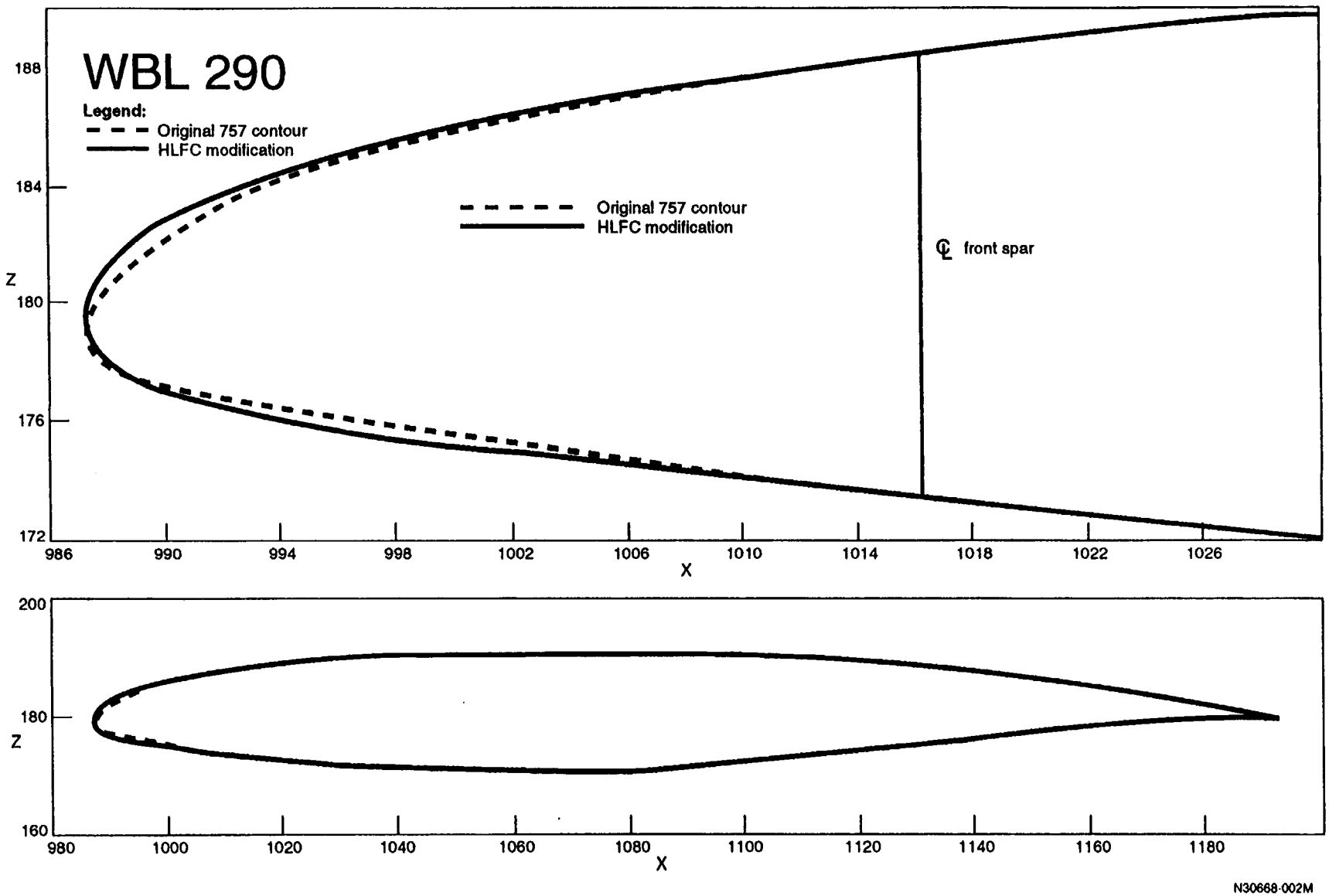

Figure A-2. HLFC and Original 757 Airfoil Contours, WBL 290

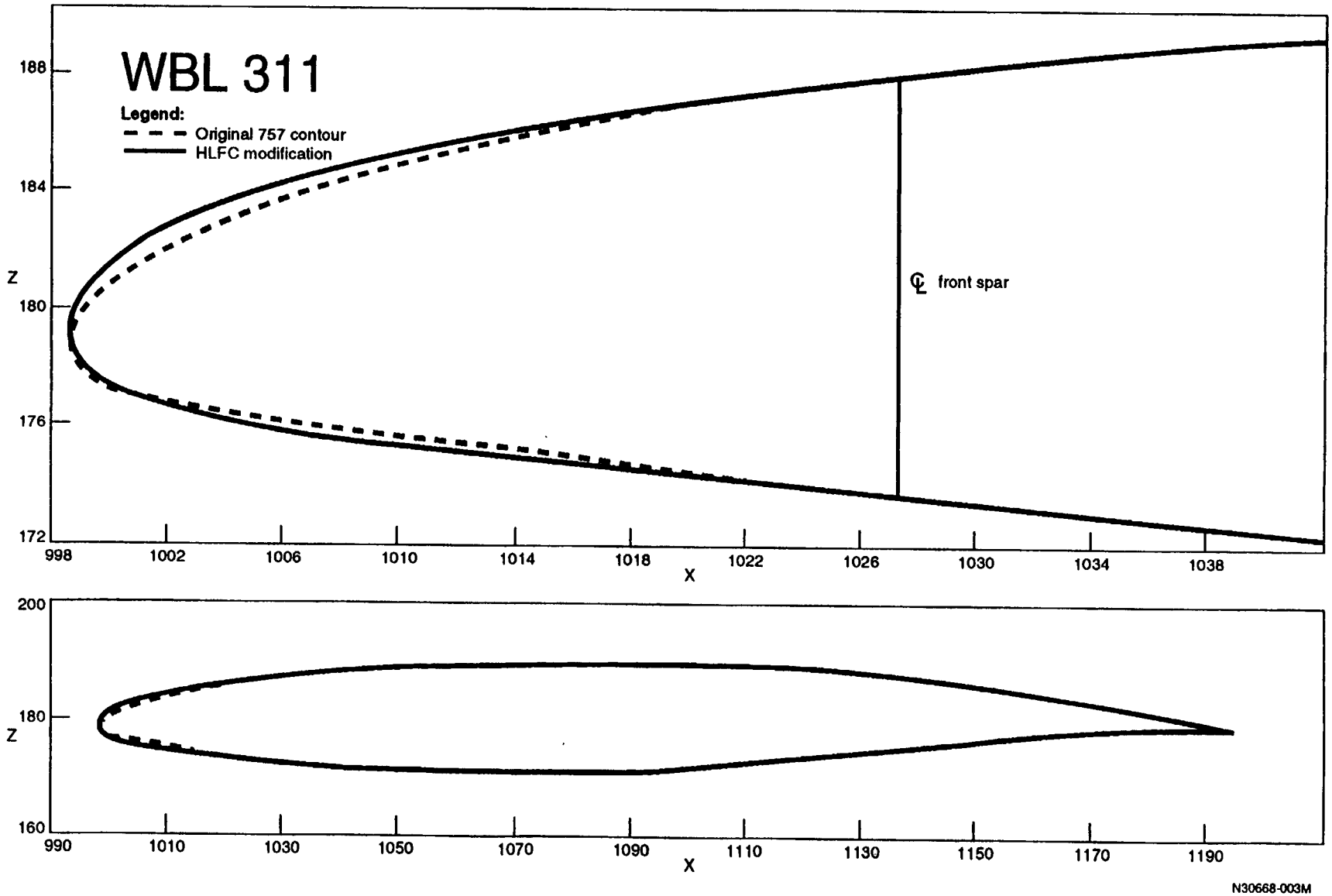

Figure A-3. HLFC and Original 757 Airfoil Contours, WBL 311

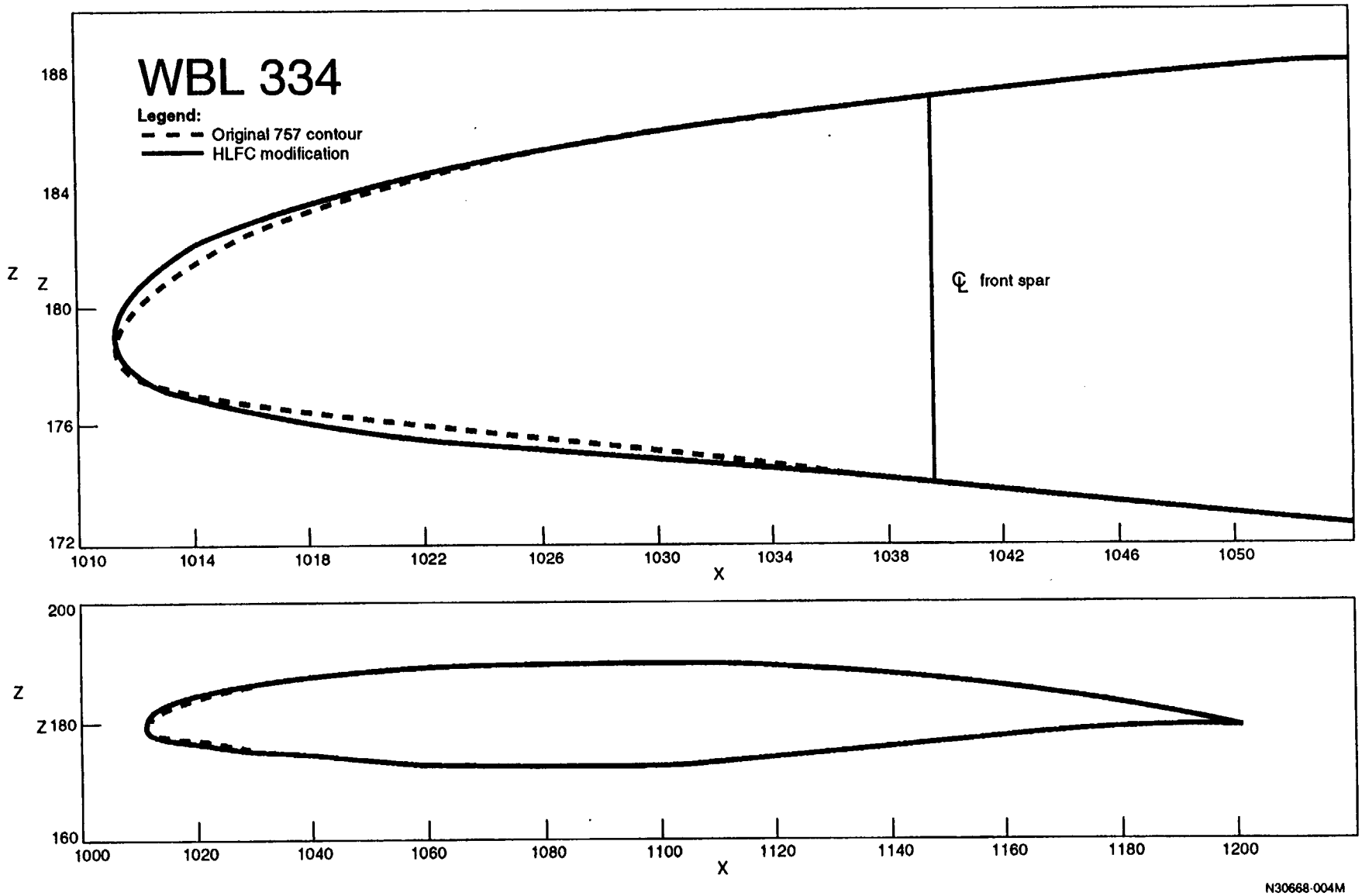

Figure A-4. HLFC and Original 757 Airfoil Contours, WBL 334

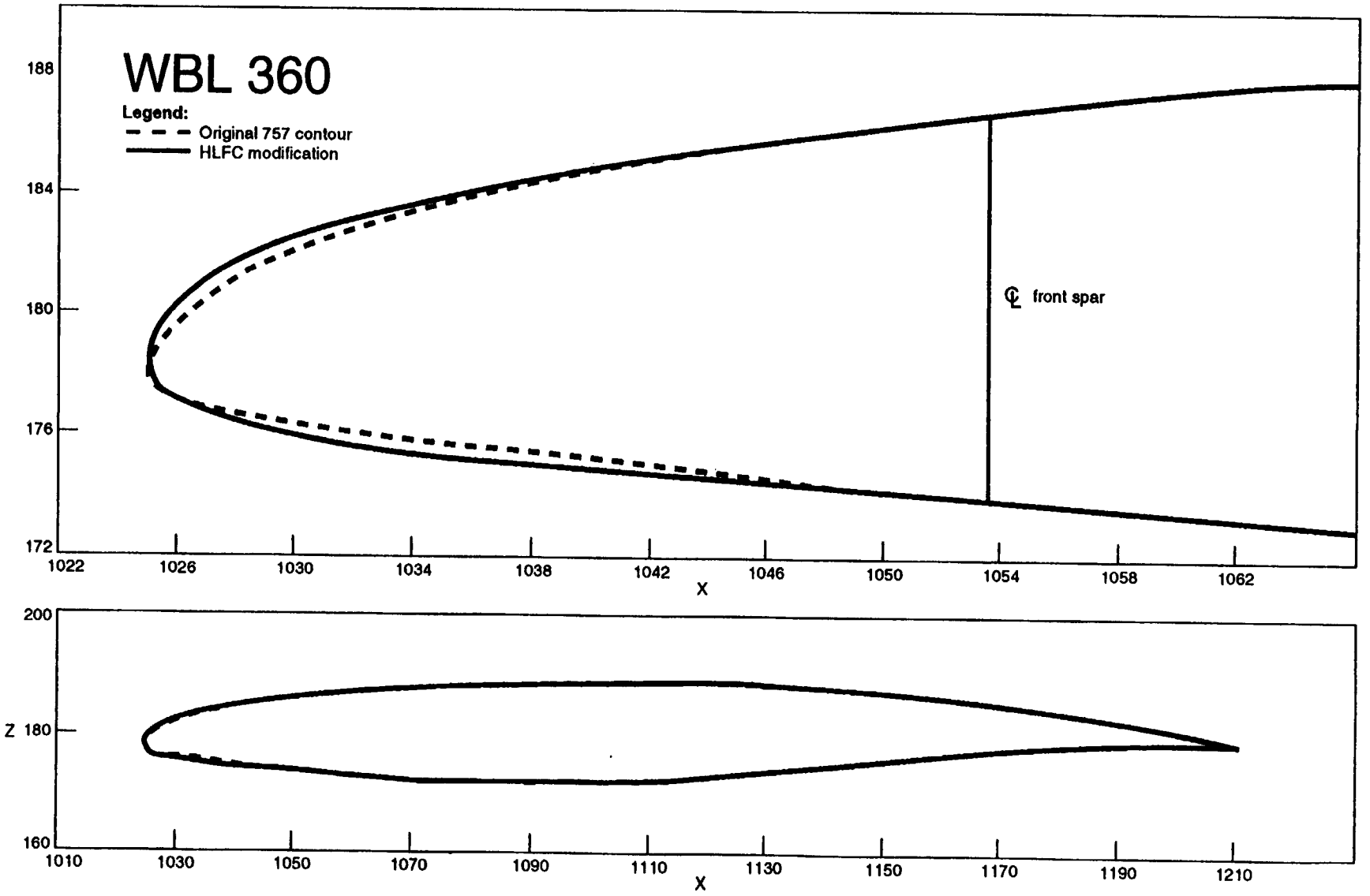

Figure A-5. HLFC and Original 757 Airfoil Contours, WBL 360

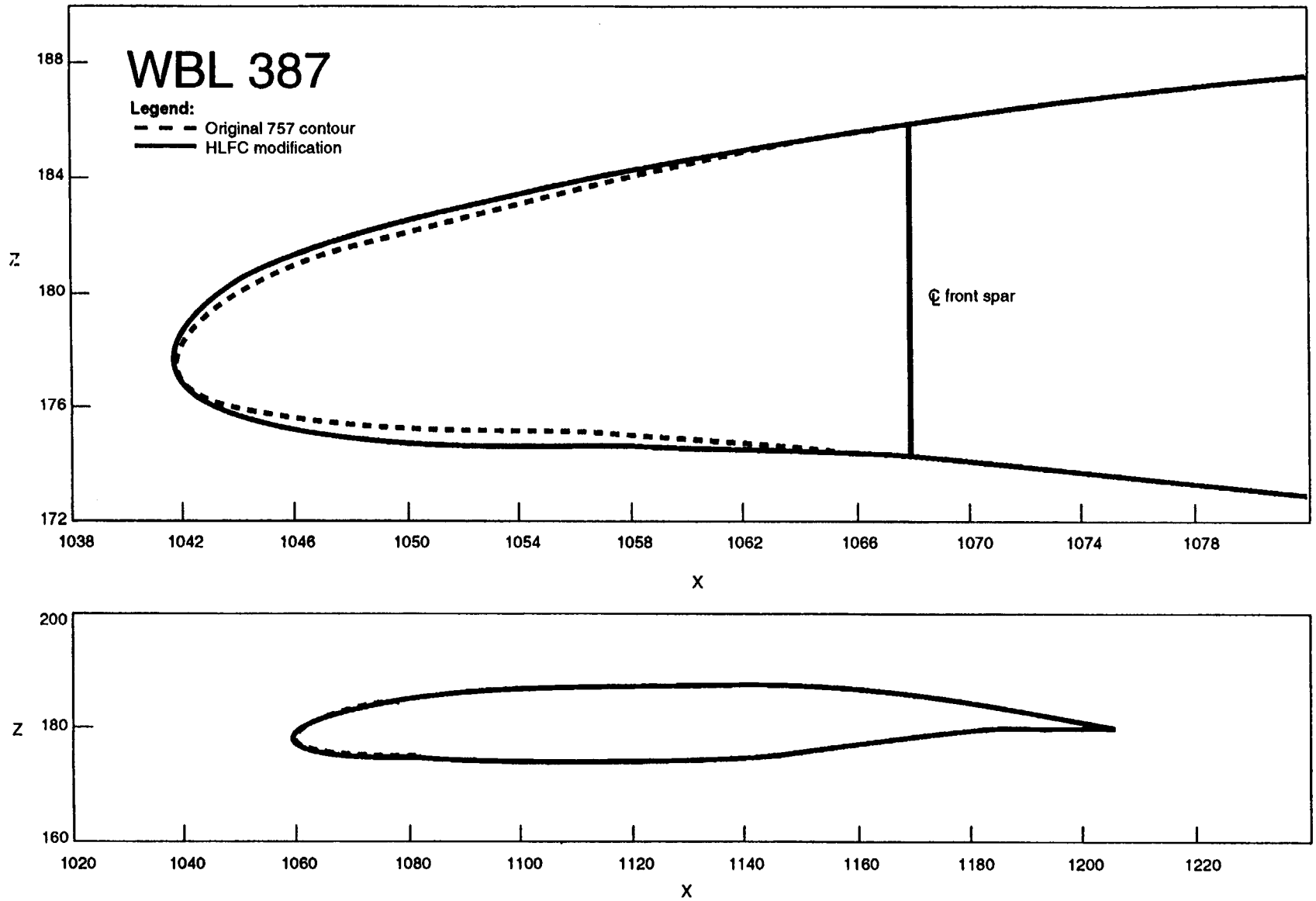

Figure A-6. HLFC and Original 757 Airfoil Contours, WBL 387

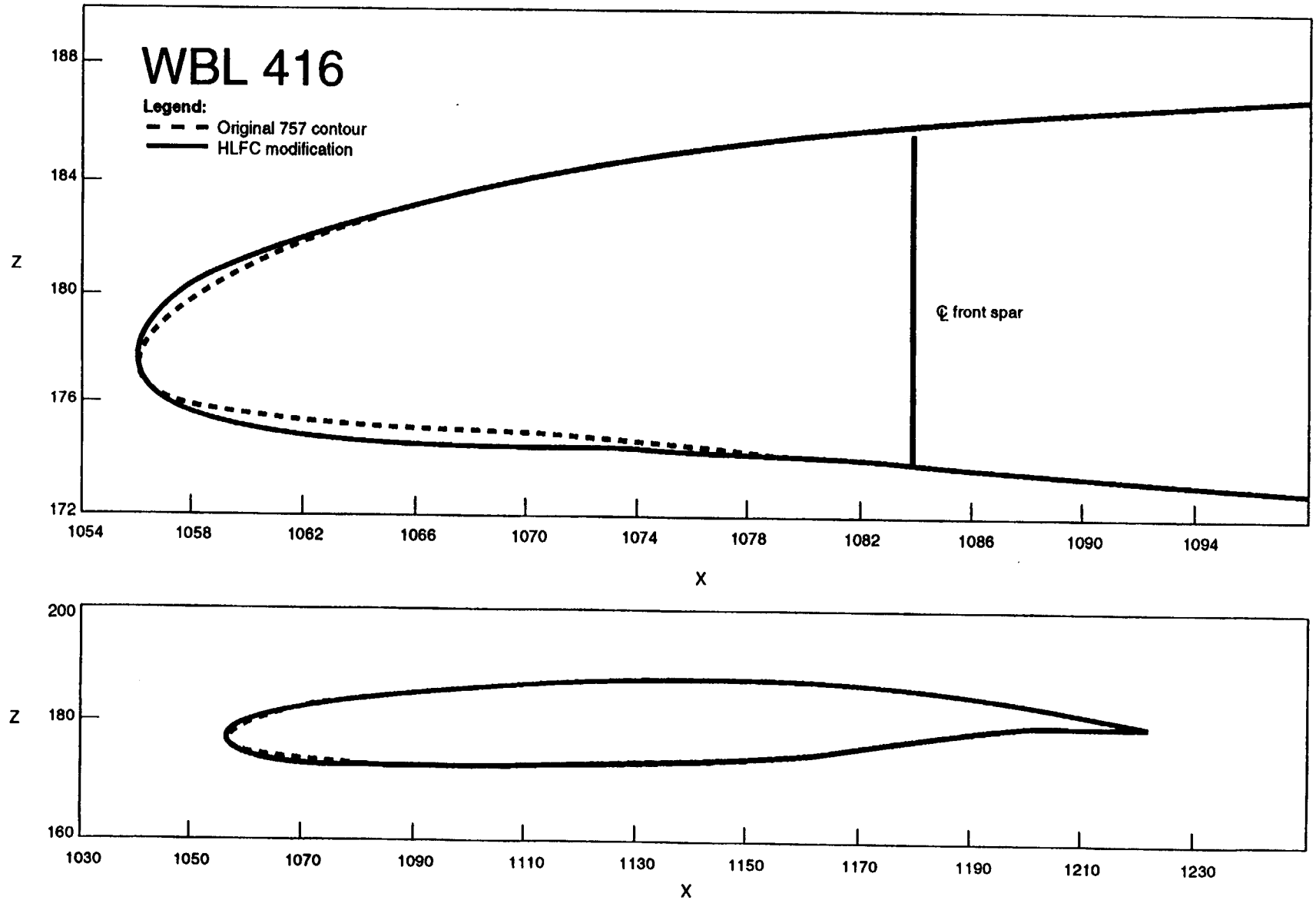

Figure A-7. HLFC and Original 757 Airfoil Contours, WBL 416

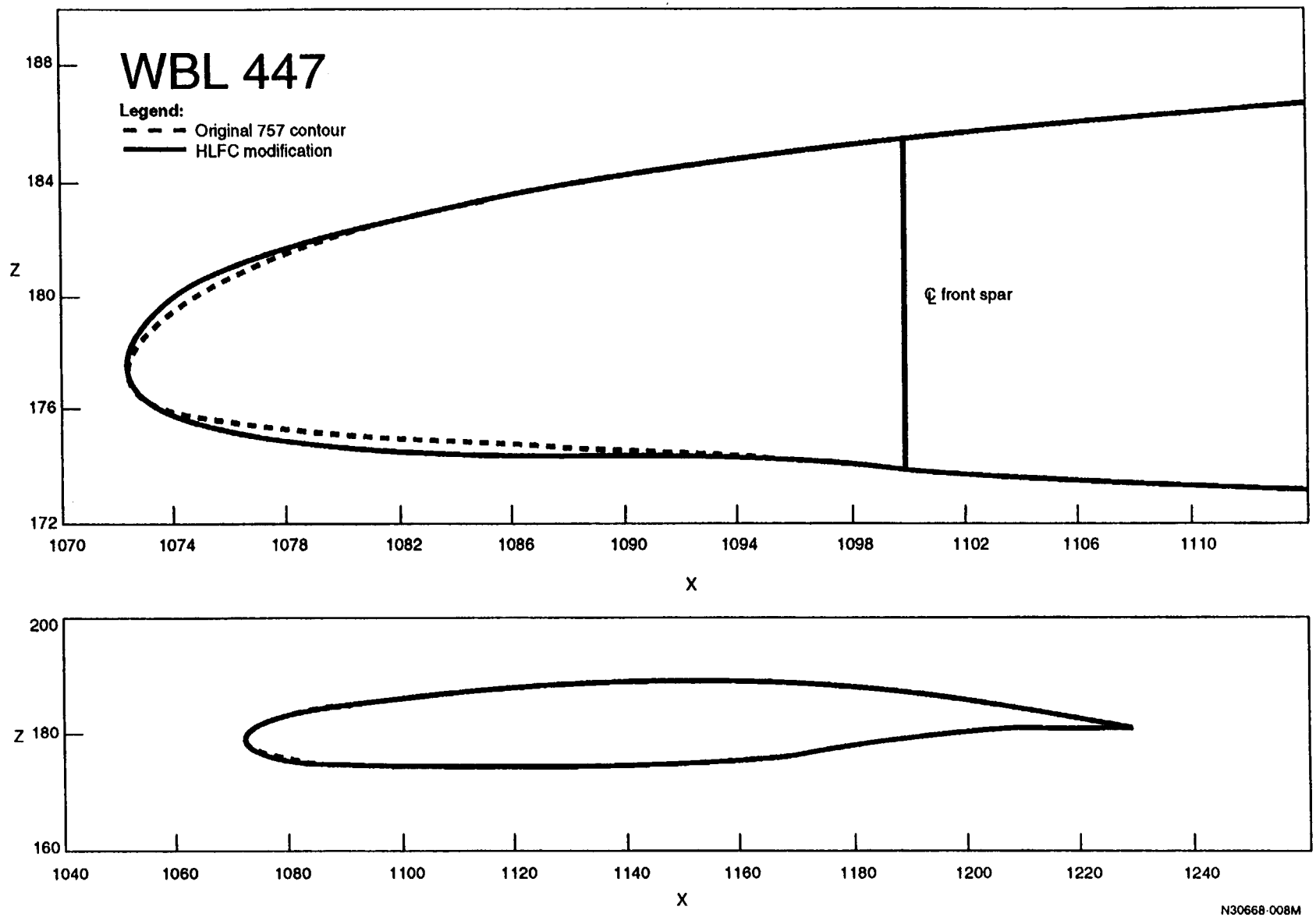

Figure A-8. HLFC and Original 757 Airfoil Contours, WBL 447

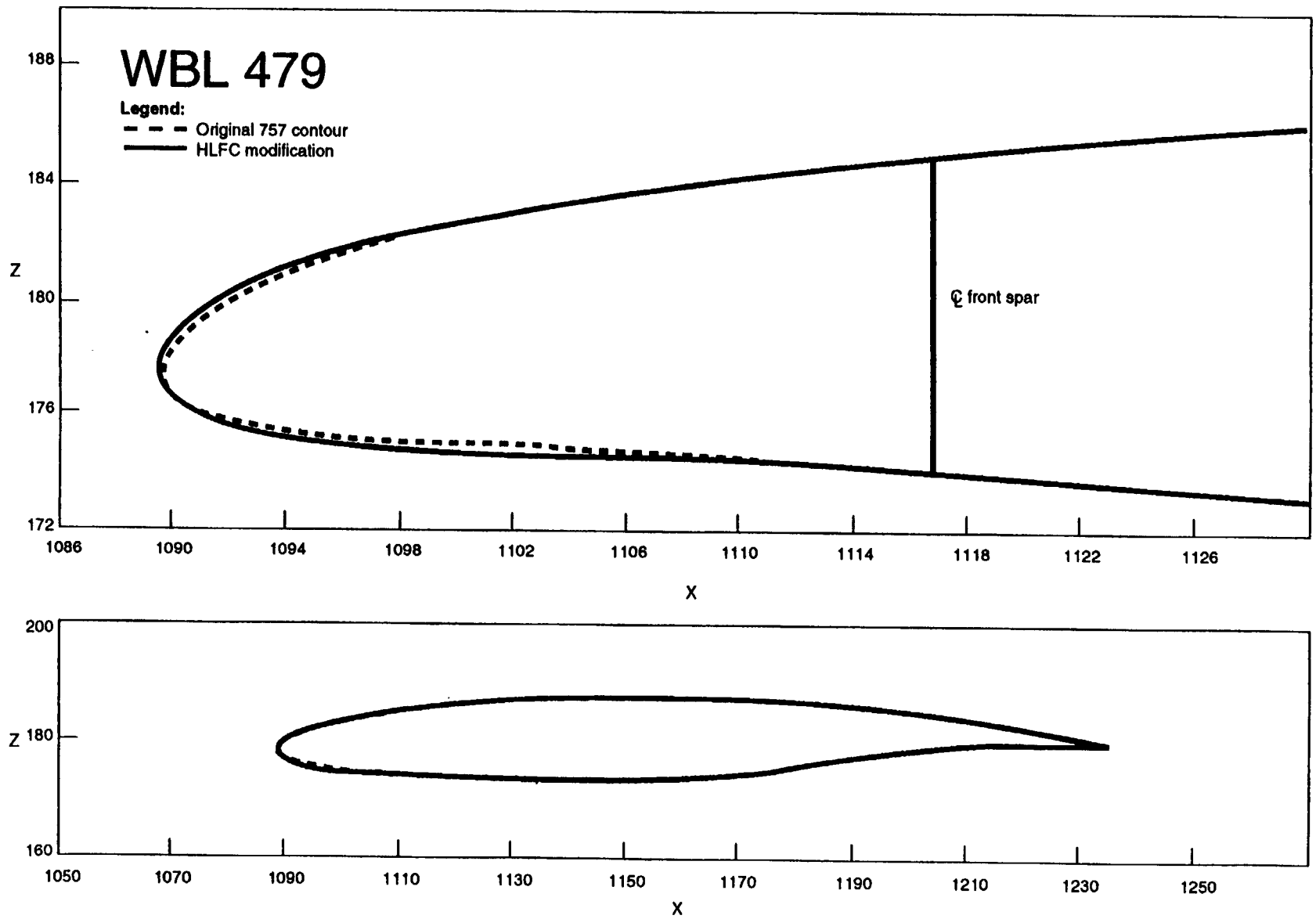

Figure A-9. HLFC and Original 757 Airfoil Contours, WBL 479

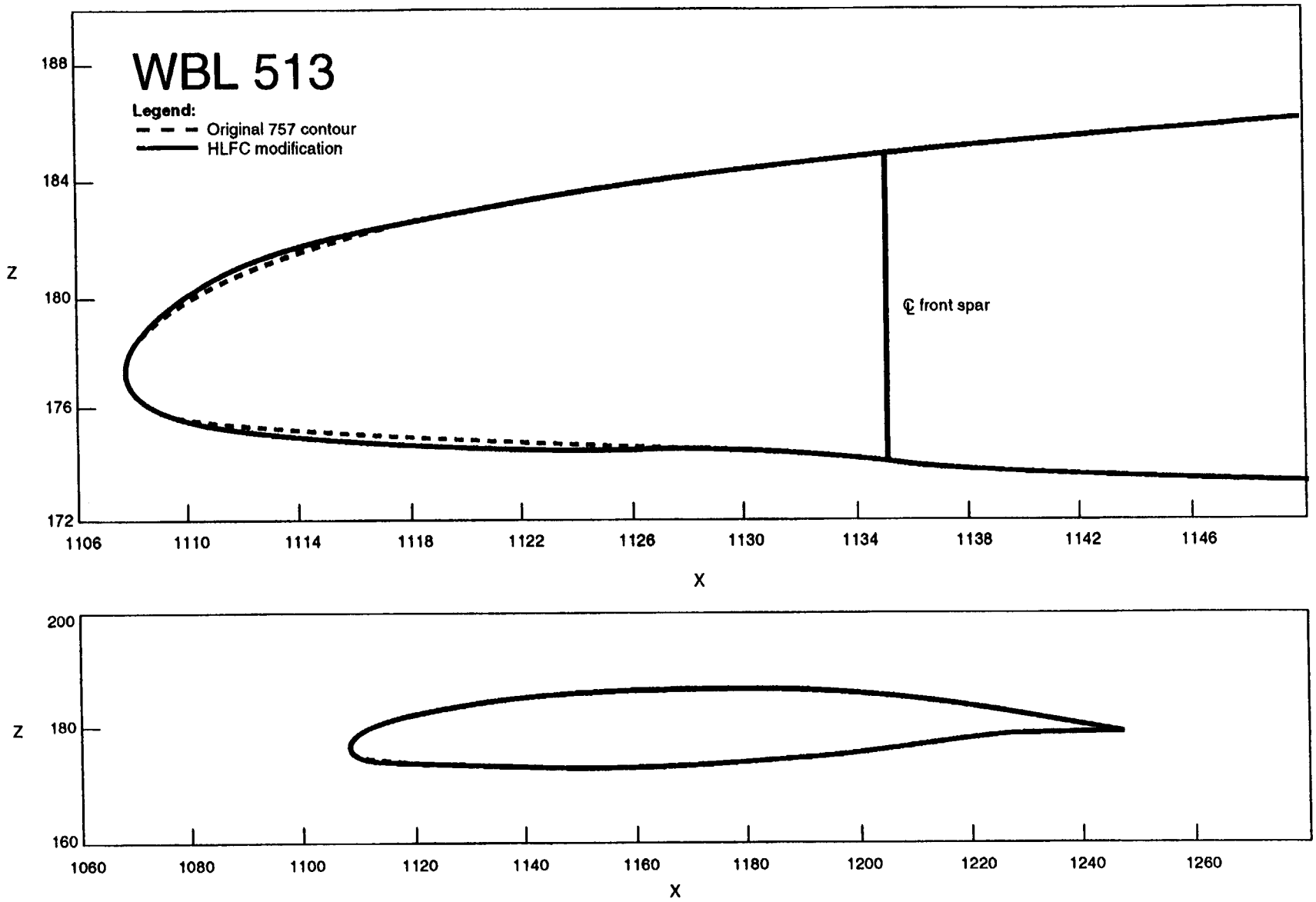

Figure A-10. HLFC and Original 757 Airfoil Contours, WBL 513

This page intentionally left blank

Appendix B

Normal Cuts of HLFC Airfoil Sections

The nose radius of a profile taken in a plane normal to the wing leading edge is the dominant parameter determining the velocity gradient normal to the attachment line, which is required for evaluation of the attachment line boundary layer momentum thickness.

This appendix shows normal cuts of the HLFC leading edge at three locations on the HLFC test panel. They are at outboard slat stations (OSS) 322, 441, and 562, as indicated in figure B-1.

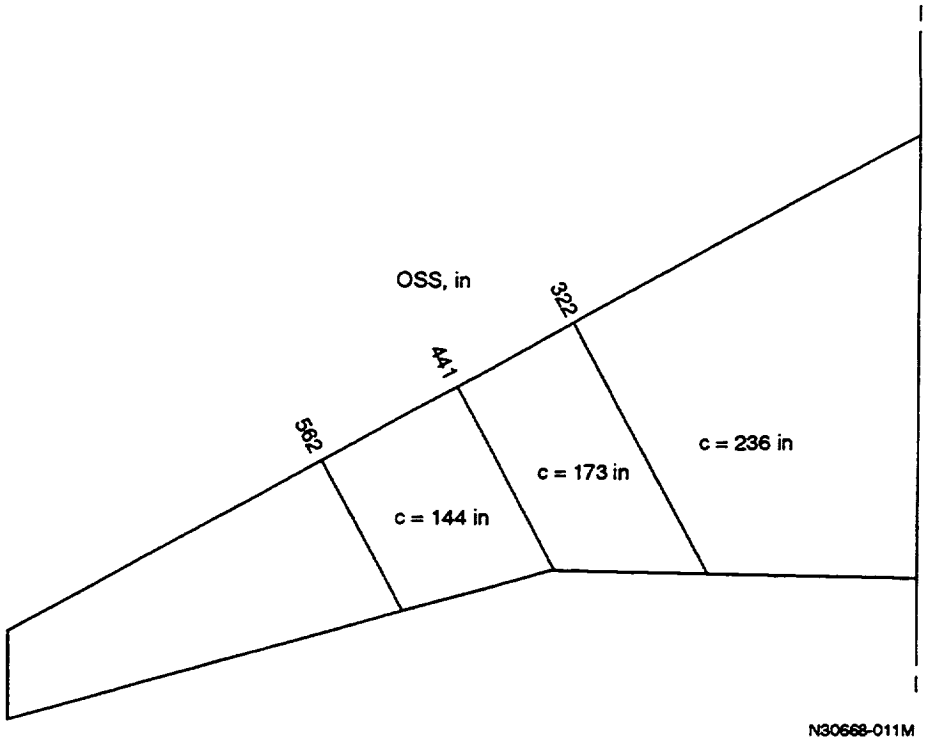

Figure B-1. Locations of Normal Cuts

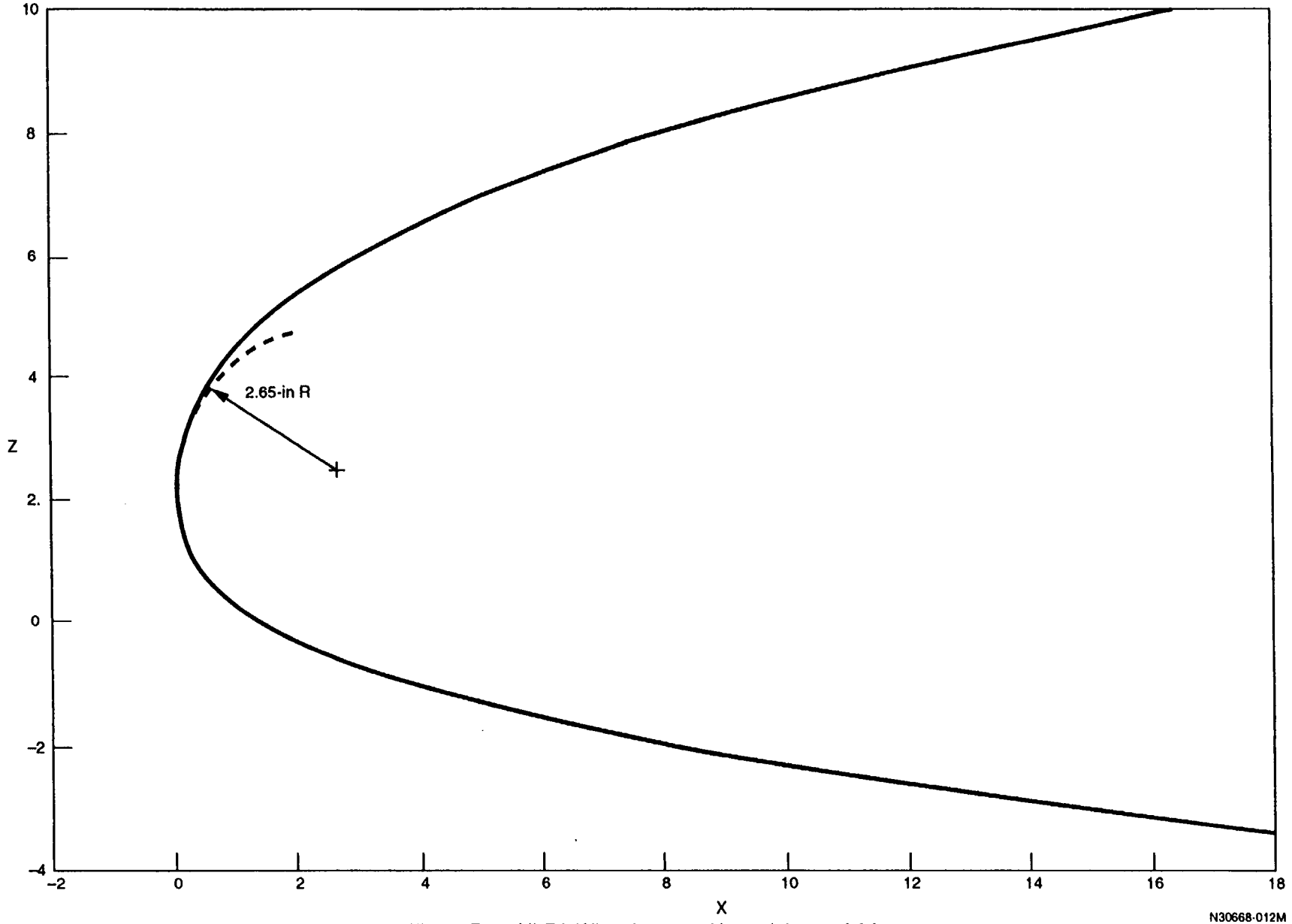

Figure B-2. HLFC Wing Contour–Normal Cut at OSS 322

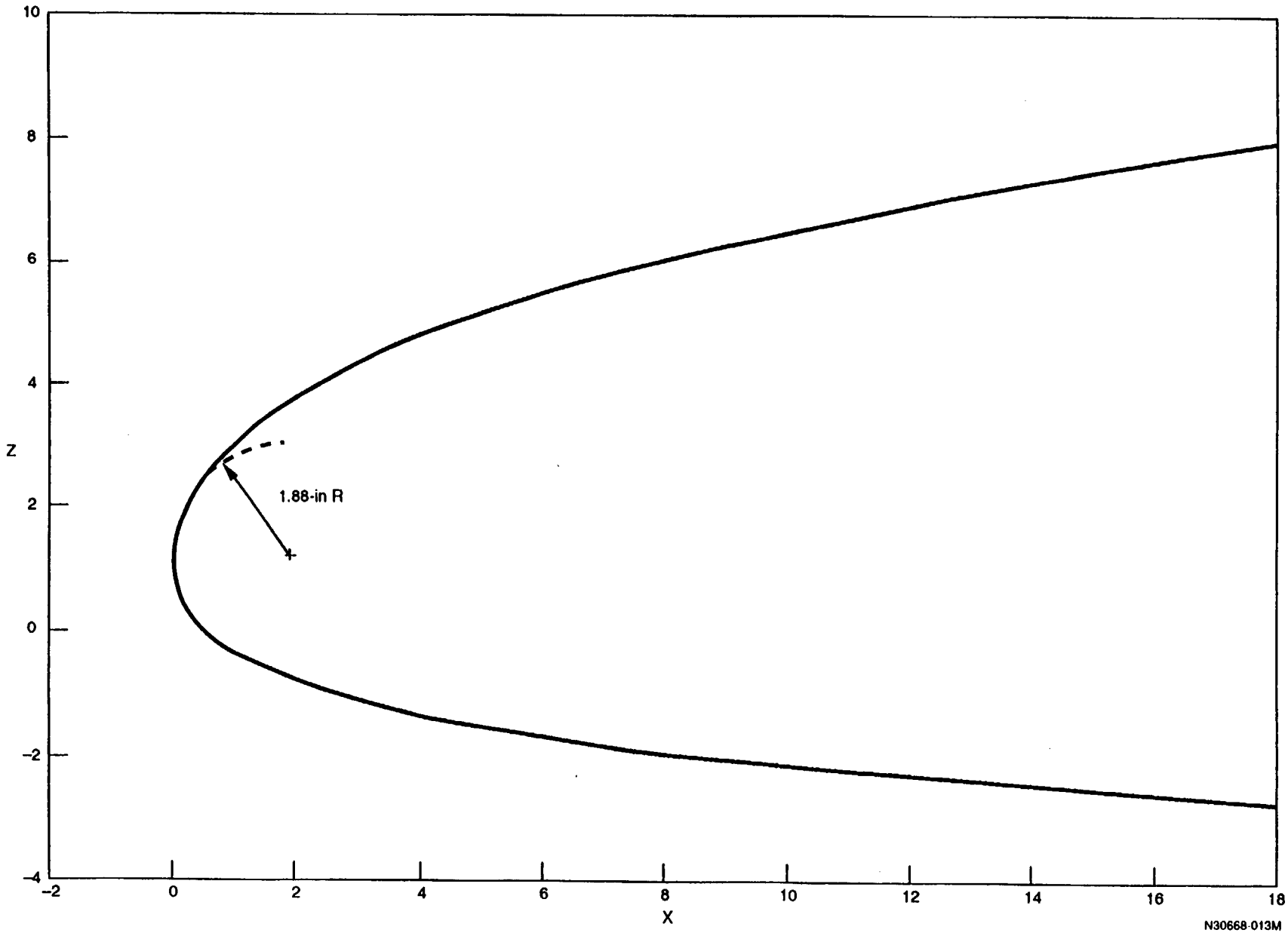

Figure B-3. HLFC Wing Contour–Normal Cut at OSS 441

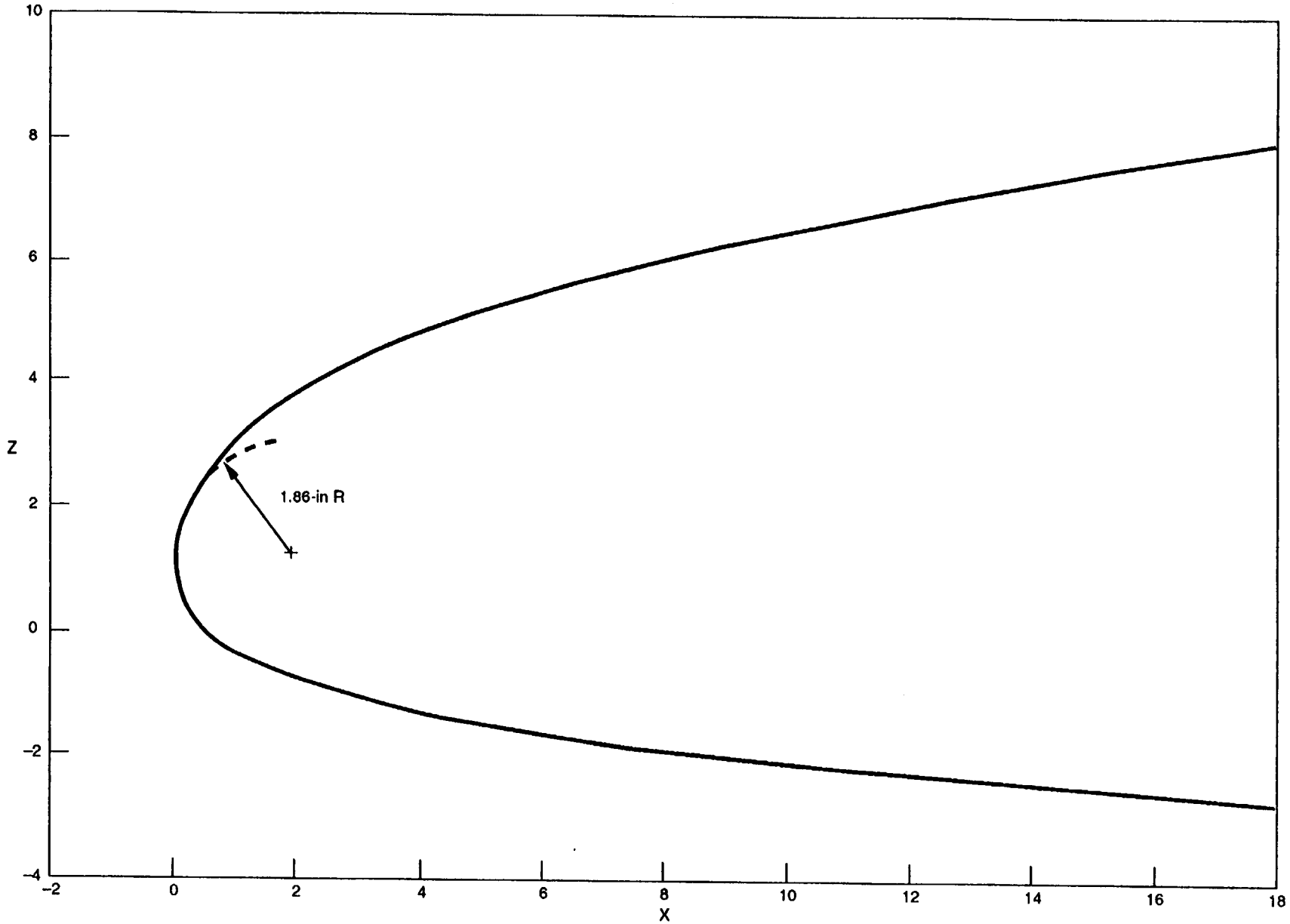

Figure B-4. HLFC Wing Contour–Normal Cut at OSS 562

This page intentionally left blank

Appendix C

Leading Edge Radius

This appendix presents a comparison between the leading edge radii of the basic 757 wing and the modified HLFC wing over the span of the test panel.

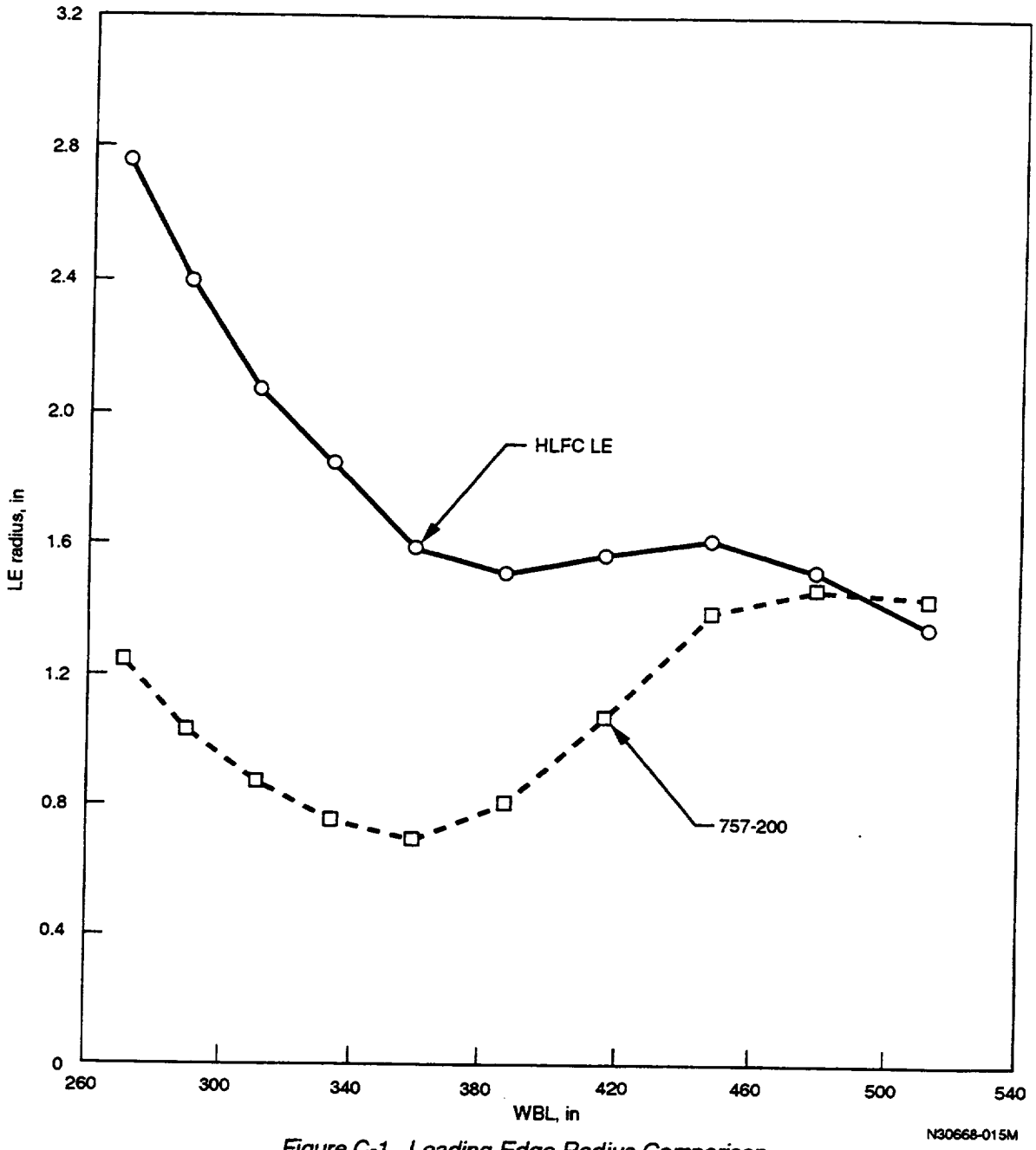

Figure C-1. Leading Edge Radius Comparison

Appendix D

Pressure Distributions at the Design Condition

This appendix shows calculated pressure coefficient distributions at the design condition (Mach 0.80 at C_L = 0.50) at 10 spanwise stations on the HLFC test panel, from WBL 270 to WBL 513. Each figure shows C_{PS} for the entire section plus an expanded-scale plot covering the forward 28% of the chord.

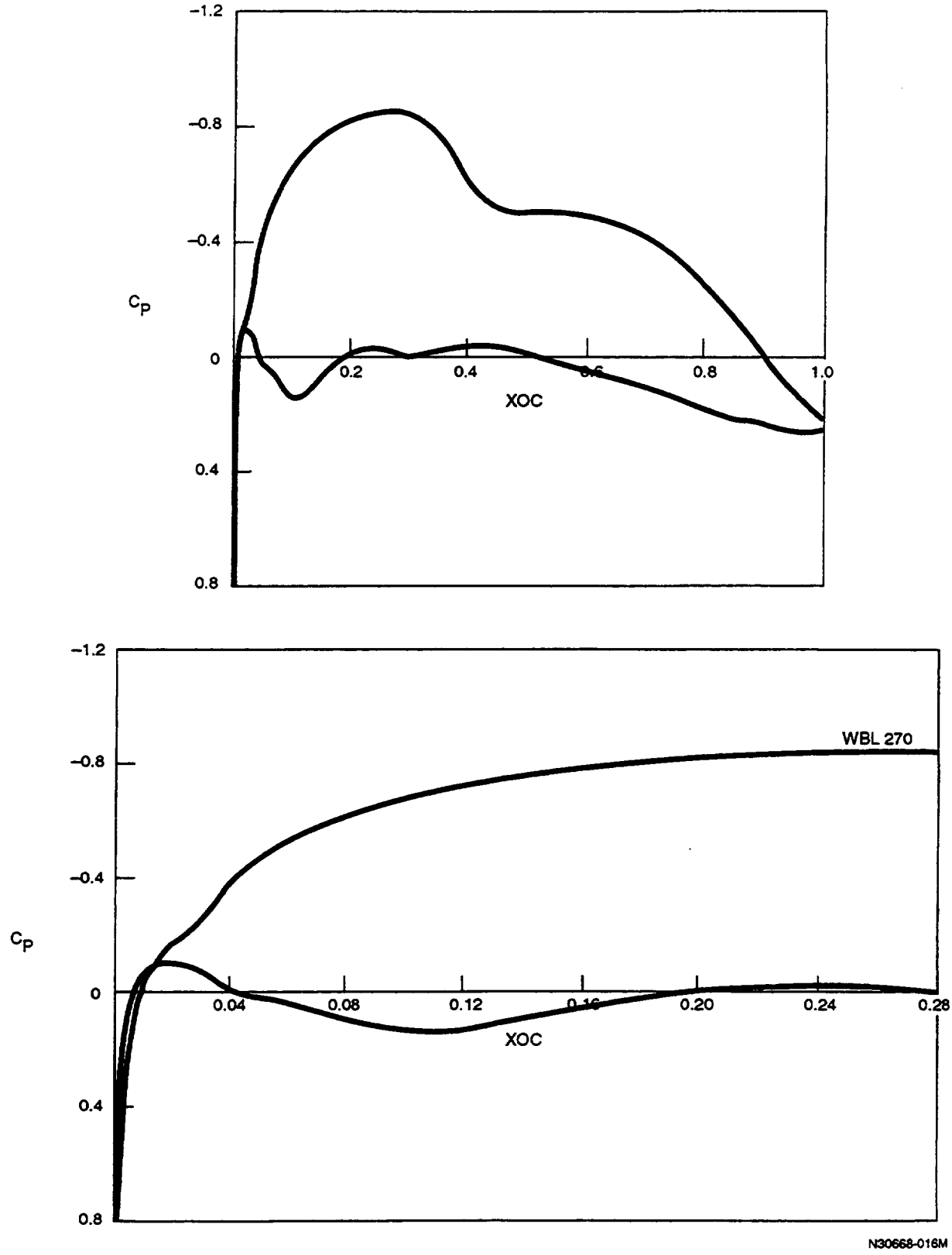

Figure D-1. Calculated C_P Distribution at C_L = 0.50, Mach = 0.80, WBL 270

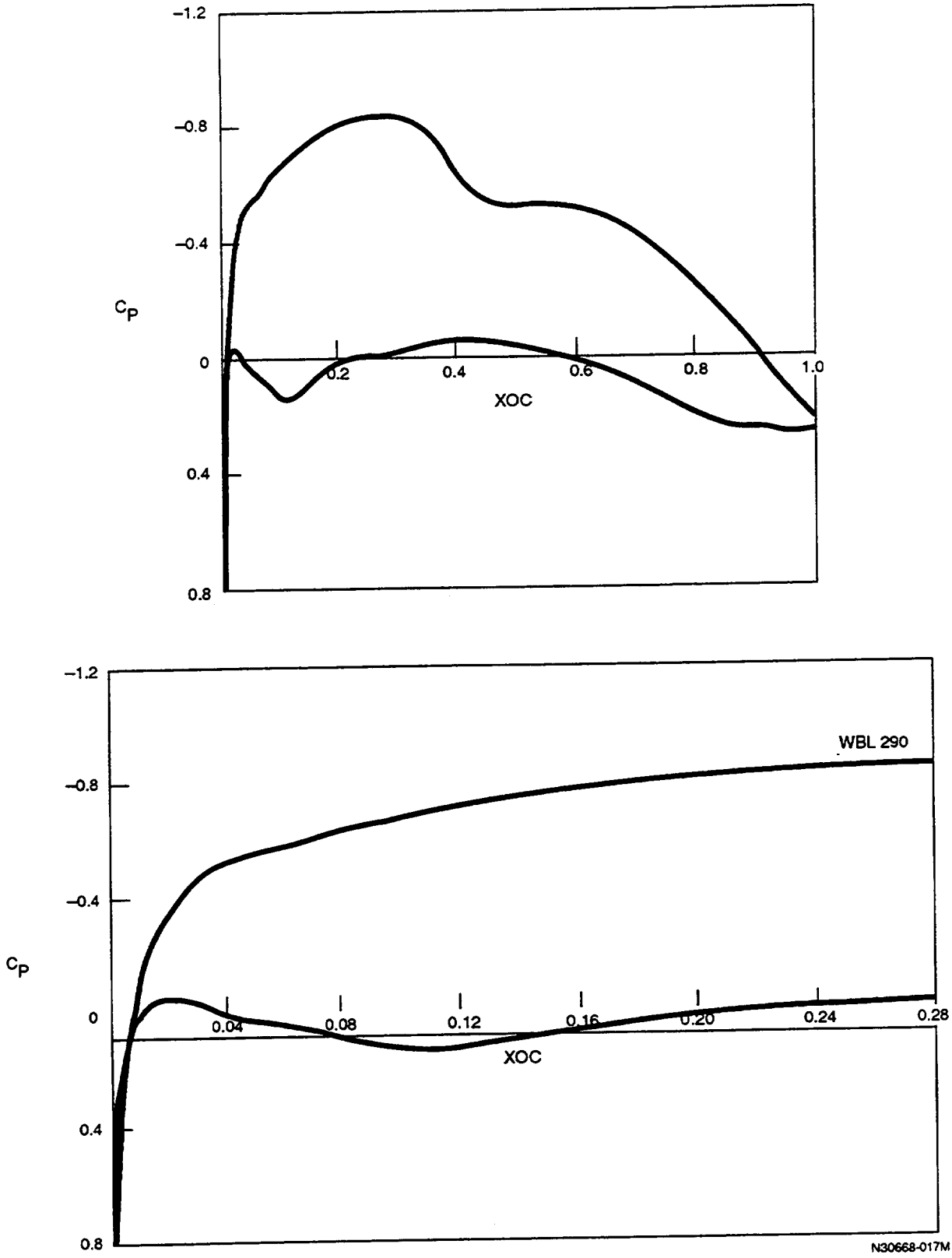

Figure D-2. Calculated C_P Distribution at C_L = 0.50, Mach = 0.80, WBL 290

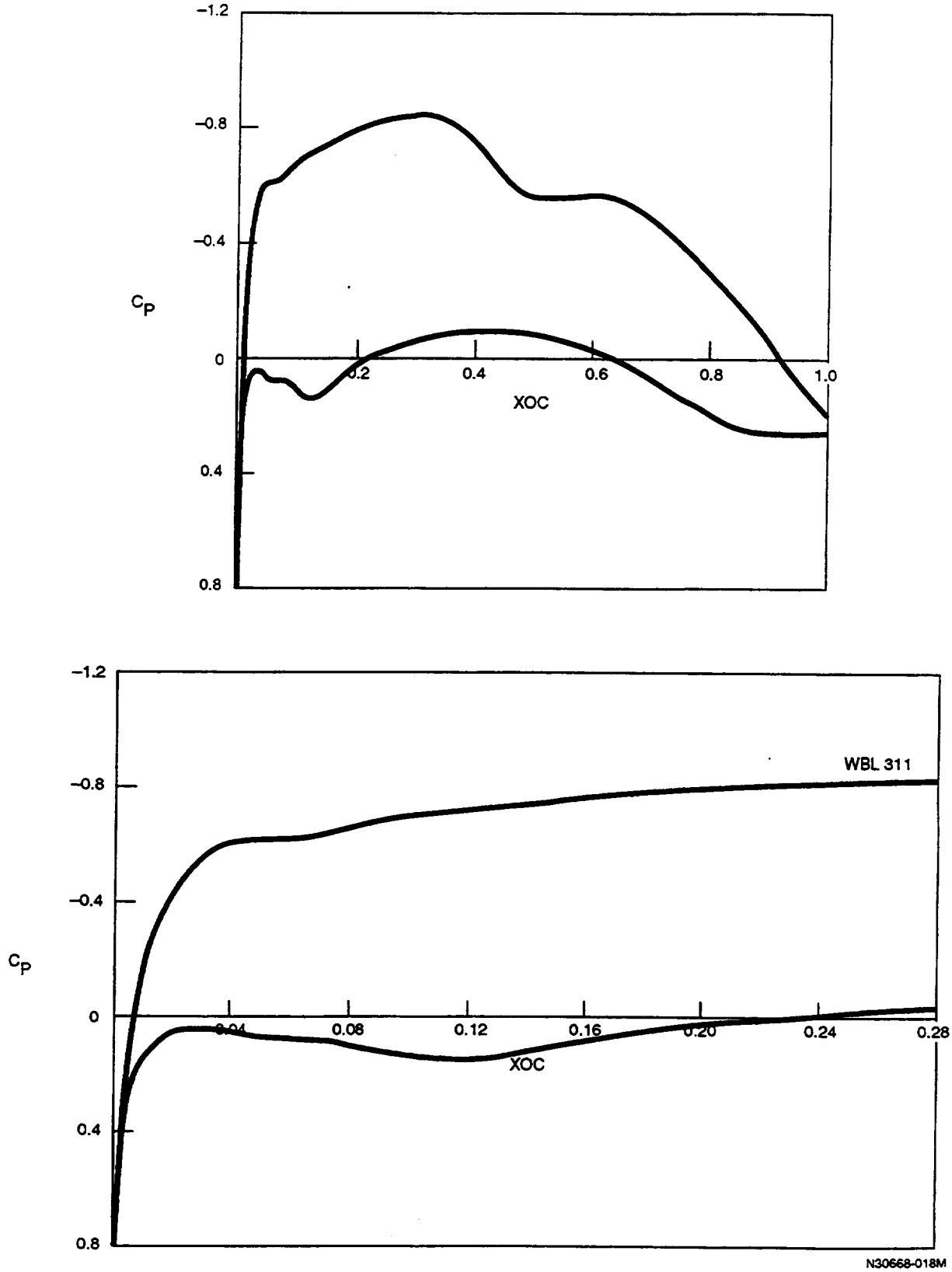

Figure D-3. Calculated C_P Distribution at C_L = 0.50, Mach = 0.80, WBL 311

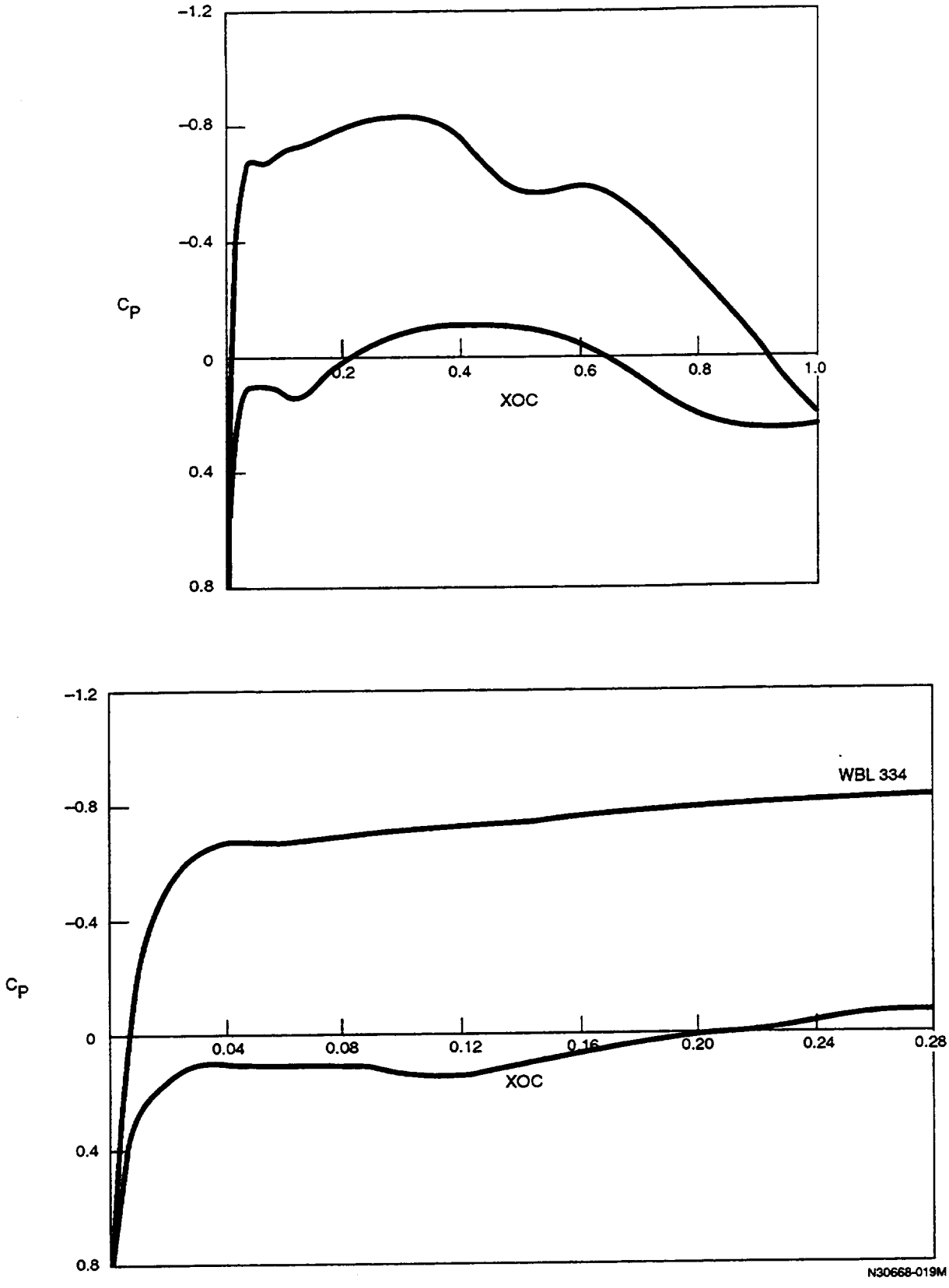

Figure D-4. Calculated C_P Distribution at C_L = 0.50, Mach = 0.80, WBL 334

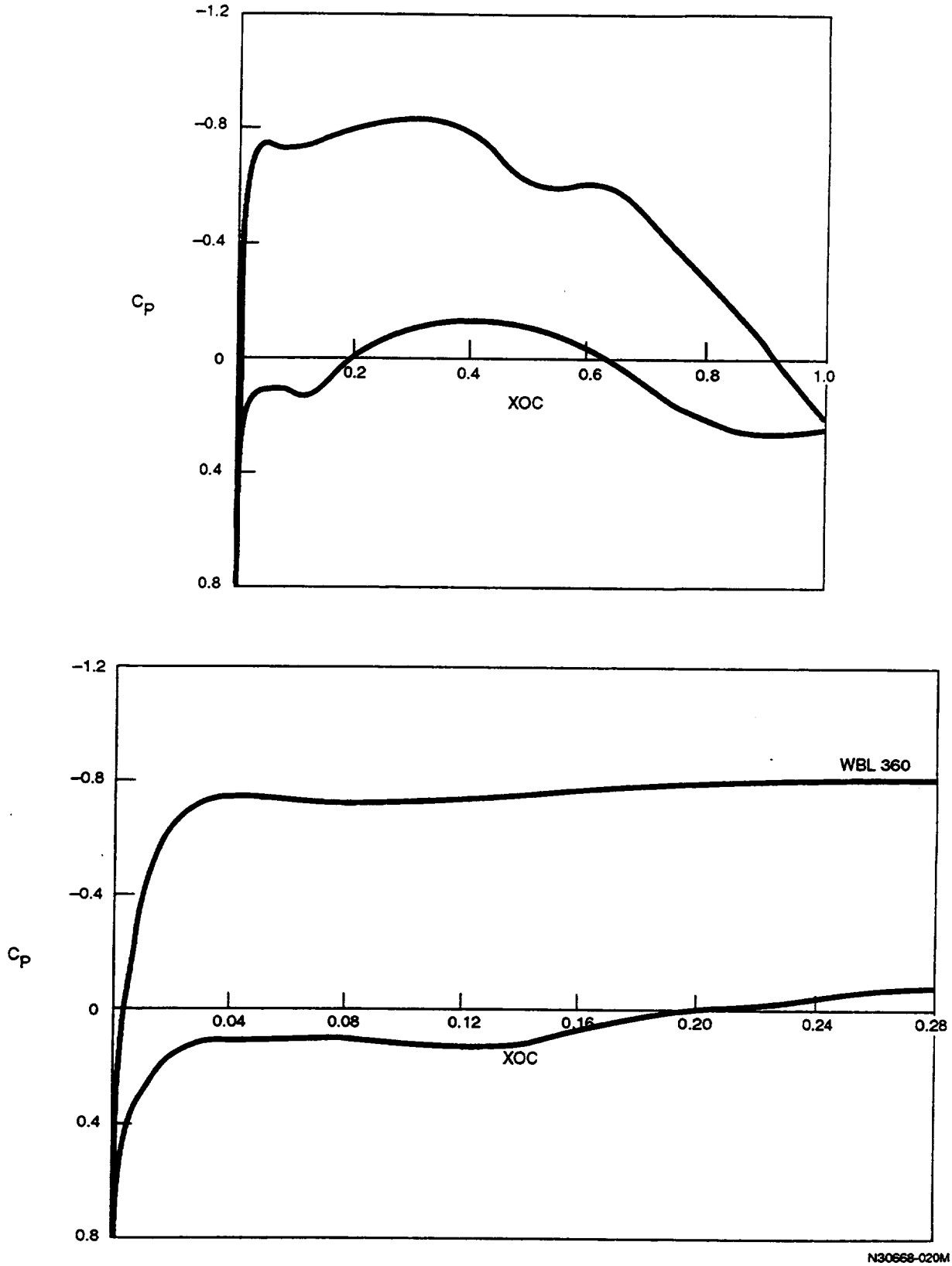

Figure D-5. Calculated C_P Distribution at C_L = 0.50, Mach = 0.80, WBL 360

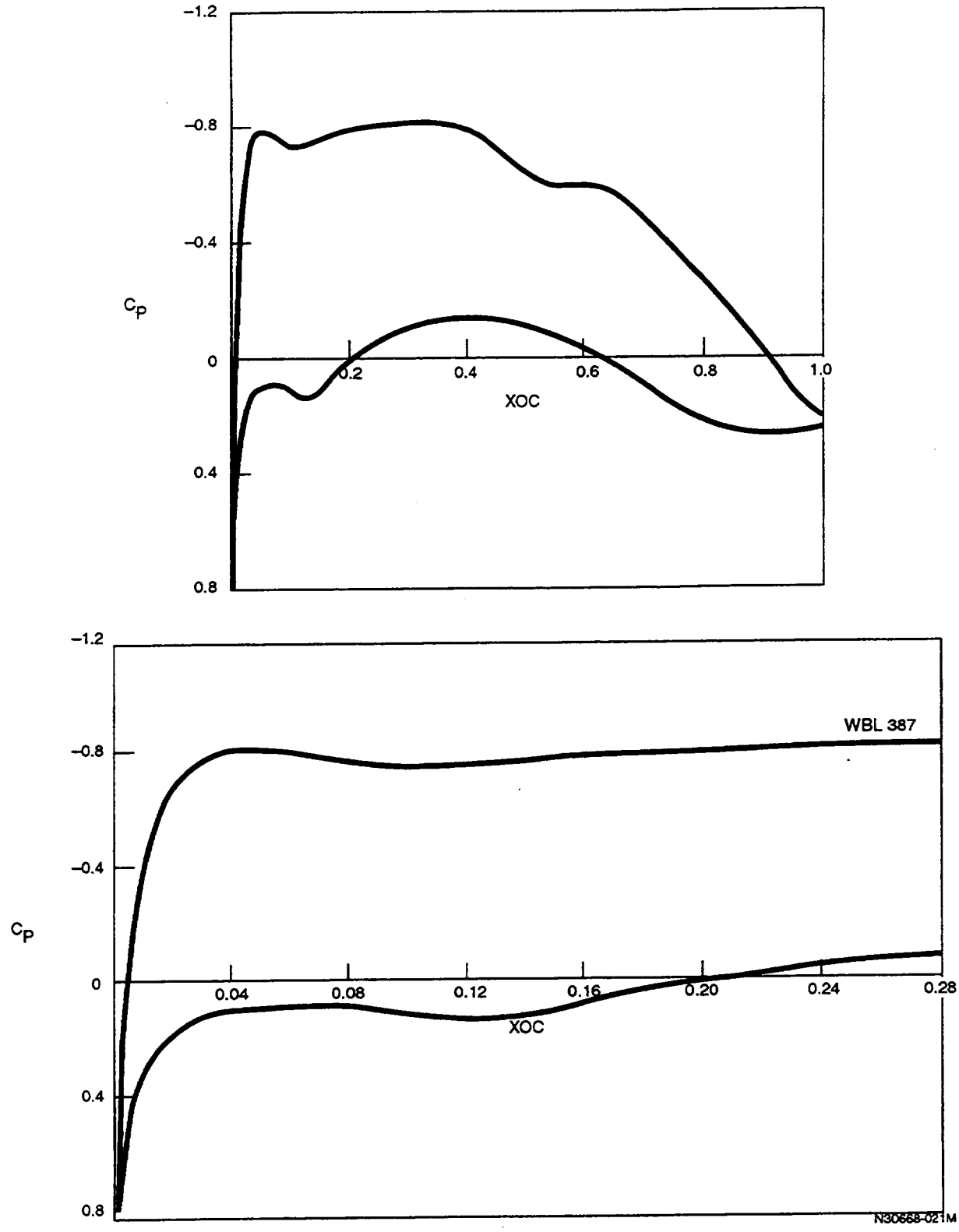

Figure D-6. Calculated C_P Distribution at C_L = 0.50, Mach = 0.80, WBL 387

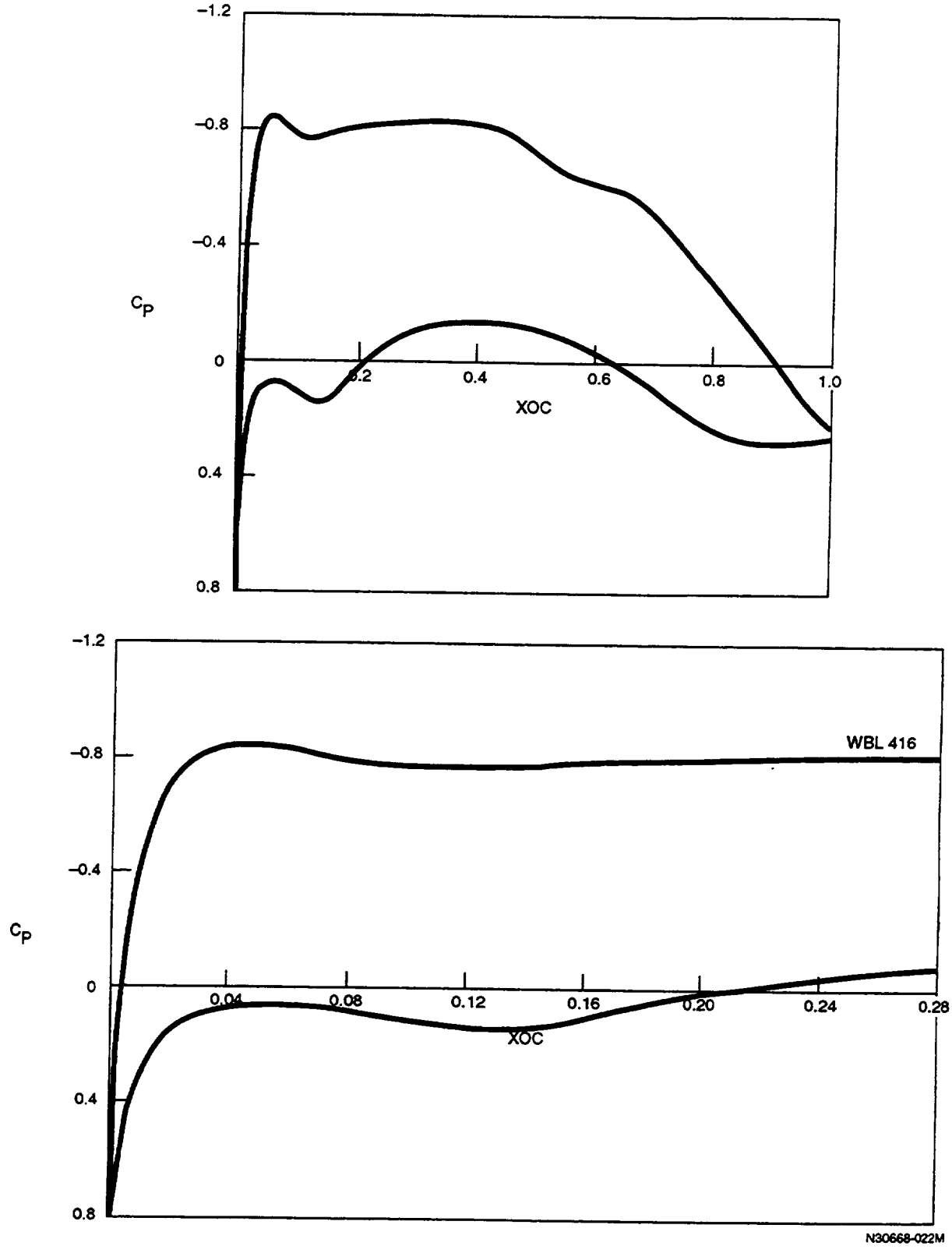

Figure D-7. Calculated C_P Distribution at C_L = 0.50, Mach = 0.80, WBL 416

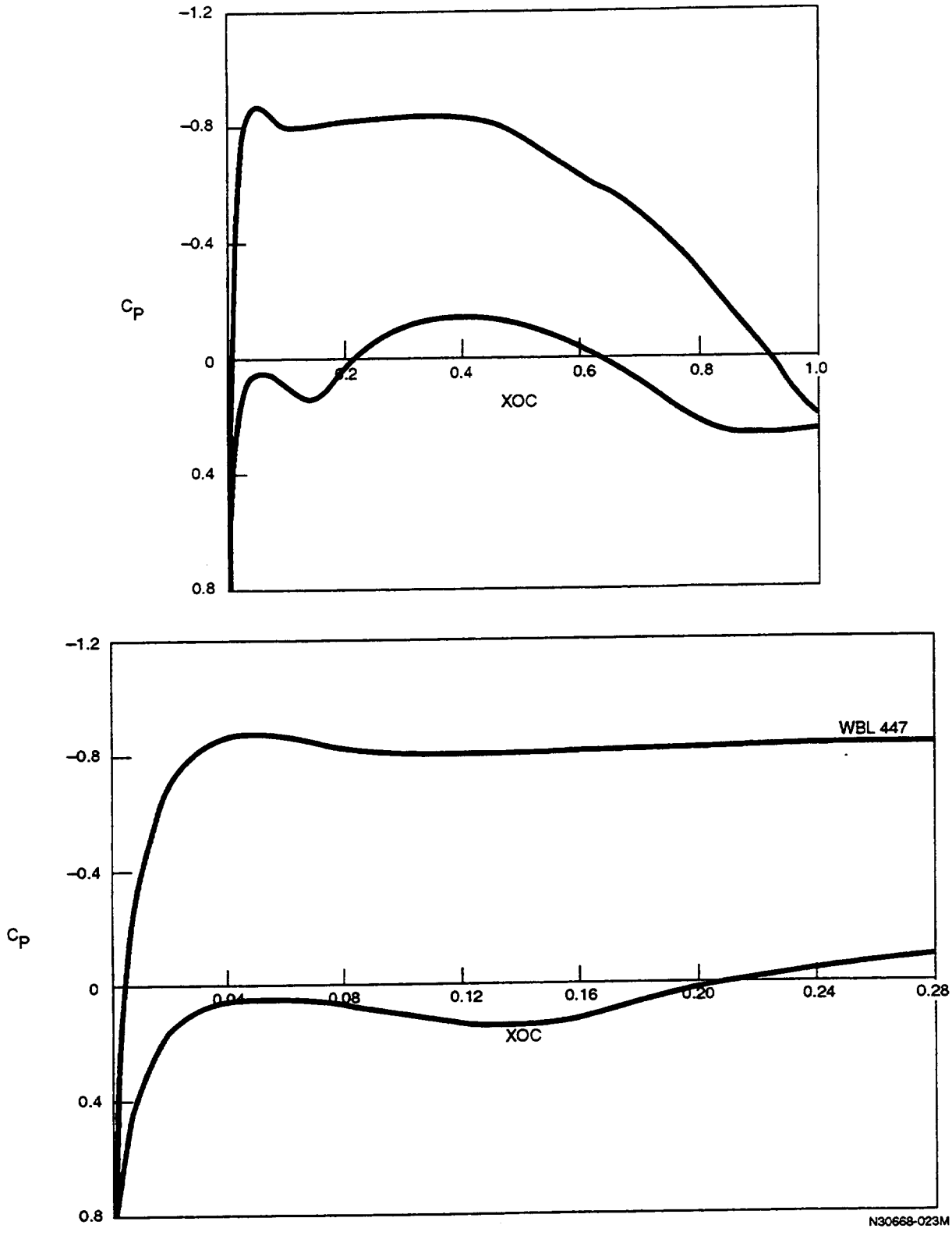

Figure D-8. Calculated C_P Distribution at C_L = 0.50, Mach = 0.80, WBL 447

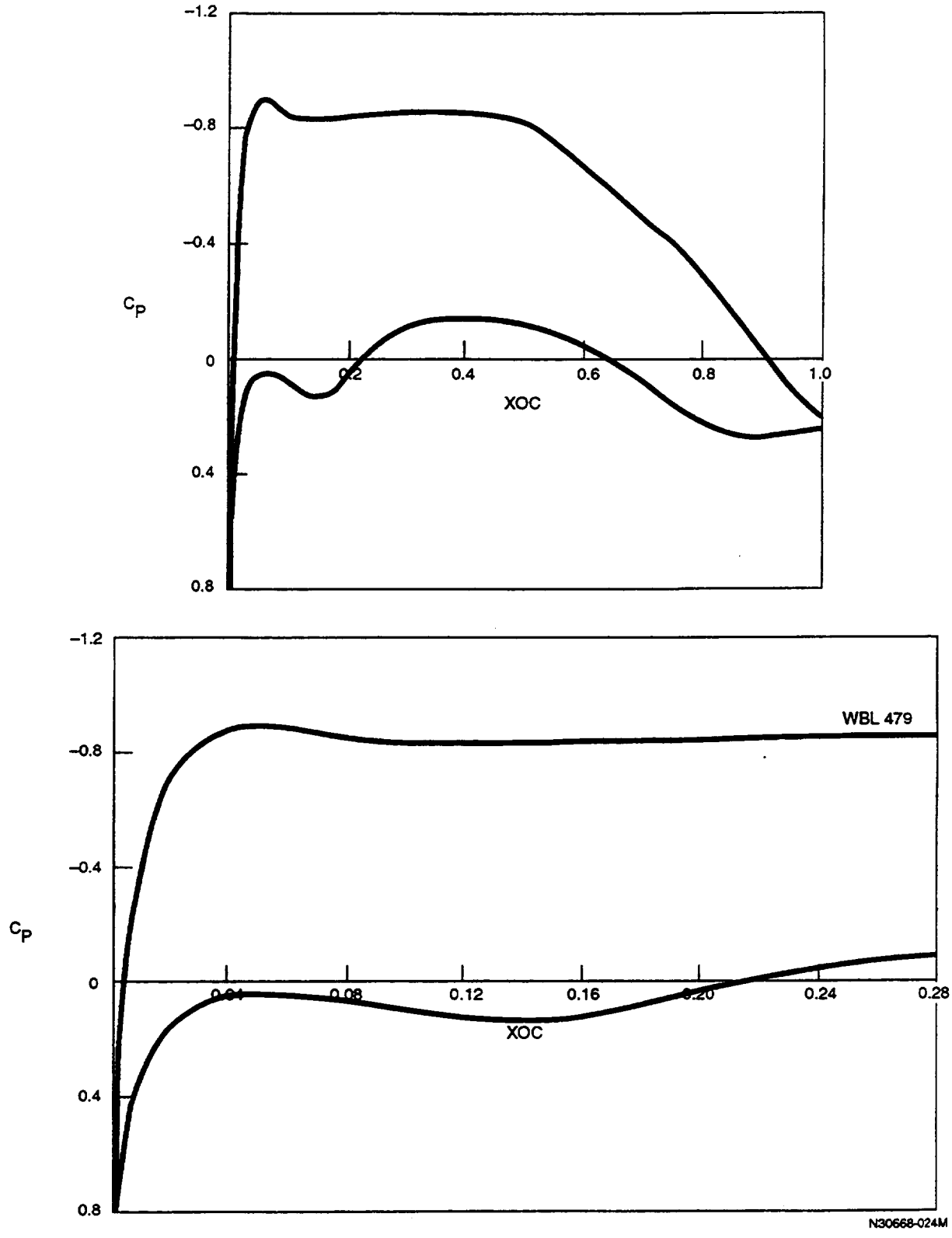

Figure D-9. Calculated C_P Distribution at C_L = 0.50, Mach = 0.80, WBL 479

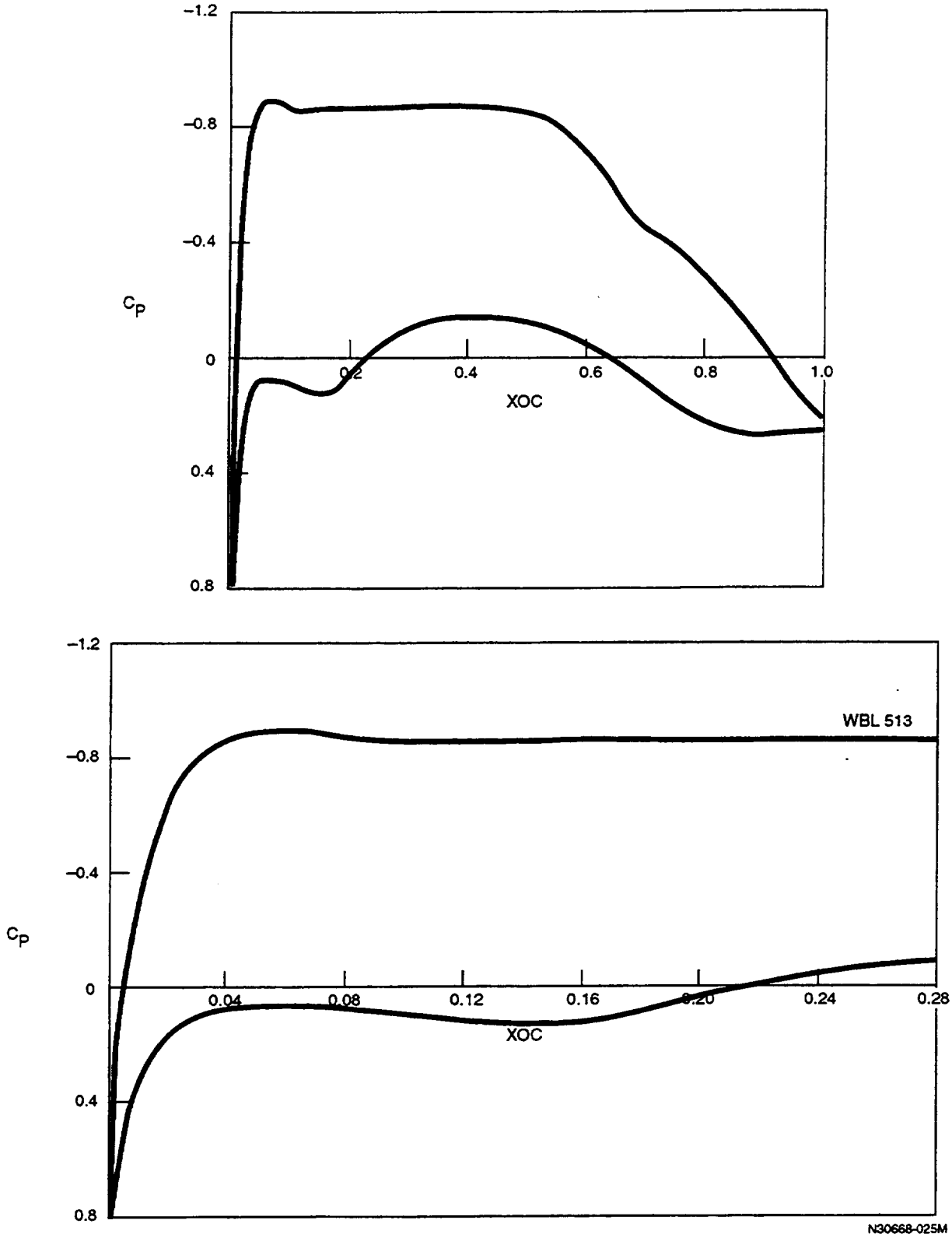

Figure D-10. Calculated C_P Distribution at C_L = 0.50, Mach = 0.80, WBL 513

This page intentionally left blank

Appendix E

Isobar Plots for the HLFC Test Panel

This appendix presents computer-generated isobar plots for the HLFC test panel at the design condition, Mach 0.80 at $C_L = 0.50$.

Figures E-1 and E-2 show upper and lower surface isobars on the right wing planform on the airplane, although the left wing was actually modified. Figure E-3 shows isobars projected on the developed wing upper surface near the leading edge. Figure E-4 shows the same data in enlarged format, this time plotted for the left wing, over a narrow portion near the attachment line.

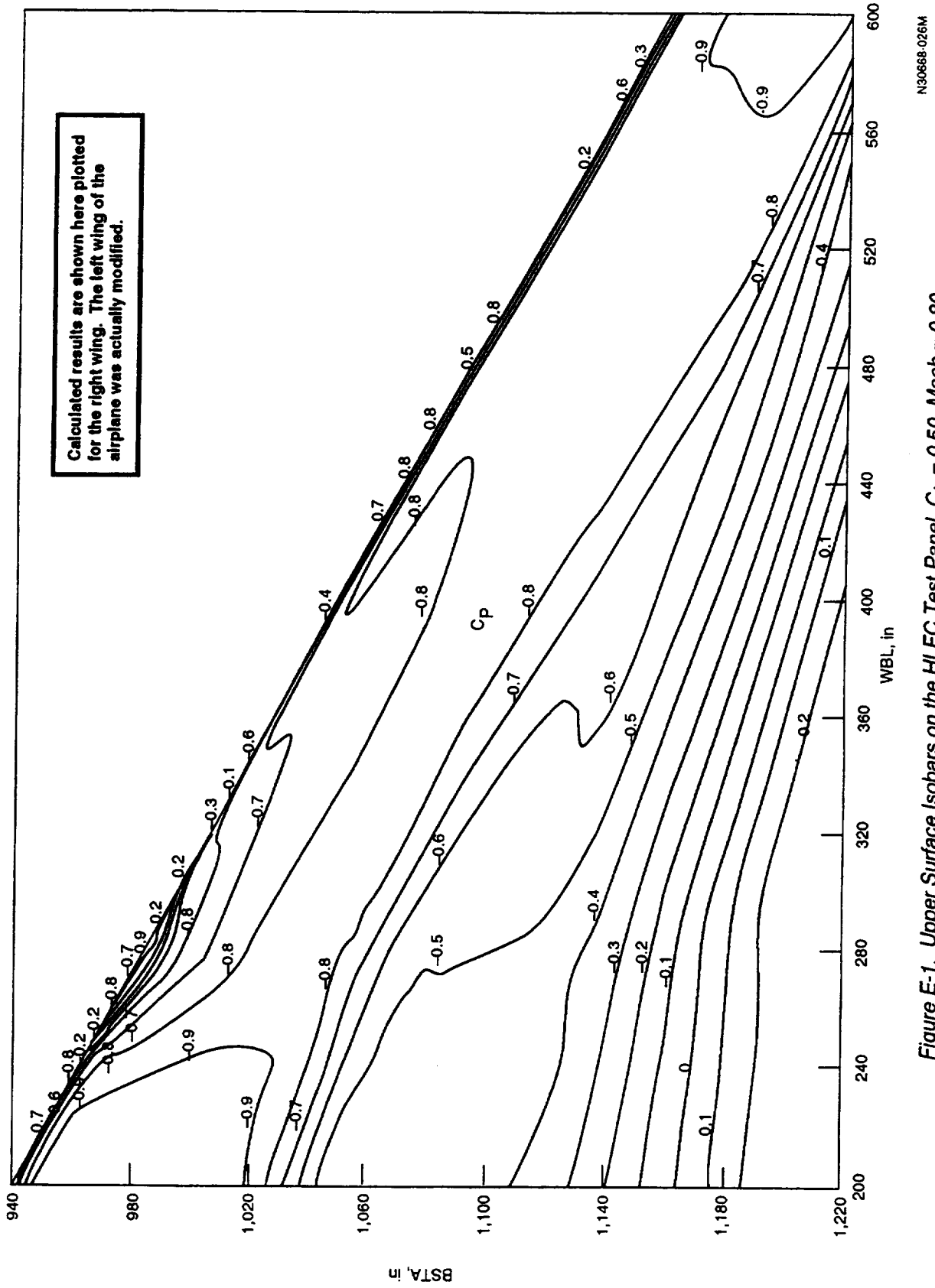

Figure E-1. Upper Surface Isobars on the HLFC Test Panel, C_L = 0.50, Mach = 0.80

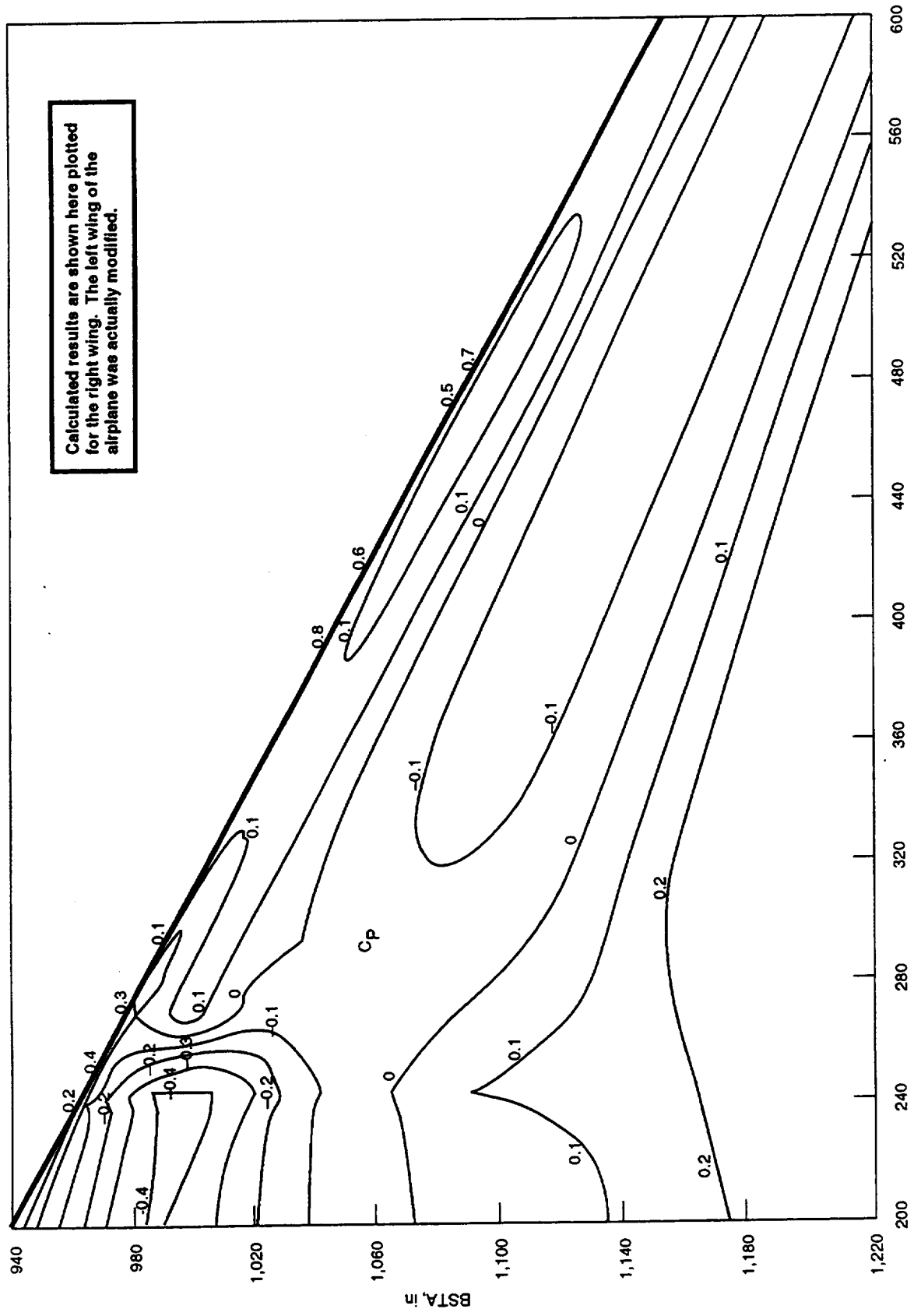

Figure E-2. Lower Surface Isobars on the HLFC Test Panel, C_L = 0.50, Mach = 0.80

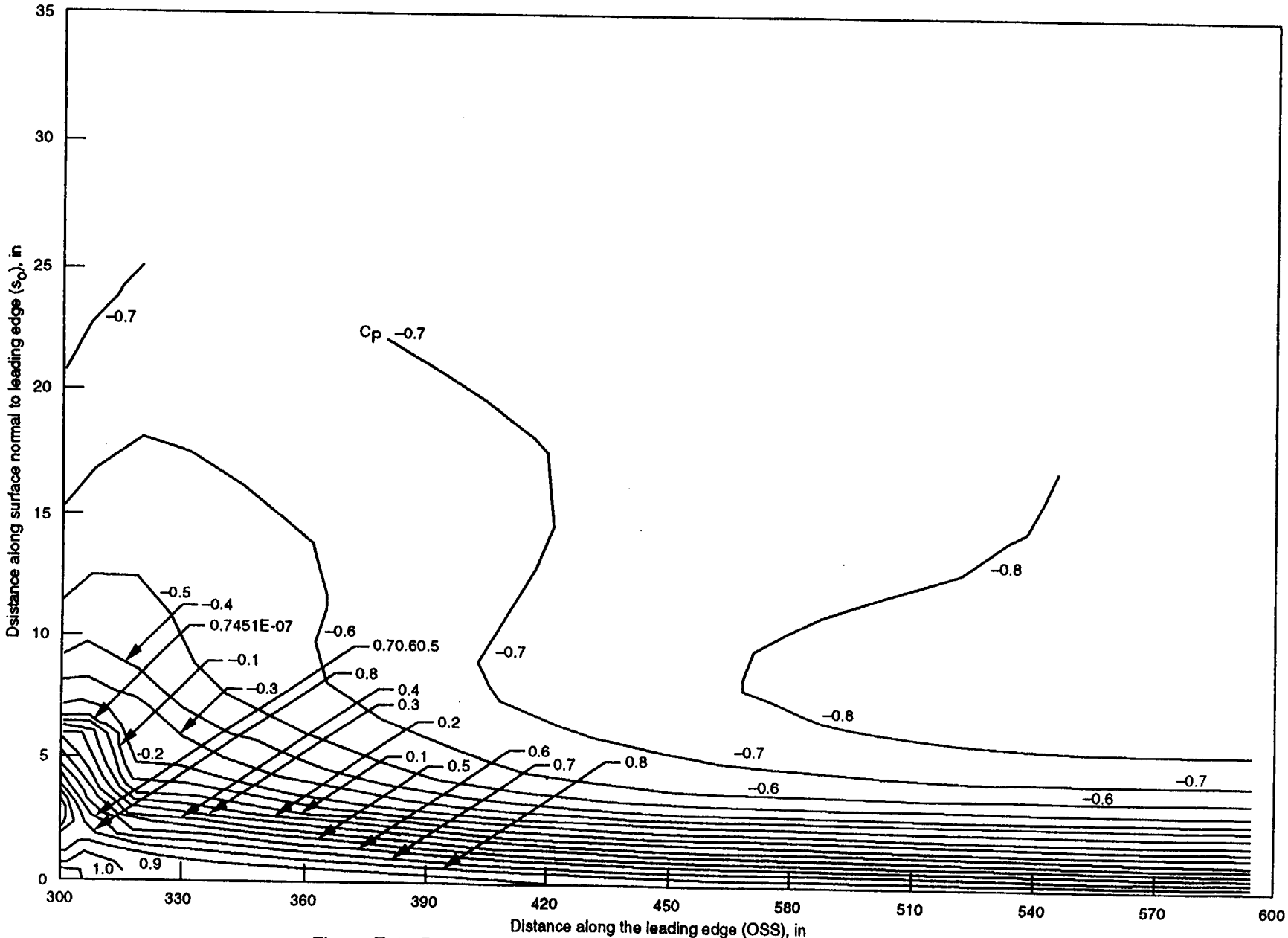

Figure E-3. Developed-Surface Plot of Upper Surface Leading Edge Isobars

N30668-028M

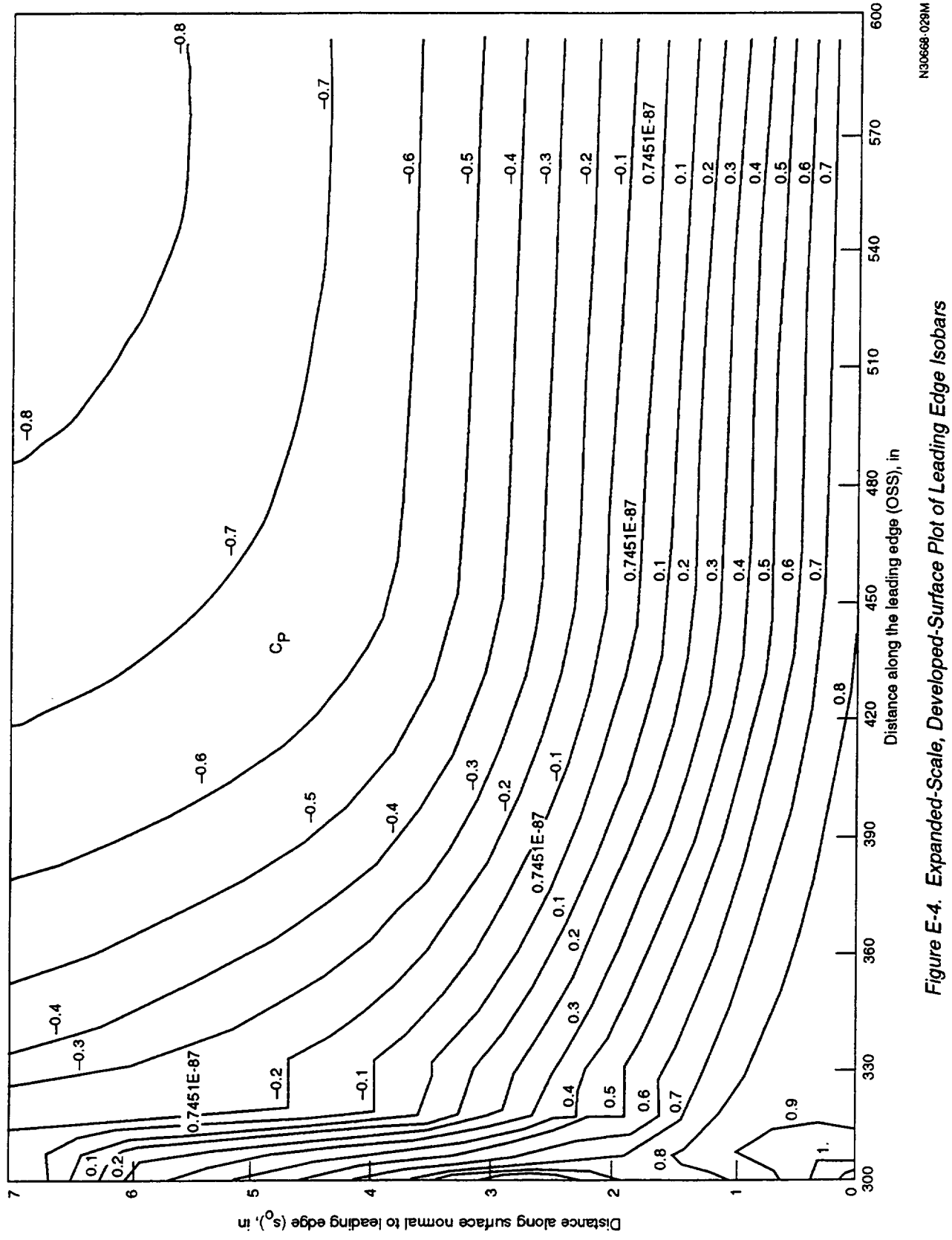

Figure E-4. Expanded-Scale, Developed-Surface Plot of Leading Edge Isobars

This page intentionally left blank

Appendix F

Boundary Layer Growth on the HLFC Test Surface

This appendix presents the calculated growth of the laminar boundary layer at three sections within the HLFC test panel: WBL 290, WBL 387, and WBL 479. These data pertain to the nominal design condition, $M = 0.80$, $C_L = 0.50$ at 39,000-ft altitude. Figure F-1 shows the boundary layer velocity thickness, δ, that is, the distance from the surface to the point where the velocity is 99% of the potential-flow value. Figure F-2 shows the displacement thickness, δ^*. Both are plotted against arc length on the airfoil surface divided by local wing chord.

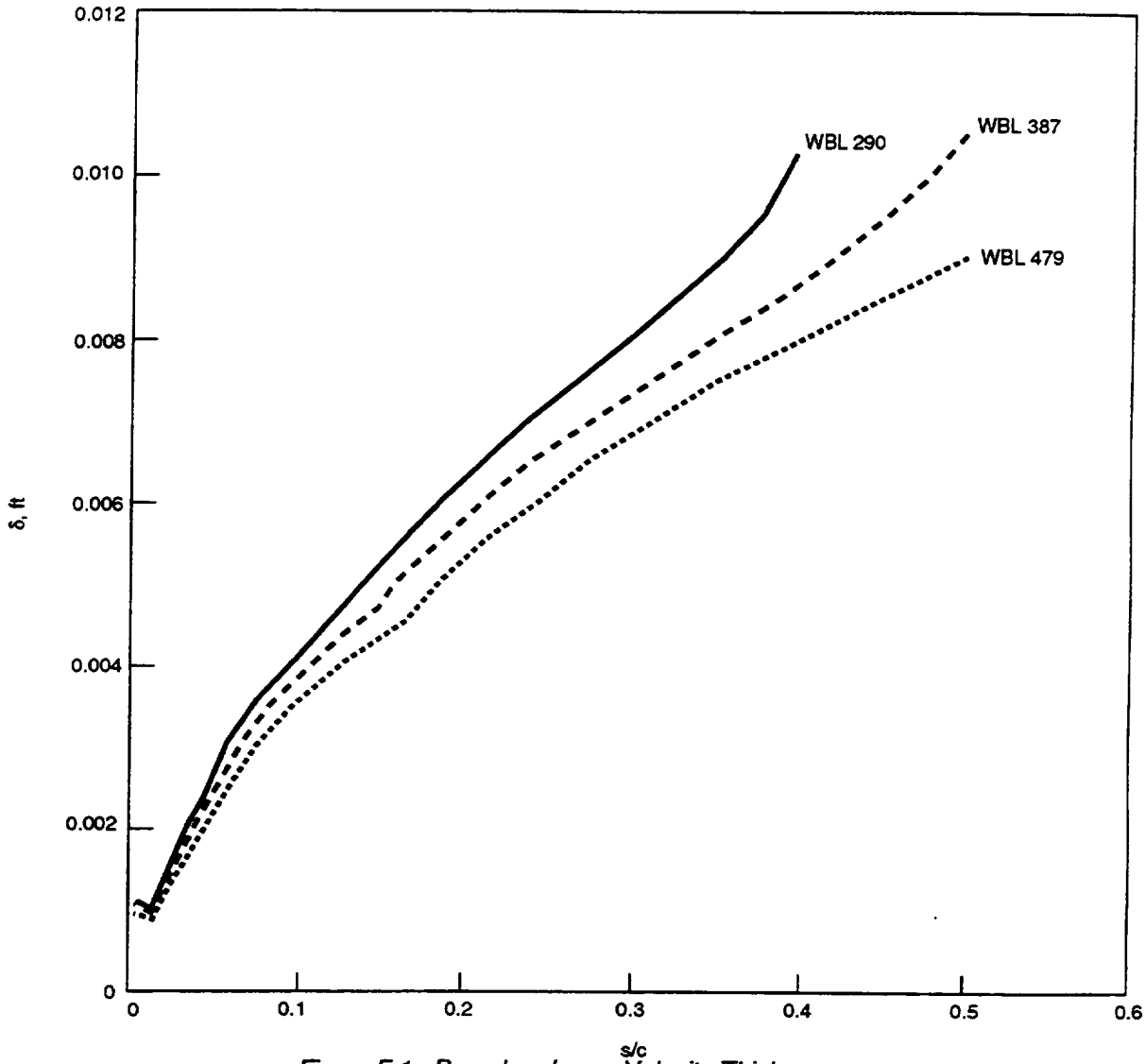

Figure F-1. Boundary Layer Velocity Thickness

N30668-030M

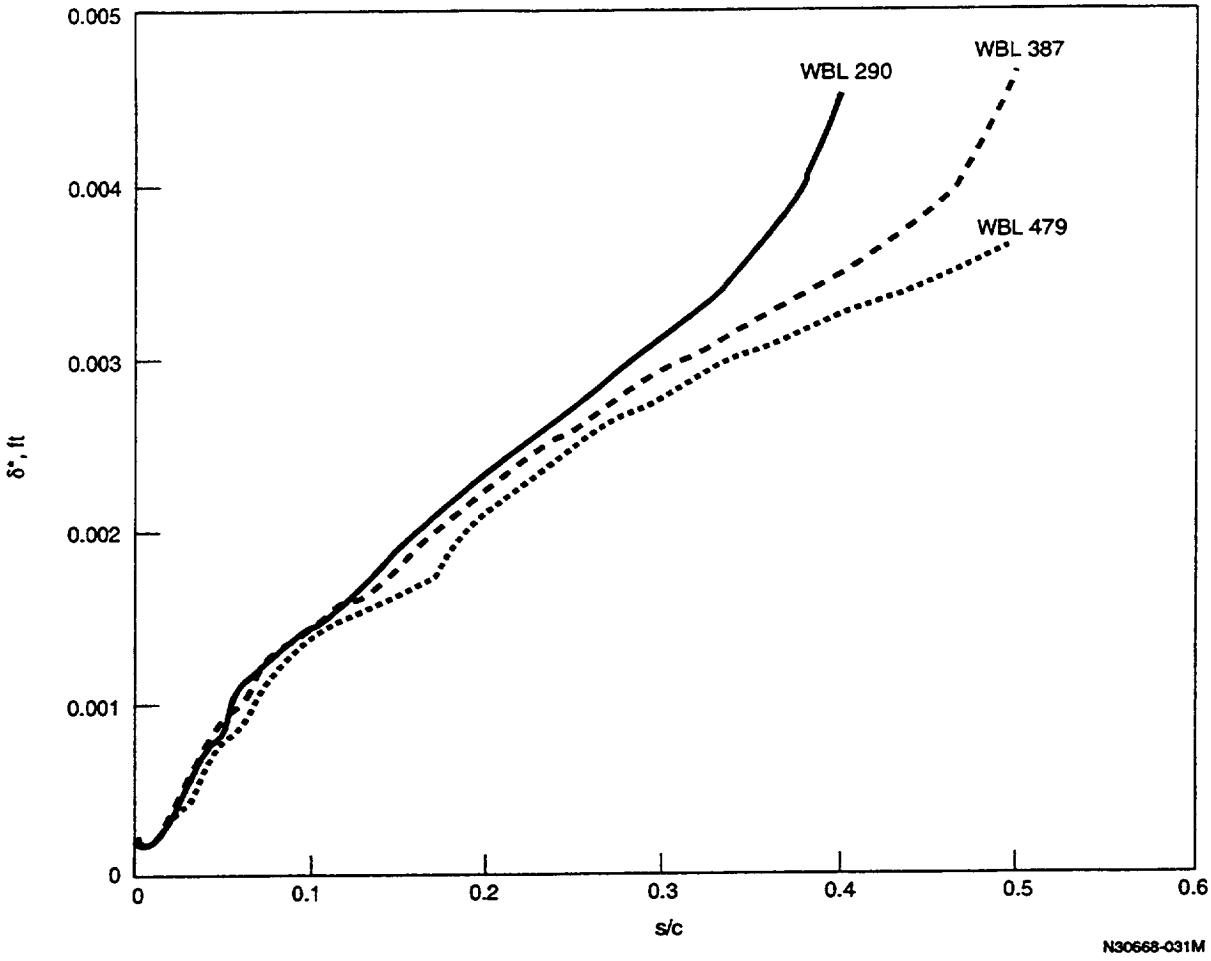

Figure F-2. Boundary Layer Displacement Thickness

This page intentionally left blank

Appendix G

Detailed Results of Boundary Layer Stability Calculations

This appendix contains computer-generated plots summarizing the stability calculations at six spanwise stations, WBL 270, 311, 360, 416, 447, and 513, at the nominal design condition of Mach 0.80, at C_L = 0.50 and 39000-ft altitude.

For each station, the following are plotted against s/c:

a. Static pressure over the first 20% of the wing upper surface arc length, s/c, and the suction distribution applied.

b. Crossflow disturbance amplification factors, N_{CF}, for a range of wave numbers, α_{CF}, at zero frequency.

c. Tollmien-Schlichting disturbance amplification factors, N_{TS}, for a range of frequencies, (ω_{TS}), at 50-deg wave angle.

In addition, there are—

d. Contour plots of CF amplification factors, $N_{CF} = f(\alpha_{CF}, s/c)$.

e. Contour plots of TS amplification factors, $N_{TS} = f(\omega_{TS}, s/c)$.

f. Comparison of CF and TS amplification factors with the transition criterion.

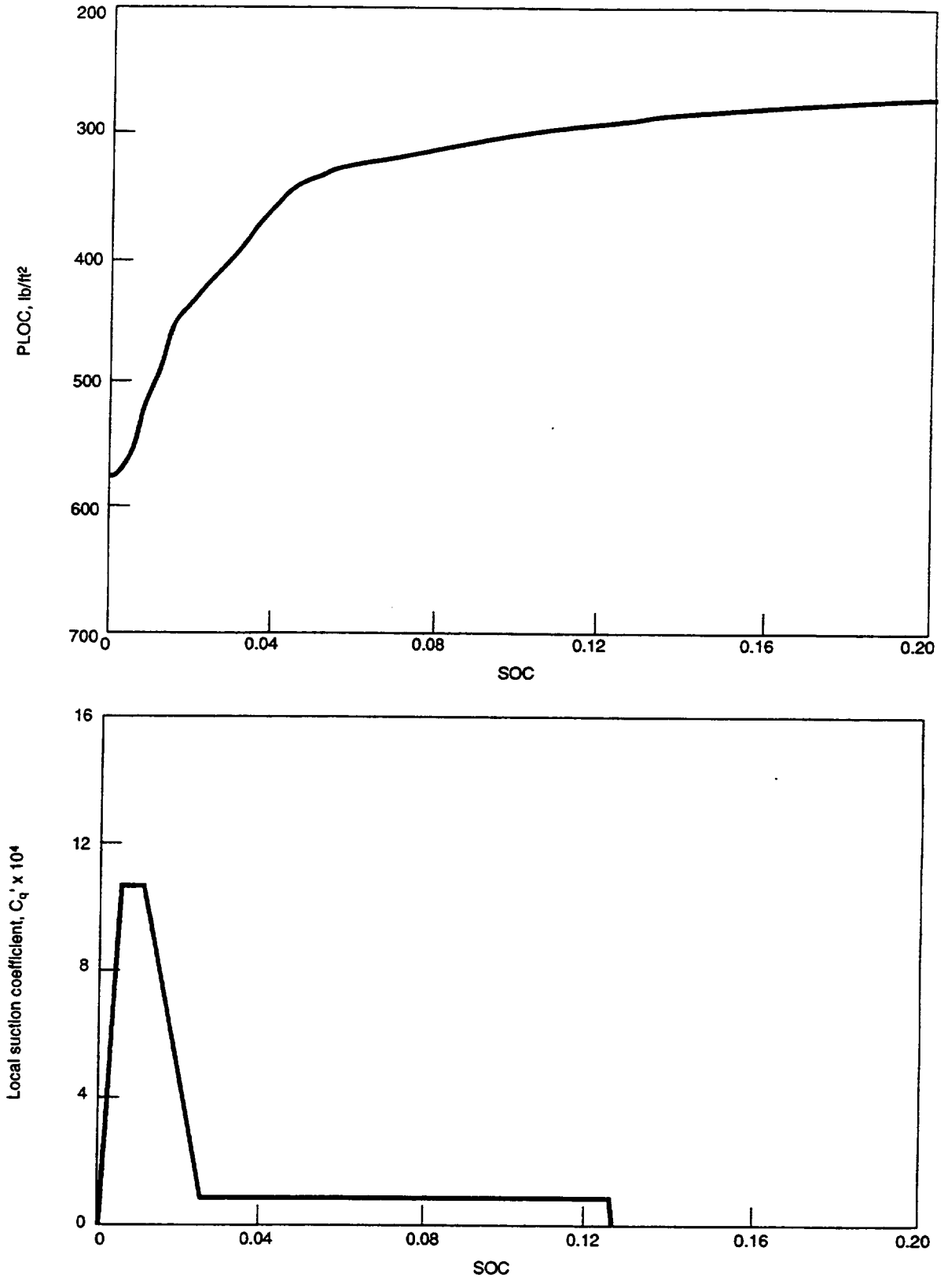

Figure G-1. External Pressure and Suction Distributions, WBL 290

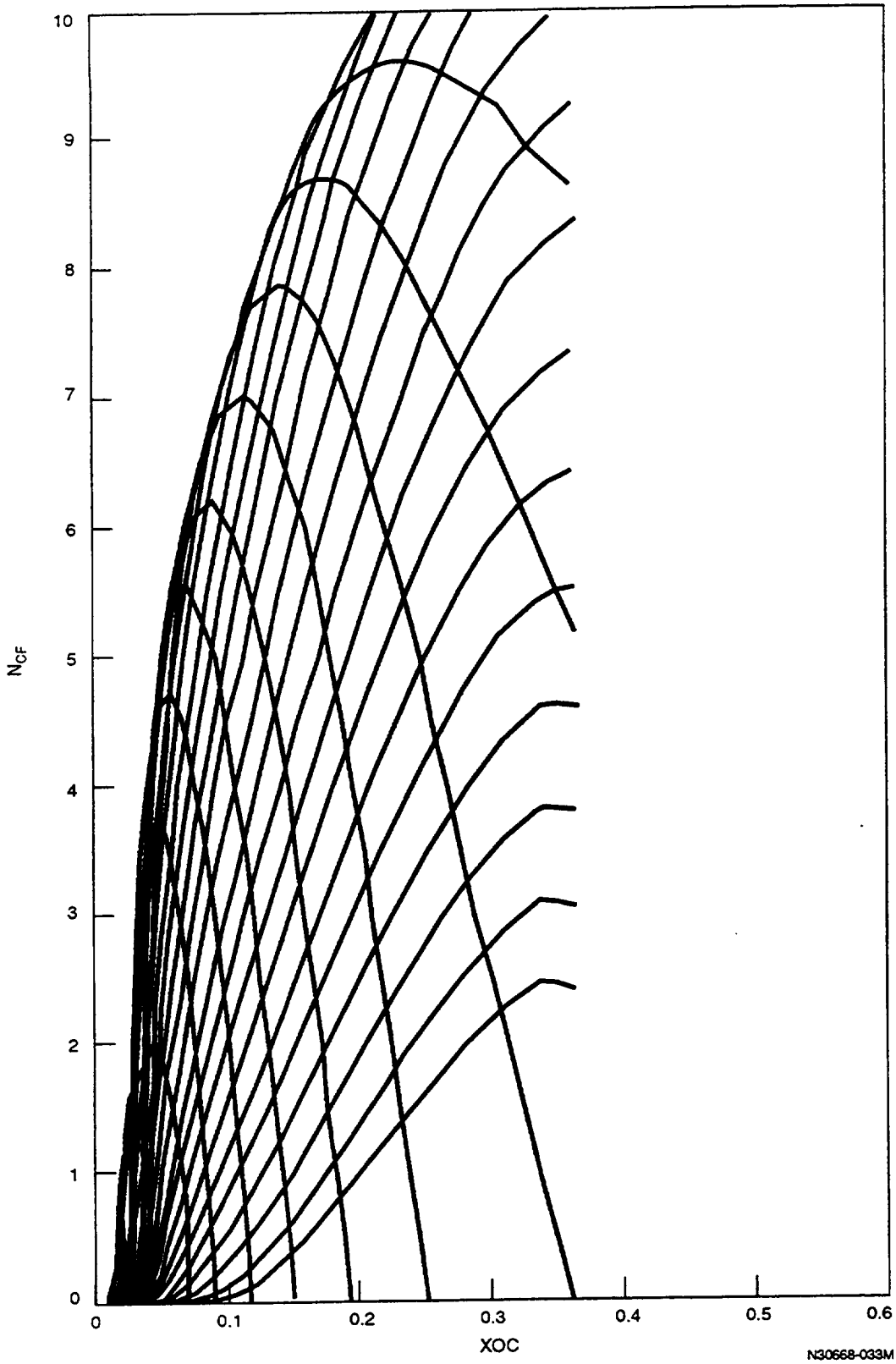

Figure G-2. Crossflow Disturbance Amplification Factors, WBL 290

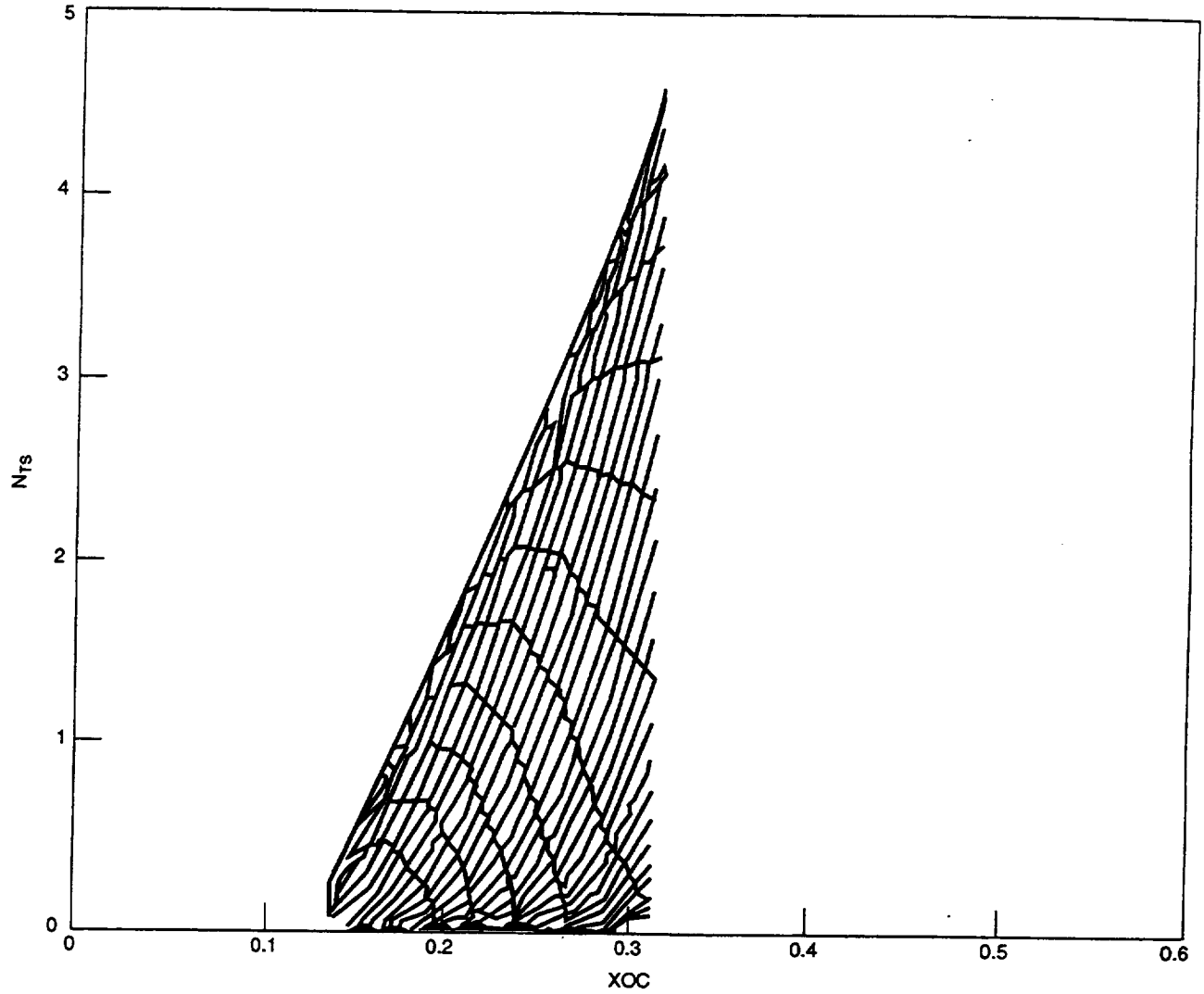

Figure G-3. Tollmien-Schlichting Disturbance Amplification Factors, WBL 290

N30668-034M

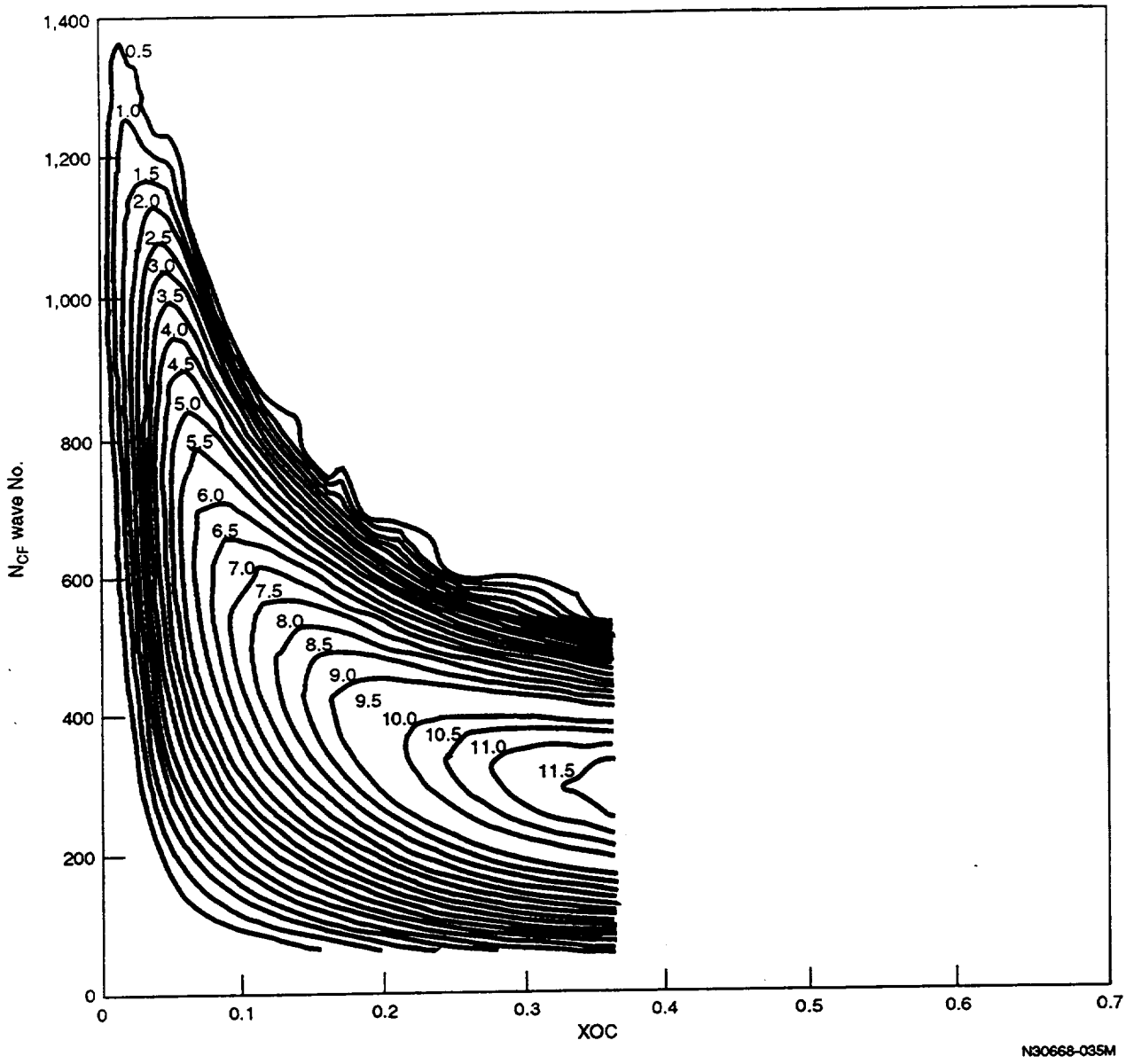

Figure G-4. Contour Plot of CF Disturbance Amplification Factors, WBL 290

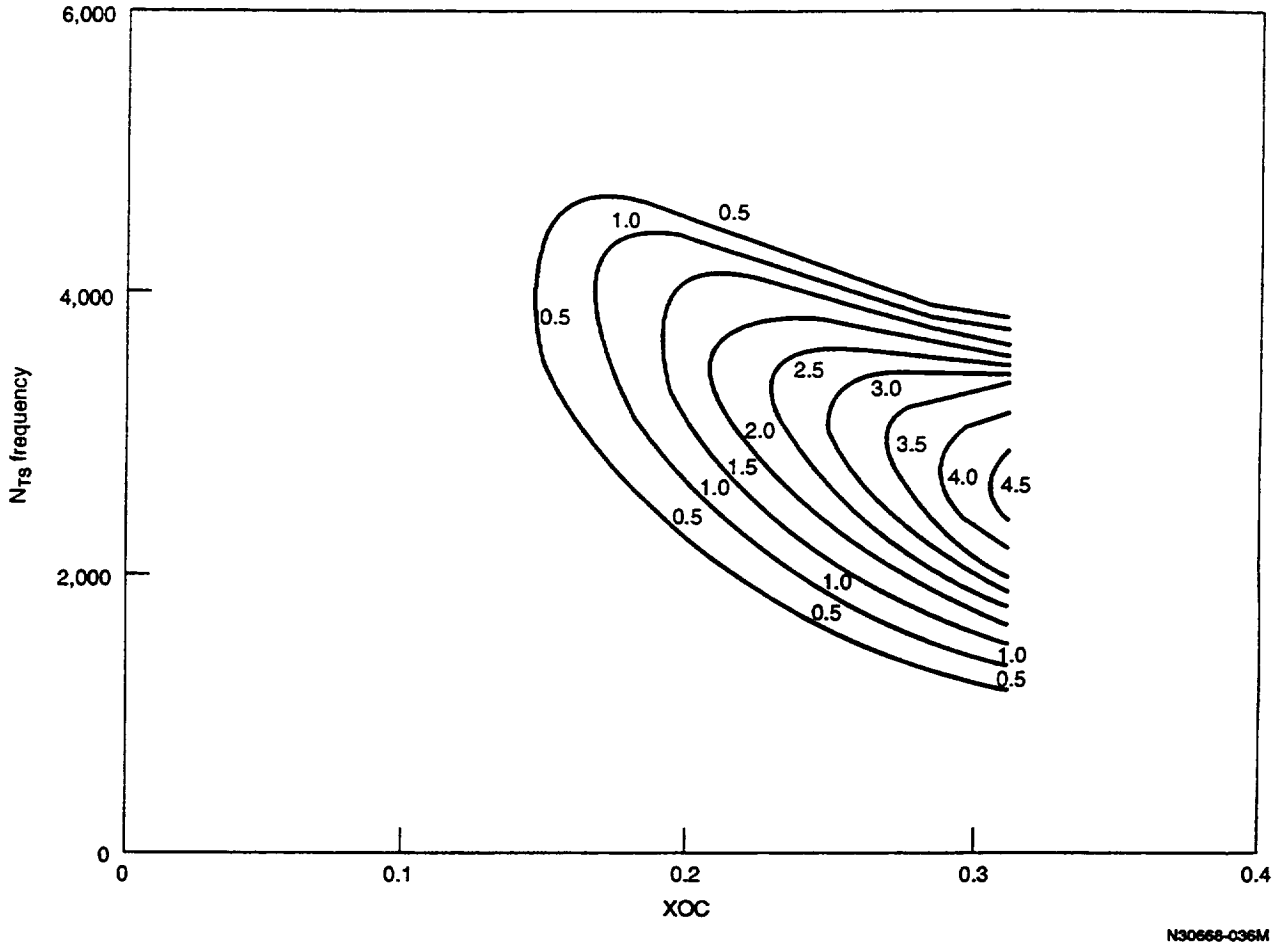

Figure G-5. Contour Plot of TS Disturbance Amplification Factors, WBL 290

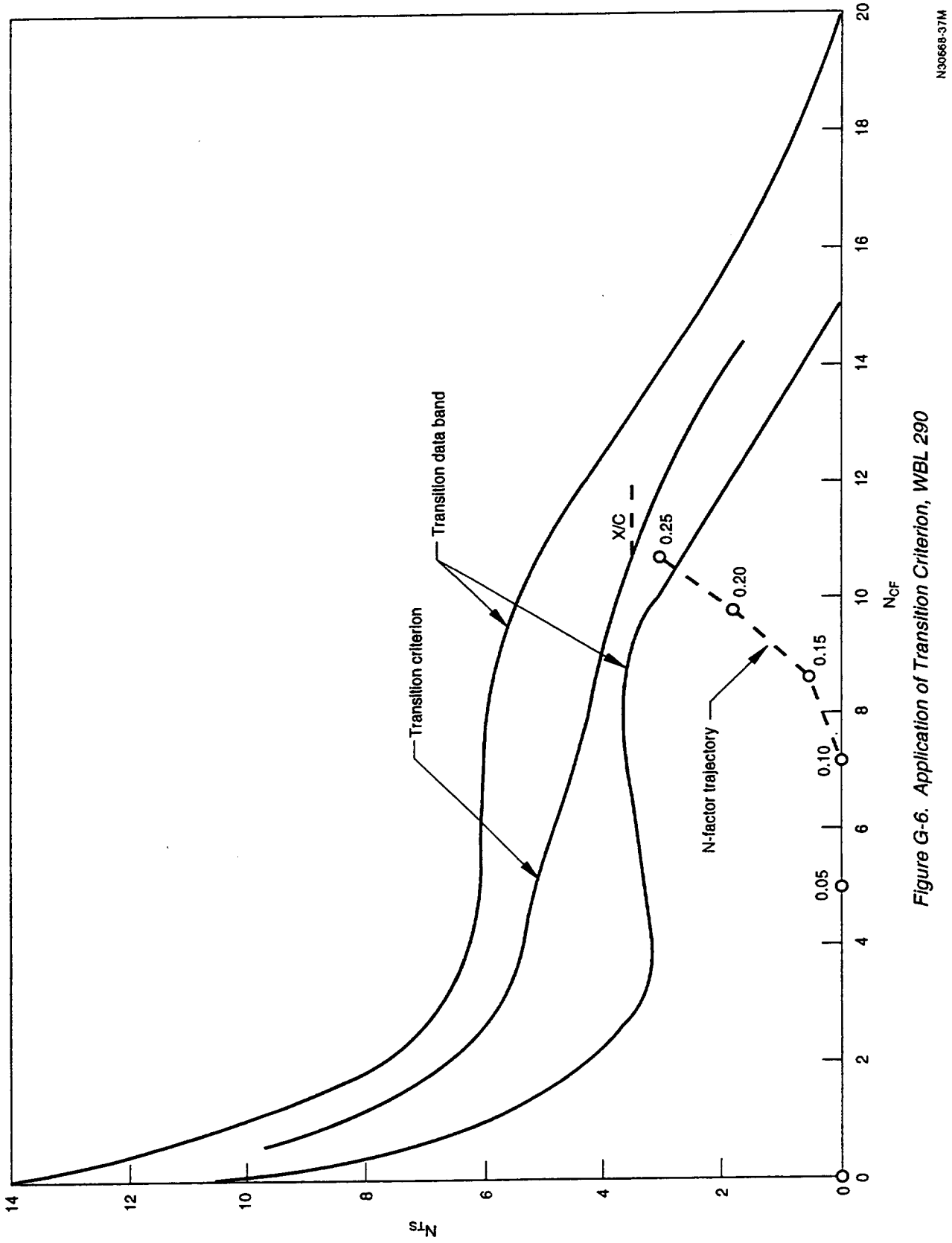

Figure G-6. Application of Transition Criterion, WBL 290

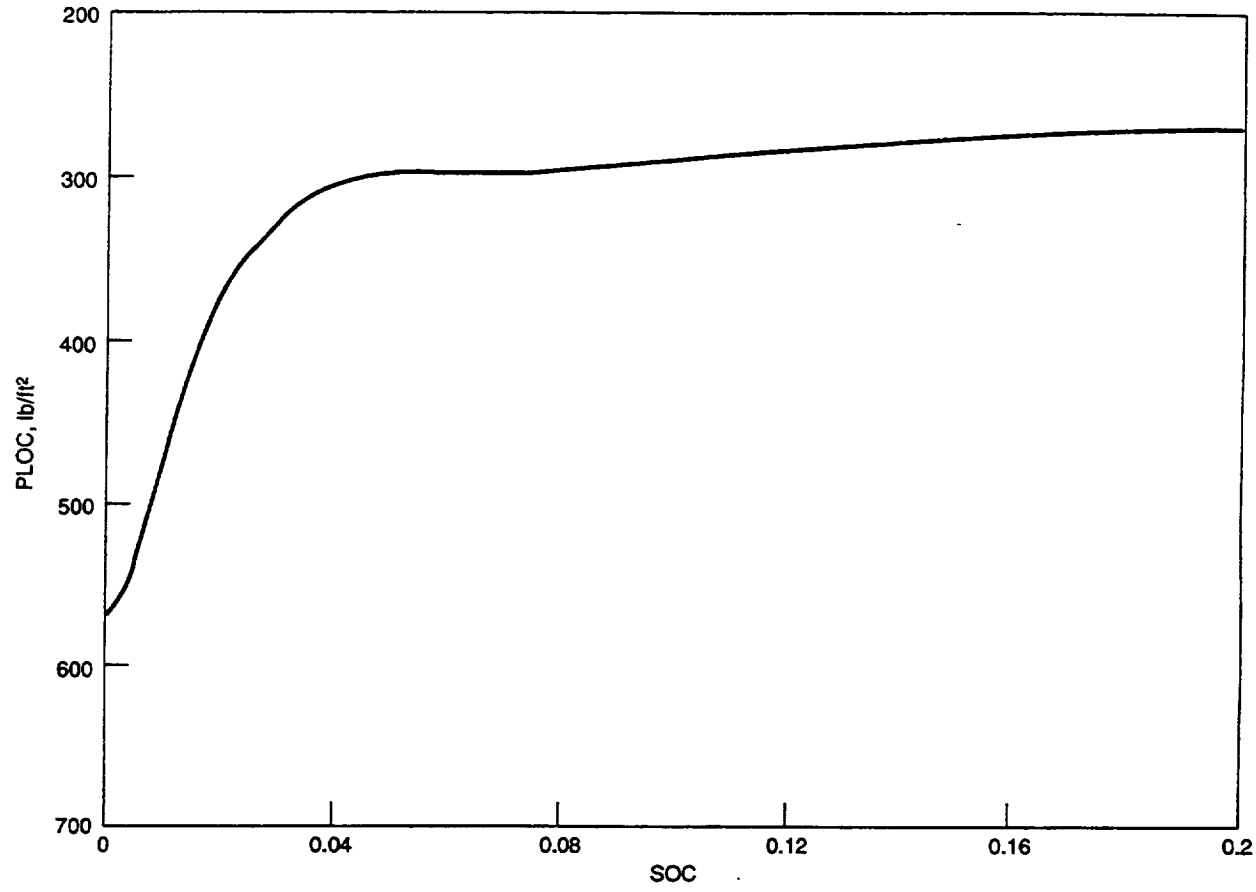

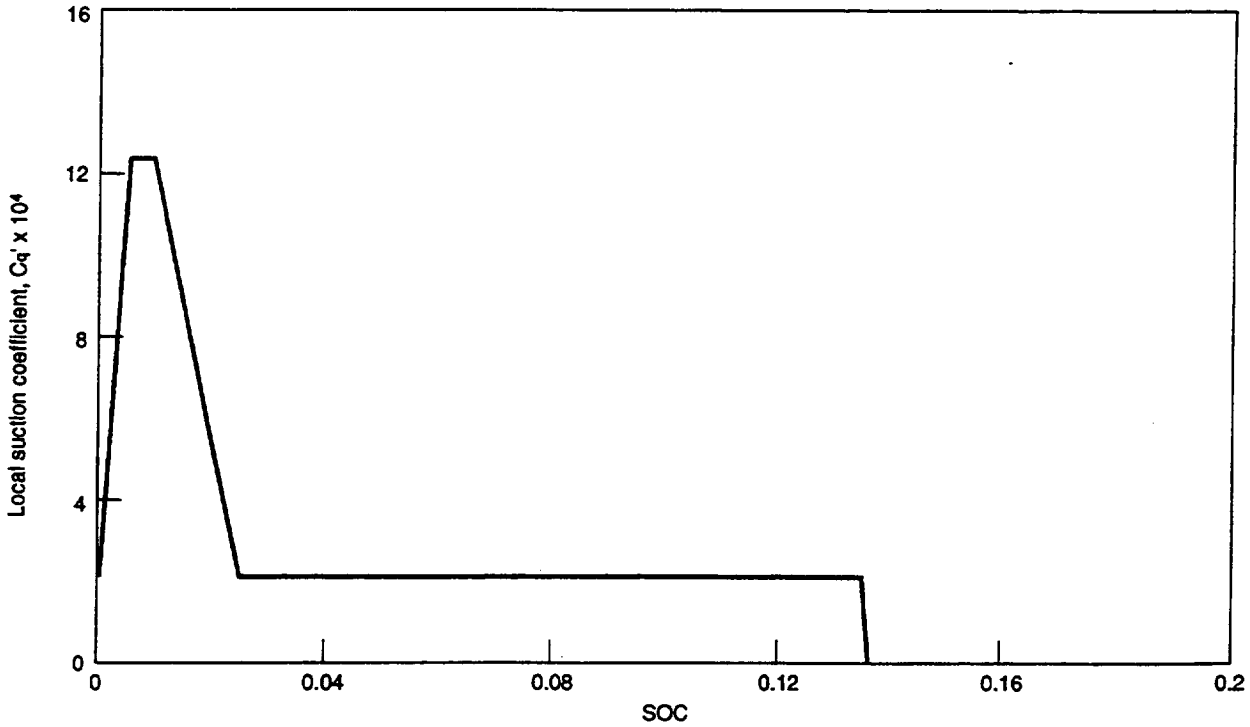

Figure G-7. External Pressure and Suction Distributions, WBL 311

N30668-038M

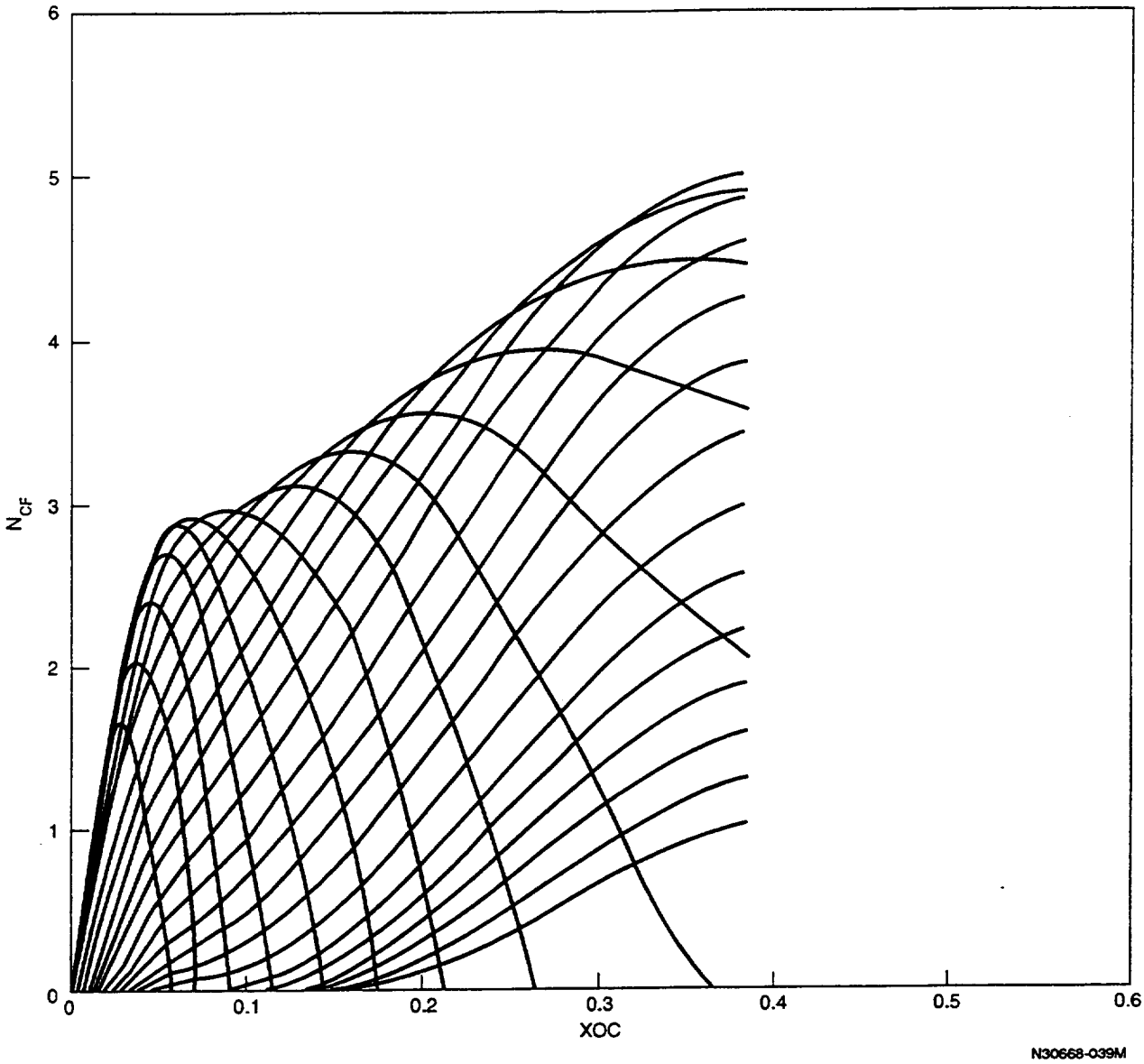

Figure G-8. Crossflow Disturbance Amplification Factors, WBL 311

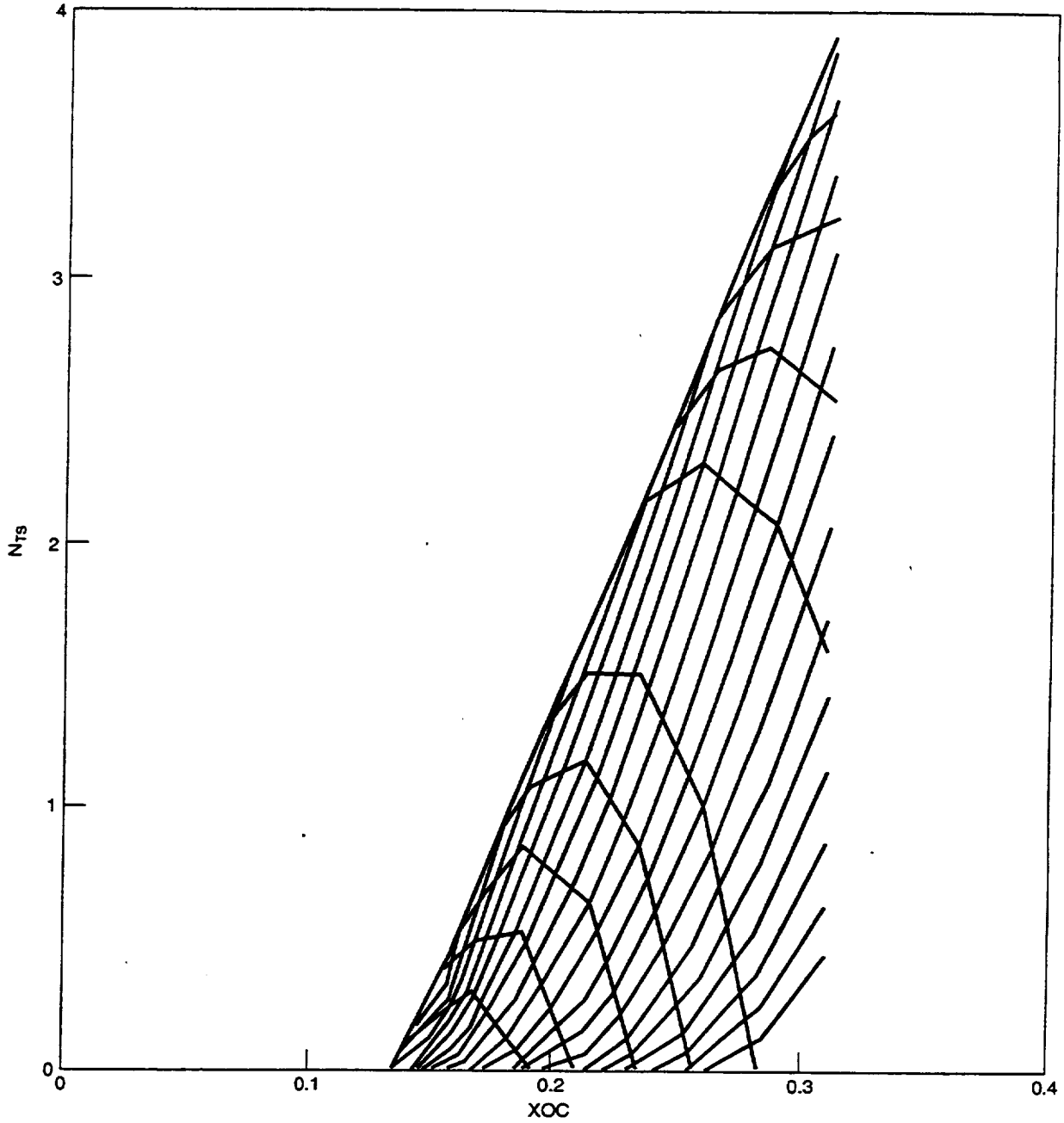

Figure G-9. Tollmien-Schlichting Disturbance Amplification Factors, WBL 311

N30568-040M

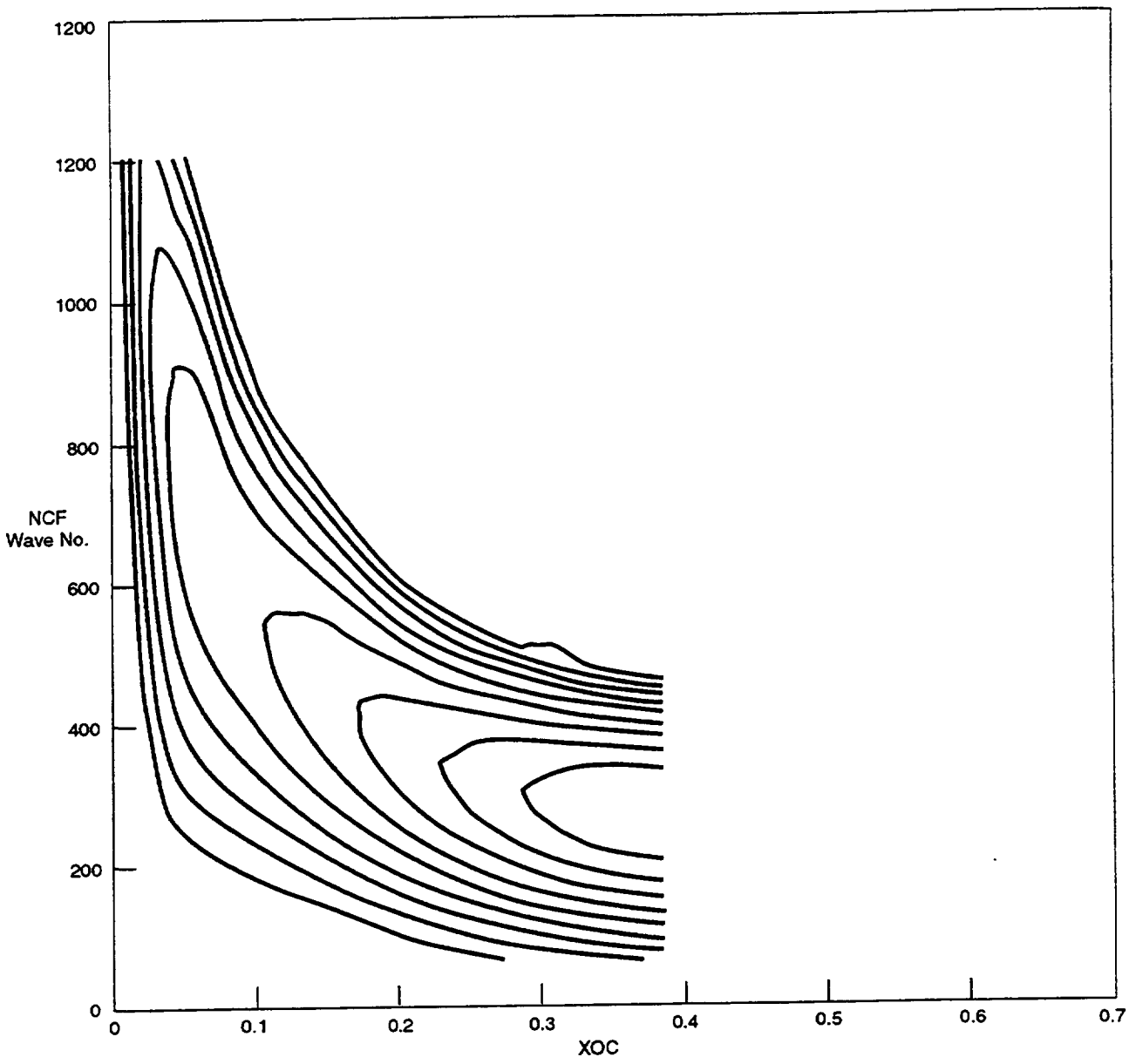

Figure G-10. Contour Plot of C-F Disturbance Amplification Factors, WBL 311

N30668-041M

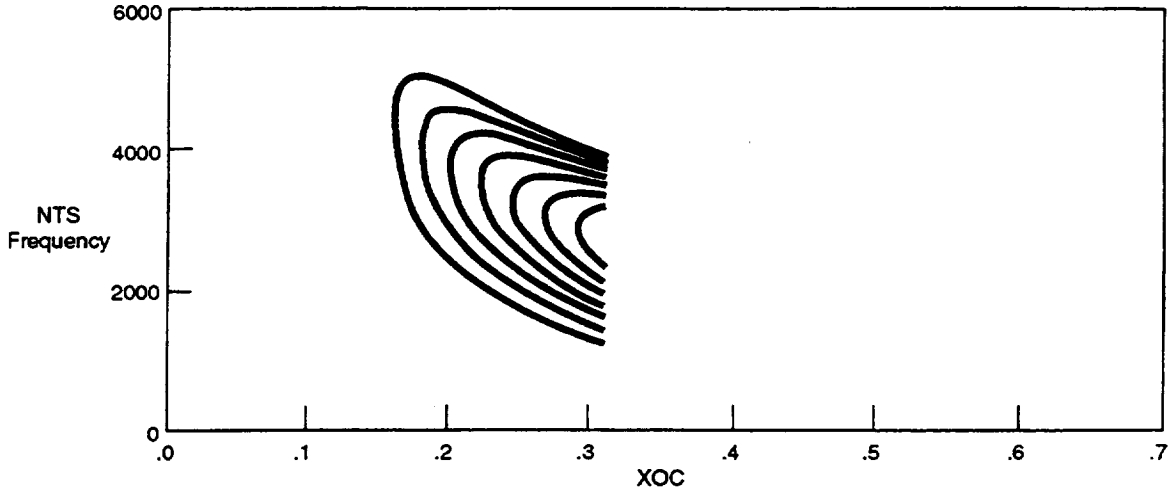

Figure G-11. Contour Plot of T-S Disturbance Amplification Factors, WBL 311

N30668-042M

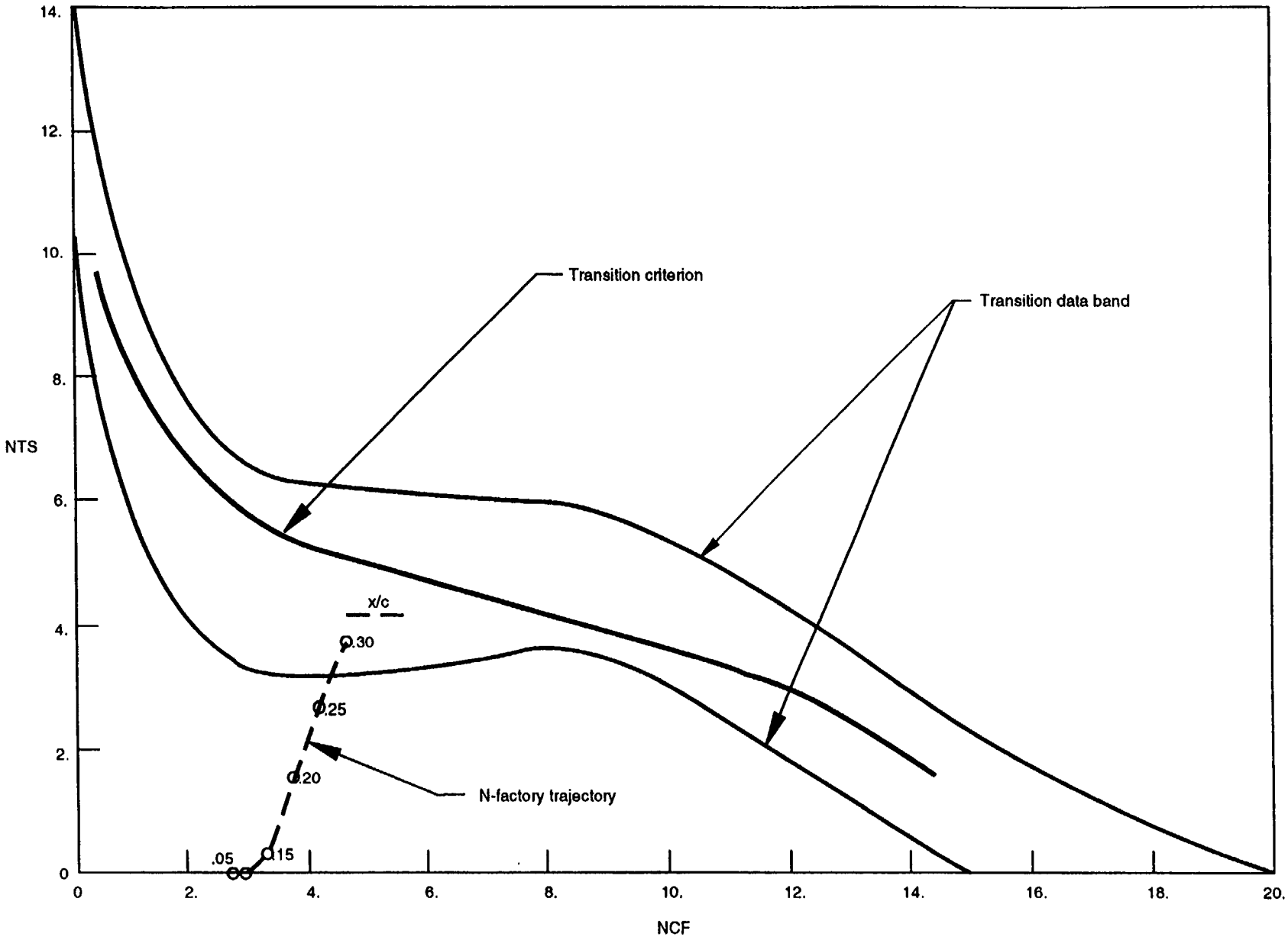

Figure G-12. Application of Transition Criterion, WBL 311

N30668-043M

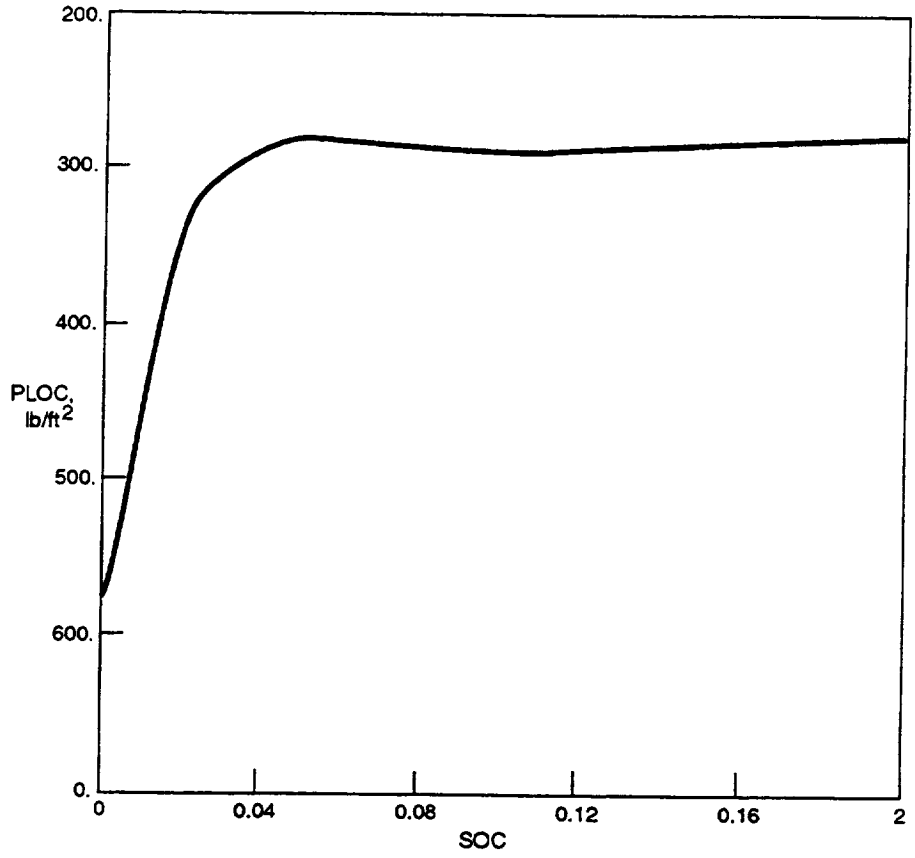

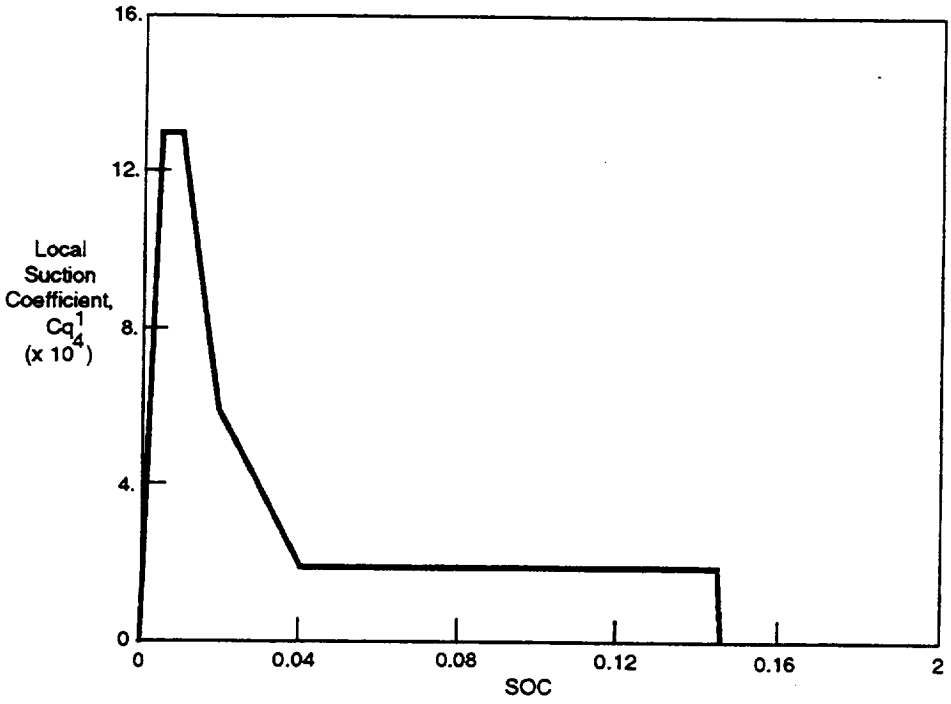

Figure G-13. External Pressure And Suction Distributions

N30668-044M

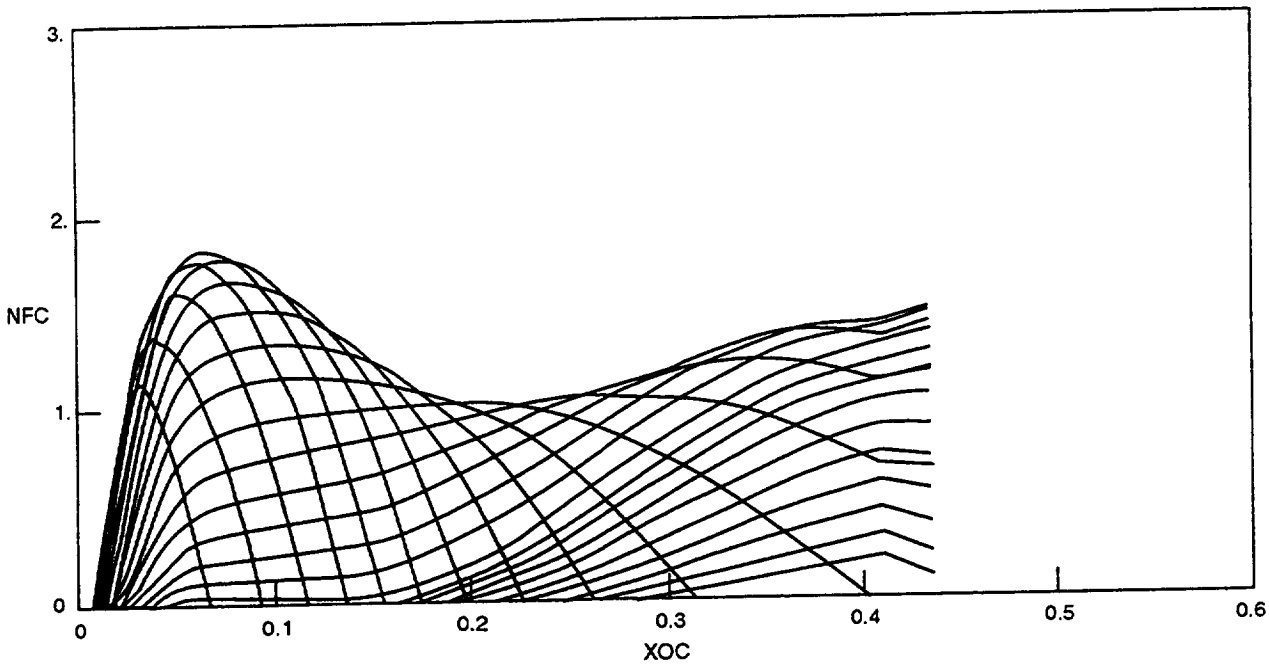

Figure G-14. Crossflow Disturbance Aplification Factors, WBL 360

N30668-045M

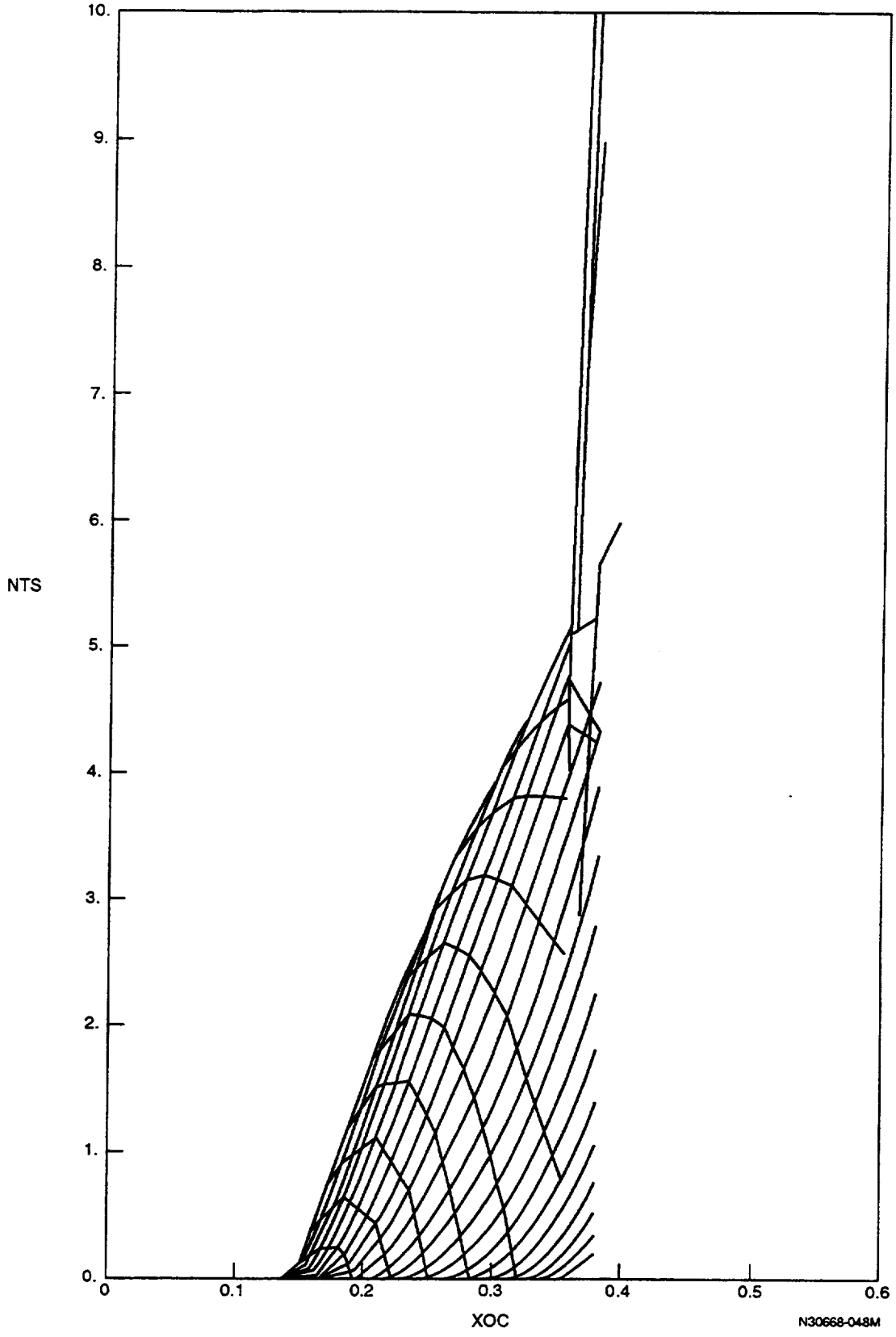

Figure G-15. Tollmien-Schlichting Disturbance Amplification Factors, WBL 360

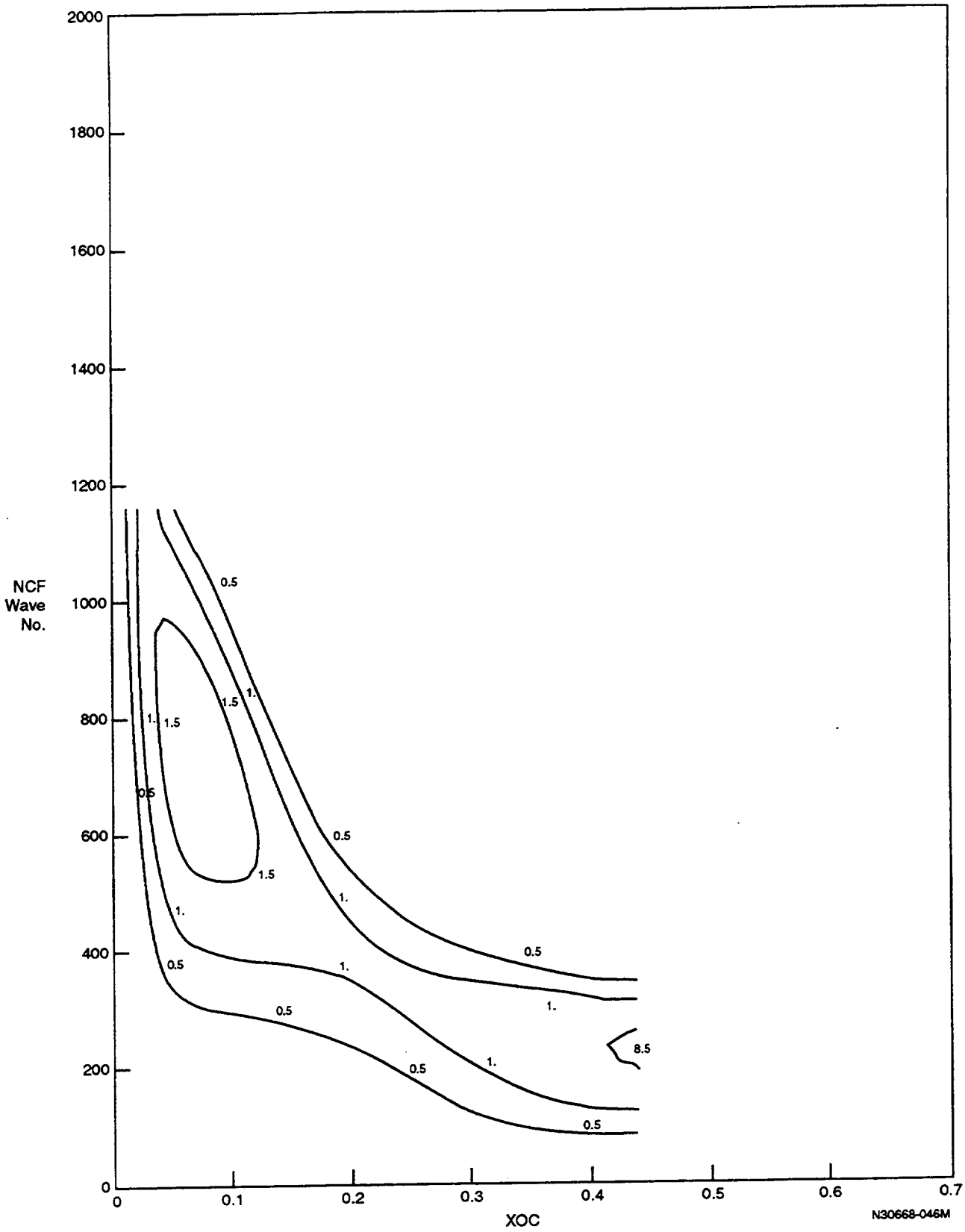

Figure G-16. Contour Plot of C-F Disturbance Amplification Factors, WBL 360

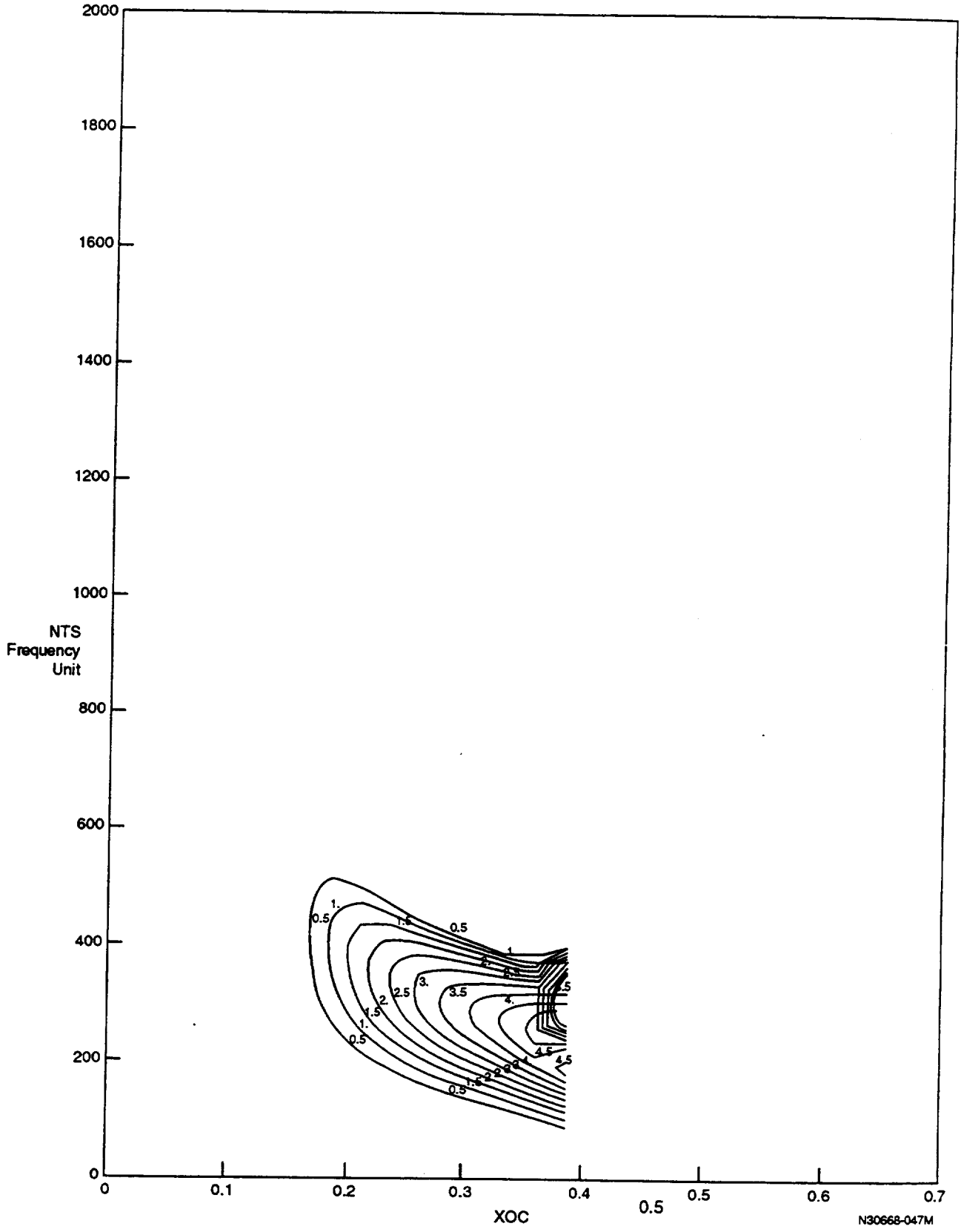

Figure G-17. Contour Plot of T-S Disturbance Amplification Factors, WBL 360

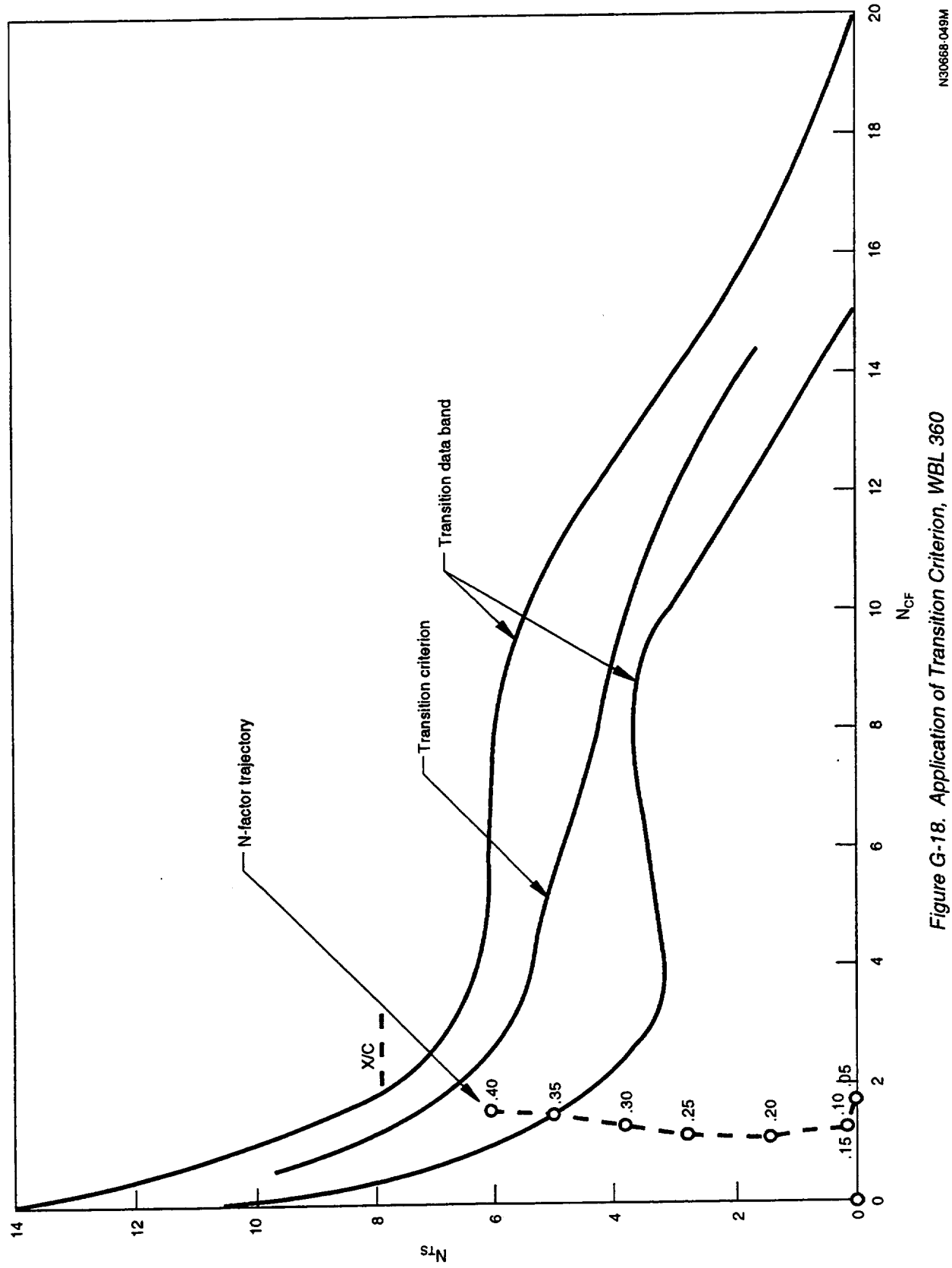

Figure G-18. Application of Transition Criterion, WBL 360

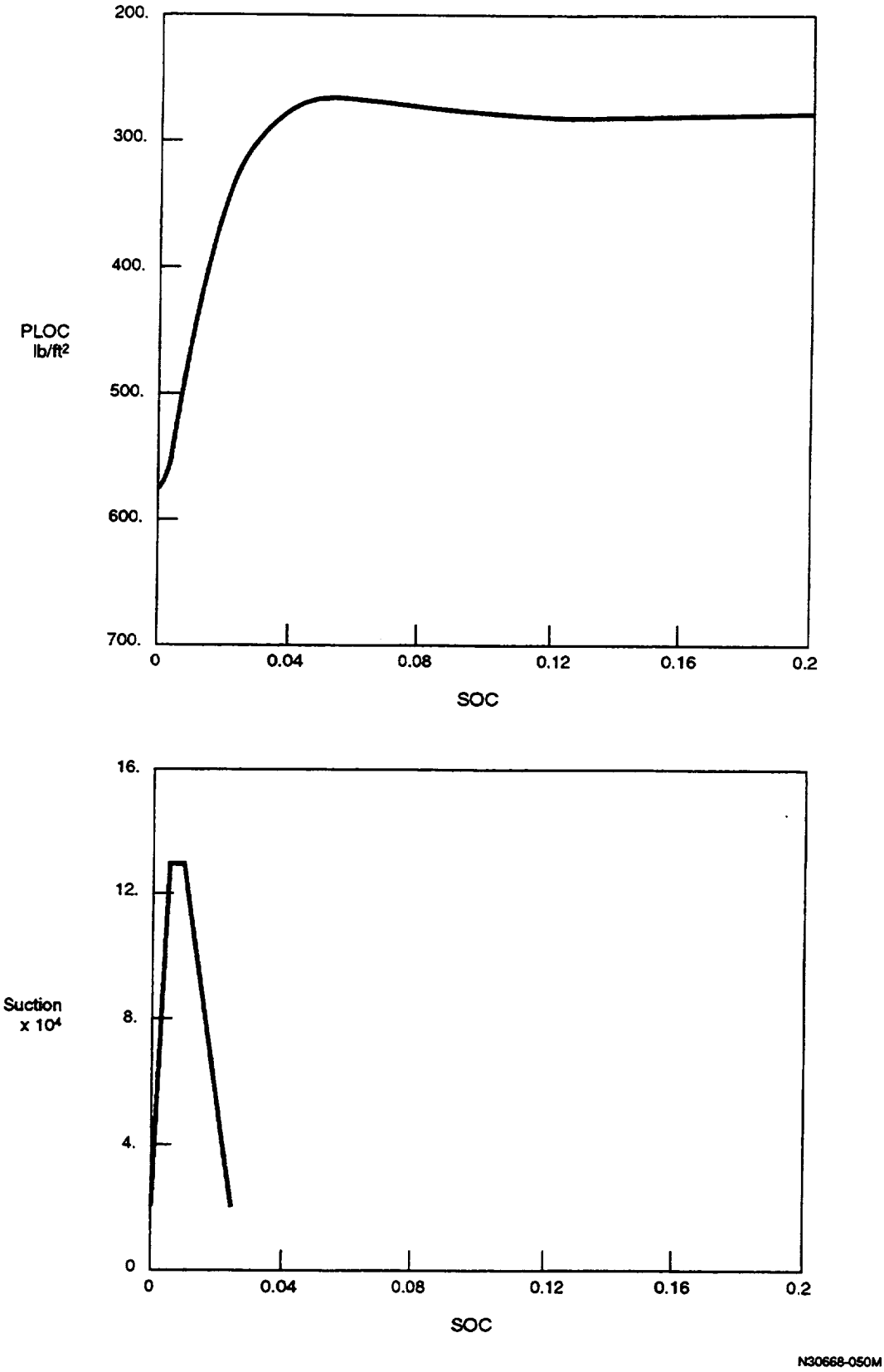

Figure G-19. External Pressure and Suction Distributions, WBL 416

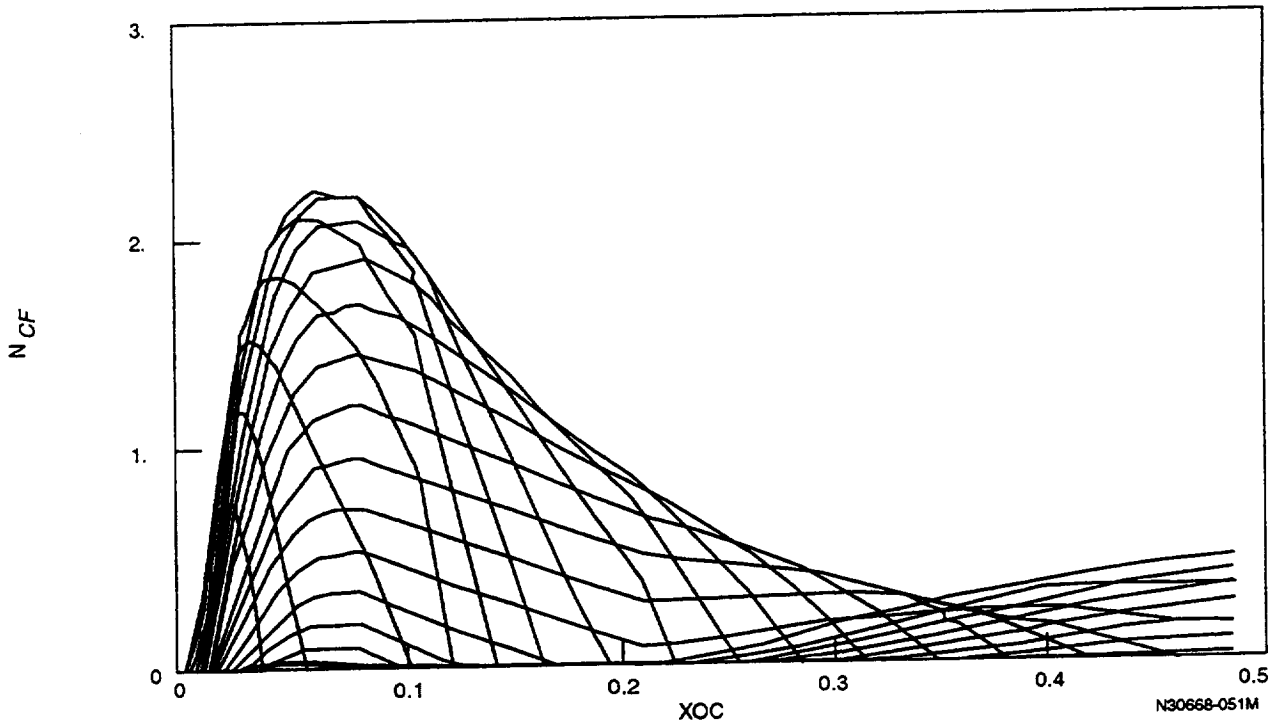

Figure G-20. Crossflow Disturbance Amplification Factors, WBL 416

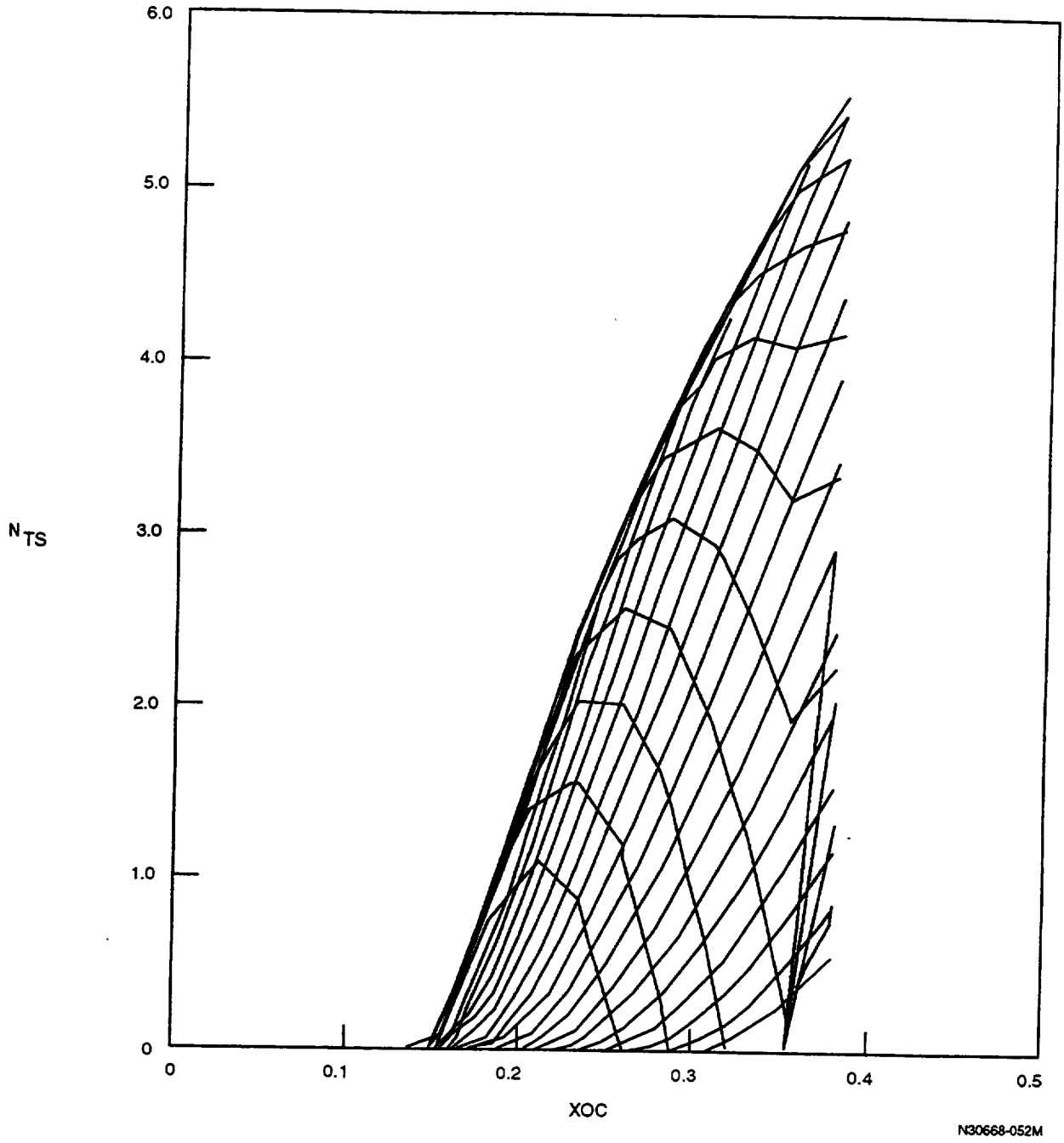

Figure G-21. Tollien-Schlichting Disturbance Amplification Factors, WBL 416

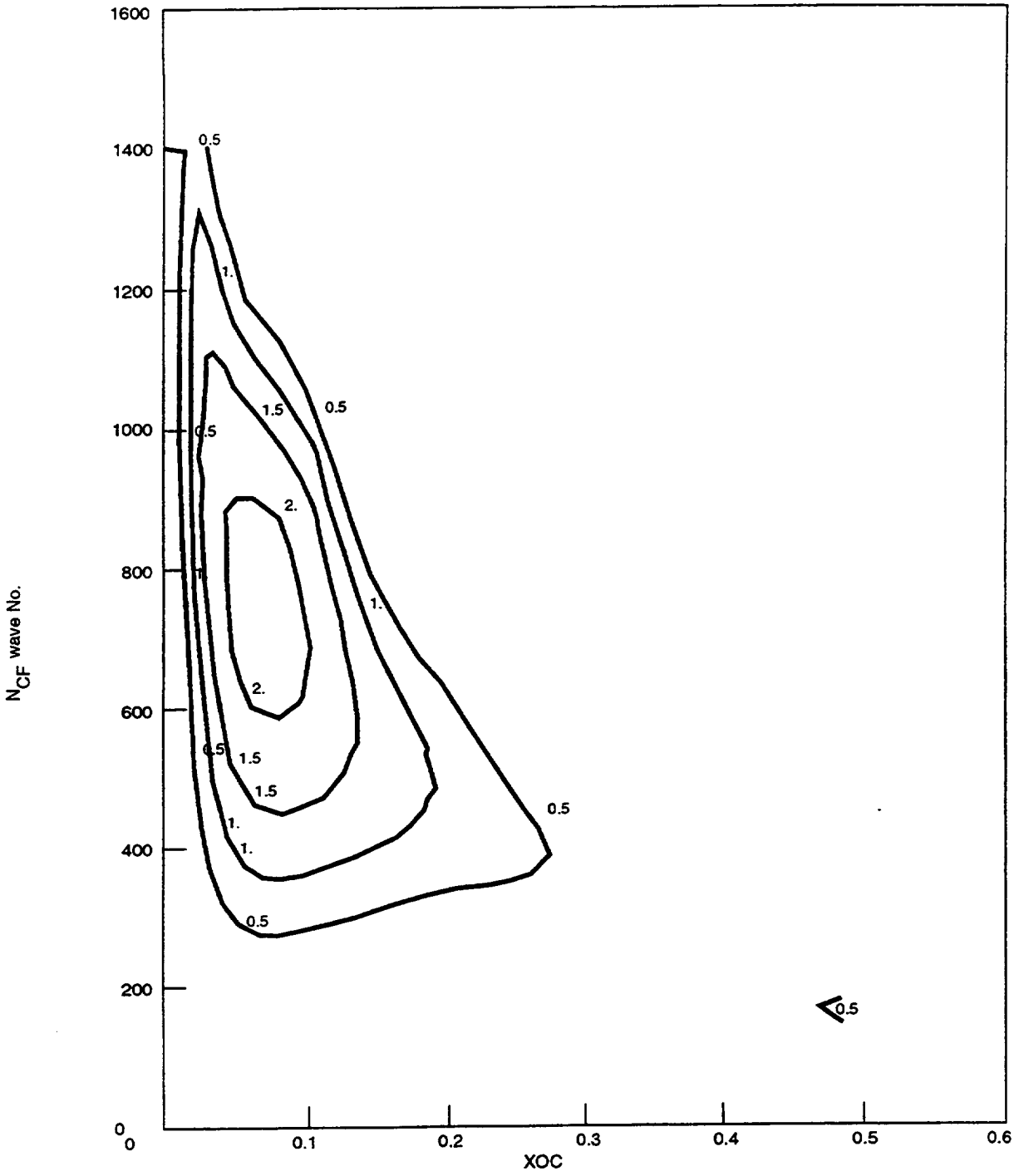

Figure G-22. Contour Plot of CF Disturbance Amplification Factors, WBL 416

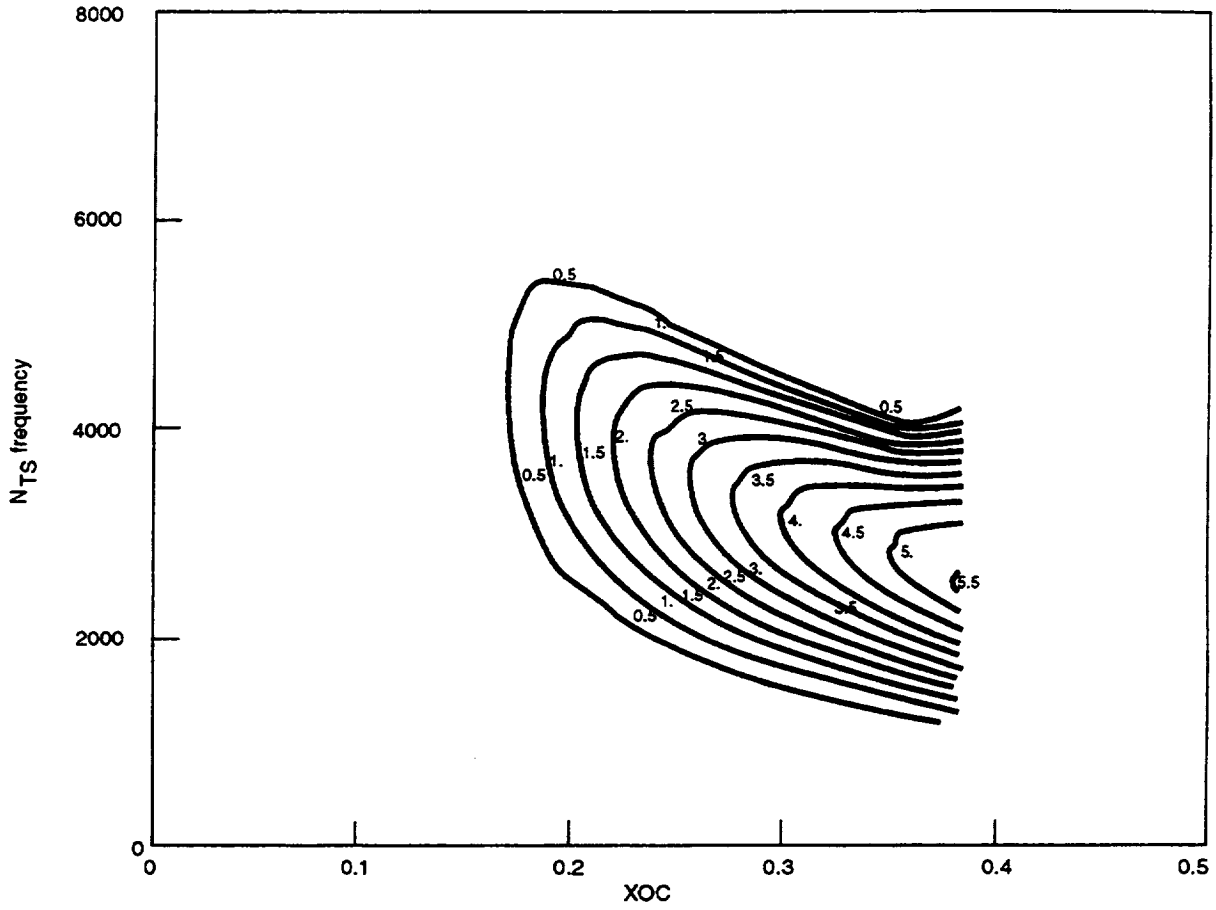

Figure G-23. Contour Plot of TS Disturbance Amplification Factors, WBL 416

N30668-054M

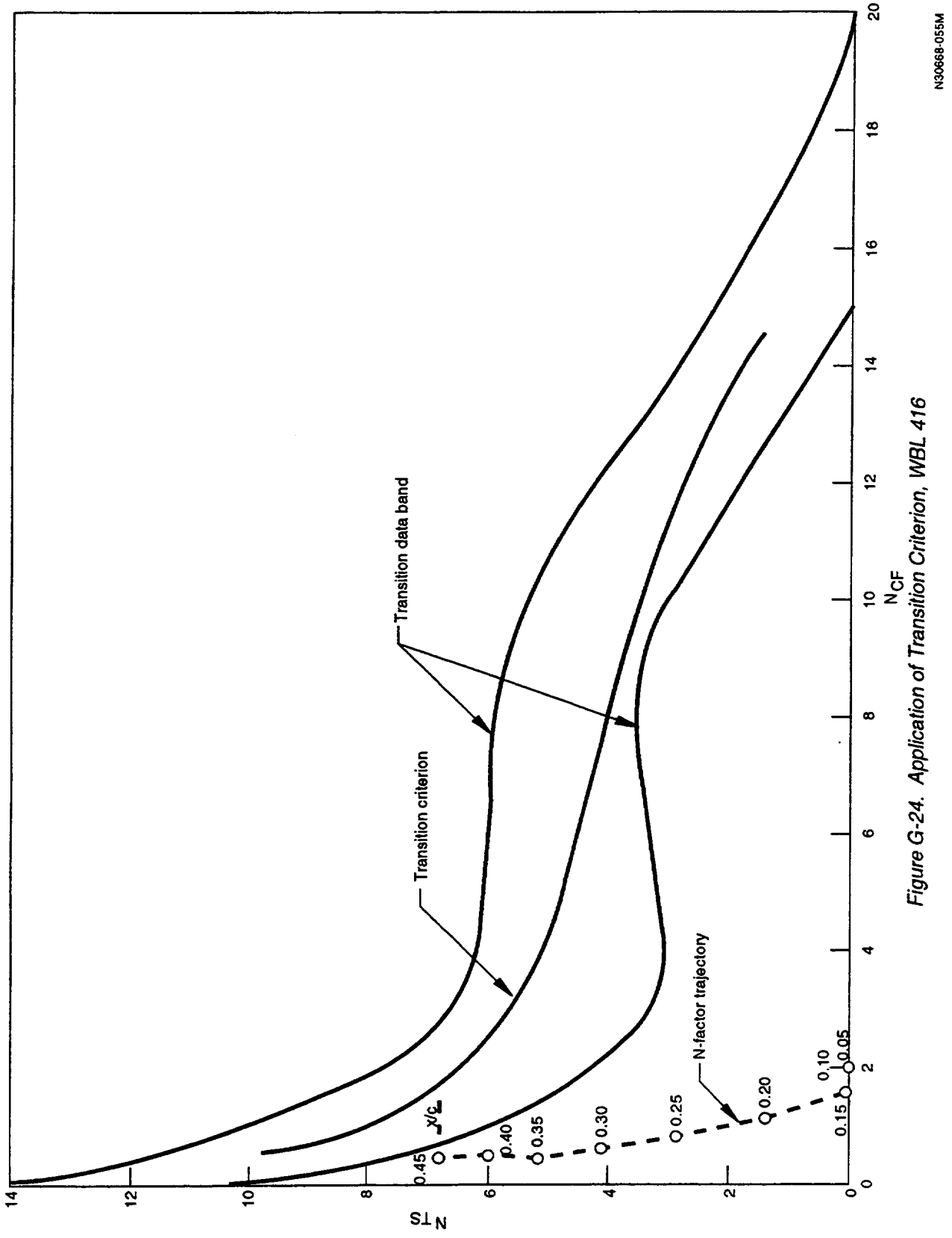

Figure G-24. Application of Transition Criterion, WBL 416

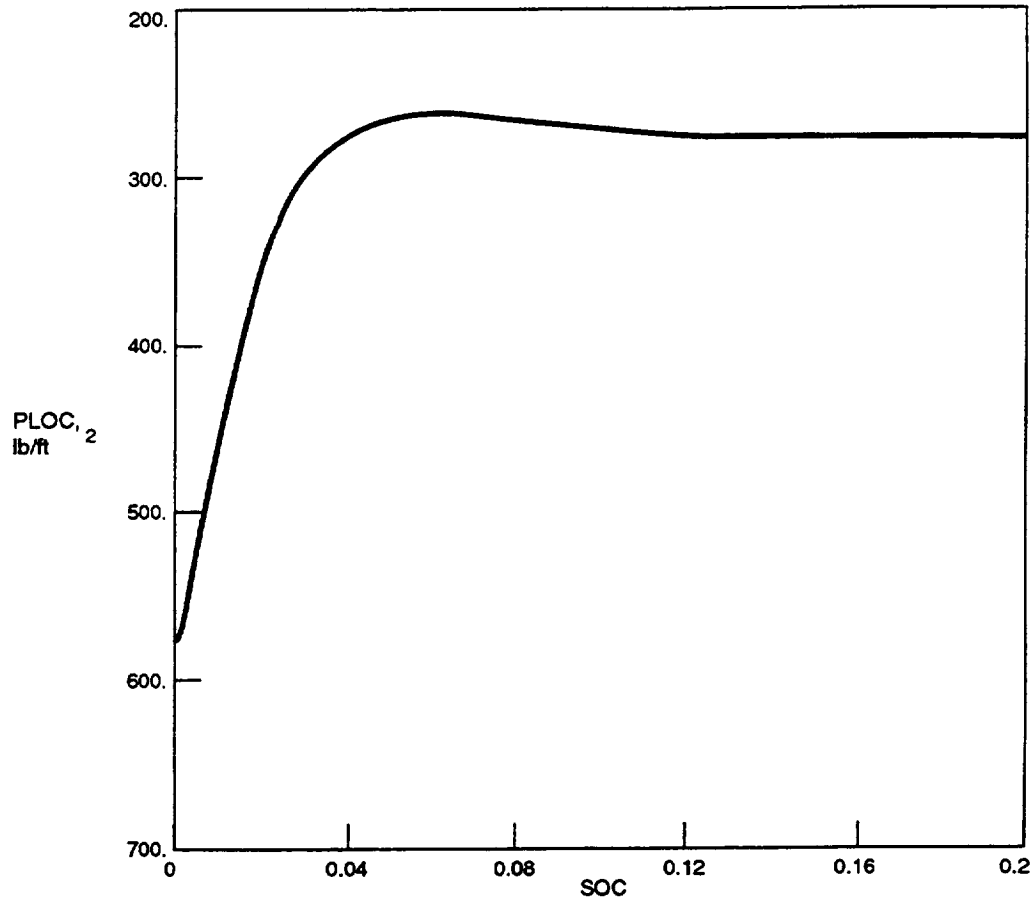

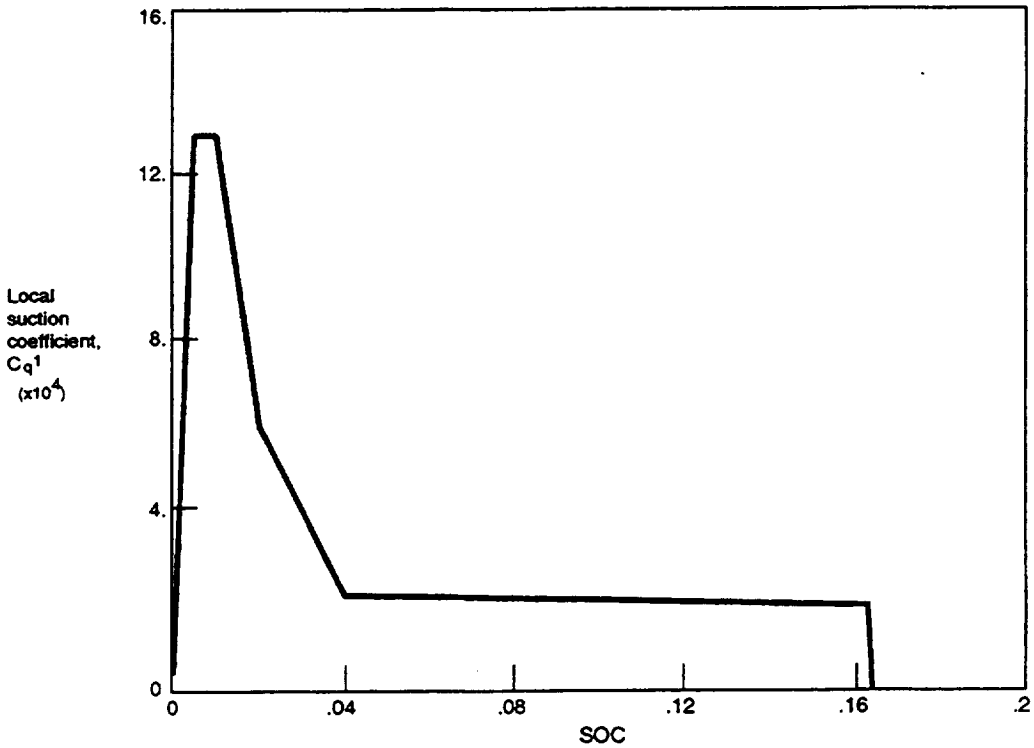

Figure G-25. External Pressure and Suction Distributions, WBL 447

N30668-060M

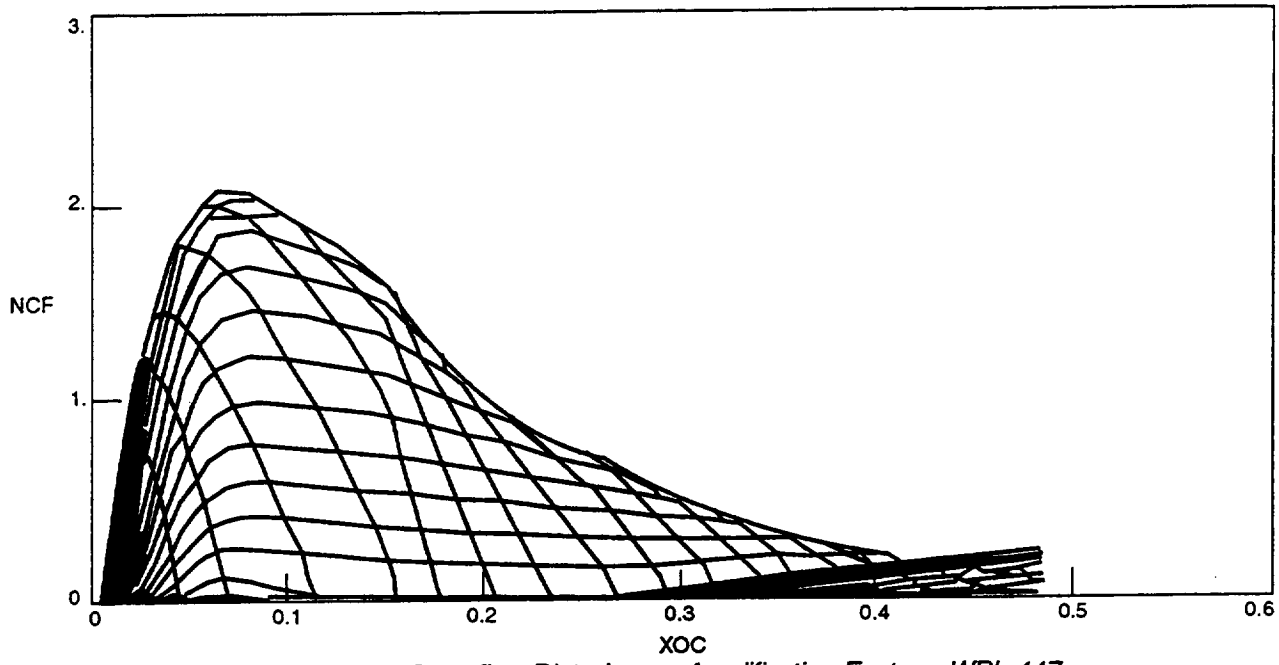

Figure G-26. Crossflow Disturbance Amplification Factors, WBL 447

N30668-056M

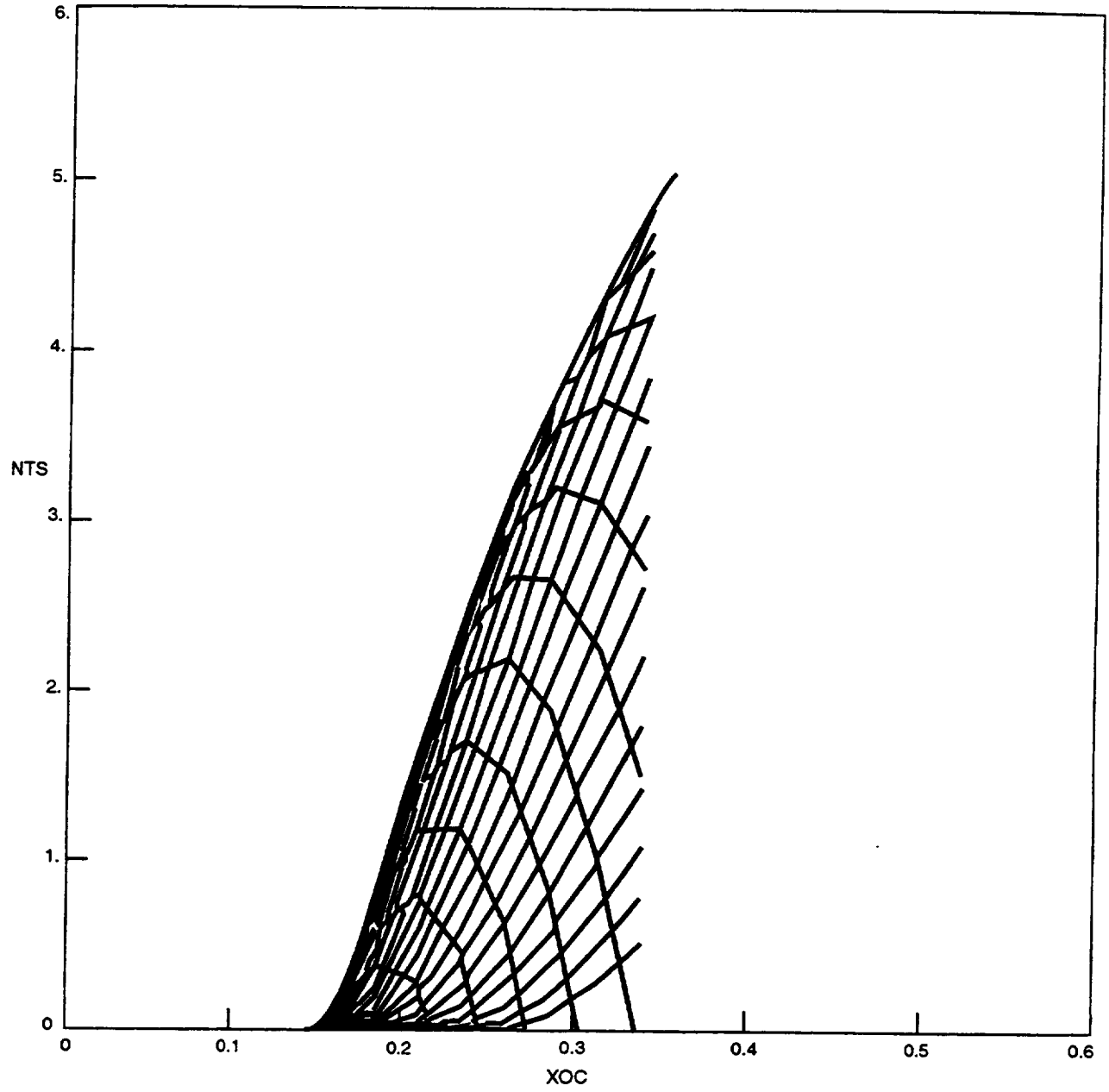

Figure G-27. Tollmein-Schlichting Disturbance Amplification Factors, WBL 447

N30668-057M

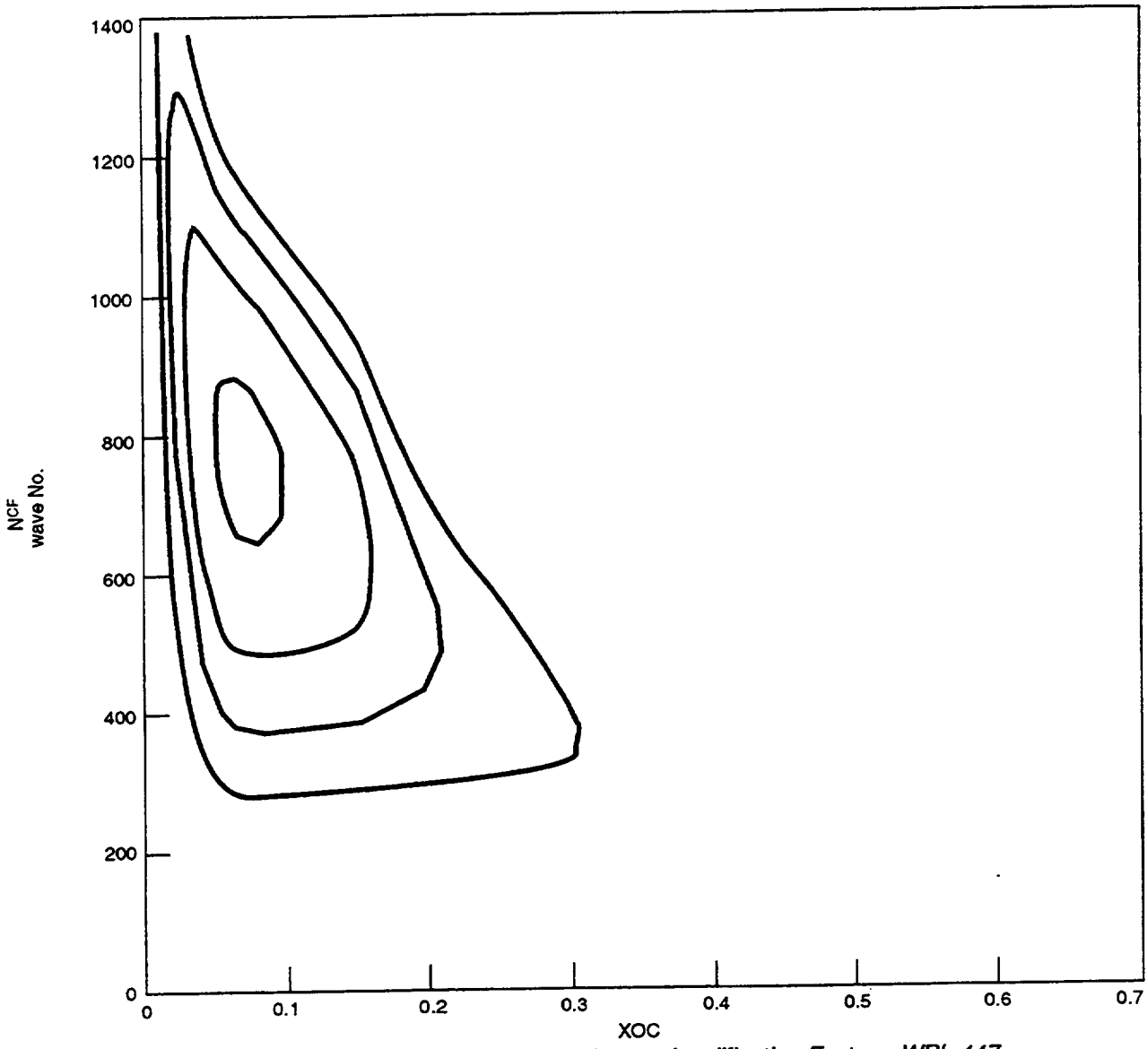

Figure G-28. Control Plot of C-F Disturbance Amplification Factors, WBL 447

N30668-058M

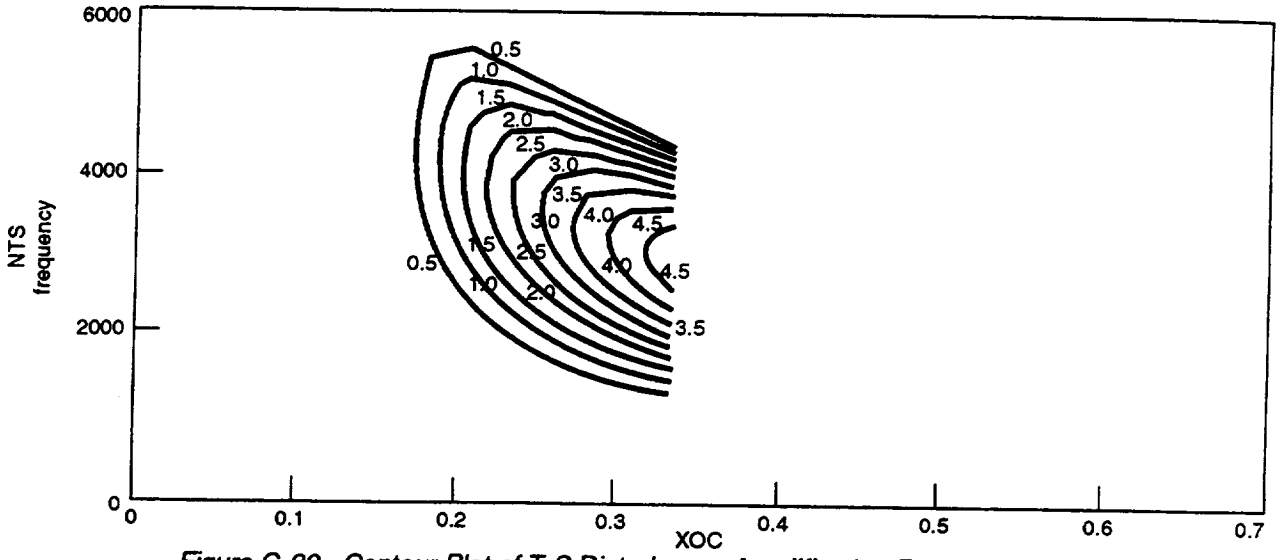

Figure G-29. Contour Plot of T-S Disturbance Amplification Factors WBL 447

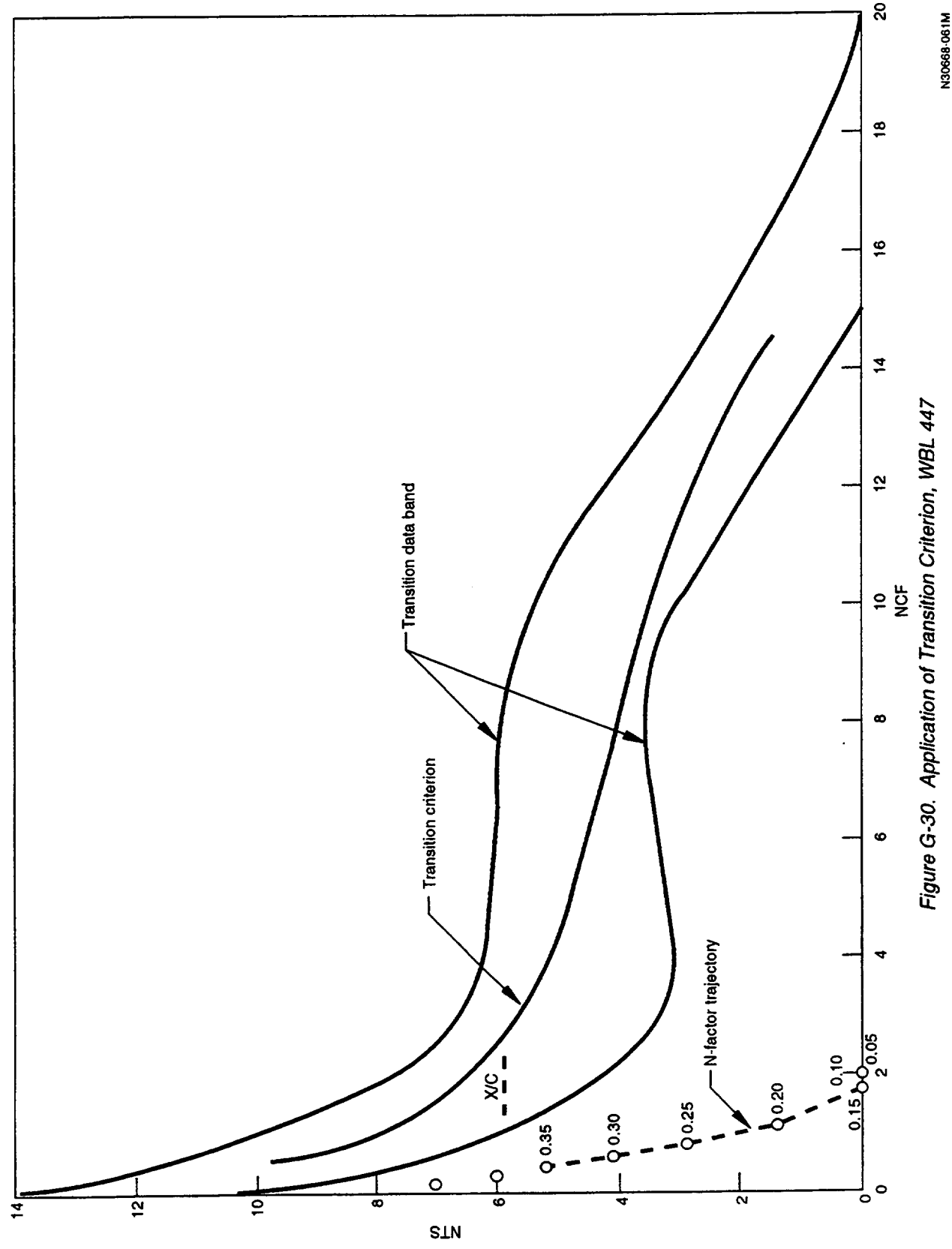

Figure G-30. Application of Transition Criterion, WBL 447

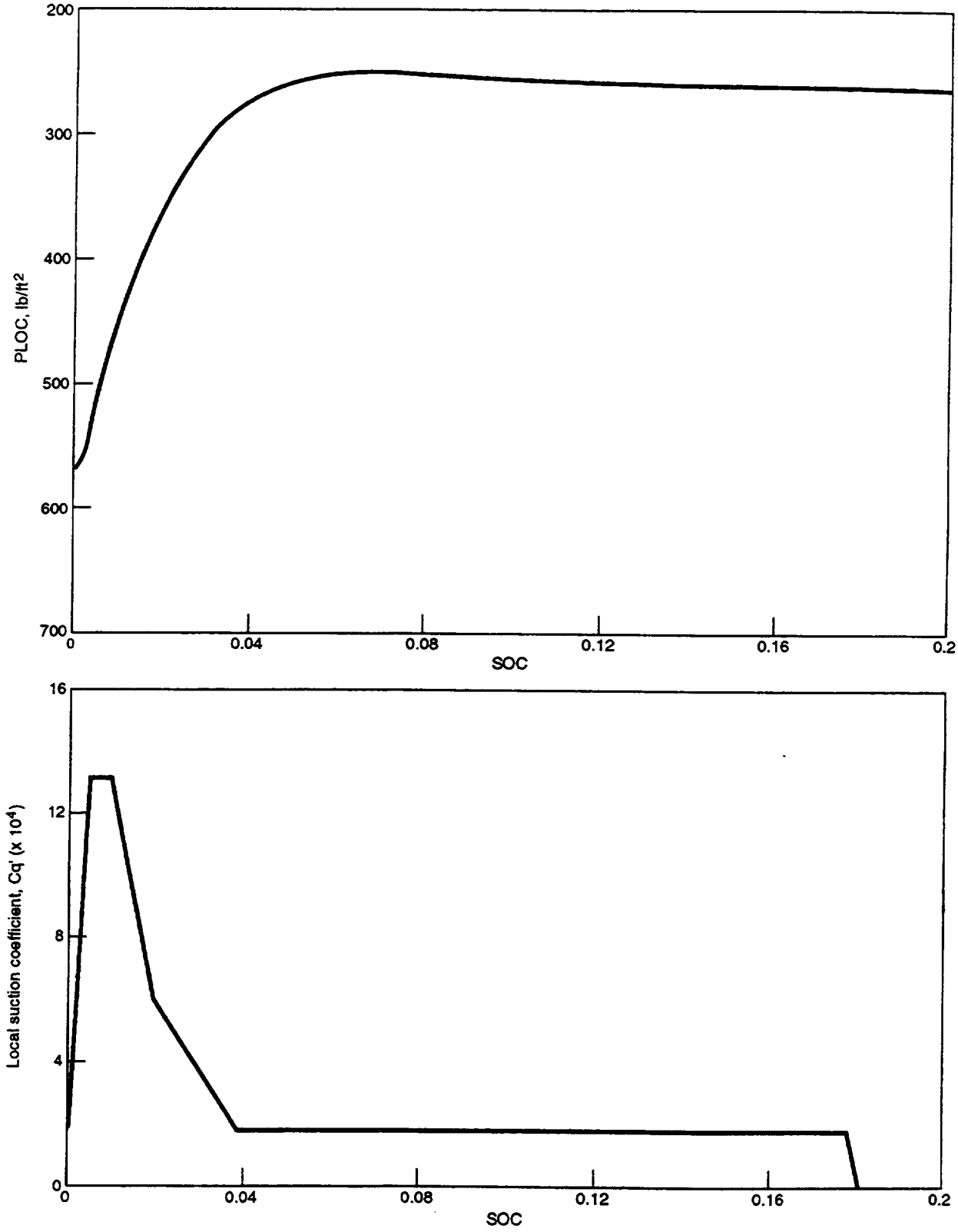

Figure G-31. External Pressure and Suction Distributions, WBL 513

N30668-062M

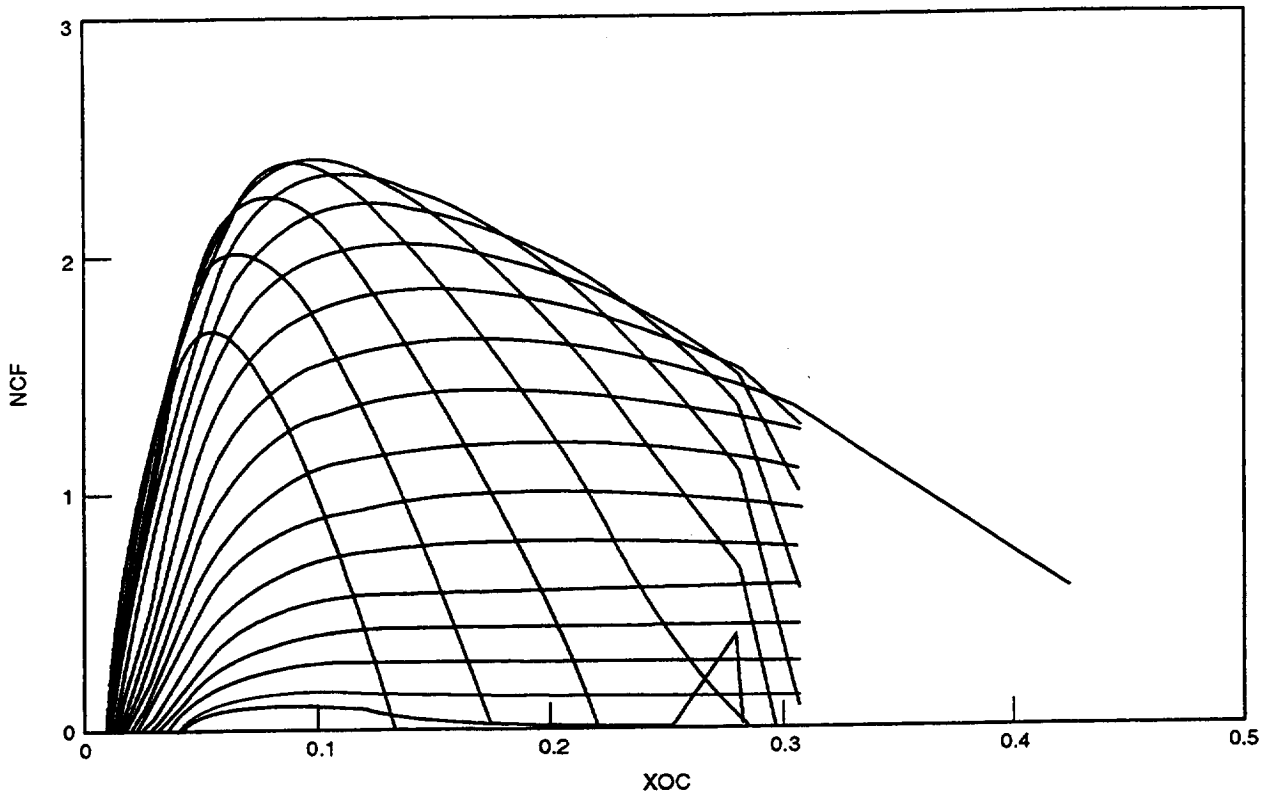

Figure G-32. Crossflow Disturbance Amplification Factors, WBL 513

N30668-063M

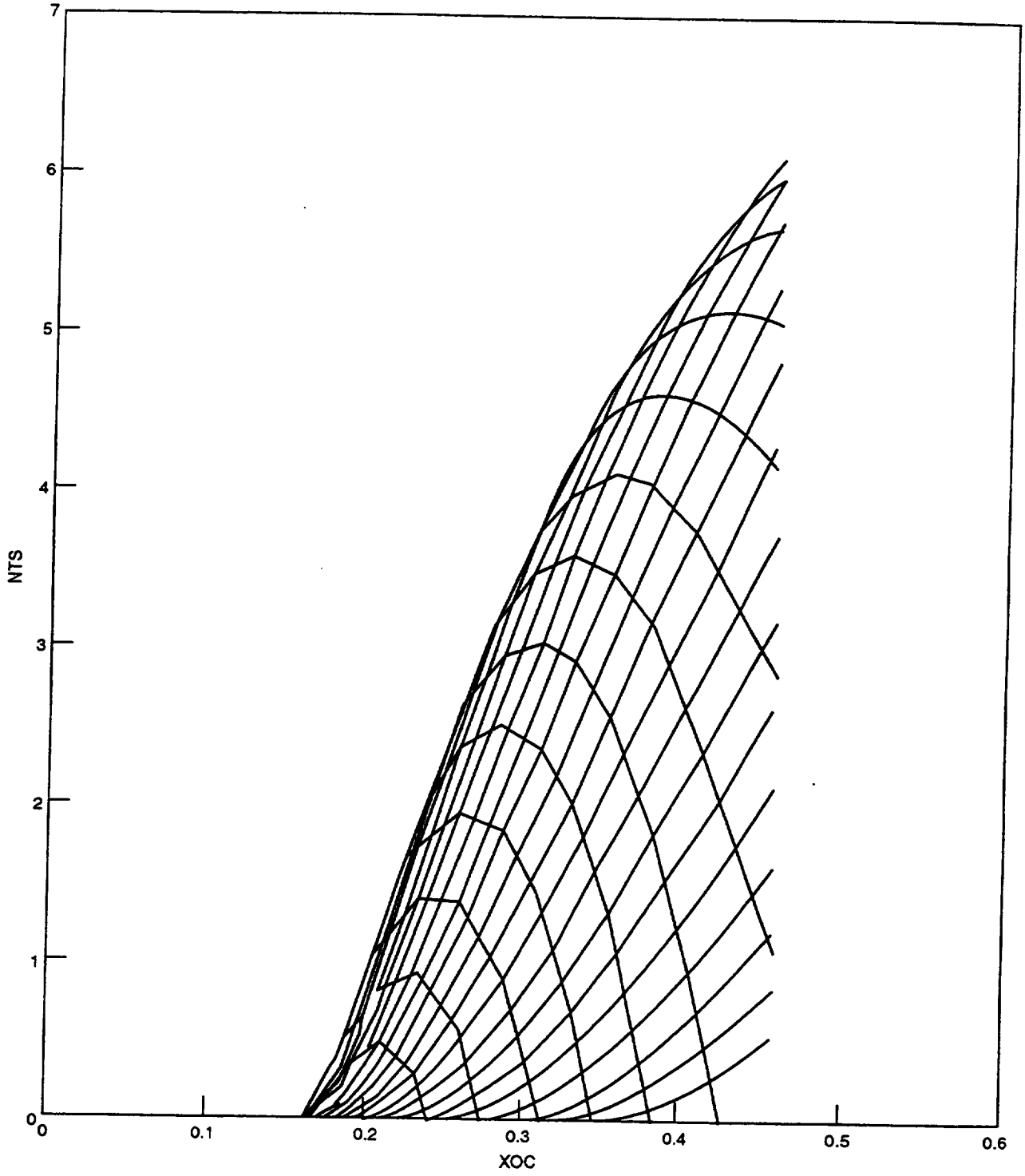

Figure G-33. Tollmien-Schlichting Disturbance Amplification Factors, WBL 513

N30668-064M

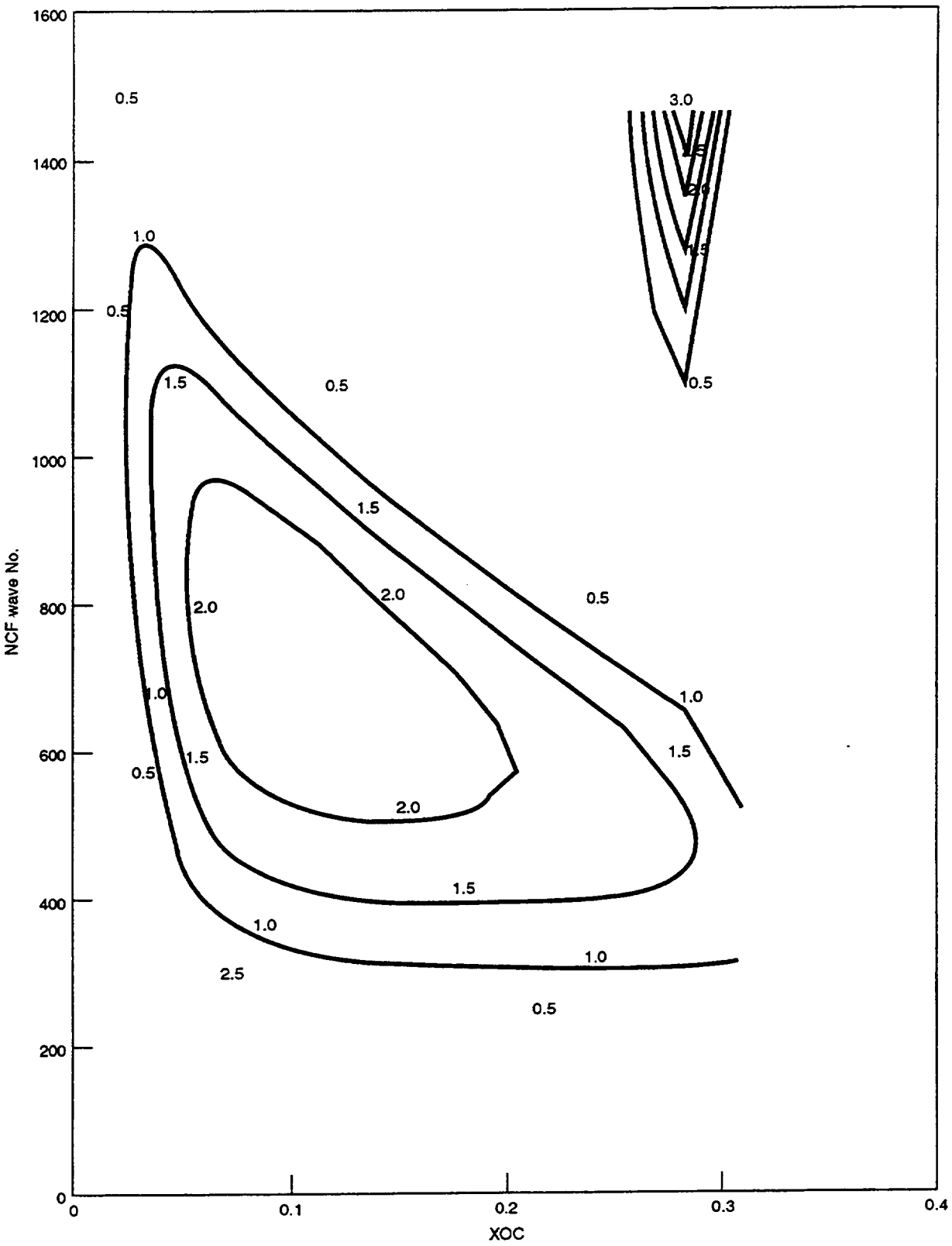

Figure G-34. Contour Plot of C-F Disturbance Amplification Factors, WBL 513

N30668-065M

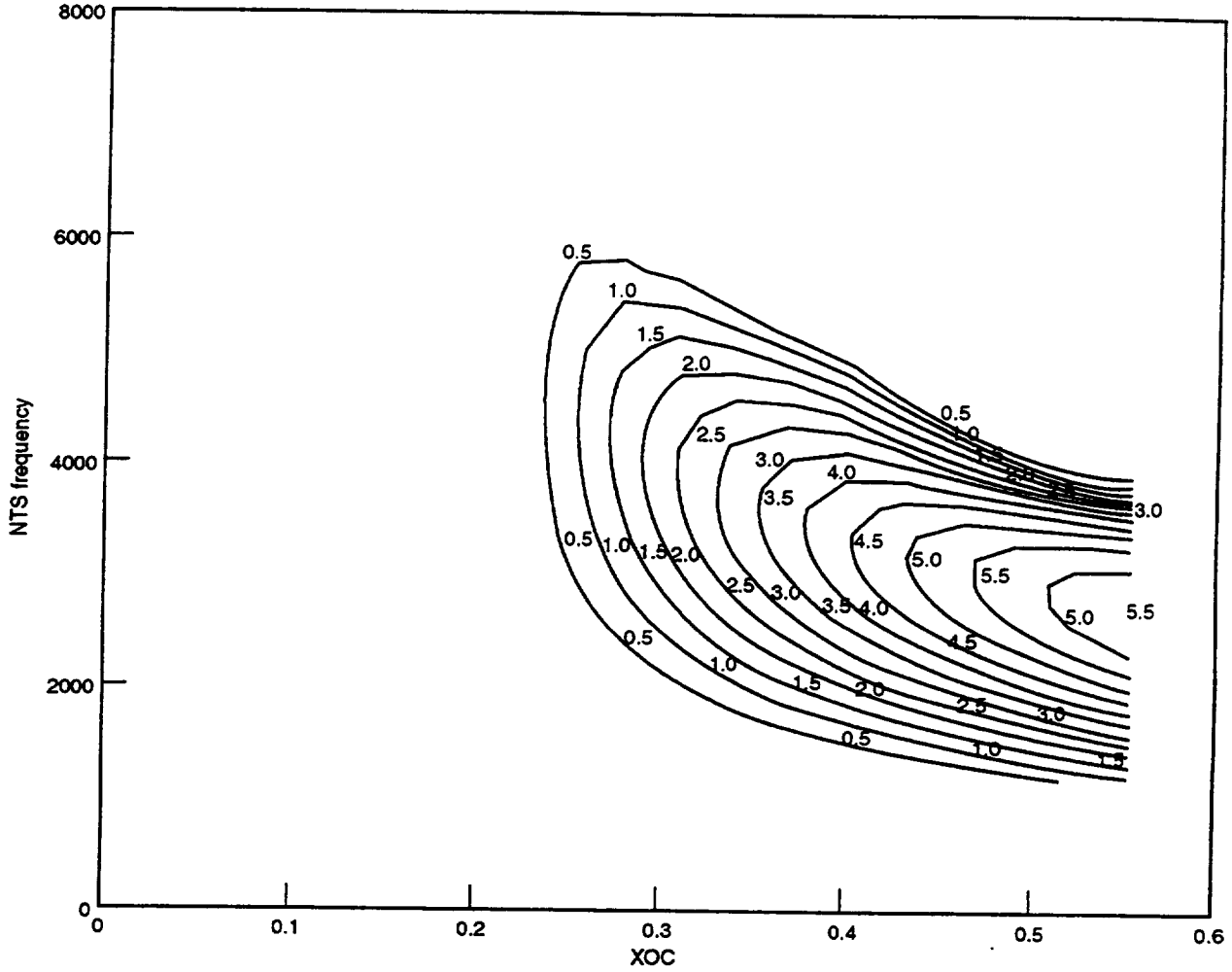

Figure G-35. Contour Plot of T-S Disturbance Amplification Factors, WBL 513

N30668-066M

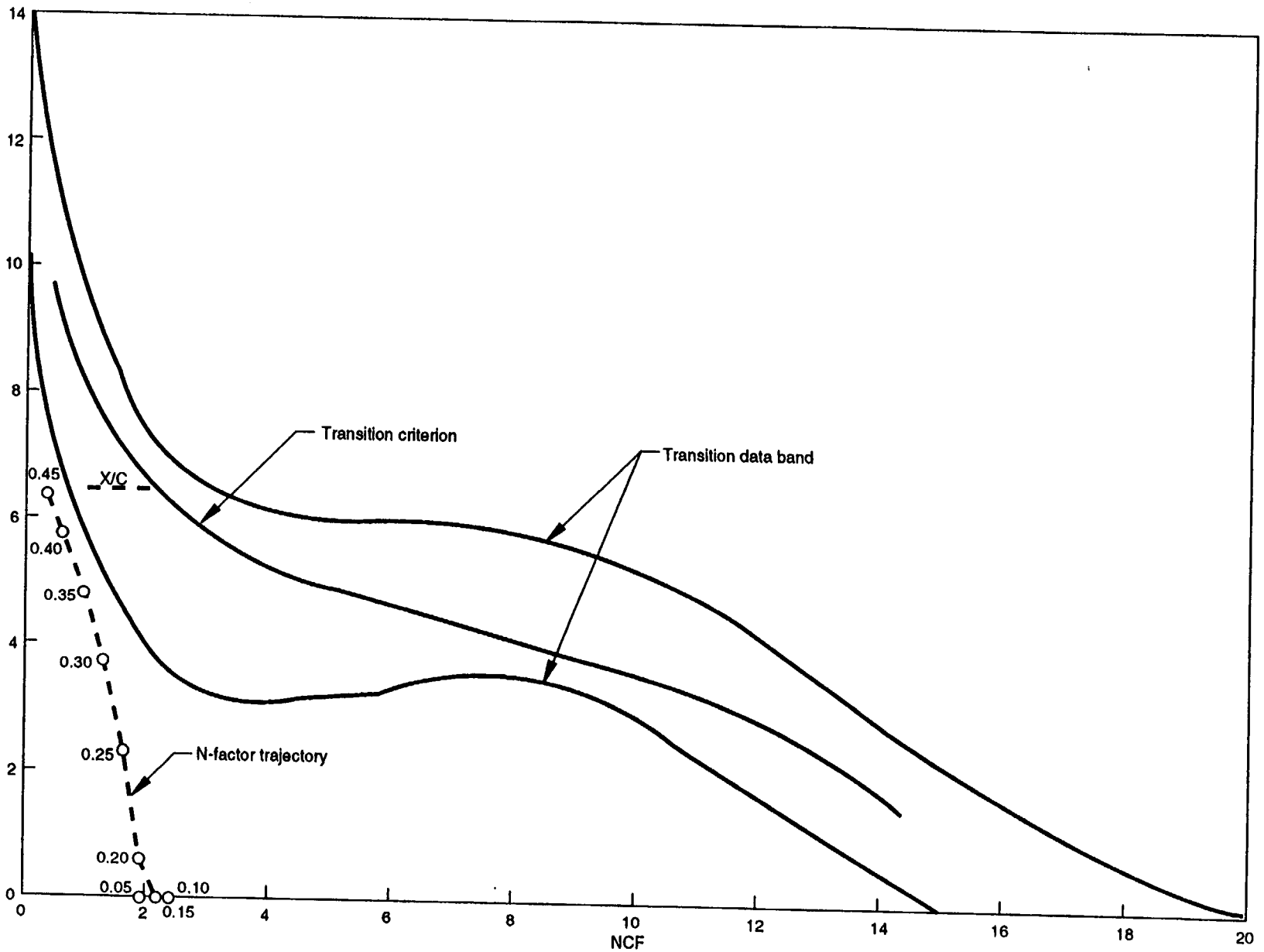

Figure G-36. Application of Transition Criterion, WBL 513

N30688-67M

REPORT DOCUMENTATION PAGE

Form Approved
OMB No. 0704-0188

1. AGENCY USE ONLY (Leave blank)	2. REPORT DATE	3. REPORT TYPE AND DATES COVERED
	April 1999	Contractor Report

4. TITLE AND SUBTITLE
High Reynolds Number Hybrid Laminar Flow Control (HLFC) Flight Experiment
II. Aerodynamic Design

5. FUNDING NUMBERS
C NAS1-18574

WU 522-32-31-01

6. AUTHOR(S)
Boeing Commerical Airplane Group

7. PERFORMING ORGANIZATION NAME(S) AND ADDRESS(ES)
Boeing Commercial Airplane Group
P. O. Box 3707
Seattle, WA 98124-2207

8. PERFORMING ORGANIZATION REPORT NUMBER

9. SPONSORING/MONITORING AGENCY NAME(S) AND ADDRESS(ES)
National Aeronautics and Space Administration
Langley Research Center
Hampton, VA 23681-2199

10. SPONSORING/MONITORING AGENCY REPORT NUMBER
NASA/CR-1999-209324

11. SUPPLEMENTARY NOTES
Langley Technical Monitor: Fayette S. Collier, Jr.
Point of Contact: Ronald D. Joslin

12a. DISTRIBUTION/AVAILABILITY STATEMENT
Unclassified-Unlimited
Subject Category 02 Distribution: Nonstandard
Availability: NASA CASI (301) 621-0390

12b. DISTRIBUTION CODE

13. ABSTRACT *(Maximum 200 words)*

This document describes the aerodynamic design of an experimental hydrid laminar flow control (HLFC) wing panel intended for use on a Boeing 757 airplane to provide a facility for flight research on high Reynolds number HLFC and to demonstrate practical HLFC operation on a full-scale commercial transport airplane. The design consists of revised wing leading edge contour designed to produce a pressure distribution favorable to laminar flow, definition of suction flow requirements to laminarize the boundary layer, provisions at the inboard end of the test panel to prevent attachment-line boundary layer transition, and a Krueger leading edge flap that serves both as a high lift device and as a shield to prevent insect accretion on the leading edge when the airplane is taking off or landing.

14. SUBJECT TERMS	15. NUMBER OF PAGES
Laminar Flow Control, Boundary Layer Suction, LFC, Flight Experiment	172
	16. PRICE CODE: A08

17. SECURITY CLASSIFICATION OF REPORT	18. SECURITY CLASSIFICATION OF THIS PAGE	19. SECURITY CLASSIFICATION OF ABSTRACT	20. LIMITATION OF ABSTRACT
Unclassified	Unclassified	Unclassified	UL

NSN 7540-01-280-5500

Standard Form 298 (Rev. 2-89)
Prescribed by ANSI Std. Z-39-18
298-102